Assessment of Drug Delivery and Anticancer Activity of Multikinase Inhibitor in Lung Cancer

THESIS

SUBMITTED IN FULFILMENT FOR THE AWARD OF THE DEGREE OF

Doctor of Philosophy

IN

PHARMACEUTICAL SCIENCES

BABASAHEB BHIMRAO AMBEDKAR UNIVERSITY
LUCKNOW
प्रज्ञा शील करुणा
ESTABLISHED 1996

Submitted By

Poonam Parashar

Enrollment no. 563/13

Supervisor

Prof. (Dr.) Shubhini A. Saraf

DEPARTMENT OF PHARMACEUTICAL SCIENCES
SCHOOL FOR BIOSCIENCES AND BIOTECHNOLOGY
BABASAHEB BHIMRAO AMBEDKAR UNIVERSITY
(A CENTRAL UNIVERSITY)
VIDYA VIHAR, RAIBARELI ROAD, LUCKNOW-226025 U.P., INDIA

(2018)

DECLARATION

I hereby declare that the thesis entitled **"Assessment of Drug Delivery and Anticancer Activity of Multikinase Inhibitor in Lung Cancer"** has been prepared by me under the supervision of **Prof. (Dr.) Shubhini A. Saraf**at Department of Pharmaceutical Sciences, School of Bioscience and Biotechnology, Babasaheb Bhimrao Ambedkar University, Lucknow (U.P.).

No part of this thesis has formed the basis for the award of my degree, diploma or fellowship previously. I further declare that the material embodied in the present work is based on original research work and indebtedness to others has been duly acknowledged at relevant places. I hereby also declare that the thesis is essentially free from all kinds of plagiarism.

Poonam Parashar
Candidate

Prof. (Dr.) Shubhini A. Saraf
Supervisor

CERTIFICATE

This is to certify that the thesis titled **"Assessment of Drug Delivery and Anticancer Activity of Multikinase Inhibitor in Lung Cancer"** submitted by **Ms. Poonam Parashar (Enrollment no. 563/13)** is an original work and has not been previously submitted in part or full for the award of any other degree or diploma to this or any other university.

The thesis submitted to Babasaheb Bhimrao Ambedkar University Lucknow satisfies all the requirements as stipulated in the Doctor of Philosophy (Ph.D.) regulations-1999 as amended in 2008/2010/2013 and it is fit for submission and evaluation for the award of the degree of Doctor of Philosophyof the University.

Date: 31st Aug 2018

Supervisor

Head of the Department

ACKNOWLEDGEMENT

My thesis represents not only my work at the pharmaceuticals; it is a milestone in more than four year of work at BBAU and specifically within the Pharmaceutics Laboratory. First and above all, I praise God, the almighty for providing me this opportunity and granting me the capability to proceed successfully.

First and foremost I wish to thank my esteemed Supervisor ***Prof Shubhini A. Saraf****, Head and Dean of the Department, School of Biosciences and Biotechnology, Babasaheb Bhimrao Ambedkar University, Lucknowfor accepting me as a Ph.D. student, for her warm encouragement, thoughtful guidance, critical comments and correction of the thesis. She helped me come up with the thesis topic and guided me through all these years. Her constant guidance, cooperation and support have always kept me going ahead. I owe a lot of gratitude to her for always being there for me and I feel privileged to be associated with a person like her during my life. She has given my career in science a purpose and a meaning full direction. And during the most difficult times when writing this thesis, she gave me the moral support and the freedom I needed to move on.*

I wish to offer my sincere thanks to Prof R.C. Sobti, Honorable Vice Chancellor of Babasaheb Bhimrao Ambedkar University, Lucknow, for providing infrastructure facilities for carrying the project advices throughout my academic career.

I convey my thanks to Dr. Gaurav Kaithwas, Dr. Sudipta Saha, Dr. Rajnikant, Dr. Vikas Mishra and Dr. Sapna Kushwaha faculty members of Deptt. of Pharmaceutical Sciences, B.B.A.U, Lucknow, for their hearty cooperation and valuable guidance throughout my research work.

I gratefully acknowledge the help rendered by my Departmental Research Committee (DRC) members of B.B.A.U, Lucknow,especially Dr. R. Venkatesh Kumar, Dr. N.K.S. More, Dr. V.Elangovan, Dr. Gaurav Kaithwas, Dr. Sudipta Saha, Dr. Vikas Mishra and Prof Shubhini A. Saraf.

I am thankful to Dr. K.P.Gupta and Prof Shailendra K. Saraf, for their patronage in scrutinizing the observations and sharing their pearls of wisdom with me to realize my research work.

I accord my thanks to the Dr. V. Elangovan and Dr. Sangeeta Saxena, BBAU, Lucknow for providing me University Science Instrumentation Centre (USIC) facilities to carry out my project.

I am thankful to the Director of Sophisticated Analytical Instrumentation Facility (SAIF), of Panjab University, Chandigarh for providing the facility for TEM studies, CDRI (SAIF), Lucknow for NMR Analysis.

I also acknowledgethe University Grant Commission, Government of Indiafor providing me with the necessary funding and fellowship to pursue research at B.B.A.U.

I would like to express sincere thanks to Dr. Sunil Goria (Librarian), Mr. O.P. Saini and Mr. Nilesh Verma (Asst. Librarian), B.B.A.U for their kind support.

My Sincere thanks to office staff and non-teaching staff, Mr. Anand, Ms. Seema, Mr. Amar, Mr. Bhandariand others who have always extended their full hearted support in carrying out my work in time.

I express my thanks to fellow labmates Mr. Chandra Bhushan Tripathi and Ms. Malti for their support, discussion, meetings, outing and jokes.

I am also grateful to my seniors Mr. Mahendra Singh, Ms. Jovita kanoujia, Ms.Pooja Singh for their support during my research work. I owe my thanks to my departmental friends Manjari Singh, Swetlana Gautam, Jitendra Kumar Rawat, Rajnish Yadav, Subhadeep Roy, Lakhveer, Amit Keshari, Vinit Raj, Amit Rai, Ashok Singh and Pranesh Nigam.

I am also grateful to my juniors Priyanka, Maurya, Samipta Singh, Raviraj, Raquibun Nisha, Nidhi Mishra,Surabhi Pal, Meena Rathore, Neelu Singh and Amit Kumarwho have supported in a number of ways and providing the pleasant environment and support during the work.

I am also appreciativeto Ms. Sapna Kushwaha and Ms. Monika Dwivedi for providing support and suggestions in various in vivo studies.

I warmly thank my beloved Father (Mr. R.B. Parashar) for his encouragement and moral support in all aspects of my life. I always miss my Mother, (Late Mrs. Bhawana Parashar) who has always stood by me like a pillar in times of need. I extend my respect to my in-laws for showing faith in me and giving me liberty to choose what I desired. This dissertation would not have been possible without Abhishek, my husband. His support and encouragement has helped me through tough times. I wouldalso like to thank my brother and sister (Shikhar and Roshni), for providing assistance in numerous ways.

Words carrying no meaning when it comes to acknowledge the love and support, I got from my little daughter Aashita. She has supported in a number of ways and always received me with warm smile and taught me how to cherish each moment.

Finally I would like to express my whole hearted gratitude to all of those, whom I may not be able to name individually, for helping directly or indirectly and I also apologize for not mentioning personally one by one.

Parashar

Poonam Parashar

CONTENTS

List of Figures

List of Tables

ABBREVIATIONS

BAX : bcl-2-associated X

BBD : Box-Behnken design

bcl-2 : B-cell lymphoma-2bromide

Cap : Capsaicin

CCD : Central composite design

Cdks : Cyclin-dependent protein kinases.

CMAs : Critical material attributes

CQAs : Critical quality attributes

DCC : N,N'-Dicyclohexylcarbodiimide

DCF : 2',7'-dichlorodihydrofluorescein

DCFDA : 2, 7-dichlorofluorescin diacetate

DMEM : Dulbecco's Modified Eagle's medium

DoE : Design of experiments

EGFR : Epidermal Growth Factor Receptor

EMEM : Eagle’s Minimum Essential Medium

FA :Folic acid

FACS : Fluorescence-activated cell sorting

FBS : Fetal Bovine Serum

FITC : Fluorescein isothiocyanate

FTIR :Fourier-transform infrared spectroscopy

Gnb :Gefitinib

GSH :Glutathione

HABA : 2-(4-hydroxyphenylazo)benzoic acid

HRP : Horse radish peroxidise

IC_{50} : Half maximal inhibitory concentration

ICH :International conference on harmonization

LC	:Lung Cancer
MMP	:Mitocondrial membrane potential
MMP-9	:Matrix metalloproteinase-9
MTT	: 3-(4,5-Dimethylthiazol-2-yl)-2,5-diphenyl tetrazolium
mV	:Milli volt
Nar	: Naringenin
NHS	: N-hydroxysuccinimide
nm	:Nanometer
PBS	:Phosphate buffer saline
PEG-bis-amine	:Poly(ethylene glycol)bis(amine)
PLGA	:Poly(lactic-co-glycolic acid)
PVA	:Poly vinyl alcohol
Rh-123	: Rhodamine-123
RIPA	: Radio Immuno Precipitation Assay
ROS	: Reactive oxygen species
SMVT	: Sodium-dependent multivitamin transporter
SOD	:Superoxide dismutase
TBARS	:Thiobarbituric acid reactive substances
TRPV1	:Transient receptor potential vanilloid 1 receptor
UV	:Ultra violet
w.r.t.	: with respect to

Chapter I

Introduction

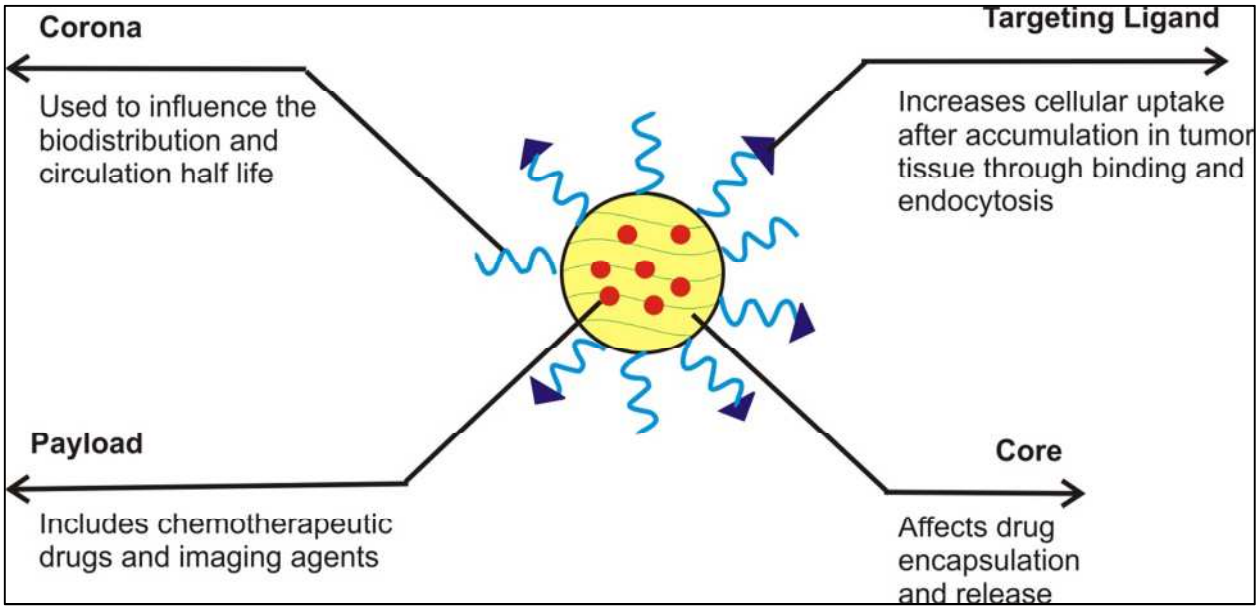

1. INTRODUCTION

1.1 Nanotechnology/Nanoparticles and cancer therapy

Most of the chemotherapeutics including xenobiotic usually offer physiochemical and pharmacological challenges, such as low aqueous solubility, poor bioavailability and narrow therapeutic index (Martin 2006). These limitations restrict their wide applications in effective cancer therapy. In past two decades newer strategies have been developed to address these fundamental drawbacks of chemotherapy (Brigger et al. 2012). The approached could be either to scheme and develop novel derivatives of chemotherapeutic agents having amended physiochemical and pharmacological characters or to develop advanced drug delivery systems. These accents may lead to specifically and unambiguously modulate the molecular processes and pathways related to tumor development (Brannon-Peppas et al. 2012). Another methodology that has been widely applied is to amend the therapeutic outcomes of the chemotherapeutic molecules through use of suitable drug delivery systems that can deliver effective payload(Izumi et al. 2003). One of the most widely used drug delivery system includes drug delivery through nanoparticles known as nanomedicine. The nanomedicines comprise of nanoparticles of chemotherapeutic entities having particle size ranging from 100-500nm. The anticancer therapy though nanoparticles is primarily focused on the development of carriers modules i.e. biodegradable polymers and methodologies, and secondary on targeting tumors. The targeting is based principle of enhanced permeation and retention effect (EPR) and/or active targeting though surface modification (Shi et al. 2017). The advantages of nanoparticle in cancer therapy are illustrated in figure 1.1.

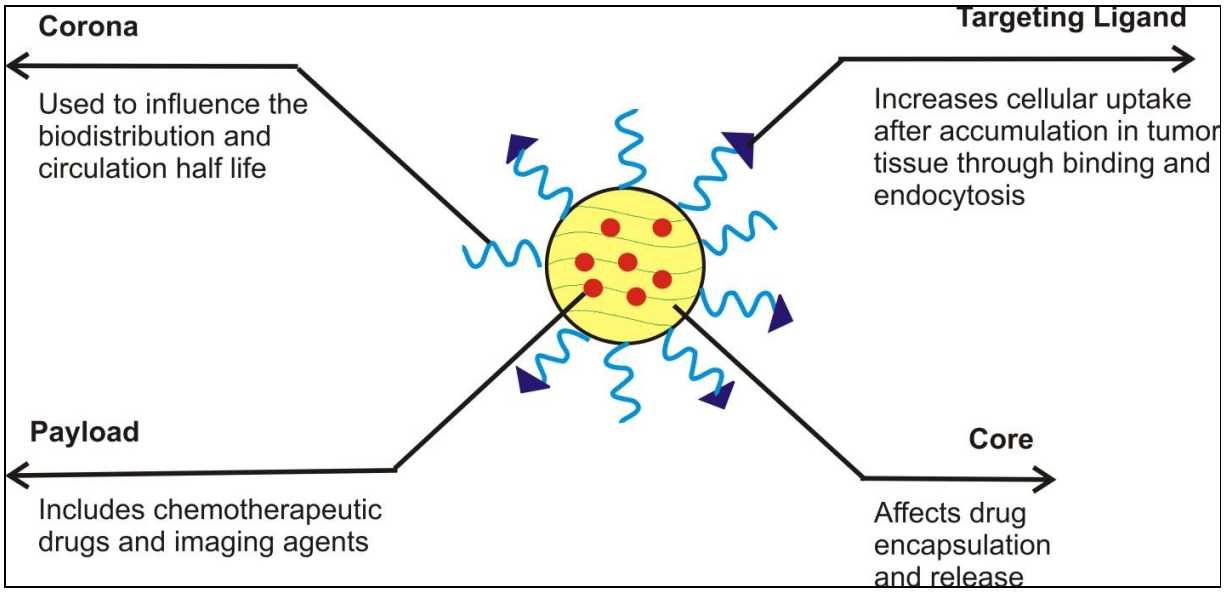

Figure 1.1. Schematic representation of nanoparticle platforms for drug delivery including corona, payload, targeting ligand and core.

The EPR effect demonstrates the accumulation of anticancer agent formed as nanoparticles (NPs) in tumor vicinity. Tumors possess high permeability, leaky vasculature and compromised lymphatic drainage. These favorable conditions of tumor facilitate NPs towards higher accumulation into the tumor site. Nanocarriers fabricated for passive targeting have been appraised clinically in mid-1980s however, approved for clinical use only after mid-1990 [6]. Some examples of the marketed products at present are Abraxane (albumin-based pacitaxel) for NSCLC (Nonsmall cell lung cancer) and breast cancer therapy, Eligard® (Leuprolide acetate and polymer (PLGA (poly(DLLactide-coglycolide)) for prostrate cancer therapy, Oncaspar®(Polymer-protein conjugate (PEGylated Lasparaginase) for leukemia and DaunoXome® (Liposomal Daunorubicin) for Karposi's Sarcoma (Mathew et al. 2007, Peer et al. 2007, Zhang et al. 2008, Wang et al. 2012).

The newer strategies are focused on developing systems that can bypass biological barriers and RES uptake at systemic, tissue, and cellular levels to achieve targeting. Recent fabrication technologies have it made possible to achieve precise delivery by making alterations in one or the other parameter such as size, surface property, and shape to give desired results (Morrissey 2006).

1.2. Ideologies of site specific drug targeting to tumor

1.2.1. Passive targeting

Passive targeting is based on the strategy of designing nanosize formulations and use of biodegradable polymers that retains in blood stream for a longer time. The repeated circulation is achieved as the NP bypasses RES uptake and reaches solid tumors where complex and leaky vasculature as well as microenvironment discriminates its entry into healthy tissues (Wakaskar 2017). Likewise, the solid tumors lack lymphatic functions hence are incompetent to eliminate extravagated drug molecule designed. This inability of tumor tissues lead to enhanced payload specifically into tumor cells and restricted/compromised entry into normal cells. This mechanism is known as enhanced permeability and retention (EPR) effect where the nanocarrier protects the drug from opsonization. The widely used nanomedicine formulations include polymeric NPs, niosomes, metallic NPs, lipoidal carriers, nanoemulsions, and so on (Perrault et al. 2009).

1.2.2. Principles of Active Targeting

Active targeting is based on the principle of interaction of NPs surface moiety, drug conjugate or drug carriers, with the targeted cell. Such kind of mechanism can be achieved through various targeting modules. The targeting ligands have very strong affinity to bind to the tumor cell surface resulting in endocytosis mediated internalization. As a result of interactions, the drug loaded NPs are delivered into the tumor-specific regions (Bae 2009). Solid tumors have different vascular endothelium from normal tissues in terms of anatomy and the expression of surface receptors. The surplus demand for nutrients and minerals needed for rapid growth and proliferation of tumor cells generates new blood vessels in order to fulfill their demands. This results in enhanced expression of receptors and enzymes (Danhier et al. 2010). Therefore, the vascular endothelium offers a platform for several targets for targeted drug delivery to cancer cells. These targeting ligands can be broadly classified as-

a) Receptor-ligand binding: biotin, folate, transferrin
b) Antibody-antigen binding: Trastuzumab, Cetuximab,Heceptin
c) Lectin based targeting: Galectins, Annexin
d) Aptamers: Pegaptanib (RNA), PNDA-3 (DNA)

The aforementioned ligands used to achieve targeting are briefly described herein.

1.2.2.1. Receptor-ligand binding is based on the principle that the cancer cells demand an additional amount of vitamins and nutrients such as biotin, folic acid, for their active proliferation. Thus a swift uptake of NPs carrying such molecules is witnessed via these **overexpressed receptors**. When surface engineered NPs reach these overexpressed receptors, they rapidly internalize into the cells, thus delivering the drug payload(Kouchakzadeh et al. 2017, Ming et al. 2017). However, non-cancerous normal cells have comparatively lesser levels of such kind of receptors on their cell surface, thus a poor accumulation of drug is witnessed.

1.2.2.2. Antibody may target tumor cells by fetching surface **antigens** that are differentially expressed in cancer cells (Scott et al. 2012). The antibodies bind to the overexpressed antigens and can cause tumor cell death by blocking pathways that are necessary for proliferation and survival of cancer cells. For example, rituximab targets CD20 in non-Hodgkin B cell lymphoma, trastuzumab targets HER2 in breast cancer, and cetuximab targets EGFR in colorectal cancer. Monoclonal antibodies such as bevacizumab trastuzumab, cetuximab and rituximab have been approved for clinical use at present.

1.2.2.3. Lectins are vastly specific proteins having affinity to bind with **carbohydrates** and widely exist in various animals, plants and bacteria. On the basis of their defensive properties and usual ability to prompt apoptosis in cells, lectins have been utilized in targeting cancer cells (Yau et al. 2015). Lectins in animals offer cell interactions in cancer therapy. The effect of galectins was studied against lung cells, fibroblast cells, thyroid cells, colon cells, prostate cells and it was revealed that it binds to T-cell, through specific integrin binding and inhibit $Ca2^{+}$-calpaincaspase-1 pathway causing cell death. These lectins recognize carbohydrate moieties such as dextrose, mannose, glucose, and their derivatives thus, been comprehensively exploited as targeting moieties. (Torchilin 2000, Allen et al. 2004, Lammers et al. 2008, Kue et al. 2016).

1.2.2.4. Aptamers, commonly known as chemical antibodies, are single-stranded **nucleic acid oligonucleotides** which possess high specificity and affinity towards their binding targets. Bestowed with their superior qualities related to conventional

antibodies, particularly small size and minor immunogenicity and minimal toxicity, aptamers have currently arisen as innovative delivery tools for antineoplastic agents specifically to cancer cells through targeting specific cancer defined hallmarks (Zhou et al. 2016).

In designing of NPs, the most widely explored systems comprises are lipid and polymer-based systems. A prominent example being poly (lactic-co-glycolic acid) (PLGA) and Polycaprolactone (PCL) has been employed in designing of study and is discussed in detail.

1.3. Polymers as a Carrier in Nanomedicine

Ever since 1970s, considerable attempts have been made on developing different polymers having various attributes to achieve desired drug delivery of therapeutic agents. The polymers selected for designing of drug delivery systems are selected on the basis of their capability to improved bioavailability, biocompatible, nature, preferred release profile, altered degradation rate and stability (Duncan 2006). PLGA and PCL are among the most recognized choices widely adapted for the formulation of NPs due to their properties of biocompatibility and biodegradability (Krause et al. 1985). These polymers were first used in 1970-80s for delivery of small peptides and low molecular weight steroids molecules like LHRH analogues as contraceptives (Beck et al. 1983). PLGA was first used back in 1989 for sustained delivery of peptides and recombinant proteins(Schrier et al. 1999). Advanced technology in 1994, emphasizes the development of modified polymers like PLA-PEG were investigated in order to get controlled release as well as extended circulation of the drug molecules (Hu et al. 2006, Makadia et al. 2011). The administration routes have also been considerably expanded, from intravenous to pulmonary, oral, intranasal and newly targeting delivery approach(Soppimath et al. 2001). The extensive research of PCL/PLGA polymers has resulted in myriad biomedical applications.

1.3.1. Types of Polymeric Nanoparticles

Polymeric NPs are broadly classified into four types which are: nanoparticles, micelles, dendrimers and drug conjugates.

Nanoparticles range from 10–1000 nm in size and are biodegradable and biocompatible in nature. They offer protection of therapeutic agents against enzymatic and biological fluid

degradation before reaching site of choice. They have been proven as potential carriers for their stealth effect and for active and passive targeting and long circulatory capability subsequent to surface modification thereby maintaining controlled and sustained release of drugs. Other advantages comprises of properties such as high entrapment efficiency, high payload and bio- stability (Reis et al. 2017).

Dendrimers have a particle size below 100nm and are highly branched monodispersed polymeric systems. They constitute a core, branches and surface. Dendrimers are bestowed with properties such as long circulation, controlled release and targeted delivery of drugs specifically to macrophages. They have been widely utilized in liver targeting. Priostar® and Astramol® are some of the examples of commercially available Dendrimers (Bae 2009, Zhou et al. 2016).

Polymeric micelles of 10–100 nm in size have desirable characteristics of high drug entrapment, high payload and stability against GIT fluids and enzymatic degradation. They have been extensively utilized in site specific active and passive targeting as theranostics (Oerlemans et al. 2010).

Polymer drug conjugates are formed by the conjugation of polymers with low molecular weight drug candidates. They are employed to deliver high molecular weight drugs and proteins. These conjugated systems lead to altered pharmacokinetic properties of drug at cellular level and are designed to be enzyme specific for a particular diseased tissue. Guided by the physiochemical properties, retention in cancer cells is facilitated for enhanced permeation and retention effect. The specificity towards enzymes enhances tumor drug accumulation into tumors and significantly minimizes entry to healthy tissues (Greco et al. 2009).

1.4. Method of Preparation of Polymeric NPs (Vauthier et al. 2009, Reis et al. 2017)

Polymeric NPs preparation method are enumerated below-

1. Emulsion and Solvent Evaporation Method
2. Spontaneous Emulsification or Solvent Diffusion Method

3. Double Emulsion and Evaporation Method
4. Salting Out Method
5. Emulsions-Diffusion Method
6. Solvent Displacement/Precipitation Method
7. Coacervation or Ionic Gelation Method
8. Polymerization Method

Some important technique are discussed as follows-

1.4.1. Emulsion and Solvent Evaporation Method (Mu et al. 2002)

Most of the antineoplastic agents have poor aqueous solubility, thus double emulsion technique is most preferred. This method is employed as both polymer and antineoplastic agent are hydrophobic in nature. Both are dissolved in organic solvents such as dichloromethane, chloroform etc. The resulting solution of drug and polymer (separately) is then mixed in aqueous solution and is being emulsified under sonication to obtained NPs. The detailed methodology is explained in scheme 1.

1.4.2. Double Emulsion and Evaporation Method (Rao et al. 2011)

It is also one of the most preferred methods employed for formulating polymeric NPs as it can be utilized for hydrophilic drugs, more so as they lack high entrapment. The detailed methodology is explained in scheme 2.

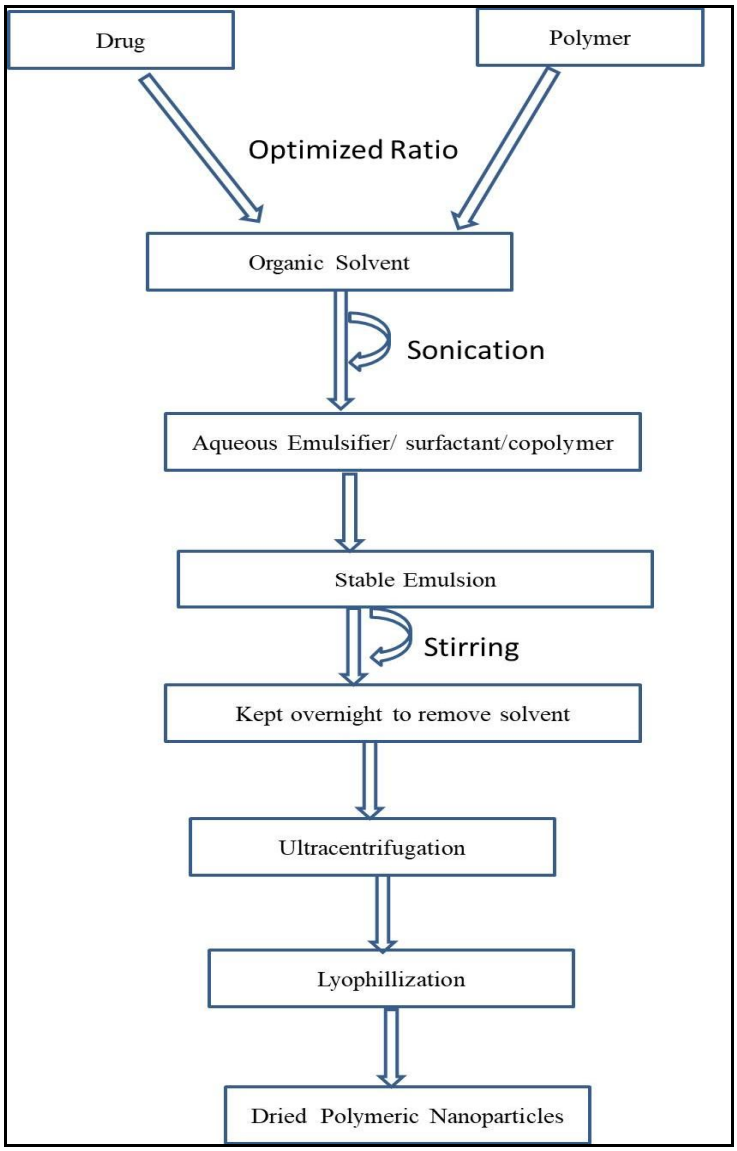

Scheme 1. Schematic representation of emulsion and solvent evaporation method employed for preparing polymeric NPs.

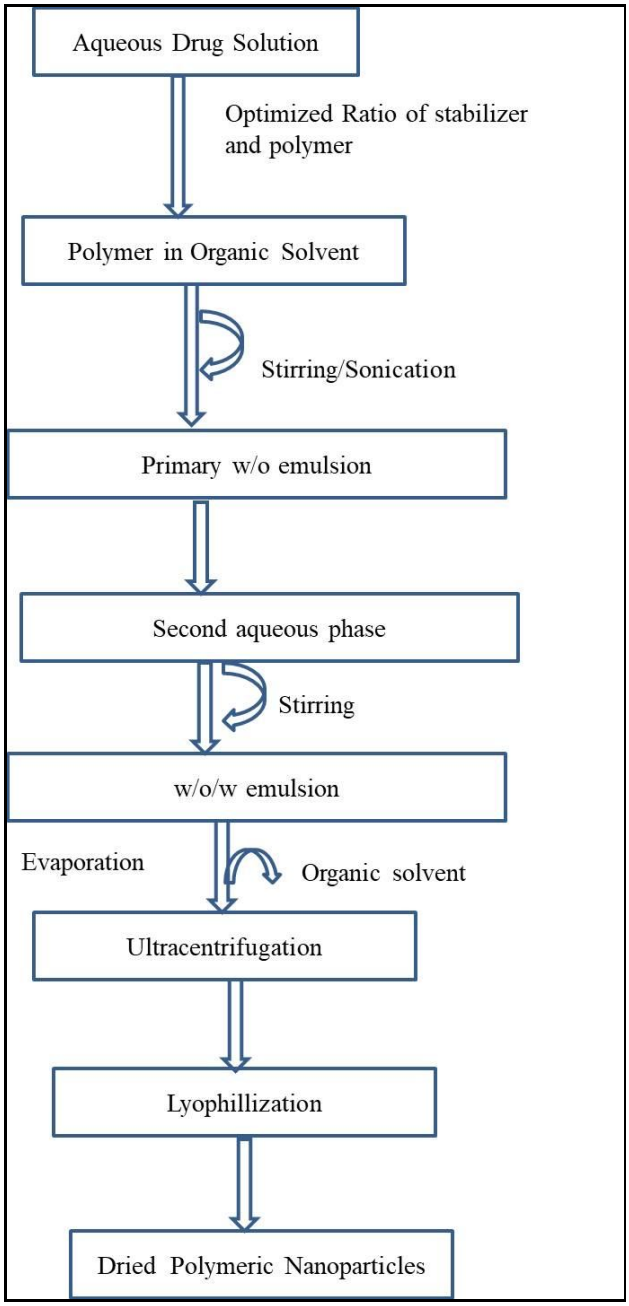

Scheme 2. Schematic representation of Double emulsion and evaporation method employed for preparing polymeric NPs.

1.5. Applications of Polymeric Nanoparticles (Nasir et al. 2015)

2. **Cancer therapy:** Conjugated NPs with surface modification and/or targeting ligand moiety used in cancer theranostics.
3. **Enhanced circulation time:** Able to bypass RES uptake and opsonization; taken up via endocytosis passively, by virtue of size.
4. I**nternalization:** Rapid uptake by cancer cells due to nanosize and presence of overexpressed factors.
5. **Targeted drug delivery:** Site specific delivery to cancer cells.

1.6. Lung Cancer

Cancer is a huge group of diverse diseases that occur due to unregulated cell growth(Aupérin et al. 2010, Stewart et al. 2017).Cancer remains one of the most lethal disease with an ever increasing number of patients across the world (Mok et al. 2017). Lung cancer (LC) holds the first position among various cancers accounting for 28% of total cancer, having low survival rate of five years, poor prognosis and lack of early diagnosis (Garon et al. 2015). LC is broadly classified as non- small cell lung cancer (NSCLC) which accounts for >80% of overall LC (Stewart et al. 2017). Second major type which covers 20% of LC is small cell lung cancer (SCLC) but its occurrence is less. NSCLC is further subcategorized as adenocarcinomas (ADC), squamous cell carcinoma (SCC) and large cell carcinoma (LCC) (Heymach et al. 2008).

1.6.1. Signs and symptoms

LC symptoms comprise persistent cough, sometimes blood or rust colored sputum at severe stages. LC may involve difficulty in breathing along with shortness of breath. Other nonspecific symptoms include loss of appetite leading to weight loss and fatigue. Lung related infections such as bronchitis and pneumonia may also be one of the signs of LC (Hammerschmidt et al. 2009).

1.6.2. Diagnosis

LC is diagnosed mostly by X-ray and CT-scans. Completely developed LC can be detected through endobronchial ultrasound and other laboratory examinations. The confirmation of

LC tumor as malignant, its severity and type, is done through biopsy or lung nodule diagnosis. However LC does not show any early symptoms, so it is often diagnosed only when it has already reached an advanced stage (Batzler et al. 2008).

1.6.3. Stages of Lung Cancer

Non-small cell lung cancer has four major stages as summarized in Table 1.

Table 1.1. Stages of Lung Cancer (Detterbeck et al. 2007)

Stage	Occurrence
I	Cancer is confined to lung and not spread outside the lung
II	Cancer develops in the lung and nearby lymph nodes
III	Cancer develops in lung and spreads to lymph nodes up to middle of the chest
III a	Cancer is found in lymph nodes of the same side of the chest where cancer growth initiated
III b	Cancer spread to lymph nodes on the opposite side of the chest and above the collarbone
IV	Cancer has spread to both lungs, and surrounding area of lungs and/or to distant organs.

1.6.4. Aggressive Lung Cancer

Most of the lung cancers are diagnosed at the stages where they have become invasive i.e., they have migrated into surrounding lymph nodes and distant organs. Molecular biomarkers of LC offer a specific treatment strategy and sensitive diagnosis. Some major protein biomarkers comprises of SCC (Squamous cell carcinoma antigen), VEGF (Vascular endothelial growth factor), EGFR (Epidermal Growth Factor), MEK1, HER2 and many more (Tatiana N. Zamay,2007). There are targeted agents that have been successful against epidermal growth factor receptor (EGFR) mutations and anaplastic lymphoma kinase (ALK) rearrangements. Through genomic testing, other molecular changes have been found including gene rearrangements of ROS1 and RET, amplification of MET and activating

mutations in BRAF, KRAS *and* HER2 genes, which might be potential targets for future therapies (Shtivelman et al. 2014).

1.6.5. Lung Cancer Treatment

Noteworthy developments have been done toward the decline of occupational health threats concomitant with LC, specifically smoking, and for the avoidance of various disorders. In recent years, immunotherapy and targeted therapy have made remarkable contributions in the LC management. Moreover, genetics and biomarkers have proven to be helpful in personalized LC therapy and its management. The foremost treatments include chemotherapy, surgery and radiotherapy. Also, immunotherapy is done to boost the body's own defense system to target cancers cells (Howington et al. 2013).

1.6.6. Treatment of Lung Cancer

Almost 40% of LC is diagnosed at stage IV. The prime aim of treating such patients is to expand survival and reduce disease-related adverse events as well as drug-related toxicity. The treatment through combined chemotherapy is the first-line treatment for LC (Tanner et al. 2017). However, it is greatly influenced by age, gender and histology. The chemotherapeutic treatment comprises of regimen of a platinum (cisplatin or carboplatin) in combination with paclitaxel/irinotecan or vinorelbine/docetaxel or gemcitabine. Radiotherapy damages DNA of cancer cells through its high-energy beams. The radiation therapy is preferred at early stages when tumor is localized within the chest (Zappa et al. 2016).

After the development of LC in a patient, the tumor should be tested for specific gene mutations like ROS1,EGFR, ALK and BRAF. On the basis of mutation the following treatment regimen should be opted (Shaw et al. 2013).

- ALK inhibitor like Crizotinib, Ceritinib and Alectinib should be selected as first treatment for ALK gene mutated LC. Once these antineoplastic agents get well tolerated other ALK inhibitors like Brigatinib should be given.

- The patients having EGFR mutation should be treated with anti-EGFR drugs like Erlotinib, Gefitinib, Imatinib etc.
- Patients having ROS1 gene mutation should be treated with Crizotinib (ALK inhibitor) as first choice.
- BRAF gene mutated patients might be opted for treatement with a combination of the targeted drugs Dabrafenib and Trametinib.

1.7. Use of Targeted Agent

In spite of extensive innovations in cancer therapy, an effective treatment still remains the foremost challenge for clinicians (Goldman et al. 2017) . Despite advances in defining the molecular mechanisms involved in lung oncogenesis, LC chemotherapy faces various hurdles due to number of factor viz. early diagnosis among patients is not observed, premature metastasis, high relapse rate and complications with surgical procedure, expensive radiation therapy, MDR against most of chemotherapeutic agents and severe side effects associated with chemotherapy (Silvestri et al. 2005). The modern era of chemotherapy, has focused oncology towards targeted therapy (Pirker 2013). Numerous molecular alterations have been observed as possible therapeutic targets and are regarded as targeted modules. These targeting modules can overcome the hurdles of chemotherapy (Shtivelman et al. 2014). The targeted therapy is loaded with advantages like minimal side effects, improved therapeutic efficacy and higher accumulation of drug at the targeted site. Amongst the various targeting approaches like antibodies, lectins, aptamers, nucleic acid-based ligand and small peptides molecules, most common targets for LC are EGFR receptor, receptor tyrosine kinases, folate receptor (FR), biotin receptor etc. The most widely investigated targeted therapy utilizing EGFR are Gefitinib and Erlotinib.For the potential therapeutic approach for HER3, clinical studies of anti-ERBB3 antibody MM-121 are ongoing in NCT00994123 and NCT01451632 including combination study with erlotinib (Brunner et al. 2013).

1.8. LITERATURE REVIEW

Table 1.2 Literature review

Author	Drug	Formulation	Inferences
(Amreddy et al. 2018)	Cis-diamine platinum	Polyamidoamine dendrimer	Improved cytotoxicity to A549 cells, enhanced accumulation at targeted site and enhanced therapeutic efficacy
(Lee et al. 2018)	Doxorubicin	Biotin conjugated bilirubin-based NPs	Specific binding to cancer cells, greater accumulation of drug into tumor and enhanced anticancer activity
(Kato et al. 2017)	-	Porphyrin-lipid NPs (porphysomes)	Enhanced cellular uptake, higher accumulation, inhibits tumor cell proliferation and greater apoptosis
(Lv et al. 2017)	Capsaicin	Folate conjugated lipid NPs	Enhanced toxicity, apoptosis and targeted delivery to cancer cells
(Wang et al. 2017)	Gemcitabinein	Folic acid-conjugated chitosan NPs	Targeted delivery to tumor, reduced organ toxicity and higher uptake into cancer cells
(Ni et al. 2017)	Gefitinib	Polymeric NPs	Enhanced antitumor effects, reduced side effects and significantly organs toxicity
(Zhang et al. 2017)	Gefitinib	Polymeric NPs	enhanced cytotoxicity, inhibits growth of tumors and enhanced therapeutic efficacy
(Qi et al. 2017)	-	Review	Improved therapeutic efficacy as two drug act by different mechanism
(Tian et al. 2017)	Paclitaxel and cisplatin	Polymeric NPs	Reduced toxicity, enhanced tumor inhibition and anticancer potential
(Wickens et al. 2017)	-	Review	CD44 receptors are overexpressed in cancer cells and hold high affinity towards hyaluronic acid
(Chang et al. 2017)	Naringenin	Naringenin extract	Downegulation of matrix metalloproteinase (MMP)-2 and −9 expression and inhibition of A549 cells migration
(Zhou et al. 2017)	Gefitinib and Doxorubicin	drug-polymer conjugate NPs	desired sequential release,4-fold enhanced anticancer efficacy

Author	Drug	Formulation	Inferences
(Mottaghitalab et al. 2017)	Gemcitabine	Peptide conjugated NPs	Reduced lung tumorvolume, higher targeting potential and enhanced survival rate
(Zhang et al. 2016)	Spermine	Folate-conjugated polyspermine	Enhanced specificity towards cancer cells and targeted gene delivery
(Clark et al. 2016)	Capsaicin	Review	Anticancer properties of Capsaicin
(Mattheolabakis et al. 2015)	-	Review	Hyaluronic acid' targeting potential can be utilized in cancer therapy
(Ren et al. 2015)	-	Review	biotin moiety is a smart choice for targeted delivery to cancer cells.
(Zhao et al. 2015)	Gefitinib	Chitosan NPs	enhanced cell apoptosis, overcome resistance and enhanced cancer potential
(Anandakumar et al. 2015)	Capsaicin	Capsaicin extract in oil base	Downregualted matrix metalloproteases 2 and 9 expression and restoration of collagen, elastin levels
(Mir et al. 2015)	Naringenin	Review	Naringenin holds anticancer potential
(Lam et al. 2014)	Gefitinib	EGFR antibody conjugated Gold NPs	Enhanced internalization, reduced vialbility in A549 cell lines and higher stability
(Chakraborty et al. 2014)	Capsaicin	Capsaicin extract	Capsaicin play an important role in down-regulation of VEGF expression and Cox-2 in a p53-dependent manner
(Chittasupho et al. 2014)	Doxorubicin	Peptide conjugated PLGA NPs	Higher binding efficiency, CXCR4-mediated internalization and targeted delivery
(Lau et al. 2014)	Capsaicin	Capsaicin extract	capsaicin-induced apoptosis in human SCLC cells and possess potent anti-neoplastic activity
(Heo et al. 2012)	Paclitaxel	Biotin functionalized Gold NPs	Reduced viability in A549 cell, enhanced apoptosis and drug accumulation.
(Zwicke et al. 2012)	various	Review	Folate expression can be exploited for targeted delivery to tumor. The overexpressed factors can facilitate drug uptake.

Author	Drug	Formulation	Inference
(Peng et al. 2011)	Cisplatin	EGFR conjugated NPs	prolonged circulation time and improved pharmacokinetics and enhanced antitumor activity
(Chahar et al. 2011)	-	Review	Anticancer potential of flavonoids
(Cataldo et al. 2011)	Erlotinib and Gefitinib	Case report	Reduced side effect and better therapeutic outcome
(Le Marchand et al. 2000)	Various flavonoids	Review	Flavonoids play an important role in cancer prevention

Based on the extensive literature search the aims, objectives and methodology of the present work were conceived.The referencing of reported literature was done through Endnote X7 software throughout the thesis utilizing author-date format.

REFERENCES

Allen, T. M. and P. R. Cullis (2004). "Drug delivery systems: entering the mainstream." Science. **303**(5665): 1818-1822. .

Amreddy, N., A. Babu, J. Panneerselvam, A. Srivastava, R. Muralidharan, A. Chen, Y. D. Zhao, A. Munshi and R. Ramesh (2018). "Chemo-biologic combinatorial drug delivery using folate receptor-targeted dendrimer nanoparticles for lung cancer treatment." Nanomedicine: Nanotechnology, Biology and Medicine **14**(2): 373-384.

Anandakumar, P., S. Kamaraj, S. Jagan, G. Ramakrishnan, S. Asokkumar, C. Naveenkumar, S. Raghunandhakumar, M. K. Vanitha and T. Devaki (2015). "The anticancer role of capsaicin in experimentallyinduced lung carcinogenesis." Journal of pharmacopuncture **18**(2): 19.

Aupérin, A., C. Le Péchoux, E. Rolland, W. J. Curran, K. Furuse, P. Fournel, J. Belderbos, G. Clamon, H. C. Ulutin and R. Paulus (2010). "Meta-analysis of concomitant versus sequential radiochemotherapy in locally advanced non-small-cell lung cancer."

Bae, Y. H. (2009). "Drug targeting and tumor heterogeneity." Journal of controlled release: official journal of the Controlled Release Society **133**(1): 2.

Batzler, W. U., K. Giersiepen, S. Hentschel, G. Husmann, P. Kaatsch, A. Katalinic, J. Kieschke, K. Kraywinkel, M. Meyer and R. Stabenow (2008). "Cancer in Germany 2003-2004 Incidence and Trends."

Beck, L. R. and T. R. Tice (1983). "Poly (lactic acid) and poly (lactic acid-co-glycolic acid) contraceptive delivery systems."

Brannon-Peppas, L. and J. O. Blanchette (2012). "Nanoparticle and targeted systems for cancer therapy." Advanced drug delivery reviews **64**: 206-212.

Brigger, I., C. Dubernet and P. Couvreur (2012). "Nanoparticles in cancer therapy and diagnosis." Advanced drug delivery reviews **64**: 24-36.

Brunner, A. M., D. B. Costa, R. S. Heist, E. Garcia, N. I. Lindeman, L. M. Sholl, G. R. Oxnard, B. E. Johnson and P. S. Hammerman (2013). "Treatment-related toxicities in a phase II trial of dasatinib in patients with squamous cell carcinoma of the lung." Journal of Thoracic Oncology **8**(11): 1434-1437.

Cataldo, V. D., D. L. Gibbons, R. Perez-Soler and A. Quintas-Cardama (2011). "Treatment of non-small-cell lung cancer with erlotinib or gefitinib." N Engl J Med **364**(10): 947-955.

Chahar, M. K., N. Sharma, M. P. Dobhal and Y. C. Joshi (2011). "Flavonoids: A versatile source of anticancer drugs." Pharmacognosy reviews **5**(9): 1.

Chakraborty, S., A. Adhikary, M. Mazumdar, S. Mukherjee, P. Bhattacharjee, D. Guha, T. Choudhuri, S. Chattopadhyay, G. Sa and A. Sen (2014). "Capsaicin-induced activation of p53-SMAR1 auto-regulatory loop down-regulates VEGF in non-small cell lung cancer to restrain angiogenesis." PloS one **9**(6): e99743.

Chang, H. L., Y. M. Chang, S. C. Lai, K. M. Chen, K. C. Wang, T. T. Chiu, F. H. Chang and L. S. Hsu (2017). "Naringenin inhibits migration of lung cancer cells via the inhibition of matrix metalloproteinases-2 and-9." Experimental and therapeutic medicine **13**(2): 739-744.

Chittasupho, C., K. Lirdprapamongkol, P. Kewsuwan and N. Sarisuta (2014). "Targeted delivery of doxorubicin to A549 lung cancer cells by CXCR4 antagonist conjugated PLGA nanoparticles." European Journal of Pharmaceutics and Biopharmaceutics **88**(2): 529-538.

Clark, R. and S.-H. Lee (2016). "Anticancer properties of capsaicin against human cancer." Anticancer research **36**(3): 837-843.

Danhier, F., O. Feron and V. Préat (2010). "To exploit the tumor microenvironment: passive and active tumor targeting of nanocarriers for anti-cancer drug delivery." Journal of controlled release **148**(2): 135-146.

Detterbeck, F. C., M. A. Jantz, M. Wallace, J. Vansteenkiste and G. A. Silvestri (2007). "Invasive mediastinal staging of lung cancer: ACCP evidence-based clinical practice guidelines." Chest **132**(3): 202S-220S.
Duncan, R. (2006). "Polymer conjugates as anticancer nanomedicines." Nature reviews cancer **6**(9): 688.
Garon, E. B., N. A. Rizvi, R. Hui, N. Leighl, A. S. Balmanoukian, J. P. Eder, A. Patnaik, C. Aggarwal, M. Gubens and L. Horn (2015). "Pembrolizumab for the treatment of non–small-cell lung cancer." New England Journal of Medicine **372**(21): 2018-2028.
Goldman, E., A. Zinger, D. da Silva, Z. Yaari, A. Kajal, D. Vardi-Oknin, M. Goldfeder, J. E. Schroeder, J. Shainsky-Roitman, D. Hershkovitz and A. Schroeder (2017). "Nanoparticles target early-stage breast cancer metastasis in vivo." Nanotechnology **28**(43): 43LT01.
Greco, F. and M. J. Vicent (2009). "Combination therapy: opportunities and challenges for polymer–drug conjugates as anticancer nanomedicines." Advanced drug delivery reviews **61**(13): 1203-1213.
Hammerschmidt, S. and H. Wirtz (2009). "Lung cancer: current diagnosis and treatment." Deutsches Ärzteblatt International **106**(49): 809.
Heo, D. N., D. H. Yang, H.-J. Moon, J. B. Lee, M. S. Bae, S. C. Lee, W. J. Lee, I.-C. Sun and I. K. Kwon (2012). "Gold nanoparticles surface-functionalized with paclitaxel drug and biotin receptor as theranostic agents for cancer therapy." Biomaterials **33**(3): 856-866.
Heymach, J. V., L. Paz-Ares, F. De Braud, M. Sebastian, D. J. Stewart, W. E. Eberhardt, A. A. Ranade, G. Cohen, J. M. Trigo and A. B. Sandler (2008). "Randomized phase II study of vandetanib alone or with paclitaxel and carboplatin as first-line treatment for advanced non–small-cell lung cancer." Journal of Clinical Oncology **26**(33): 5407-5415.
Howington, J. A., M. G. Blum, A. C. Chang, A. A. Balekian and S. C. Murthy (2013). "Treatment of stage I and II non-small cell lung cancer: diagnosis and management of lung cancer: American College of Chest Physicians evidence-based clinical practice guidelines." Chest **143**(5): e278S-e313S.
Hu, F.-Q., G.-F. Ren, H. Yuan, Y.-Z. Du and S. Zeng (2006). "Shell cross-linked stearic acid grafted chitosan oligosaccharide self-aggregated micelles for controlled release of paclitaxel." Colloids and Surfaces B: Biointerfaces **50**(2): 97-103.
Izumi, H., T. Torigoe, H. Ishiguchi, H. Uramoto, Y. Yoshida, M. Tanabe, T. Ise, T. Murakami, T. Yoshida and M. Nomoto (2003). "Cellular pH regulators: potentially promising molecular targets for cancer chemotherapy." Cancer treatment reviews **29**(6): 541-549.
Kato, T., C. S. Jin, H. Ujiie, D. Lee, K. Fujino, H. Wada, H.-p. Hu, R. A. Weersink, J. Chen and M. Kaji (2017). "Nanoparticle targeted folate receptor 1-enhanced photodynamic therapy for lung cancer." Lung Cancer **113**: 59-68.
Kouchakzadeh, H., T. Soudi, N. H. Aghda and S. A. Shojaosadati (2017). "Ligand-modified Biopolymeric Nanoparticles as Efficient Tools for Targeted Cancer Therapy." Current pharmaceutical design **23**(35): 5336-5348.
Krause, H.-J., A. Schwarz and P. Rohdewald (1985). "Polylactic acid nanoparticles, a colloidal drug delivery system for lipophilic drugs." International journal of pharmaceutics **27**(2-3): 145-155.
Kue, C. S., A. Kamkaew, K. Burgess, L. V. Kiew, L. Y. Chung and H. B. Lee (2016). "Small Molecules for Active Targeting in Cancer." Med Res Rev **36**(3): 494-575. .
Lam, A. T. N., J. Yoon, E.-O. Ganbold, D. K. Singh, D. Kim, K.-H. Cho, S. Y. Lee, J. Choo, K. Lee and S.-W. Joo (2014). "Colloidal gold nanoparticle conjugates of gefitinib." Colloids and Surfaces B: Biointerfaces **123**: 61-67.
Lammers, T., W. E. Hennink and G. Storm (2008). "Tumour-targeted nanomedicines: principles and practice." Br J Cancer **99**(3): 392-397.
Lau, J. K., K. C. Brown, A. M. Dom, T. R. Witte, B. A. Thornhill, C. M. Crabtree, H. E. Perry, J. M. Brown, J. G. Ball and R. G. Creel (2014). "Capsaicin induces apoptosis in human small cell lung cancer via the TRPV6 receptor and the calpain pathway." Apoptosis **19**(8): 1190-1201.

Le Marchand, L. c., S. P. Murphy, J. H. Hankin, L. R. Wilkens and L. N. Kolonel (2000). "Intake of flavonoids and lung cancer." Journal of the National Cancer Institute **92**(2): 154-160.
Lee, Y., S. Lee and S. Jon (2018). "Biotinylated Bilirubin Nanoparticles as a Tumor Microenvironment-Responsive Drug Delivery System for Targeted Cancer Therapy." Advanced Science: 1800017.
Lv, L., Y.-x. Zhuang, H.-w. Zhang, N.-n. Tian, W.-z. Dang and S.-y. Wu (2017). "Capsaicin-loaded folic acid-conjugated lipid nanoparticles for enhanced therapeutic efficacy in ovarian cancers." Biomedicine & Pharmacotherapy **91**: 999-1005.
Makadia, H. K. and S. J. Siegel (2011). "Poly lactic-co-glycolic acid (PLGA) as biodegradable controlled drug delivery carrier." Polymers **3**(3): 1377-1397.
Martin, C. R. (2006). "Welcome to nanomedicine."
Mathew, R., S. Kongara, B. Beaudoin, C. M. Karp, K. Bray, K. Degenhardt, G. Chen, S. Jin and E. White (2007). "Autophagy suppresses tumor progression by limiting chromosomal instability." Genes & development **21**(11): 1367-1381.
Mattheolabakis, G., L. Milane, A. Singh and M. M. Amiji (2015). "Hyaluronic acid targeting of CD44 for cancer therapy: from receptor biology to nanomedicine." Journal of drug targeting **23**(7-8): 605-618.
Ming, H., L. Fang, J. Gao, C. Li, Y. Ji, Y. Shen, Y. Hu, N. Li, J. Chang and W. Li (2017). "Antitumor Effect of Nanoparticle 131I-Labeled Arginine-Glycine-Aspartate–Bovine Serum Albumin–Polycaprolactone in Lung Cancer." American Journal of Roentgenology **208**(5): 1116-1126.
Mir, I. A. and A. B. Tiku (2015). "Chemopreventive and therapeutic potential of “naringenin,” a flavanone present in citrus fruits." Nutrition and cancer **67**(1): 27-42.
Mok, T. S., Y.-L. Wu, M.-J. Ahn, M. C. Garassino, H. R. Kim, S. S. Ramalingam, F. A. Shepherd, Y. He, H. Akamatsu and W. S. Theelen (2017). "Osimertinib or platinum–pemetrexed in EGFR T790M–positive lung cancer." New England Journal of Medicine **376**(7): 629-640.
Morrissey, S. (2006). "Nanotechnology in food and agriculture." Chem Eng News **84**: 31-31.
Mottaghitalab, F., M. Kiani, M. Farokhi, S. C. Kundu, R. L. Reis, M. Gholami, H. Bardania, R. Dinarvand, P. Geramifar and D. Beiki (2017). "Targeted Delivery System Based on Gemcitabine-Loaded Silk Fibroin Nanoparticles for Lung Cancer Therapy." ACS applied materials & interfaces **9**(37): 31600-31611.
Mu, L. and S.-S. Feng (2002). "Vitamin E TPGS used as emulsifier in the solvent evaporation/extraction technique for fabrication of polymeric nanospheres for controlled release of paclitaxel (Taxol®)." Journal of Controlled Release **80**(1-3): 129-144.
Nasir, A., A. Kausar and A. Younus (2015). "A review on preparation, properties and applications of polymeric nanoparticle-based materials." Polymer-Plastics Technology and Engineering **54**(4): 325-341.
Ni, X. L., L. X. Chen, H. Zhang, B. Yang, S. Xu, M. Wu, J. Liu, L. L. Yang, Y. Chen and S. Z. Fu (2017). "In vitro and in vivo antitumor effect of gefitinib nanoparticles on human lung cancer." Drug delivery **24**(1): 1501-1512.
Oerlemans, C., W. Bult, M. Bos, G. Storm, J. F. W. Nijsen and W. E. Hennink (2010). "Polymeric micelles in anticancer therapy: targeting, imaging and triggered release." Pharmaceutical research **27**(12): 2569-2589.
Peer, D., J. M. Karp, S. Hong, O. C. Farokhzad, R. Margalit and R. Langer (2007). "Nanocarriers as an emerging platform for cancer therapy." Nature nanotechnology **2**(12): 751.
Peng, X.-H., Y. Wang, D. Huang, Y. Wang, H. J. Shin, Z. Chen, M. B. Spewak, H. Mao, X. Wang and Y. Wang (2011). "Targeted delivery of cisplatin to lung cancer using ScFvEGFR-heparin-cisplatin nanoparticles." Acs Nano **5**(12): 9480-9493.
Perrault, S. D., C. Walkey, T. Jennings, H. C. Fischer and W. C. Chan (2009). "Mediating tumor targeting efficiency of nanoparticles through design." Nano letters **9**(5): 1909-1915.

Pirker, R. (2013). "EGFR-directed monoclonal antibodies in non-small cell lung cancer." Targeted oncology **8**(1): 47-53.
Qi, S.-S., J.-H. Sun, H.-H. Yu and S.-Q. Yu (2017). "Co-delivery nanoparticles of anti-cancer drugs for improving chemotherapy efficacy." Drug delivery **24**(1): 1909-1926.
Rao, J. P. and K. E. Geckeler (2011). "Polymer nanoparticles: preparation techniques and size-control parameters." Progress in polymer science **36**(7): 887-913.
Reis, C. P., R. J. Neufeld and F. Veiga (2017). Preparation of Drug-Loaded Polymeric Nanoparticles. Nanomedicine in Cancer, Pan Stanford**:** 197-240.
Ren, W. X., J. Han, S. Uhm, Y. J. Jang, C. Kang, J.-H. Kim and J. S. Kim (2015). "Recent development of biotin conjugation in biological imaging, sensing, and target delivery." Chemical Communications **51**(52): 10403-10418.
Schrier, J. A. and P. P. DeLuca (1999). "Recombinant human bone morphogenetic protein-2 binding and incorporation in PLGA microsphere delivery systems." Pharmaceutical development and technology **4**(4): 611-621.
Scott, A. M., J. D. Wolchok and L. J. Old (2012). "Antibody therapy of cancer." Nature Reviews Cancer **12**(4): 278.
Shaw, A. T., D.-W. Kim, K. Nakagawa, T. Seto, L. Crinó, M.-J. Ahn, T. De Pas, B. Besse, B. J. Solomon and F. Blackhall (2013). "Crizotinib versus chemotherapy in advanced ALK-positive lung cancer." New England Journal of Medicine **368**(25): 2385-2394.
Shi, J., P. W. Kantoff, R. Wooster and O. C. Farokhzad (2017). "Cancer nanomedicine: progress, challenges and opportunities." Nature Reviews Cancer **17**(1): 20.
Shtivelman, E., T. Hensing, G. R. Simon, P. A. Dennis, G. A. Otterson, R. Bueno and R. Salgia (2014). "Molecular pathways and therapeutic targets in lung cancer." Oncotarget **5**(6): 1392.
Silvestri, G. A. and M. P. Rivera (2005). "Targeted therapy for the treatment of advanced non-small cell lung cancer: a review of the epidermal growth factor receptor antagonists." Chest **128**(6): 3975-3984.
Soppimath, K. S., T. M. Aminabhavi, A. R. Kulkarni and W. E. Rudzinski (2001). "Biodegradable polymeric nanoparticles as drug delivery devices." Journal of controlled release **70**(1-2): 1-20.
Stewart, B. and C. P. Wild (2017). "World cancer report 2014." Health.
Tanner, N. T., A. Porter, M. K. Gould, X.-J. Li, A. Vachani and G. A. Silvestri (2017). "Physician assessment of pretest probability of malignancy and adherence with guidelines for pulmonary nodule evaluation." Chest **152**(2): 263-270.
Tian, J., Y. Min, Z. Rodgers, K. M. Au, C. T. Hagan, M. Zhang, K. Roche, F. Yang, K. Wagner and A. Z. Wang (2017). "Co-delivery of paclitaxel and cisplatin with biocompatible PLGA–PEG nanoparticles enhances chemoradiotherapy in non-small cell lung cancer models." Journal of Materials Chemistry B **5**(30): 6049-6057.
Torchilin, V. P. (2000). "Drug targeting." Eur J Pharm Sci **11**(2): S81-91.
Vauthier, C. and K. Bouchemal (2009). "Methods for the preparation and manufacture of polymeric nanoparticles." Pharmaceutical research **26**(5): 1025-1058.
Wakaskar, R. R. (2017). "Passive and active targeting in tumor microenvironment." International Journal of Drug Development and Research **9**(2).
Wang, A. Z., R. Langer and O. C. Farokhzad (2012). "Nanoparticle delivery of cancer drugs." Annual review of medicine **63**: 185-198.
Wang, F., Y. Wang, Q. Ma, Y. Cao and B. Yu (2017). "Development and characterization of folic acid-conjugated chitosan nanoparticles for targeted and controlled delivery of gemcitabinein lung cancer therapeutics." Artificial cells, nanomedicine, and biotechnology **45**(8): 1530-1538.
Wickens, J. M., H. O. Alsaab, P. Kesharwani, K. Bhise, M. C. I. M. Amin, R. K. Tekade, U. Gupta and A. K. Iyer (2017). "Recent advances in hyaluronic acid-decorated nanocarriers for targeted cancer therapy." Drug discovery today **22**(4): 665-680.
Yau, T., X. Dan, C. C. W. Ng and T. B. Ng (2015). "Lectins with potential for anti-cancer therapy." Molecules **20**(3): 3791-3810.

Zappa, C. and S. A. Mousa (2016). "Non-small cell lung cancer: current treatment and future advances." Translational lung cancer research **5**(3): 288.
Zhang, L., F. Gu, J. Chan, A. Wang, R. Langer and O. Farokhzad (2008). "Nanoparticles in medicine: therapeutic applications and developments." Clinical pharmacology & therapeutics **83**(5): 761-769.
Zhang, M., Y.-K. Kim, P. Cui, J. Zhang, J. Qiao, Y. He, J. Lyu, C. Luo, L. Xing and H. Jiang (2016). "Folate-conjugated polyspermine for lung cancer–targeted gene therapy." Acta Pharmaceutica Sinica B **6**(4): 336-343.
Zhang, Y., Q. Zhang, J. Sun, H. Liu and Q. Li (2017). "The combination therapy of salinomycin and gefitinib using poly (D, L-lactic-co-glycolic acid)-poly (ethylene glycol) nanoparticles for targeting both lung cancer stem cells and cancer cells." OncoTargets and therapy **10**: 5653.
Zhao, L., G. Yang, Y. Shi, C. Su and J. Chang (2015). "Co-delivery of Gefitinib and chloroquine by chitosan nanoparticles for overcoming the drug acquired resistance." Journal of nanobiotechnology **13**(1): 57.
Zhou, G., G. Wilson, L. Hebbard, W. Duan, C. Liddle, J. George and L. Qiao (2016). "Aptamers: A promising chemical antibody for cancer therapy." Oncotarget **7**(12): 13446.
Zhou, Z., M. Jafari, V. Sriram, J. Kim, J.-Y. Lee, S. J. Ruiz-Torres and S. E. Waltz (2017). "Delayed Sequential Co-Delivery of Gefitinib and Doxorubicin for Targeted Combination Chemotherapy." Molecular pharmaceutics **14**(12): 4551-4559.
Zwicke, G. L., G. Ali Mansoori and C. J. Jeffery (2012). "Utilizing the folate receptor for active targeting of cancer nanotherapeutics." Nano reviews **3**(1): 18496.

Research Envisaged

1.9. Research Envisaged

In the current scenario a paradigm shift in nanotechnology-based targeted drug delivery has been made in cancer therapy. Nanotechnology has emerged as one of the paramount technique that covers challenges related to safety, efficacy, delivery and stability of antineoplastic agents and hence it has gained a vital role in cancer therapy. Broadly two targeting mechanisms, comprising passive targeting to achieveenhanced permeation and retention (EPR) effect through nanosize particles and ligand mediated active targeting have been employed extensively in rationale design of targeted delivery systems.

The present study envisages formulation and assessment of a targeted polymeric nano-particulate system for delivery of anticancer drug(s). Also, the feasibility of a cotherapy through combination of naturally existing phytoconstituent and synthetic antineoplastic agents has been exploredto investigate its potential to overcome drug resistance as well as for its synergistic effects in cancer therapy. Such a combination may enhance the chemotherapeutic efficacy of the system as two drugs may act through different mechanism and pathways. Thus in order to target multiple growth-promoting pathways, combination therapies using different anticarcinogenic agents has been investigated.

Also, most of the xenobiotic agents suffer a major challenge of being expelled out from the cells due to efflux pumps present in prokaryotes and eukaryotes leading to multidrug resistance (MDR). These efflux pumps facilitate the efflux of intracellular toxic elements including drugs out of the cell. Thus phytoconstituents are also expelled out of the cells; hence fails to attain desirable therapeutic concentrations in the cells subsequently leading to resistance. Formulating them as surface modified receptor specific nanoformulations can lead to higher internalization of phytoconstituent into the targeted cells as a result of better interaction and rapid uptake by overexpressed factors due to the presence of targeting moieties.

Utilizing this approach in cancer therapy may be beneficial in improving therapeutic efficacy of selected drug candidate(s), avoiding systemic toxicity, effective dose reduction, enhanced circulation, improving stability against enzymatic and GIT fluid degradation, safety and improving patient compliance and many more. The advanced experimental and computational methodologies will be supportive in formulation development forsubsequent scale-up and clinical use from bench to bedside.

1.9.1. Objectives of the researchwork

The objective of present study is to develop and evaluate targeted polymeric nanoparticles for site specific delivery of anticancer drug(s) utilizing synergistic approach. The targeted drug nanocarriers should be competent to specially deliver chemotherapeutic(s) to the

preferred site utilizing some guiding modules thereby delivering drug payload in the tumor, while constraining the drug delivery to the normal cells. Further, co-therapy through combination of drug as separate nanoparticle may potentiate the therapeuticefficacy, reduce dose and also provide an antioxidant shield to the normal cells through phytomedicinal agent thereby lowering drug related side effects as well as preventing MDR.

The specific objectives were:

1) To develop hyaluronic acid functionalized PCL nanoparticles for site specific drug delivery and its assessment for therapeutic efficacy and targeting potential over A549 cell lines and urethane-induced cancer model in rats.
2) To develop folic acid functionalized PLGA nanoparticles for targeted drug delivery and its assessment for synergy, therapeutic efficacy and targeting potential over A549 cell lines and urethane-induced cancer model in rats.
3) To develop biotin functionalized PCL nanoparticles for targeted drug delivery and its assessment for synergy, therapeutic efficacy and targeting potential over A549 cell lines and urethane-induced cancer model in rats.

1.9.2. Hypothesis

It was hypothesized that the outcome of current study would be development of effective, stable and safe polymeric nanoparticles of Gefitinib in combination with Capsaicin/Naringenin for cancer therapy. Since the cancer cells undergo rapid growth, proliferation they require excessive amount of nutrients including vitamins and minerals. Subsequently, the receptors involved in uptake of the vitamins are overexpressed on the surface of cancer cells. When a surface modified nanoparticle approaches, these overexpressed receptors rapidly internalize it and the drug is directly delivered to these cells. Accordingly, it was thought worthwhile to designate such overexpressed agents (folic acid, biotin, oligopeptides etc.) as a tumor targeting molecule for delivery of chemotherapeutic agents. Entrapping chemotherapeutic agents in nanoparticles is a strategy to protect the agent from RES uptake during its circulation in the blood stream and may serve the dual purpose of targeting cancer cells while protecting normal nontargeted tissues from toxicity. Also, the approach of combination therapywould potentiate the therapeutic efficacy of gefitinib in comparison to individual therapy through gefitinib alone. The co-therapy resulting in synergistic approachmay facilitate the cancer management therapy with greater safety and efficacy.

Plan of Work

1. Literature Survey & Procurement of Materials
2. Preformulation study
    - Identification and characterization of Drug
    - Selection of analytical method
3. Selection of excipients
4. Preparation of nanocarriers system
    - Pharmaceutical considerations
    - Physiological considerations
    - Pharmacological considerations
    - Optimization of drug delivery systems
5. *In vitro* Characterization of nanocarriers
    - Entrapment efficiency
    - Drug content and drug loading
    - In vitro release studies
    - Zeta potential and size distribution studies
    - Surface morphology (TEM)
    - Surface modification of nanocarriers and its characterization
6. Cell lines study (A549 lung cancer cell lines)
    - MTT assay
    - Cell Cycle Analysis
    - Cell proliferation study
    - Reactive Oxygen Species estimation
    - Mitochondrial membrane potential
    - Cellular uptake study
    - Cellular internalization
    - Apoptosis
7. Stability Studies
8. *In vivo* Studies
    - Tumor volume
    - Animal weight
    - Animal survival
    - Biochemical Estimation
    - Histopathological evaluations
    - Western blotting

- Biodistribution
- Metabolomics

9. Statistical analysis
10. Computation and Compilation of work

Chapter II

Drug Profile & Preformulation Studies

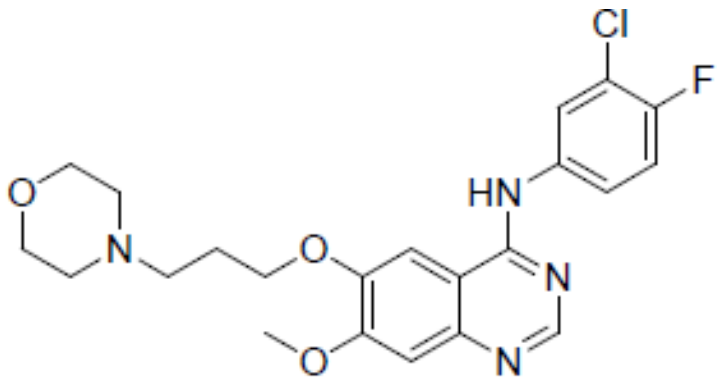

2. Drug profile and Pre-formulation studies

The drug selected for the present study was Gefitinib. It is classified as a signal transduction inhibitor EGFR (epidermal growth factor receptor) tyrosine kinase inhibitor. Gefitinib is used for the treatment of advanced and metastatic non-small cell lung cancer. Gefitinib is one of the most widely used anticancer drugs worldwide.

2.1 The drug Gefitinib (Gnb)

It is an antineoplastic agent which is chemically designated as N-(3-chloro-4-fluoro-phenyl)-7-methoxy-6-(3-morpholin-4-ylpropoxy) quinazolin-4-amine

2.1.1 Chemical structure

The structural formula of Gnb is

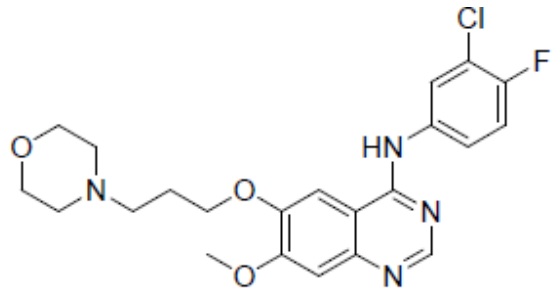

N-(3-chloro-4-fluoro-phenyl)-7-methoxy-6-(3-morpholin-4-ylpropoxy) quinazolin-4-amine

2.1.2 Molecular formula: $C_{22}H_{24}ClFN_4O_3$

2.1.3 Molecular weight: 446.902 g/mol

2.1.4 Category: Antineoplastic, anticancer, protein kinase inhibitor

2.1.5 Chemistry and Structure: Gnb is a tyrosine kinase inhibitor. It consists of the quinazoline moiety linked to N-(3-chloro-4-fluoro-phenyl)-7-methoxy-6-(3-morpholin-4-ylpropoxy) and amine group at 4^{th} position.

2.1.6 Mechanism of action: Gnb inhibits tyrosine kinases receptor, epidermal growth factor receptor (EGRF)-TK. Gnb competitively blocks the binding of adenosine triphosphate to its binding site in the tyrosine kinase domain of EGFR, thereby inhibiting autophosphorylation

and blocking downstream signalling. Gefitinib also inhibits ATP-binding cassette transporter-mediated drug efflux, which in turn strongly increases the intracellular concentrations of co-administrated drug molecules that are transporter substrates. After oral administration, Gefitinib is widely distributed throughout the body. Gefitinib is metabolized in the liver by cytochromes (Cataldo et al. 2011).

2.1.7 Pharmacokinetics

2.1.8 Absorption & Distribution: Half-life for distribution of gefitinib is 48 hours. Volume of distribution is found to be 1400 L indicating extensive distribution into tissue.

2.1.9 Metabolism & Excretion: Gefitinib undergoes oxidative metabolism through CYP3A4, a major P450 isozyme. N-propylmorpholino group, demethylation of the methoxy substituent on the quinazoline and oxidative defluorination of the halogenated phenyl group are the three sites of biotransformation. The foremost metabolite recognized in human plasma is O-desmethyl gefitinib. It has 14-fold less potential than the parent drug gefitinib for inhibiting EGFR, thus its contribution to therapeutic outcome is insignificant. Gefitinib has a total plasma clearance of 500 mL/min approximately, and is excreted mainly through the faeces.

2.1.10 Protein binding: 90%

2.1.11 Physicochemical properties: According to official monographs (IP 2014) it is a white colored crystalline powder, with a poor aqueous solubility of 0.027 mg/mL; freely soluble in glacial acetic acid and pyridine; moderately soluble in ethanol, methanol.

2.1.12 Sotrage: It should be stored in well-closed containers, between 20°C-25°C .

2.1.13 Adverse Effects:

Some of the adverse effects associated with Gnb is thrombocytopenia, peripheral edema, diarrhoea, and vomiting, dry skin (incidence rate 1-6%). The most severe adverse effects include hepatic malfunction, interstitial lung disease, weight loss, ocular disorders comprising keratitis and hyperbilirubinemia. Gnb can cause fetal harm when administered during pregnancy.

2.2 Identification of drug

2.2.1 Percentage purity Percentage purity assay was done according to Indian pharmacopoeia 2014 (Pharmacopoeia 2014).

2.2.2 Physical Appearance

Drug was a white coloured crystalline powder.

2.2.3 Melting point

Melting point of Gnb was assessed through melting point apparatus. The drug sample was filled in three separate capillaries and melting temperature range was recorded. The melting range was found to be 119-120°C.

2.2.4 Fourier transforms infrared spectrum (FTIR)

FTIR analysis of Gnb was performed to check the purity of the drug. The FTIR scanning was done in a range from 4000 to 500 cm-1 using Nicolet 6700, Thermoscientific, spectrophotometer. The principal peaks were displayed at 3400 cm^{-1} (N-H), 2956 cm^{-1} (CH_2, C-H ;alkyl), 2808 cm^{-1}, 1625 cm^{-1}(C=C, C=N), 1578 cm^{-1}, 1532 cm^{-1}, 1500 cm^{-1} (HC=CH; aryl), 1472 cm^{-1}, 1429 cm^{-1}, 1398 cm^{-1}, 1227 cm^{-1}, 1219 cm^{-1}, 1110 cm^{-1} (C-O), 1028 cm^{-1} (C-F), 847 cm^{-1}, and 542 cm^{-1} respectively (**Figure 2.1**).

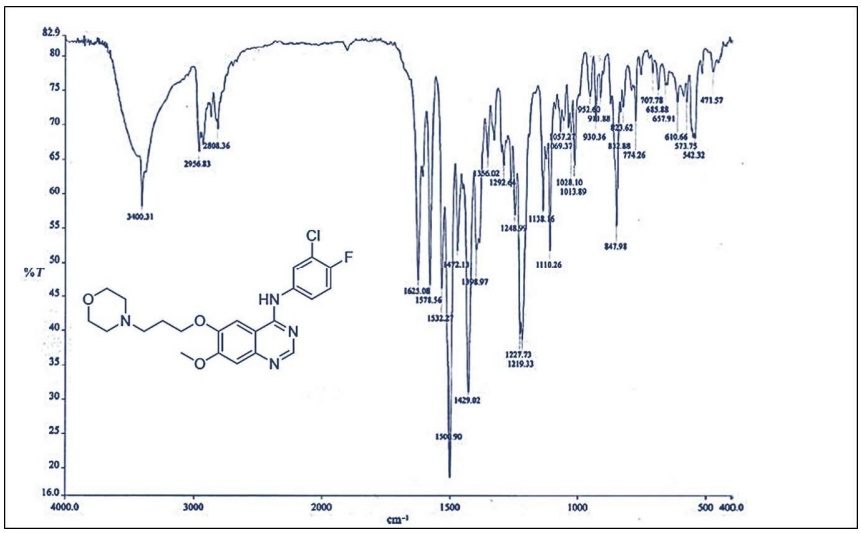

Figure. 2.1 FTIR spectrum of gefitinib

2.3. The drug Capsaicin (Cap)

Capsaicin is derived from a plant of the genus *capsicum annum* which belongs to the family Solanaceae. It is a homovanillic acid derivative and the major spicy constituent in chilli peppers. It is an alkaloid extracted from chilli pepper that has been recognised as analgesic, antioxidant, anti-inflammatory, anti-obesity agent, anticancer and anti-proliferative.

2.3.1. Chemical structure

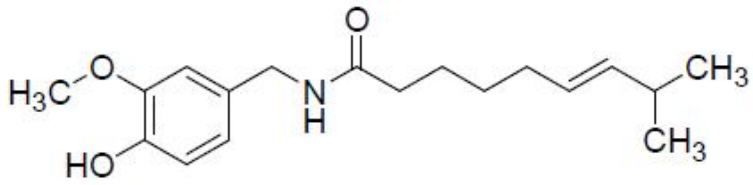

Trans -8-methyl-n-vanillyl-6-nonenamide

2.3.2 Molecular formula: $C_{18}H_{27}NO_3$

2.3.3 Molecular weight: 305.42 g/mol

2.3.4 Category: Antineoplastic, anticancer, analgesic, antiproliferative.

2.3.5 Chemistry and Structure: It is a trans-8methyl-N-vanillyl-6-nonenamide) homovanillic acid derivative having a benzene ring, a long hydrophobic carbon tail with a polar amide group.

2.3.6 Mechanism of action: Anticancer mechanism of Cap is by suppression of MMP-2 and MMP-9 expression thereby preventing the migration of carcinoma cells. Another underlying mechanism for apoptosis, is the property of Cap to produce heat-sensation over cancer cells, mediated by the transient receptor potential vanilloid 1 (TRPV1) receptor(Reyes-Escogido et al. 2011, Hong et al. 2015, Zhang et al. 2017).

2.3.7 Pharmacokinetics

2.3.8 Absorption & Distribution: Half-life for distribution of capsaicin is 1.64 hours. Volume of distribution is found to be 807.95 L.

2.3.9 Metabolism & Excretion: Cap majorly gets metabolised in the liver, generating three major metabolites, 16,17-hydroxycapsaicin, 17-hydroxycapsaicin, and 16-hydroxycapsaicin. It is expected that cytochrome P450 (P450) enzyme plays a vital role in hepatic drug metabolism of Cap. Cap mainly undergoes renal excretion, in its unchanged form as well as in the glucuronide form.

2.3.10 physicochemical properties: It is a hydrophobic, colorless, odorless, crystalline powder. It is practically insoluble in water, freely soluble in alcohols, benzene, chloroform and dimethyl sulpoxide.

2.3.11 Sotrage: It should be stored in well-closed containers at room temperature.

2.3.12 Adverse Effects:

Cap causes burning sensation over skin and mucous layers. It has a characteristic strong pungent odor and taste, detectable in 1 part in 100,000.

2.4 Identification of drug

2.4.1 Percentage purity

Percentage purity assay was performed in order to assess purity of phytoconstituents.

2.4.2 Physical Appearance

Drug is a colorless and crystalline powder.

2.4.3 Melting point

Melting point of Cap was assessed through melting point apparatus. The drug sample was filled in three separate capillaries and melting temperature range was recorded. The melting range was found to be 63-65°C.

2.4.4 Fourier transforms infrared spectrum (FTIR)

FTIR analysis of Cap was performed to check the purity of the drug. The FTIR scanning was done in a range from 4000 to 500 cm-1 using Nicolet 6700, Thermoscientific, spectrophotometer. The principal peaks were displayed at 3314cm^{-1} (N-H stretch), 2862cm^{-1} (C=O), 1629cm^{-1} (C-C) and 1556 cm^{-1} (C-H) respectively (**Figure 2.2**).

.

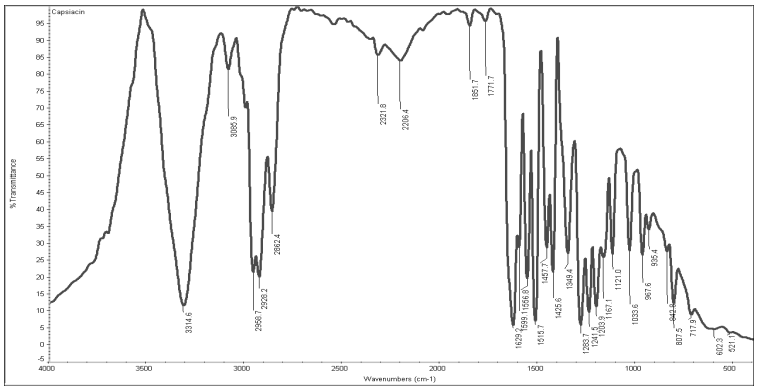

Figure 2.2 FTIR spectrum of capsaicin

2.5 The drug Naringenin (Nar)

NAR is a flavanone (5,7,4-trihydroxyflavanone or 5,7-dihydroxy-2-(4-hydroxyphenyl)chroman-4-one) found especially in citrus fruits, and grapefruit. Nar has been reported to possess anticancer, antimutagenic, anti-inflammatory, antiatherogenic, antifibrogenic and free radical scavenging properties (Jin et al. 2009, Benevenuto et al. 2015).

2.5.1 Chemical structure

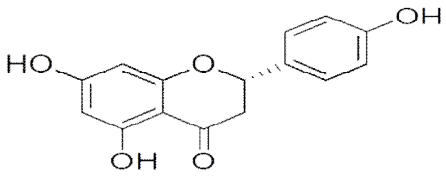

5,7,4-trihydroxyflavanone or 5,7-dihydroxy-2-(4-hydroxyphenyl)chroman-4-one

2.5.2 Molecular formula: $C_{15}H_{12}O_5$

2.5.3 Molecular weight: 272.26 g/mol

2.5.4 Category: Antidiabetic, Anti-inflammatory, Antioxidant, Anticancer

2.5.5 Chemistry and Structure: Chemically **i**t is 5,7-dihydroxy-2-(4-hydroxyphenyl)-2,3-dihydro-4H-chromen-4-one.

2.5.6 Mechanism of action: NAR inhibits both cell proliferation and motility by interfering with the phosphoinositide 3-kinase (PI3K) and Mitogen-activated protein kinase MAPK pathways which results in cell growth inhibition and upregulation of autophagic protein followed by autophagy-mediated cell death (Lee et al. 2007, Chang et al. 2017).

2.5.7 Pharmacokinetics

2.5.8 Absorption & Distribution: The half-life of Nar is 2.3 hours. Nar is widely distributed in the body including highest concentration in liver and lower concentration in organs like stomach, small intestine, kidney, lung, heart, spleen. Its volume of distribution is 1.6 L and serum clearance of $0.16/mim^{-1}$.

2.5.9 Metabolism: Nar predominantly gets metabolised in the liver, generating glucuronide intermediates. **Nar** mainly undergoes renal excretion. It was reported that approximately 8.5-8.8% of administered dose is excreted through urine.

2.5.10 Physicochemical properties: It is a hydrophobic, colorless, odorless, crystalline powder. It is practically insoluble in water, while completely soluble in organic solvents such as alcohol, DMSO, ethyl acetate, methanol, isopropanol, n-butanol, petroleum ether and hexane.

2.5.11 Storage: It should be stored in a well-closed container at room temperature.

2.5.12 Identification of drug

2.5.12.1 Percentage purity

Percentage purity assay was done to assess the purity of phytoconstituents.

2. 5.12.2 Physical Appearance

Drug sample is colorless powder having bitter taste.

2. 5.12.3 Melting point

Melting point of Nar was assessed through melting point apparatus. The drug sample was filled in three separate capillaries and melting temperature range was recorded. The melting range was found to be 249-250°C.

2.5.13 Fourier transforms infrared spectrum (FTIR)

FTIR analysis of Nar was performed to check the purity of the drug. The FTIR scanning was done in a range from 4000 to 500 cm-1 using Nicolet 6700, Thermoscientific, spectrophotometer. The major peaks were displayed at 3284.0cm^{-1} (-C-OH stretch), 835.1cm^{-1} for (-C-OH Bending), 2919.1, cm^{-1} (-C-H stretching) and 1634.2 cm^{-1} (-C=O) respectively (**Figure 2.3**).

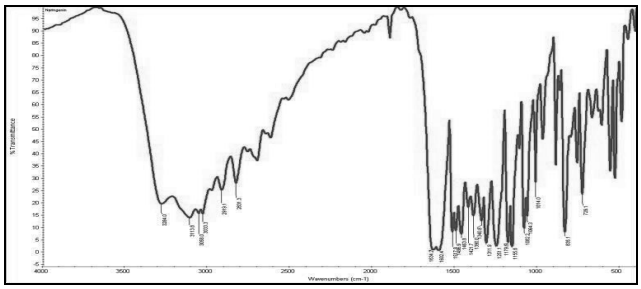

Figure 2.3 FTIR spectrum of naringenin

2.6 Development of UV-spectrophotometric method

2.6.1 Development of calibration plot of Gnb, cap and Nar through UV-spectrophotometer

Standard plots (n=3) for API Gnb, phytoconstituents Cap and Nar were constructed each in methanol to evaluate concentration of drug(s) in various *in vitro* studies. A stock solution of the drug (100µg/ml each) was prepared in methanol. The scanning of the drug(s) was performed in range of 200 to 400 nm on UV/VIS spectrophotometer for wavelength of maximum absorption (each drug separately). The absorption maxima (λ_{max}) of Gnb, Cap and Nar were recorded as 338, 279 and 285nm respectively (**Figure 2.4 a-c**). The obtained data was further analysed for regression and regression equation along with r^2 values were derived for further use **(Figure 2.5, 2.6&2.7)**. All the readings were taken in methanol.

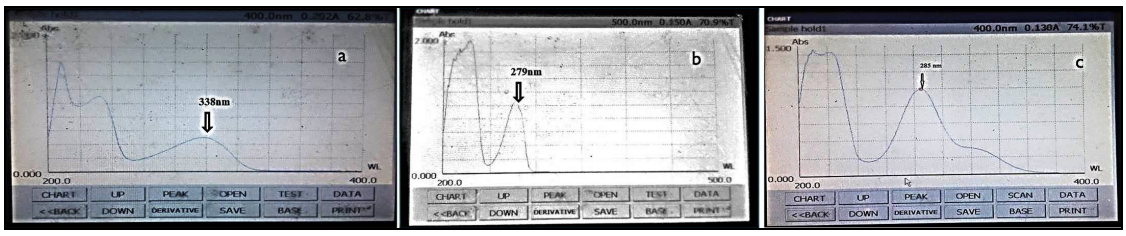

Figure 2.4 UV spectra of a) Gnb b) Cap c) Nar in methanol

Table 2.1 Concentration and average absorbance of gefitinib in methanol

S. No.	Concentration (µg/ml)	Absorbance (mean±SD)
1.	0	0.000±0.000
2.	2	0.0187±0.003
3.	4	0.279±0.004
4.	6	0.432±0.008
5.	8	0.625±0.012
6.	10	0.769±0.005
7.	12	0.878±0.009

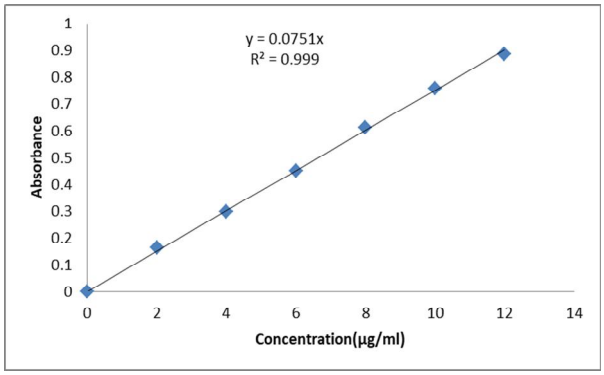

Figure 2.5 Standard curve of Gnb in methanol

The UV-Vis spectrophotometer method employed for Gnb analysis displayed linearity in the concentration ranges of 1.0-12 µg/mL in methanol with r^2 = 0.9990 respectively (n=6).

Table 2.2 Concentration and average absorbance of Cap in methanol

S. No.	Concentration (µg/ml)	Absorbance (mean±SD)
1.	0	0.000±0.000
2.	10	0.046±0.001
3.	20	0.093±0.003
4.	30	0.145±0.005
5.	40	0.192±0.09
6.	50	0.241±0.010

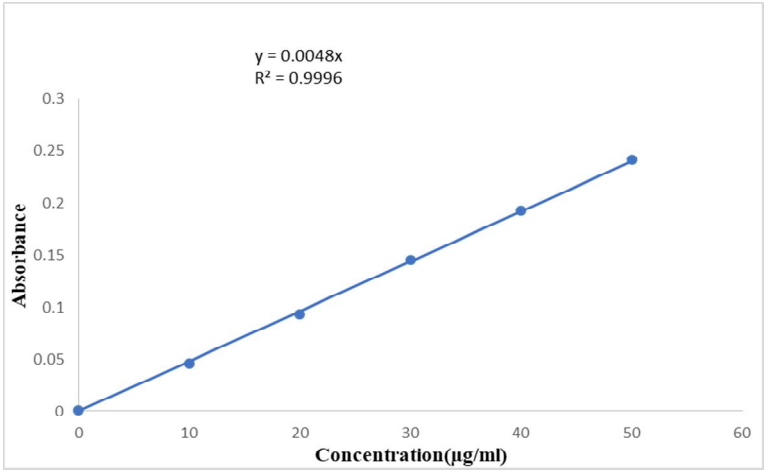

Figure 2.6 Standard curve of Cap in methanol

The UV-Vis spectrophotometer method employed for Cap analysis displayed linearity in the concentration ranges of 10-50 µg/mL in methanol with r^2 = 0.9996 respectively (n=5).

Table 2.3 Concentration and average absorbance of Nar in methanol

S. No.	Concentration (µg/ml)	Absorbance (mean±SD)
1.	0	0.000±0.000
2.	1	0.102±0.003
3.	2	0.226±0.004
4.	4	0.424±0.013
5.	6	0.618±0.014
6.	8	0.822±0.09
7.	10	0.999±0.010

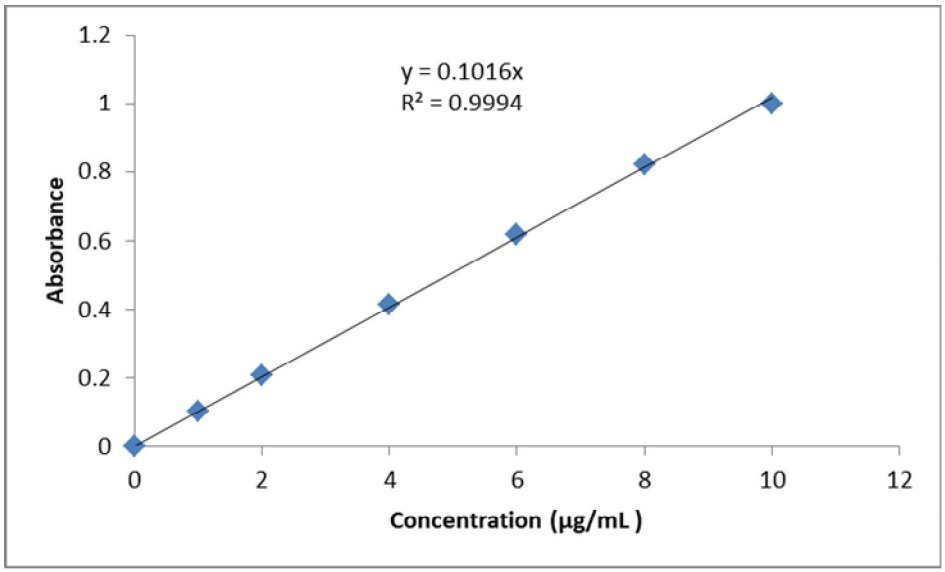

Figure 2.7 Standard curve of Nar in methanol

The UV-Vis spectrophotometer method employed for Nar analysis displayed linearity in the concentration ranges of 1-10 µg/mL in methanol with r^2 = 0.9994 respectively (n=6).

2.6.3. Standard curve of Gnb in plasma

Calibration curve of Gnb was prepared in plasma using HPLC method, with slight modification (Pandey et al. 2014). A 50 µl volume of methanol containing known concentration of Gnb (0.05-1 µg/ml) was added to the plasma (50 µl) followed by vortexing for few seconds to assure proper mixing. The resultant mixture was centrifuged for 15min at 15,000 rpm (Spinwin MC-01, Tarsons), and the supernatant was collected into tubes and kept for drying at 40°C for 8 h for to obtain residue. The residue obtained after evaporation was dissolved in 0.5 ml of mobile phase and centrifuged for 15 min at 10,000 rpm. The samples were filtered through 0.22 µm membrane filter and 20 µL was injected in the HPLC system. For test samples, 100 µL of test plasma and 100 µL blank acetonitrile were taken and processed similarly through previously mentioned method.

HPLC system, (Waters 2489, Milford, Massachusetts, USA with UV-Visible Detector), was equipped with Spherowsorb C18, 3.5 µm, 4.6×250 mm column at flow rate 1.0 mL/min. The mobile phase comprised of methanol and 0.1 M potassium dihydrogen phosphate in a ratio

of 40:60 (v/v) and a flow rate of 1.0 mL/min with runtime 20 min. Detection was done at 254nm.The calibration curve was prepared by plotting peak area ratio verses Gnb concentration in plasma (**Figure 2.8**).

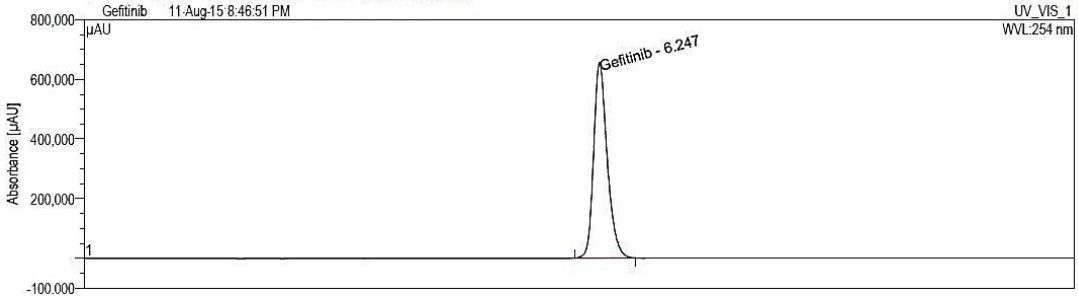

Figure 2.8 HPLC chromatogram of Gnb

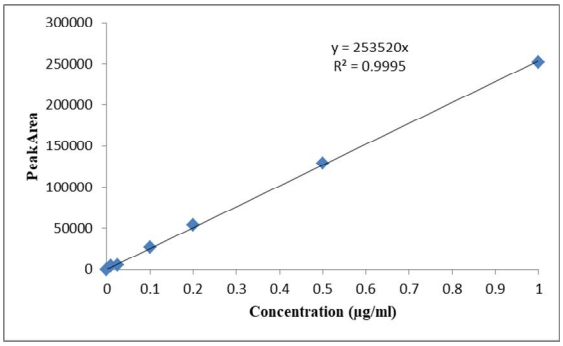

Figure 2.9 Standard curve of Gnb in plasma

Table 2.4 Calibration curve of Gnb in plasma

S. No.	Conc. (µg/ml)	Average AUC (mean±SD)
1.	0.01	4729
2.	0.025	5305
3.	0.1	29081
4.	0.2	54924
5.	0.5	128577
6.	1	241776

The HPLC method performed for Gnb analysis in plasma showed linearity in the concentration ranges of 0.01-1.0 µg/mL in rat plasma with R2 value of = 0.9995 as shown in Figure 2.9.

2.6.3.2 Standard curve of Cap in plasma

The calibration curve of cap was prepared in plasma using HPLC method as described above for Gnb, with slight modification (Othman et al. 2011). The Cap concentration was measured through the validated HPLC method (Waters 2489, Milford, Massachusetts, USA). The system was equipped with Spherisorb C18, 3.5 µm, 4.6×250 mm column at flow rate 1.5 mL/min. The mobile phase comprised of water-acetonitrile in 50:50 ratios and a flow rate of 1.5 mL/min with runtime 15 min and detection was done at 222nm. The calibration curve was prepared by plotting peak area ratio verses Cap concentration in plasma (**Figure** 2.10).

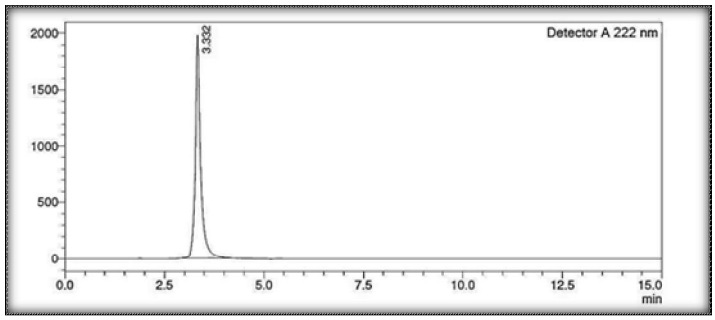

Figure 2.10 HPLC chromatogram of Cap

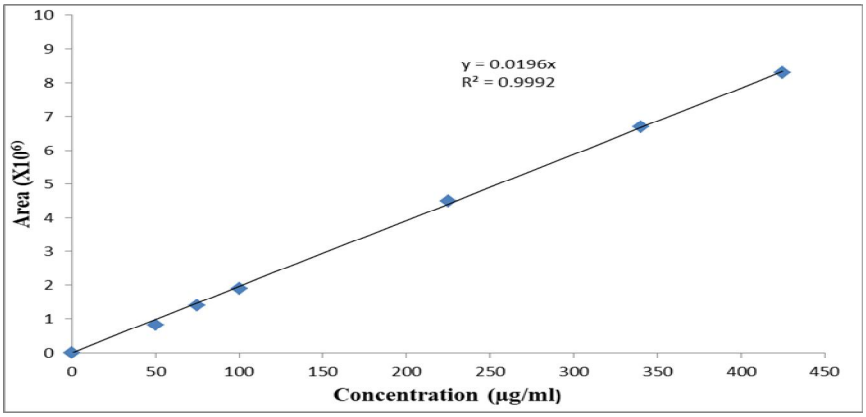

Figure 2.11 Standard curve of Cap in plasma

2.7 Excipient Profiles

2.7.1 Poly(lactic-co-glycolic acid) (PLGA)

PLGA [poly(lactic-co-glycolic acid)] is a synthetic copolymer, biodegradable and biocompatible in nature and is approved by Food and Drug Administration (FDA) for therapeutic use. PLGA is synthesized by direct polycondensation of lactic acid and glycolic acid (Avgoustakis 2008). It is a crystalline solid colorless to white in colour.

2.7.1.1 Structure

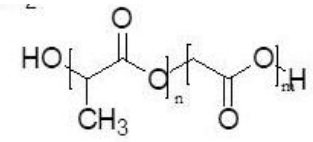

PLGA

2.7.1.2 Molecular formula and molecular weight: $C_5H_{10}O_6$, 30,000-60,000.

2.7.1.3 Solubility: PLGA is freely soluble in acetone, tetrahydrofuran, ethyl acetate and chlorinated solvents. PLGA is poorly soluble in water and degrades in the presence of water by hydrolysis of its ester linkages.

2.7.2 Poly E-caprolactone (PCL)

PCL (Poly E-caprolactone) is a biodegradable polymer and is commercially used as a carrier molecule for delivery of therapeutic agents. It is biodegradable and biocompatible in nature and is approved by Food and Drug Administration (FDA) for therapeutic use. It is a white semicrystalline solid and has polyglycolic acid (PGA), poly-L lactide (PLLA) as its copolymers. (Abedalwafa et al. 2013).

2.7.2.1 Structure

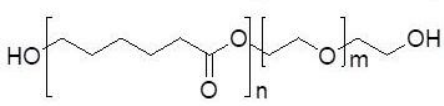

PCL

2.7.2.2 Molecular formula and molecular weight: $(C_6H_{10}O_2)_n$, 50,000 to 80,000 g/mol

2.7.2.3 Solubility: PCL is soluble in chloroform, dichloromethane, carbon tetrachloride, toluene and benzene. It displayed poor solubility in acetone, and ethyl acetate, and is insoluble in alcohol, and diethyl ether.

2.7.3 Folic Acid

Folic acid is vitamin B9 and also known as folate and folacin. Folate is an essential component necessary for proper cellular metabolism and cell survival, specifically during the rapid cell division phase which is characteristic of cancerous cells. Folate receptors are thus over-expressed in various type of cancers such as lung, liver, breast, colon, brain and kidney.

2.7.3.1 Molecular formula and Molecular weight: $C_{19}H_{19}N_7O_6$, 441.404 g/mol

2.7.3.2 Physical form: Yellowish-orange crystalline solid, odorless

2.7.3.3 Melting Point: 248-252 °C

2.7.4 Biotin

Biotin (vitamin H or B-7) is a growth promoter at the cellular level, and its concentration in tumors is significantly higher than that in normal tissues. Biotin receptors are overexpressed in a number of cancer cells such as leukemia (L1210FR), breast (MMT06056), colon (Colo-26), lung (NCI-H69, A549) and many more.

2.7.4.1 Molecular formula and Molecular weight: $C_{10}H_{16}N_2O_3S$, 244.31g/mol

2.7.4.2 Physical form: White crystalline needles

2.7.4.3 Melting Point: 230-232 °C

2.8 Discussion

The preformulation studies aim at establishing the physiochemical properties of the drug, and are a essential milestones for designing and developing of a dosage form. They also reduce the challenges during formulation development. This includes the analysis of physiochemical properties of the drug and its compatibility aspect with the excipients of choice for developing a stable dosage form.

It is essential to analyse the purity of drug, as impurities or a compromised concentration may have undesirable manifestations. Gefitinib was standardized as per the specifications given in the monograph in IP 2014 and the analysis complies with the official monographs. The physiochemical properties of drugs capsaicin and naringenin also comply with the previously published literature (Lau et al. 2014, Pharmacopoeia 2014, Chang et al. 2017).

Suitable methods of UV spectrophotometry were utilized to prepare standard curves of Gnb, Cap and Nar. The result of calibration curve in methanol revealed that Beer Lambert's law is followed in the concentration range 1-12 µg/ml for Gnb, 10-50 µg/ml for Cap and 1-10 µg/ml for Nar respectively in UV spectroscopy. Beer-Lambert law states the relationship between absorbance and concentration of the solution, describing that the absorbance is directly proportional to concentration of the solution.

High-performance liquid chromatography (HPLC) is a convenient and useful analytical technique extensively used for the analysis of pharmaceuticals, phytomedicines and polymers. The chromatograms revealed that the linearity was observed in concentration range of 0.01-1.0 µg/mL with correlation coefficient of 0.9995. It was concluded that the method recognized for HPLC assay has been successfully used in analysis of drug in physiological fluids (plasma, serum) intravenous administration of Gnb nanoparticles in mice model.

REFERENCES

Abedalwafa, M., F. Wang, L. Wang and C. Li (2013). "Biodegradable poly-epsilon-caprolactone (PCL) for tissue engineering applications: a review." Rev. Adv. Mater. Sci **34**(2): 123-140.

Avgoustakis, K. (2008). "Polylactic-co-glycolic acid (PLGA)." Encyclopedia of biomaterials and biomedical engineering. New York: Informa Healthcare USA, Inc: 2259-2269.

Benevenuto, C. G., L. O. Guerra and L. R. Gaspar (2015). "Combination of retinyl palmitate and UV-filters: phototoxic risk assessment based on photostability and in vitro and in vivo phototoxicity assays." European Journal of Pharmaceutical Sciences **68**: 127-136.

Cataldo, V. D., D. L. Gibbons, R. Perez-Soler and A. Quintas-Cardama (2011). "Treatment of non-small-cell lung cancer with erlotinib or gefitinib." N Engl J Med **364**(10): 947-955.

Chang, H. L., Y. M. Chang, S. C. Lai, K. M. Chen, K. C. Wang, T. T. Chiu, F. H. Chang and L. S. Hsu (2017). "Naringenin inhibits migration of lung cancer cells via the inhibition of matrix metalloproteinases-2 and-9." Experimental and therapeutic medicine **13**(2): 739-744.

Hong, Z.-F., W.-X. Zhao, Z.-Y. Yin, C.-R. Xie, Y.-P. Xu, X.-Q. Chi, S. Zhang and X.-M. Wang (2015). "Capsaicin enhances the drug sensitivity of cholangiocarcinoma through the inhibition of chemotherapeutic-induced autophagy." PloS one **10**(5): e0121538.

Jin, C.-Y., C. Park, J.-H. Lee, K. T. Chung, T. K. Kwon, G.-Y. Kim, B. T. Choi and Y. H. Choi (2009). "Naringenin-induced apoptosis is attenuated by Bcl-2 but restored by the small molecule Bcl-2 inhibitor, HA 14-1, in human leukemia U937 cells." Toxicology in Vitro **23**(2): 259-265.

Lau, J. K., K. C. Brown, A. M. Dom, T. R. Witte, B. A. Thornhill, C. M. Crabtree, H. E. Perry, J. M. Brown, J. G. Ball and R. G. Creel (2014). "Capsaicin induces apoptosis in human small cell lung cancer via the TRPV6 receptor and the calpain pathway." Apoptosis **19**(8): 1190-1201.

Lee, E.-R., Y.-J. Kang, H.-Y. Choi, G.-H. Kang, J.-H. Kim, B.-W. Kim, Y. S. Han, S.-Y. Nah, H.-D. Paik and Y.-S. Park (2007). "Induction of apoptotic cell death by synthetic naringenin derivatives in human lung epithelial carcinoma A549 cells." Biological and Pharmaceutical Bulletin **30**(12): 2394-2398.

Othman, Z. A. A., Y. B. H. Ahmed, M. A. Habila and A. A. Ghafar (2011). "Determination of capsaicin and dihydrocapsaicin in Capsicum fruit samples using high performance liquid chromatography." Molecules **16**(10): 8919-8929.

Pandey, M., S. Sultana and K. P. Gupta (2014). "Involvement of epigenetics and microRNA-29b in the urethane induced inception and establishment of mouse lung tumors." Experimental and molecular pathology **96**(1): 61-70.

Pharmacopoeia, I. (2014). "Govt. of India, Ministry of Health and Family Welfare, Delhi, Ghaziabad, 2014." Vol. II **2066**.

Reyes-Escogido, M. d. L., E. G. Gonzalez-Mondragon and E. Vazquez-Tzompantzi (2011). "Chemical and pharmacological aspects of capsaicin." Molecules **16**(2): 1253-1270.

Zhang, S.-s., Y.-h. Ni, C.-r. Zhao, Z. Qiao, H.-x. Yu, L.-y. Wang, J.-y. Sun, C. Du, J.-h. Zhang and L.-y. Dong (2017). "Capsaicin enhances the antitumor activity of sorafenib in hepatocellular carcinoma cells and mouse xenograft tumors through increased ERK signaling." Acta Pharmacologica Sinica.

Chapter III

Hyaluronic Acid Conjugated Nanoparticles

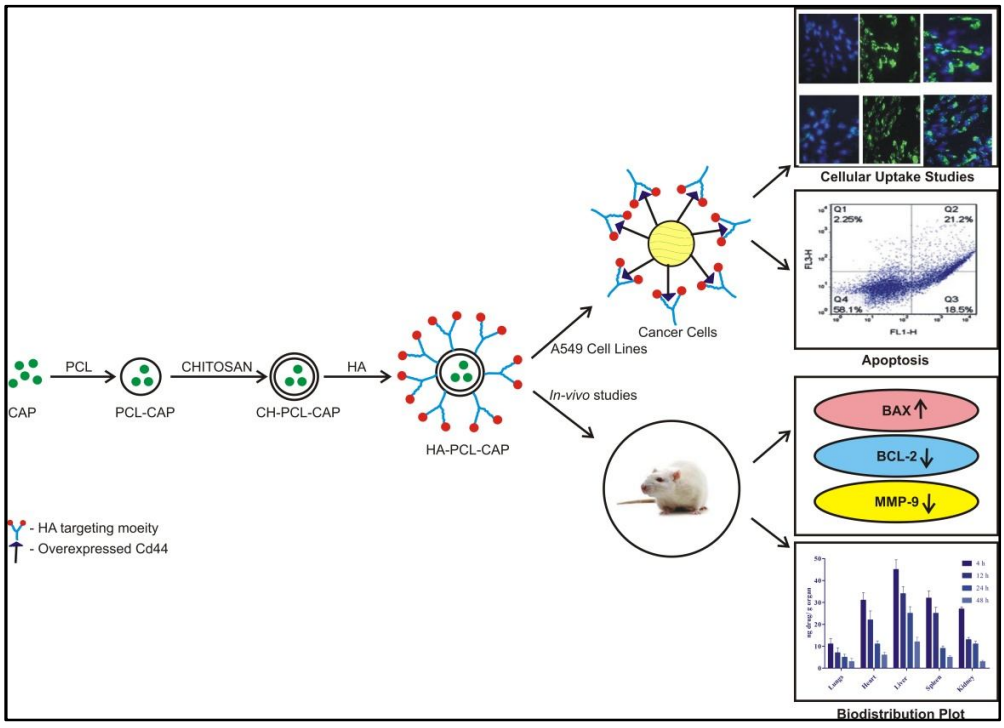

3. Fabrication and Assessmentof Hyaluronic Acid Functionalized PCL Nanoparticlesof Capsaicin

3.1 Introduction

Polymeric nanoparticles like PCL and PLGAare bestowed with properties such as biodegradability, biocompatibility, modified release and can be easily surface modified for site specific targeted delivery to tumor cells(Najlah et al. 2017). The development of newer targeted delivery systems utilizing such polymers are beingvastly designed specifically for targeting over-expressed factors, such as folate receptor, EGFR (epidermal growth factor receptor), cluster determinant 44 receptor (CD44) etc.(Muralidharan et al. 2015).It has been reported that these surface engineered polymeric nanoparticles (NPs) have longer circulation repeatability as they hold the abilityto shield the carrier moiety and drug from reticuloendothelial system (RES) uptake during blood circulation. Thenanosize, surface modification and repeated circulation of NPs,have promising outcomes forsite specific targeting of cancer cells, while safeguarding normal (non-cancerous)cells from toxicity(Wickens et al. 2017). The other important advantages of targeted drug delivery system comprisehigher accumulation and bio-distribution of drug into targeted organ, as well as improved cellular uptake of thedrug (Chen et al. 2010). This results in prevention of undesired toxic side effects of the drug on non-targeted cells/tissues.

Capsaicin (trans-8methyl-N-vanillyl-6-nonenamide) is a derivative of homovanillic acid and is the chief spicy component of chili peppers belonging to genus *Capsicum annum*. Ithas been well reported that capsaicin (CAP) possessesmedicinal values viz.anticancer and anti-proliferative activity, analgesic, antioxidant, anti-inflammatory and anti-obesity properties.CAPhas been broadly studied for a variety of cancers including lung(Chakraborty et al. 2014). On the other hand, Hyaluronic acid (HA) is a linear mucopolysaccharidewithrepeated *N*-acetyl glucosamine and glucuronic di-saccharide units alternately.HA is one of the important components of extracellular matrix, and has been reported to haveanti-inflammatory, wound healing as well as tissue regeneration and inhibitionof cancer metastasis, due to the action of HA degrading enzyme-hyaluronidases(Vangara et al. 2013, Gao et al. 2017). HA constitutes the foremostconstituent of the extracellular matrix consequentlyfacilitating enhanced interaction

with the biological membranes(Wang et al. 2017).HA is known to interact and bind with non-small cell lung cancer overexpressed with CD44. Jing et al. stated improved drug accumulation of doxorubicin in tumor cells and enhanced antitumor efficiency of chemotherapeutic agent by making use of HA modified polymeric NPs(Li et al. 2012). Kuanet al. successfully formulated and evaluated sinulariolide conjugated hyaluronic acid NPs, describing improved *in vitro* efficiency against lung adenocarcinoma cells (Hsiao et al. 2016). HA modification is focused to targeted delivery of chemotherapeutic agent to achieve better management of cancer therapy.

This chapter explores the fabrication and characterization aspects ofCAP loadedHA modified PCL nanoparticles. The present study was aimed to develop CAP loaded HA NPs utilizing layer by layer technique and optimization through 2^3 factorial designs to achieve enhanced and precise delivery as well as target specificity. The HA functionalized NPs were comprehensively characterized for various parameters viz.particle size, zeta potential, *in vitro* release and cytotoxicity on A549 cells. The formulations were also evaluated *in vivo* in urethane-induced lung carcinoma in rat model.

3.2 Materials

Capsaicin, polymer Poly-ε-caprolactone (PCL) (Mw: 42,500–65,000), and surface modifier hyaluronic acid (HA) (Mw: 200 kDa) were purchased from M/s Sigma Aldrich, St. Louis, MO, USA. Chitosan, Cremophore EL and urethane were purchased from M/s Hi-media chemicals, Mumbai, India. All other chemicals were of analytical grade and purchased from Merck Specialities Pvt. Ltd. Mumbai, India. Propidium Iodide, RNase A, DMEM (Dulbecco's Modified Eagle's medium), Fetal Bovine Serum (FBS) (previously heat-inactivated), tris-buffered saline (TBS) and tween 20 (TBST), MTT (3-(4,5-Dimethylthiazol-2-yl)-2,5-diphenyl tetrazolium bromide), DAPI 2-(4-amidinophenyl)-1H -indole-6-carboxamidine, Nonidet P-40 (NP-40s) were purchased from M/s Sigma Aldrich, MO, USA. All antibodies were purchased from M/s Santa Cruz, CA, USA. In-house double distilled water was used throughout the experiment.All chemicals were of analytical grade.

3.2.1. Animals

The *in vivo* study was performed according to the Declaration of Helsinki for humans and the European Community guidelines as accepted principles for the use of experimental

animals and approved by the Institutional Animal Ethics Committee as per approval number SDCOPVS/AH/CPCSEA/01/0028. Albino wistar rats (male/female, seven weeks-old) were fed with synthetic pellet diet (M/S Provimi Animal Nutrition India Pvt. Ltd. Bangalore) and water ad libitum. Animals were kept in a well-ventilated animal house at temperature 22°C±2°C in polypropylene cages. Animals were divided into 05 groups having 9 animals each, under a 12 h light/ dark cycle, and acclimatized for 2 weeks. All animals were handled as per institutional animal ethics norms, and care was taken that all guidelines were followed with a human approach.

3.2.2.Cell Lines

Human non-small-cell lung carcinoma (NSCLC) cell lines (A549) were obtained from American Type Culture Collection (ATCC, Rockville, MD, USA). Cells were maintained in appropriate culture medium in Dulbecco's Modified Eagle's Medium DMEM supplemented with 10%v/v fetal bovine serum and 1%v/v antibiotic (penicillin) solution. A549 cells were maintained at 37°C with 5% CO_2 in incubator.

3.3. Methods

3.3.1. Preparation of Capsaicin Loaded Poly-ε-caprolactoneNanoparticles (PCL-CAP)

CAP loaded PCL nanoparticles were developed using nano-precipitation method reported elsewhere(Zhang et al. 2006). Briefly, PCL was dissolved in acetone in variable concentration of 1% w/v, 0.5% w/v and 0.75% w/v (10 mL). The drug (CAP10 mg) was dissolved in acetone (1 mL). The resulting solution was added drop wise with the help of a syringe into 10 mL of 0.5% v/v Cremophore-EL (10 mL) and kept under continuous stirring (magnetic stirrer -Tarsons-Spinot MC 01, Delhi, India). This solution was stirred overnight to remove any organic solvent. After the completion of process,CAP loaded PCL NPs were obtaineddesignated as PCL-CAP NPs. The resulting sample was lyophilized (Christ Alpha 1-4 lyophilizator, Osterodo, Germany) to obtain dry powdered NPs and stored at room temperature, till further use.

3.3.2.Surface Modification of PCL-CAP

Layer by layer technique (LBL) was employed for surface modification of PCL-CAP NPs (Parashar et al. 2018). LBL technique is a facile process in which a layeris coatedover

another layer based on the principle of charge interaction. Here, PCL layer was coated with chitosan and again chitosan was coated with HA with the help of charge interaction. PCL and HA both are positively charged hence HA cannot directly be coated or bound to PCL as it would cause charge repulsion. Thus,to coat HA over the PCL-CAPNPs, an in-between layer of chitosan (owing to its positive charge) was introduced in between PCL and HA. Concisely, CAP loaded PCL NPs (PCL-CAPNPs) were added drop wise into 0.01% w/v chitosansolution in 1:2 ratio, and stirred continuously for 2 h (Tarsons-Spinot MC 01, Delhi, India). The process formed a chitosan layer/coat over PCL-CAP NPs and formation of chitosan coated nanoparticles CH-PCL-CAP NPs. The zeta potential of thus formed NPs was assessed to confirm the charge reversal from (positive to negative) after coating through, zeta/nano particle analyzer Particulate System Analyzer (NanoPlus-3,Yokohama, Japan).

After confirmation of charge reversal, the CH coated NPs i.e. CH-PCL-CAPNPs were added to 0.01% w/v of HA solutionin 1:3 ratios to obtain HA functionalized CAP NPs (HA-PCL-CAP NPs). The formation of HA functionalized NPs (HA-CH-PCL-CAP)was again confirmed through charge reversal (NanoPlus-3, Yokohama, Japan). Lastly, the prepared HA functionalized HA-PCL-CAP NPs were lyophilized (Christ Alpha 1-4 lyophilizator, Osterodo, Germany) and stored at a low temperature of 4°C till further use.

3.4. Characterization of Prepared HA-PCL-CAPNPs

3.4.1. Particle Size Analysis and Surface Charge

The particle size, PDI of HA-PCL-CAP NPs was measured through particle size analyzer and the surface charge was measured through zeta/nano particle analyzer (NanoPlus-3, Yokohama, Japan) based on dynamic light scattering (DLS) method. The samples were reconstituted in phosphate buffer pH 7.4 prior to loading cuvettes and analyzed. Laser beam operated at a scattering angle of 90° was used to determine particle size at 25°C.The experiments were performed in triplicate and values were expressed as mean ± standard deviation.

3.4.2. Transmission Electron Microscopy

The surface morphology of HA modified HA-PCL-CAP NPs was analyzed through TEM (H-750, Hitachi, Tokyo, Japan). For sample preparation,previously diluted sample was mounted over 400 mesh copper grid and allowed to air dry, followed by IR lamp drying. The excess sample was removed with the help of filter paper. After completion of sample preparation, analysis was done under 2000 magnification and 100 kV voltages. The photomicrographs were captured for interpretation of results.

3.4.3. Entrapment Efficiency (%EE)and Drug loading

Entrapment efficiency was determined by ultracentrifugation method. About 1.5 mL of each formulations was centrifuged (REMI CPR-24) for 15 min at 10,000 rpm at 4°C to separate free drug. The pellet and supernatant were separated. The supernatant was collected to determine free drug present in it and the concentration of free drug was measured by determining absorbance at 279 nm through UV spectrophotometer (Labtronics LT-2910, India). For determining drug loading, the pellet obtained after centrifugation was redispersed in acetone. The amount of drug was determined through UV spectrophotometer (Labtronics LT-2910, India) at 279 nm. All the experiments were performed in triplicate and mean values reported. The entrapment efficiency was calculated using equation (i&ii)-

$$\%EE = \frac{Wintial\ drug - Wfree\ drug}{Winitial\ drug} X\ 100 \ldots(i)$$

$$\%\ DL = \frac{\text{Initial amount of drug in NPs} - \text{free drug}}{\text{Mass of NPs recovered}} \times 100 \ldots\ldots (ii)$$

3.4.4. In Vitro Dissolution Studies

The*in-vitro* drug release of CAPfromPCL-CAP, CH-PCL-CAP and HA-PCL-CAP NPs was performed using dialysis membrane method having specifications, molecular weight cut off range 12,000–14,000 dalton (Hi-media, Mumbai, India). The dialysis membrane was pretreated prior to experiment and glycerin based contents were removed by keeping itin running water for 12 h. Sulfur-based contents present in membrane were removed by treatment with 0.3% w/v sodium sulfite at 70°C for 20 min. After that, the membranes were

kept for 2 min in water maintained at 70°C and then dipped into 0.2% v/v sulfuric acid solution for 5 min. The treated membranes were kept in PBS till further use for *in-vitro* drug release studies.

The *in vitro* release study was carried out in USP dissolution apparatus type-II (Veego, Mumbai, India). CAP equivalent to 10 mg from each formulation was taken and packed in the sac made of a pretreated dialysis membrane; the sac was knotted to the paddle of the shaft in such a way that membrane just touches the surface of dissolution medium PBS pH 7.4(0.1% w/v sodium lauryl sulfate), maintained at 37°C and 50 rpm. Sodium lauryl sulfate was added to increase the solubility of poorly soluble CAP in dissolution media and to maintain sink condition.

The release study was carried out over a period of 48 h. An aliquot of 3 mL of the sample was withdrawn at preset time intervals and restocked with fresh medium. The aliquots were filtered through 0.45 μm membrane filters. Drug concentration was estimated spectrophotometrically at 279 nm using UV spectrophotometer (Labtronics-2910, India). Cumulative percent drug release was plotted as a function of time, to determine the release of CAP from various formulations. All experiments were performed in triplicate.

3.4.5. Release Kinetics Modeling

The optimized formulation HA-PCL-CAP was subjected to graphical treatment to forecast the mechanism of drug release using goodness of data fit methodology. The obtained *in vitro* release data was analyzed for various kinetic models viz. zero order, first order, Higuchi model, Korsmeyer-Peppas etc.

3.5. In Vitro Cell Culture Study

3.5.1. Cell Cytotoxicity Study by MTT Assay

Cytotoxicity of CAP was assessed on cancer cells by means of MTT assay to evaluate the anticancer efficacy over A549 cells. Lung cancer cell lines A549 were cultured in 96 well plate with cell density ($1X10^3$ cells/well) and incubated overnight at 37°C, 5% CO_2 in DMEM media comprising 10%v/v FBS. This helped in adhesion of cell to the well surface. The cells were treated with various concentrations of CAP, PCL-CAP and HA-PCL-CAP

ranging from 0 to 50 µM equivalents CAP (n=3). Plain PBS was taken as control i.e. untreated cells. After 48 h of incubation, MTT dye (8 µL, 5 mg/mLin PBS) was added to each well and incubated for 4 h.This leads to development of MTT-formazan crystal as the viable cells internalize MTT intotheir mitochondria and metabolize it to form blue formazan crystals. The optical density was determined via Elisa plate reader at 540 nm (Synergy H1,M/s Biotech Inc, USA)(Lee et al. 2007).

3.5.2. Quantitative and Qualitative Cellular Uptake Study

FITC (Fluorescein isothiocyanate) loaded NPs were developed using same procedure as used for PCL-CAP and HA-PCL-CAP to assess the delivery system in terms of enhanced uptake of drug into the cancer cells. Drug accumulation in A549 cells was evaluated by FACS (fluorescence activated cell sorter) instrument (BD Biosciences, FACS Aria, Heidelberg, Germany). A549 cells ($3X10^3$cells/well) were cultured in a 6 well plate in fresh DMEM media following similar method as described in MTT assay and incubated in CO_2 incubator for 24 h at 37°C. Afterwards, the cells were treated with FITC-labeled PCL-CAP and HA-PCL-CAP for 4 h. The cells were washed thrice with PBS after incubation and analyzed through flow cytometric analysis at an excitation wavelength of 480 nm and an emission wavelength of 550 nm.

3.5.3. Cell proliferation studies

The cell proliferation assay of various formulations was performed utilizing Alamar blue® reduction method. The A549 cell lines ($3x10^3$cells/well)) were placed in 96 well plates and incubated for 24 h at 37℃. The cells were treated with various formulations at sub IC_{50}concentration equivalent of CAP for 24 h. Afterwards, Alamar blue® was added (final concentration 5% v/v) to wells and again incubated at 37°C for 4 h. The plates were read at 570/600 nm in a multimode reader (Synergy H1, M/s Biotech Inc, USA) and cellular proliferation percentage was assessed calorimetrically. The untreated cells were taken as control (O'brien et al. 2000).

3.5.4. Mitochondrial membrane potential assay (MMP) and Reactive Oxygen Species (ROS) generation analysis

Mitochondrial membrane potential assay was conducted employing dye Rhodamine 123 (Rh-123). Specified A549 cells were seeded in 96 well culture plate ($3X10^3$cells/well) in

DMEM culture media in CO_2 incubator for 24 h at 37°C and treated with HA modified and unmodified nanoformulations, while untreated cells were taken as control. The plates were read using a multimode reader (Synergy H1, Biotech Inc, USA) at 540/570 nm (Excitation/ Emission) at 100% sensitivity. Nexttocompletion of incubation period, Rh-123 was added in a concentration of 10 µM for 30 min in dark in a conventional incubator maintained at 37°C, 5% CO_2 and fluorescence was measured. ROS estimation was done throughDCFDA(cellular reactive oxygen species detection assay) kit against various modified and unmodified nanoformulations. Specified A549 cells were seeded in 96 well culture plates ($3X10^3$cell/well) as stated above for 24 h, 10 µM of DCFDA was added to each well after the completion of the incubation period and the plates were incubated in dark for 30 min, as above. Subsequently, washing was done with PBS to remove the dye and cells were re-suspended in 100 µL PBS.The relative fluorescence of plate was read at 495/529 (Excitation/ Emission) at 100% sensitivity in a multimode reader (Synergy H1, Biotech Inc, USA). DCFDAis a fluorescent dye which gets deacetylated by cellular esterase after diffusion into the cell. Afterwards, deacetylated form is furtheroxidized by ROS into 2',7'-dichlorofluorescein (DCF) to a non-fluorescent compound, (Perry et al. 2011).

3.5.5. Apoptosis assay

Apoptosis event in A549 cells was evaluated by dual Annexin V/Propidium iodide (PI) assay through flow cytometry using FACS (fluorescence activated cell sorter) instrument (BD Biosciences, FACS Aria, Heidelberg, Germany). The quantitative perception of apoptotic cells and necrotic cells designates the apoptotic effect of CAP, PCL-CAP and HA-PCL-CAP on A549 cells. The cells were cultured in 6 a well plates in the above described media and culture conditions. The A549 cells were treated with various formulations in equivalent to sub IC_{50} concentration of CAP. The treated A549 cells were incubated for 24 h at above mentioned conditions, and afterwards collected in PBS forflow cytometry analysis after Annexin-PI dual staining(Agrawal et al. 2016).

3.6. In Vivo Study

3.6.1. *In Vivo* Therapeutic Efficacy of HA-PCL-CAPNPs

The protocol for animal testing was approved through Institutional Ethical Committee, approval no. SDCOPVS/AH/CPCSEA/01/0028. Albino wistar rats both male and female, weighing 120-150 g were used for the experiment. Animals were randomized and divided into five groups having 12 animals each. Lung cancer was induced by three consecutive i.p. injections of urethane, within a gap of 48 h over a period of one week. The development of lung tumors was initiated over a period of 8-12 weeks. To confirm the tumor development one animal was taken as a representative from each group (except negative control) and sacrificed at 4, 8 and 12weeks. The other animals in the group were considered to be LC positive if the sacrificed one was found to be so. The treatment was initiated after complete development of tumors ie. 16^{th} week and continued over a period of one month.After completion of the study, the blood samples were collected through retro orbital plexus under chloroform anesthesia. The collected blood samples were incubated at 37°C for 1 h and serum was separated by centrifugation at 10,000 rpm for 15 min. The serum samples were stored at -20°C till further use. Animals were sacrificed on the 16^{th} week after treatment and lung tissues were isolated and stored at -80°C till further evaluation (Pandey et al. 2014). The groups of animals received various treatment as described.

Group I (negative control)

Group II (toxic control, toxicant Urethane 1 g/kg, i.p.)

Group III (Urethane 1 g/kg, i.p; CAP, 20 mg/kg)

Group IV (Urethane 1 g/kg, i.p; PCL-CAP dose: 20 mg/kg, i.v.)

Group V (Urethane 1 g/kg, i.p; HA-PCL-CAP 20 mg/kg, i.v.)

3.6.2. Histopathology

Lung tissues from all the five groups were isolated and stored in 10% buffered formalin for histopathological investigation. The tissues were embedded with paraffin wax, and sections of 3-5 µm made using rotary Microtome (YSI-060 Yorco, Ghaziabad, India). The fine sections were unruffled over the glass slide, deparaffinized, and stained with

hematoxylin and eosin. The sections were observed under 40X magnification and images were captured using digital biological microscope (N120, BR-Biochem Life Sciences, New Delhi, India.

3.6.3. Oxidative stress markers

The tumor-bearing lungs challenged by urethane were isolated from all the five groups, and investigated for oxidative stress. The isolated LC tissues homogenates were analyzed for oxidative stress markers viz thiobarbituric acid reactive substances (TBARS), superoxide dismutase (SOD), catalase and Protein carbonyl in accordance with previously established procedures(Kaithwas et al. 2012). Experiments were performed in triplicate and statistically analyzed using software Graph Pad Prism (5.01), San Diego, California.

3.6.4. Western Blotting

Lung tissues were excised and washed with buffer containing 10 mMTris/HCl, pH 7.4, and 150 mMNaCl. Tissue was homogenized in chilled RIPA buffer (50 mm Tris/HCl, 150 mm sodium chloride, 1%w/w NP-40 lysis buffer, 0.5%v/v sodium deoxycholate, 0.1% w/v SDS, pH 7.6). After homogenization, tissue was kept over ice for 30 min and sonicated three times each for 10 sec using probe sonicator (Labsonic-M, Sartorius Stedium). After sonication, the samples were centrifuged for 10 min at 10,000 g and supernatant removed. Protein concentration was determined using Bradford method. For western blot analysis, 50µg proteins were resolved each by 8-14% w/v SDS PAGE, transferred to PVDF membranes (0.45µm, molecular weight <15 kD, Millipore; Billerica, MA). A membrane was blocked using 3% w/v BSA in TBST for 2 h, incubated overnight with primary antibody and then incubated with the corresponding secondary antibody (anti-rabbit or anti-goat) at room temperature (1h). Proteins were detected by using chemiluminescent HRP (Horseradish peroxidase) substrate (Millipore)-based detection system in Imager Quant LAS 4010 Chemidoc (GE 210 Healthcare, Little Chalfont, UK). Blots were stripped and reused whenever possible.

Antibodies and dilutions for immunoblotting were as follows: Anti caspase-9 (rabbit polyclonal 1:500), Anti-actin (rabbit polyclonal 1: 500), Bcl-2 (mouse monoclonal 1:500), BAX (mouse monoclonal 1:500), and HRP-conjugated secondary antibodies (anti-rabbit,

1:500). β-actin (MA5-15739-HRP) was used as a standard reference.Quantitative analyses of protein expression in immunoblots were performed using scanning densitometry (ImageJ, NIH).

3.6.5. Biodistribution studies

Biodistribution of HA functionalized, PCL-CAP NPs and plain CAP were evaluated to determine the targeting potential of the HA conjugation. Biodistribution of the formulations was examined by injecting CAP, PCL-CAP and HA-PCL-CAPNPs equivalent dose to 20 mg/kg of CAP, through tail vein of urethane-induced LCs rats. Various body organs, *viz.*, lungs, liver, heart, kidney, spleen were excised after sacrificing animals at programmed time points i.e. 4, 12, 24 and 48 h respectively. The isolated organs were stored at -80°C till further analysis. The organs were weighed and homogenized. The concentration of CAP was measured through the validated HPLC method (Waters 2489, Milford, Massachusetts, USA). The system was equipped with Spherowsorb C18, 3.5 µm, 4.6×250 mm column at flow rate 1.0 mL/min. The mobile phase comprised of acetonitrile-water (70:30) with a flow rate of 1 mL/min and run time 6 minutes, at a detection wavelength of 280 nm. The sample injection volume was 20 µL(Guo et al. 2015).

3.7. Stability Studies

Stability studies of HA-PCL-CAP were done as per International Conference on Harmonization (ICH) guidelines over a period of 90 days. The formulations were kept in transparent containers at 5±2° and 25±2° (60±5% RH). Samples were assessed at 0, 15, 30, 45, and 90 days. The formulations were evaluated for particle size, zeta potential and drug content. All experiments were performed in triplicate and mean values reported.

3.8. Factorial Design

A 2^3 randomized full-factorial design was used in this study. In this design, three prime factors or variables were evaluated, each at two levels. A factorial design evaluating three factors at all combinations for each level would result in a full factorial design consisting of 9 runs. Thus, experimental trials were performed at all nine possible combinations. The amount of PCL (A) and Cremophore EL (B) were selected as independent variables along

with the stirring speed (C) as third variable. The particle size and %EE were the outputs as dependent variables.

3.8.1.Statistical analysis

All results were presented as the mean ± standard deviation (n=3). One-way analysis of variance (ANOVA) followed by the Turkey-Kramer multiple comparison test was performed to compare differences between formulations using Graph Pad Instat software (Graph Pad Software Inc. CA, USA). Levels of significance were set at $p<0.05$ explaining significant difference in the therapeutic efficiency of all formulations in comparison to HA-PCL-CAP.

3.9. Results

Formulation of HA functionalized CAP Nanoparticles and Characterization

Present investigation ensured the designing of HA functionalized layer by layer assembled PCL NPs sandwiched with CH for targeted delivery to mitigate lung cancer.

PCL NPs were optimized using 2^3 factorial designs, in which PCL concentration, Cremophore-EL concentration and varying stirring speed were taken as independent variables. The effects of independent variables on dependable variable viz. particle size and entrapment efficiency were taken as responses, to form batches **(Table 3.1).** Total, nine pre-optimized formulations of different composition were proposed through Design Expert® software. The data obtained after the analysis revealed that the independent factor i.e., PCL concentration has a significant effect on particle size while chermophore-EL and stirring speed plays an insignificant role on particle size. The quantitative estimation of the significant modal terms directed that a nonlinear quadratic relationship was perceived among A, B and C factors with all the dependent variables. It was observed that as the PCL concentration increases, the particle size increases. Further, chermophore-EL and PCL plays a significant role in entrapment efficiency.It was perceived that anincrement in their concentration enhances the %EE increases **(Figure 3.1 A-B).**The percentage entrapment increases as the concentration of both the factors increases. Nevertheless, the stirring speed independently plays an insignificant role in the process, though it acts significantly in terms

of BC factors taken together (stirring speed and Cremophore-EL) as shown in **Figure3.1C**. The relationship is best explained with the equations given below.

Particle size =+179.25+35.00A-4.00*B-5.25*C+6.50*BC…..(iii)

Entrapment efficiency =+55.87+3.88*A+0.875*B-0.3750*C+1.37*AB+1.12*BC …..(iv)

3.9.1. Optimization and validation

After analysis of the regression equations, detailed illustration of correlation between the dependent and independent variables, escalated process of optimization and validation was executed, employing design expert software (Design Expert 8.0 software; Trial version, M/s Stat-Ease, Minneapolis, USA). The design space/area (desirable range/value of characteristics) and the optimal formula for modified NPs depended on the rigid criteria of minimization of particle size (<200 nm) and %EE (>50%). The composition of the optimum formulation was identified as 0.75%w/v PCL (factor A), 0.75 %v/v cremophore-EL (factor B) and stirring speed of 500 rpm (factor C), which satisfied the requirements of optimization. At these points, the predicted values of particle size and percent entrapment were found to be 179.25±3.90nm and 55.87±2.76% respectivelyas shown in **Figure 3.1 D**. As per results of the advance validation of predicted values by this model, a new batch of modified NPs (HA-PCL-CAP) were prepared and characterized. This optimized batch exhibited particle size of 194±3.75 nm and percentage entrapment of 52.89±1.1%, which was in righteous orientation with the predicted values.

The surface modification was done by CH followed by HA coat on the outer surface for CD44 receptors targeting. The particle size of the CH coated PCL-CAP (CH-PCL-CAP NP) and HA anchored HA-PCL-CAP was found to be 192±3.17nm and 194±3.75 nm having a polydispersity index of 0.031 and 0.245 respectively, indicating that the formulation was homogenous with respect to particle size.

Table 3.1 Effect of various independent variables on dependable parameters for PCL NPs prepared through 2^3 factorial design (All values expressed are mean ± SD; *n* = 3).

Run	Factor A PCL concentration (%)	Factor B Cremophore-EL concentration (%)	Factor C Stirring speed(rpm)	Particle size(nm)	Entrapment efficiency (%)
1	0.5	0.5	400	156±2.67	54±1.22
2	1	0.5	400	234±3.32	59±1.09
3	0.5	1	400	138±1.90	51±1.34
4	1	1	400	210±2.11	61±2.98
5	0.5	0.5	600	144±1.98	51±2.09
6	1	0.5	600	199±3.87	56±1.11
7	0.5	1	600	139±2.90	52±3.65
8	1	1	600	214±1.99	63±1.05
9	0.75	0.75	500	189±2.57	55±1.99

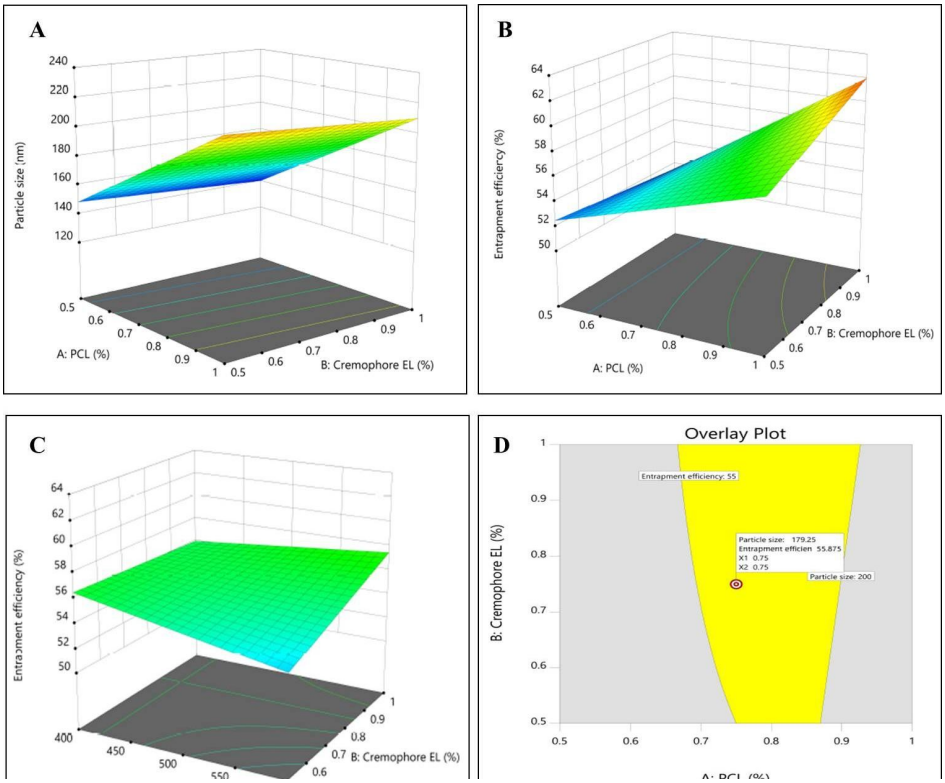

Figure3.1. Surface response plot showing influence of independent variables on (A) particle size (B) percent entrapment and (C) combined effect of stirring speed and cremophore-EL on entrapment efficiency (D) overlay plot depicting predicted values for particle size and percent entrapment in the desirable region (design space) as highlighted area for the nanoparticles.

Surface modification employing LBL technique was confirmed by measuring the surface charge after coating of each layer through different materials viz. PCL as first layer, CH as intermediate second layer and HA as outermost third layer. Therefore, the zeta potential of developed LBL assembly system was measured after coating of each layeri.e. in between each coating during fabrication of modified nanoparticles. Zeta-potential of PCL-CAP was found to be -21.34±0.21 mV as PCL retains the negative charge. The coating of chitosan was confirmed by the reversal of charge in CH-PCL-CAP from -21.34±0.21 mV to 15.72±0.37 mV as chitosan coating gives a positive surface charge as revealed by **Figure3.2.** In the final step HA coating being cationic in nature, reverses charges back to negative side, from 15.72±0.37 mV to -27.87±3.21 mV **(Figure3.2).** The threshold value of

±20 mV for zeta potential is often considered to be stable for particles, even though it is not always true as NPs of much lesser zeta potential have been reported to be stable.

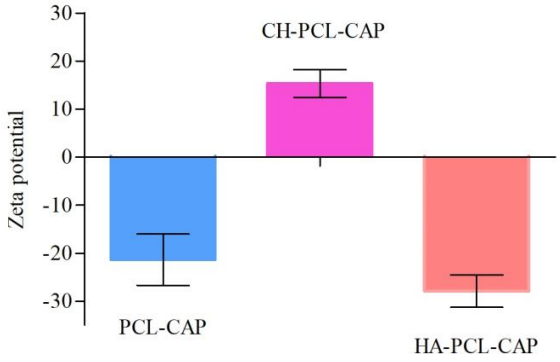

Figure3.2. Zeta potential values of PCL-CAP,CH-PCL-CAP and HA-PCL-CAP NPs, illustrating charge reversal at various steps during fabrication through LBL technique.

3.9.2. Surface Morphology

The surface morphology of HA-PCL-CAP NPs was inspected by Transmission Electron Microscopy (TEM). As depicted in **Figure 3.3**, TEM micrograph of HA-PCL-CAP NPs revealed smooth surfaced spherical particles and a mean particle size ranging from 50-200 nm.

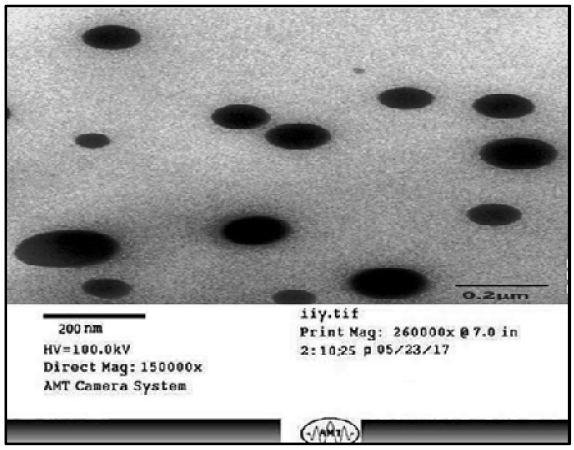

Figure 3.3.TEM image of HA-PCL-CAP NPs.

3.9.3. Drug Loading and Entrapment Efficiency

The %EE of PCL-CAP, CH-PCL-CAP and HA-PCL-CAP NPs was found to be 54.20±3.25%, 53.11±1.67% and 52.89±2.19% respectively. The loading efficiency of PCL-CAP, CH-PCL-CAP and HA-PCL-CAP NPs was found to be 14.2±0.43%, 12.5±0.05%and 13±0.37%, respectively. The drug loading and entrapment efficiency of all formulations is recorded in **Table 3.2**. A slight decrease in %EE was observed after HA modification which could be due to loss of free drug during fabrication steps. However an insignificant change in particle size was observed after HA modification.

Table 3.2. Characterization of CAP loaded HA functionalized and unmodified nanoparticle

Formulation	Particle size (nm)	%Entrapment	Drug loading (%)
PCL-CAP	187±1.32	54.20±3.25	14.2 ± 0.43
CH-PCL-CAP	192±3.17	53.11±1.67	12.5±0.05
HA-PCL-CAP	194±2.90	52.89±2.19	13±0.37

3.9.4. In vitro Dissolution Study

The release study of the unmodified and modified formulations was performed for 48 h, in PBS pH 7.4 (0.1% w/v SLS) as shown in **Figure3.4.** The release of Cap from PCL-CAP, CH-PCL-CAP and HA-PCL-CAP NP displayed biphasic release. A slower release was observed within 4 h in case of CH-PCL-CAP and HA-PCL-CAP, while a fast release was observed in case of PCL-CAP. Approximately 41.23±1.27% drug release within 4 h was observed with PCL-CAP, while only 19.32±1.98% and 16.30±2.76% of drug was released from CH-PCL-CAP and HA-PCL-CAP NP respectively. However, a slower release profile in the later hours was observed for modified formulations. About 61.23±3.22% cumulative release of CAP from HA-PCL-CAP NPs was observed over a period of 24 h. The sustained release patternobserved in case of HA-PCL-CAP NPs could probably be the CH coating over the PCL-NPs surface that increases the coat density, which detained erosion and dissolution medium took more time to penetrate through the polymer matrix into the interior of the NPs, resulting in sustained drug release. The CH-PCL-CAP NPs and HA-PCL-CAP NPs have similar release profile due to the presence of CH coating. It may be noted that the presence of targeting moiety did not display any significant change in the*in vitro* release.

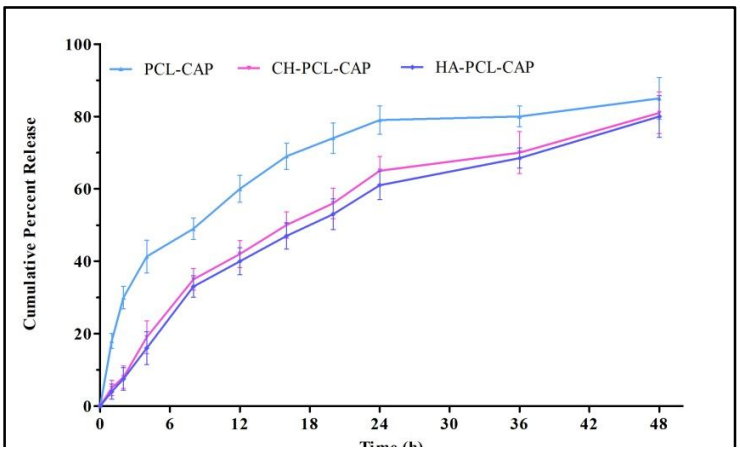

Figure3.4. *In Vitro* release profile comparison of PCL-CAP, CH-PCL-CAP and HA-PCL-CAP NPs. [Data is presented as mean±SD (n=3)]

3.9.5. Determination of Kinetic Model for Release of HA-PCL-CAP NPs

Different kinetic models were applied to the data obtained from release study for categorizing the kinetics of drug release as shown in**Table 3.2**. It was observed that Higuchi model is most suitable for describing the release of the CAP from HA-PCL-CAPNPs. The results revealed that the release of CAP from PCL NPs was diffusion controlled(Singh et al. 2017).The data obtained revealed the following sequence of drug release from PCL nanoparticles:

The dissolution media enters into polymeric matrix of the NPs through pores and penetrate into inner layers, gradually dissolving the drug and finally CAP is released via diffusion mechanism in the dissolution media.

3.9.6. *In Vitro* cell line studies

3.9.6.1. Cell cytotoxicity study by MTT assay

Cytotoxicity of HA-PCL-CAP NPs was evaluated on A549 lung cancer cells through MTT assay. The CAP, PCL-CAP and HA-PCL-CAP were incubated with A549 cells in the concentration range of 50–1.5 µM for 48 h. The results depicted through **Figure3.5a**, revealed a significant decline ($p<0.01$) in the IC_{50} of HA-PCL-CAP (39.74±2.11 µM) when compared with PCL-CAP (46.76±1.22 µM) and CAP (52.1±3.17 µM). The results witnessed a greater cytotoxic effect on A549 cells when treated with a lower concentration of CAP

with respect to CAP and PCL-CAP when formulated as HA functionalized NPs i.e. HA-PCL-CAP.

3.9.6.2. Quantitative and qualitative cellular uptake study

The HA anchored HA-PCL-CAP NPs displayed a higher cellular uptake and cellular internalization of CAP in A549 cells **(Figure3.5b).** HA-PCL-CAP, demonstrated about 1.5 times higher payload of CAP when compared to polymeric PCL-CAP NP. Enhanced cellular uptake can be correlated with decreased value of IC_{50} of HA-PCL-CAP NPs. The uptake study served as relevant proof for functionalization of HA modified nanoparticles. **Figure3.5c** revealed a higher degree of internalization of HA anchored NPs when compared to unmodified NPs.

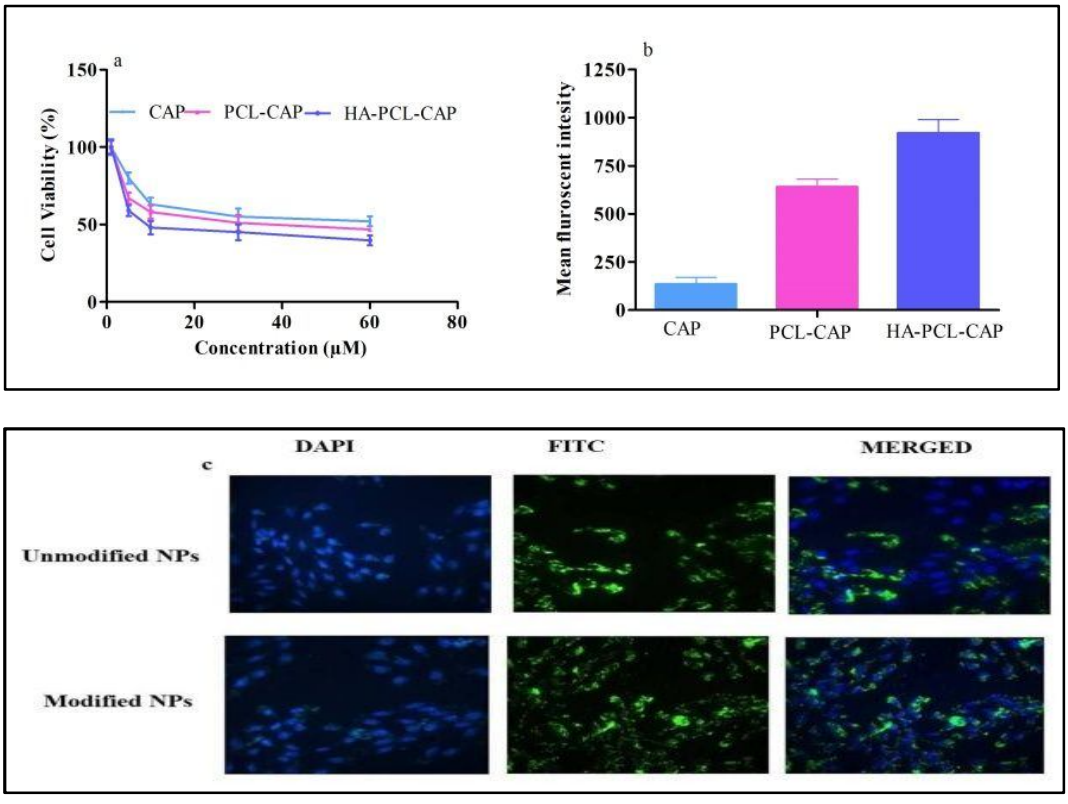

Figure 3.5.(a) Cytotoxic effect of various concentrations of CAP as pure CAP, PCL-CAP NPs and HA-PCL-CAP NPs on A549 cells (b) bar graph representation of Cell uptake study: CAP; PCL-CAP; and HA-PCL-CAP NPs and (c) Fluorescence images of A549 cells incubated with FITC-labeled unmodified NPs and HA-modified NPs: cell nuclei stained with DAPI.

3.9.6.3. Cellular apoptosis

Apoptosis assay demonstrated the outcome of treatment of A549 cells with CAP, PCL-CAP and HA-PCL-CAP which initiated cells to move towards programmed cell death process. **Figure3.6** displayed a significantly higher ($p<0.05$) apoptotic potential of HA-PCL-CAP in A549 cells and which was found 1.5 times higher than PCL-CAP.Approximately two fold increase in cell death was observed when compared with free CAP. The observed apoptotic percent was 16.4% and 18.5% in CAP and PCL-CAP treatedA549 cells. However an elevated apoptotic percentage of 28.51% was displayed afterHA-PCL-CAP treatment.

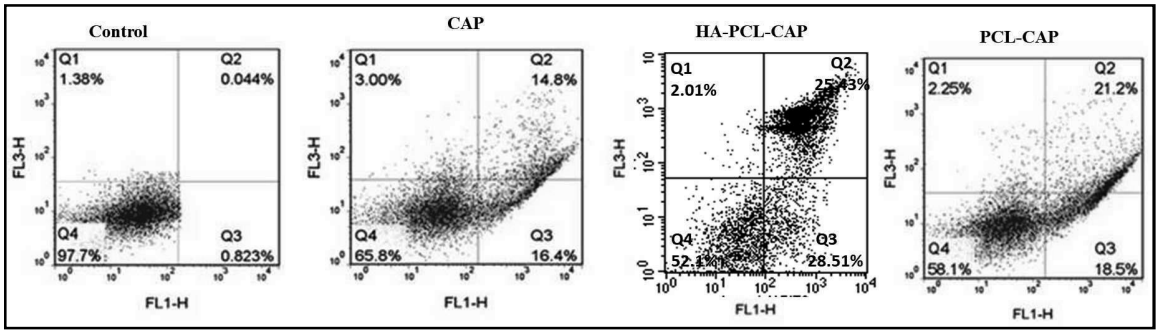

Figure3.6. Representative apoptosis in A549 cells after treatment with various formulations at sub IC_{50} drug concentration. Analysis was performed using flow cytometry ($n = 3$) ($p< 0.05$).

3.9.6.4. MMP assay and ROS generation analysis

Supreme disruption of mitochondrial membrane potential (MMP) in A549 cells was prompted by HA-PCL-CAP which was found significantly higher when compared with control samples ($p<0.01$). It was observed that HA-PCL-CAP and PCL-CAP playsa significant role in MMP disruption; however a declined effect was observed in CAP as compared to HA-PCL-CAP. A significant difference in MMP disruption was observed when a comparison was made between modified and unmodified NPs ($p<0.05$). Figure3.7asignifies the fluorescence intensity (indicating cell viability) of cells which alters differentially when treated with various formulations. Higher fluorescence intensity in control revealed least lethal capability while least fluorescence intensity in the case of HA-PCL-CAP which indicated highest mortality in A549 cells. The effect of the formulations on the MMP can be clarifiedin terms of lower uptake and retention of the Rhodamine-123 in

the mitochondria of cells undergoing apoptosis. Rhodamine-123 uptake is MMP-dependent and favors accumulation in the mitochondria of the living cells. This effects the quenching of fluorescence and consequences in red spectral shifts indicating that the cells are undergoing apoptosis.This enhanced mortality gives supplementary evidence of HA functionalization.

Inhibition of ROS by HA-PCL-CAP was found to be significantly higher ($p < 0.001$), when compared to free CAP as shown in **Figure3.7b.** Moreover, supremacy of modified NPs over unmodified NPs was also noticeable, with a significant level of $p<0.01$. A higher fluorescence of DCF in the A549 cells treated with PCL-CAP and CAP was observed, demonstrating raised cell population and production of higher ROS that oxidized the reduced form of DCF to fluorogenic oxidized form. On the contrary least fluorescence was observed with the HA-PCL-CAP treated group representing higher cell death (**Figure3.7b)**. DCFDA, a fluorogenic dye is widely used for direct measurement of the oxidation-reduction state of the live cell.

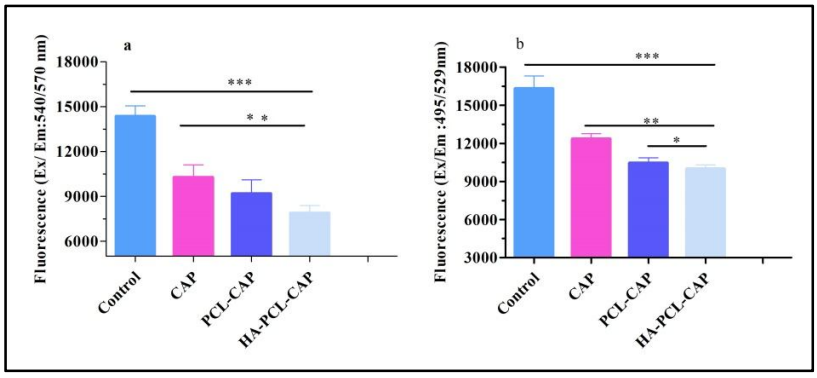

Figure3.7. (a)Loss of mitochondrial membrane potential in A549 cells (b) Intracellular ROS level in A549 cells after modified and unmodified CAP NPs measured by fluorimetry. [Data presented as the Mean±SD, n=3. *** $p<0.001$, ** $p<0.01$, * $p<0.05$ with respect to control, **a $p<0.01$ with respect to the CAP and the PCL-CAP groups]

3.9.7. *In Vivostudies*

3.9.7.1. Tumor regression study

The therapeutic effect of HA-PCL-CAP NPs was compared with the effects of CAP and PCL-CAP NPs *in vivo* in urethane-induced tumor model. The HA-PCL-CAP NPs treated group displayed major regression in tumor marked by comparative low tumor volume,

whereas PCL-CAP NPs displayed minor regression in tumor at the end point of experiment **(Figure3.8a–c)**.. The results displayed a significant augmentation of therapeutic efficacy ($p<0.01$) when compared to toxic group. Survival plot illustrated a significant reduction in animal death in both the groups receiving therapy, through HA-PCL-CAP NPs and PCL-CAP when compared to toxic group ($p < 0.05$). A lesser animal mortality was observed in group reciving drug therapies, while toxic group displayed a high mortality amomg animals. Weight variation plots for test animals throughout the study period exhibited reduced weight loss in test animals on HA-PCL-CAP NPs therapy when compared with toxicant, CAP and PCL-CAP NPs groups. A constant weight loss was observed with the toxic group, however a lesser percent weight loss was observed with HA-PCL-CAP therapy.The effect could be associated with the antioxidant potential of CAP for anti-proliferative activity and reported mechanism of reducing MMP-2 and MMP-9 in lung cancer cells to inhibit cell proliferation.

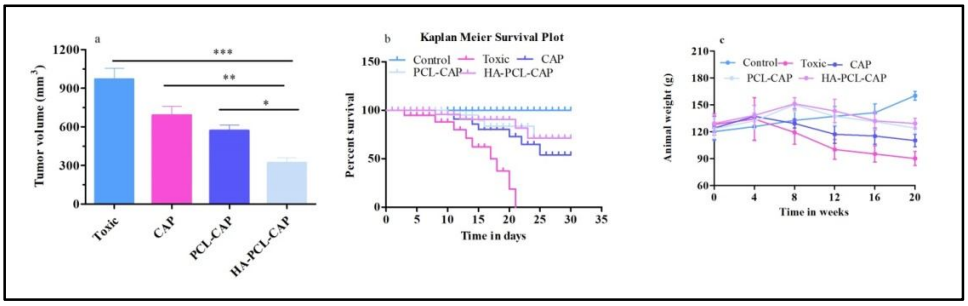

Figure3.8. (a) Bar graph of tumor volume in isolated lungs from urethane-induced rat tumor model after CAP, PCL-CAP, HA-PCL-CAP NPs therapy (dosing start after induction of tumor); (b) survival graph with percent test animal survived versus time; and (c) weight variation in animals during study.

3.9.7.2. Histological evaluation of tumors

The lung tissues were examined histopathologically for any histological changes, as shown in **Figure3.9.** Black arrows represented histological changes that occurred at the end of study.Toxic group displayed clear tumor stroma cells. The structural integrity of the lung was less affected and retained towards normal in animals receiving HA-PCL-CAP NPs followed by the PCL-CAP and pure CAP therapy group. However this was insignificant in nature. The toxic group displayed profound tumor stroma cells which lasted up to the end of the study, while a reduction in tumor stroma cells was displayed by therapy groups.

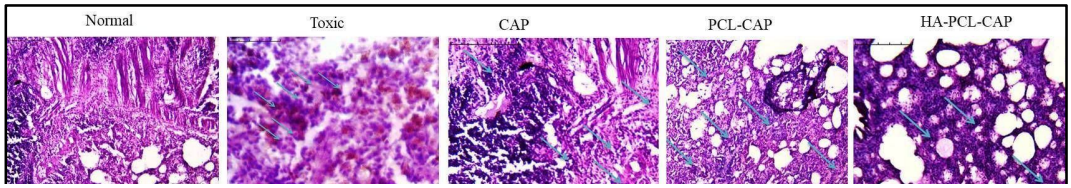

Figure3.9. H-E staining micrographs of tumor tissue after treatment with CAP, PCL-CAP, HA-PCL-CAP NPs (arrows indicate tumor stroma cells).

3.10. Oxidative stress markers

The effect of pure CAP, PCL-CAP NPs and HA-PCL-CAP NPs on oxidative stress markers, i.e., TBARs, SOD, Catalase and Protein Carbonyl, was investigated. The TBARs and SOD levels significantly increased after urethane administration and were markedly restored to normal levels after HA-PCL-CAP NPs therapy. The results displayed that HA-PCL-CAP NPs also significantly (p<0.5) restores the tissue catalase and protein carbonyl level that had previously reduced after urethane administration. Therefore, HA-PCL-CAP NPs expressed an overall, overlaid antioxidant effect to restore the redox balance in HA-PCL-CAP NPs administered group in comparisons to therapy through PCL-CAP, and pure CAP and toxicant group as recorded in **Table 3.3.**This could be attributed to the passive and active targeting. The HA modified NPs when reached CD44 overexpressed cell their swift uptake is facilitate through the same leading to enhanced payload.

Table 3.3. Effect of pure CAP, HA modified NPs and unmodified NPs on oxidative stress markers, from lung homogenate in Urethane-induced lung cancer. (Significant values * p< 0.05, ** p< 0.01, *** p< 0.001).

Groups	TBARs (nm of MDA/µg of Protein	SOD (Units of SOD/mg of Protein)	Catalase (nm of H_2O_2/min/mg of Protein)	Protein carbonyl *n*mol/mg of Protein
Control	195.20 ± 5.23	0.0356 ± 0.011 *	0.413 ± 0.012 ***	17.10 ± 0.05
Toxicant	511.83 ± 11.10	0.054 ± 0.036	0.113 ± 0.10	51.32 ± 3.70
CAP	398.2± 10.21	0.049 ± 0.021	0.121± 0.30	43.90 ± 2.87
PCL-CAP Therapy	284.5 ± 15.3 ***	0.04 ± 0.012 ***	0.129 ± 0.09	34.05 ± 1.54
HA-PCL-CAP Therapy	201.3 ± 11.10 ***	0.029 ± 0.03***	0.351 ± 0.021 ***	23.34 ± 0.12

3.11. Biodistribution studies

A delivery system conceiving higher targeting potential is the benchmark for an effective targeted anticancer therapy. Thus biodistribution of HA-PCL-CAP NPs was investigated to authenticate its targeting ability. A comparative interpretation of the CAP distribution in the various organs is presented in **Figure3.10**. It was revealed from the study that there was higher concentration of CAP in tumor tissue in HA-PCL-CAP administrated animals when compared with unmodified NPs and plain CAP administered groups. **Figure3.10 a-c,** demonstrated a significantly higher ($p<0.001$) accumulation of CAP in tumor tissues after HA-PCL-CAP therapy i.e 49.31±2.13 ng/g at 4 h respectively. Conversely, considerably low levels of CAP were retained in tumor organ at 4 h (31.15±3.27 ng/g) and over a period of 12 h (11.67±1.35 ng/g) in case of PCL-CAP treated group. Approximately, a 5 fold improved accumulation of CAP in tumor tissues was observed when compared with free CAP at all the time points. This indicated that CAP retains in tumor locality over a long span of time. The interaction and accumulation of the HA modified NPs with overexpressed CD44 receptors present in lung tumor cells was thus stipulated. This further evidences the ability of HA functionalized NPs to localize specifically into the tumor tissue when compared to free CAP, indirectly suggesting its reduced entry into other vital organs. This property could be beneficial in reduced toxicity to non-targeted tissues with enhanced payload at targeted site. This also evidences the utilization of overexpressed factors that facilitates drug uptake into the cancer cells.

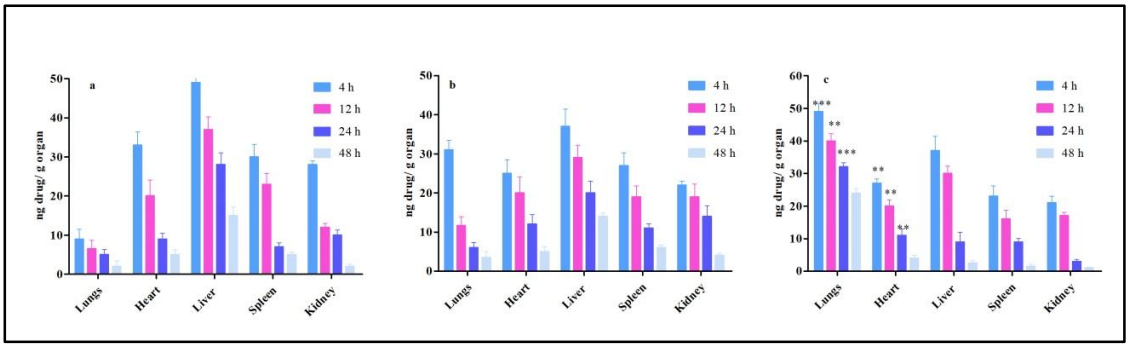

Figure3.10. Biodistribution of CAP in various organs (a) Plain CAP (b) PCL-CAP and(c) HA-PCL-CAP through tail vein (20 mg/kg CAP equivalent dose) [Values are presented as Mean ± SD (n=6); *** $p<0.001$ as compared to CAP and PCL-CAP]

3.12.*Western analysis*

Western blot analysis was performed to further elucidate the possible mechanisms underlying the superior antitumor effect of HA functionalized NPs. The results of our study (**Figure3.11 a&b**) indicate varied influences on the expression of different pro-apoptotic (BAX, Caspase-9) and anti-apoptotic (Bcl-2 and MMP-9) proteins. Concomitantly, an upregulation of pro-apoptotic proteins and down regulation of anti-apoptotic proteins was displayed subsequent to HA-PCL-CAP therapy. The results of immunoblots suggested that HA-PCL-CAP was intimately involved in the process of enhanced cell apoptosis. The western analysis revealed that the treated groups restored various markers toward normal levels when compared with toxic group, positively indicating apoptosis (**Figure3.11b**). Moreover, therapy through HA-PCL-CAP produced the higher restoration of the anti-apoptotic and pro-apoptotic markers in comparison to the plain CAP ($p<0.05$) evidencing its superiority over plain CAP. The result suggested that therapy through HA functionalized NPs competently restricted the lung carcinoma cell proliferation and invasion in the cancer-induced animals. Further, it has been demonstrated that the aforementioned proteinsare significant factors for proliferation and invasion of lung carcinoma.

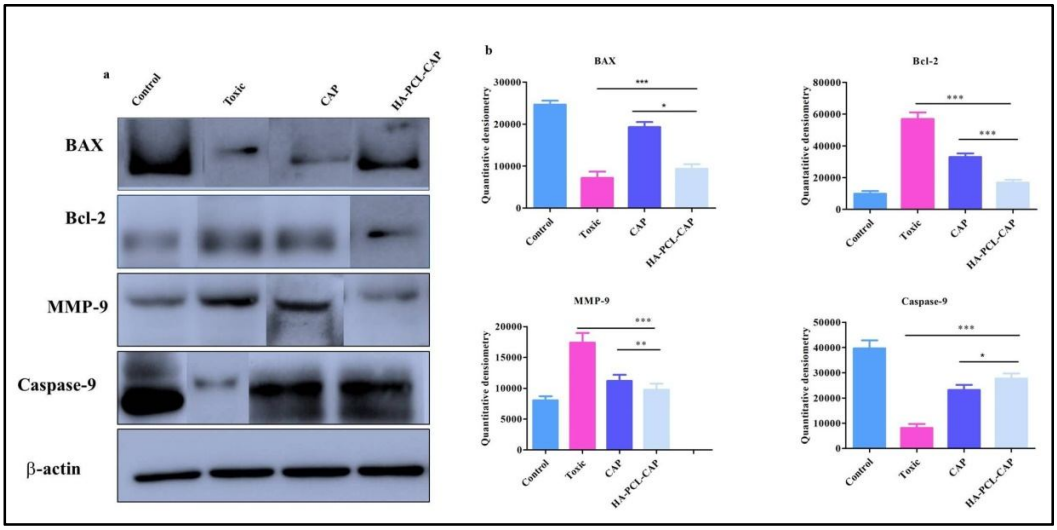

Figure3.11. (a) Immunoblot representing the regulation of mitochondria associated apoptosismodulating proteins isolated from lung tumor tissue of individual groups. (b) Level of proteins *viz.* BAX, caspase-9, bcl-2 and MMP-9, extracted for individual groups *i.e.* Control, toxic control, CAP and HA-PCL-CAP therapy. β-Actin was used as loading control. [Values are presented as Mean ± SD (n=3). The test groups were compared to the toxic group (*$p<0.05$, **$p<0.01$, ***$p<0.001$).]

3.13. Stability Studies

This study was designed to investigate the storage stability of the developed HA-PCL-CAP NPs over a prolonged period. The HA-PCL-CAP NPs was stored under refrigeration (4±1℃) and ambient temperatures (25±5℃) and their stability was evaluated at pre-determined time points during 90 daysof study period. The samples were withdrawn at regular intervals and were investigated for particle size, zeta potential and drug loading as the indicators of stability. In our experiment, we found that the particle size, zeta potential and drug loading does not significantly changes after storage up to three months under stipulated conditions, which indicates that the developed formulations were stable over the experimental period. The data is presented in **Table 3.4**.

Table 3.4. Stability study data (in respect of particle size, zeta potential and percent drug loading) of HA-PCL-CAP for 3 months at 25℃ ± 2 ℃ and 4 ℃ ± 1 °C.

Sr. No.	Sampling Interval (Days)	Particle Size (nm)		Zeta Potential (mV)		% Drug Loading	
		25 ℃ ± 5 ℃	4 ℃ ± 1 ℃	25℃±5℃	4℃±1℃	25℃±5℃	4℃ ± 1℃
1	0	194±2.90	194±2.90	-27.87 ± 3.21	-27.87± 3.21	13±0.37	13±0.37
2	30	197.5±3.21	195.6 ± 2.90	-26.10 ± 2.89	-27.13± 4.30	13±1.22	13±0.54
3	60	201.6±4.22	199.4 ± 3.82	-25.9 ± 0.90	-26.5± 0.99	12.5±1.30	12.9±0.15
4	90	203±1.99	201.5 ± 1.36	-25.6 ± 1.54	-25.9± 0.51	12.2±0.94	12.89±0.74

3.14. Discussion

PCL is a hydrophobic, biocompatible and biodegradable polymer which has been successfully utilized as carrier systems. Effective and safe chemotherapy as well as low toxicity are the foremost concern for management of cancer therapy. Addressing these issues, numerous attempts have been made for development of effective delivery systems for natural anticancer agents (Tiwari et al. 2012). However, itis a challenging task to develop an effective delivery system for such natural agents (Mahato et al. 2011, Ng et al. 2013). Xenobiotics, comprising phytopharmaceutical agents are expelled out from the cells due to efflux pumps present in prokaryotes and eukaryotes, leading to sub-therapeutic concentrations at desired site (Deeley et al. 2006). Formulating them as surface modified, receptor specific, nanoformulations can lead to improved internalization into the targeted cells. As a result, better interaction and rapid uptake by overexpressed factors due to presence of targeting moiety, is seen(Gottesman et al. 2002).

In the present study, anticancer potential of CAP has been investigated for impeding urethane-induced lung carcinoma. PCL has a fast releasing profile. Thus, release was modified, by incorporating CH surface coating over PCL NPs that control the release of NPs and overcomethe limitations of PCL delivery (Sahay et al. 2015). Furthermore HA anchoring facilitates cellular internalization overcoming efflux mediated expulsion.

Factorial design aids in selection and proper outputs for respective variables in designing a most suitable nanocarriers system.The process adopted in formulation yielded PCL NPs within the nano range having low polydispersity index indicating the system to be homogenous. The <0.5 value of PDI indicated a narrow size distribution of particle size in the system. The developed PCL NPs were characterized for their size, surface charge, percent drug loading and entrapment efficiency (Semete et al. 2010). The particle size of HA-PCL-CAP and PCL-CAP NPs was found to be 194±2.90nm and 187±1.32 nm respectively which was found to be in the desirable range for targeted delivery. A slight increase in particle size in HA-PCL-CAP was observed which could be due to the multilayer coat of CH. The gradual slight decrease in entrapment efficiency may be attributed to the loss of free drug present on the surface during fabrication steps which lead to drug loss. PCL-CAP and HA-PCL-CAP displayed zeta potential values of -21.34±0.21 and -27.87±3.21 mV whereas a shift of zeta potential towards the positive side was seen after CH

coating from -21.34±0.21 to 15.72±0.37 mV respectively. However, the positive zeta potential after HA coating was shifted again towards the negative side due to HA and the effective charge on HA-PCL-CAP surface was found to be -27.87±3.21 mV. The CH coated (modified and unmodified) formulations exhibited a slow release in the later stage because of the slower penetration of dissolution media into the multiple polymeric layers resulting in slow erosion of the polymer, and the drug was made available for dissolution only after the polymeric layers erodes. This was further proven by Higuchi fit model, which indicates that the release was diffusion controlled. From these results, the possible mechanism of the drug release from PCL nanoparticles can be that dissolution media enter into polymeric matrix of the NPs through pores, gradually dissolving the drug and finally releasing it into the dissolution media (Gao et al. 2017, Singh et al. 2017).

Four parameters *vis-à-vis* enhanced cellular uptake, reduced cell viability, depressed IC_{50} and higher drug payload in tumor tissue in case of modified NPs is attributed to HA functionalization. It has been reported that surface modification of NPs with hydrophilic polymers culminates in improved cellular uptake and permits them to escape the opsonization process, regardless of their particle size (Parveen et al. 2011, Hosseinzadeh et al. 2012). This could be due to repetitive circulation and opsonizing RES uptake, which enables NPs to be taken up by cancer cells owing to overexpression of CD44. These NPs specifically enter into tumors due to enhanced permeability and retention (EPR) effect typical of nanosize. Also, the specific binding to CD44-receptor leads to reduced expectation of efflux expulsion. Additionally, the hyaluronidase-1 (Hyal-1) is widely distributed in the acidic tumor extracellular matrix, which degrades HA coating and the drug is delivered into tissues and cells (Bhattacharjee 2016). The higher cytotoxicity can be attributed to the fact that modified NPs enter the cells through HA receptor-mediated endocytosis resulting in higher accumulation within the cells.

In view of high toxicity and resistance development associated with chemotherapy, the use of natural agent having chemotherapeutic potential holds promise. Further, the developed HA functionalized CAP NPs were investigated for their therapeutic efficacy as well as targeting potential. It has been reported in previous literature that CAP possesses apoptosis producing potential through inhibition of NF-κ activation via hindering its nuclear migration

leading to apoptosis. Subsequently, tumor necrosis factor-α–stimulates the degradation of IκBα, a factor associated with the inhibiting proteasome activity (Zhang et al. 2017). CAP is known to alter the generation of reactive oxygen species by inhibition of the NADH dependent plasma membrane electron transport system with a consequent disruption of mitochondria trans-membrane potential (Kim et al. 2015).These altered ROS and peroxynitrite levels result in inhibition of NADH oxidase activity in cancer cells.This wasclearly supported by the results of ROS and MMP analysis in our study. Another underlying mechanism of enhanced apoptosis, is the property of CAP to produce heat-sensation over cancer cells, mediated by the transient receptor potential vanilloid 1 (TRPV1) receptor (Reyes-Escogido et al. 2011). This mechanism causes amplified sensitivity of cancer cells, because of which they respond better to the chemotherapeutic agents resulting in enhanced apoptosis.

The results of western analysis of our study are in good agreement with the ability of CAP to induce DNA damage through an up regulation of pro-apoptotic proteins BAX suggesting that this could be one reason for enhanced apoptosis. To further address the underlying mechanism of this enhanced cell apoptosis, the activity of MMP-9 expression was examined in tumor tissue via western analysis. These findings indicate that HA-PCL-CAP therapy restricts cancer cell invasion by suppressing MMP-9 activity. The results indicate down regulation of MMP-9, which could be a primary reason for reduced tumor volume and improved survival of animals in the groups receiving HA-PCL-CAP NPs (Yang et al. 2013).

Oxidative stress markers viz., SOD, TBARS, GSH, catalase etc. strongly evidence diminished oxidative stress supporting antioxidant potential of CAP which could be attributed to antioxidant potential of CAP. Histopathological results also evidenced supremacy of HA-PCL-CAP NPs over other therapy through plain CAP and PCL-CAP, which could be attributed to enhanced targeting potential of HA as well as the property of CAP to cut oxidative stress (Reyes-Escogido et al. 2011). As described in preceding studies, intracellular ROS accumulation, consecutive inactivation of Akt pathway, and the successive alteration of apoptotic regulated proteins can trigger the apoptotic cascade resulting in improved therapeutic outcome (Joe et al. 1994). The biodistribution studies further strengthen the evidences for targeting potential of HA anchored NPs into tumor. This may be explained on the basis of the presence of CD44 receptors on tumor tissues that

favored discriminatory entry of HA-PCL-CAP in tumors. The stability study of HA-PCL-CAP NPs indicates that the opted method for formulating and optimization of NPs was accurate and precise. The possible reason for stability of formulation with respect to particle size, zeta potential and drug loading could be attributed to the HA and CH coat over the PCL(Khan et al. 2013). Newer promising natural agents could also be investigated for formulating targeted modules in future studies. Further, formulating them as modified NPs enables better interaction with biological membranes, enhanced targeting potential and higher drug payload in the tumor cells.

3.15. Conclusions

Surface functionalized PCL nanoparticles containing CAP were successfully developed, which were anchored with HA for tumor targeting. The HA-PCL-CAP NPs ascertained potential in treating NSCLC and exhibited enhanced cytotoxic, anti-proliferate and apoptotic attributes of CAP in A549 lung cancer cells. HA-PCL-CAP NPs displayed significant decrease in tumor development and restoration of oxidative stress markers, when compared with plain CAP and PCL-CAP NPs. Drug release comparisons demonstrated a sustained release pattern of HA modified NPs.The results of *in vivo* studies and western immunodensity suggested that the developed nano-formulation has potentiated the therapeutic effect of CAP. Further, biodistribution studies suggested higher drug payload and targeting potential of HA functionalized NPs into the cancer tissues. From the above confirmations, it can be concluded that the proliferative and migratory effects of urethane-induced lung carcinoma are reduced through HA-PCL-CAP NPs by means of activation the mitochondrial-mediated apoptotic pathway and down- regulation of anti-apoptotic proteins. The insights gained give hope for possible strategies which could benefit in development of such formulations which can be further translated from bench to bedside. This could offer a substitute to the conventional formulations in management of lung carcinoma therapy. Further, the translational potential of this drug delivery system could prove favorable for patients after appropriate clinical assessments, as future scope.

REFERENCES

Agrawal, S., H. Ahmad, M. Dwivedi, M. Shukla, A. Arya, K. Sharma, J. Lal and A. K. Dwivedi (2016). "PEGylated chitosan nanoparticles potentiate repurposing of ormeloxifene in breast cancer therapy." Nanomedicine**11**(16): 2147-2169.

Bhattacharjee, S. (2016). "DLS and zeta potential–What they are and what they are not?" Journal of Controlled Release**235**: 337-351.

Chakraborty, S., A. Adhikary, M. Mazumdar, S. Mukherjee, P. Bhattacharjee, D. Guha, T. Choudhuri, S. Chattopadhyay, G. Sa and A. Sen (2014). "Capsaicin-induced activation of p53-SMAR1 auto-regulatory loop down-regulates VEGF in non-small cell lung cancer to restrain angiogenesis." PloS one**9**(6): e99743.

Chen, S., X. Zhao, J. Chen, J. Chen, L. Kuznetsova, S. S. Wong and I. Ojima (2010). "Mechanism-based tumor-targeting drug delivery system. Validation of efficient vitamin receptor-mediated endocytosis and drug release." Bioconjugate chemistry**21**(5): 979-987.

Deeley, R. G., C. Westlake and S. P. Cole (2006). "Transmembrane transport of endo-and xenobiotics by mammalian ATP-binding cassette multidrug resistance proteins." Physiological reviews**86**(3): 849-899.

Gao, S., J. Wang, R. Tian, G. Wang, L. Zhang, Y. Li, L. Li, Q. Ma and L. Zhu (2017). "Construction and Evaluation of a Targeted Hyaluronic Acid Nanoparticle/Photosensitizer Complex for Cancer Photodynamic Therapy." ACS applied materials & interfaces**9**(38): 32509-32519.

Gao, X., J. Zhang, Q. Xu, Z. Huang, Y. Wang and Q. Shen (2017). "Hyaluronic acid-coated cationic nanostructured lipid carriers for oral vincristine sulfate delivery." Drug development and industrial pharmacy**43**(4): 661-667.

Gottesman, M. M., T. Fojo and S. E. Bates (2002). "Multidrug resistance in cancer: role of ATP–dependent transporters." Nature Reviews Cancer**2**(1): 48.

Guo, C.-L., H.-Y. Chen, B.-L. Cui, Y.-H. Chen, Y.-F. Zhou, X.-S. Peng and Q. Wang (2015). "Development of a HPLC method for the quantitative determination of capsaicin in collagen sponge." International Journal of Analytical Chemistry**2015**.

Hosseinzadeh, H., F. Atyabi, R. Dinarvand and S. N. Ostad (2012). "Chitosan–Pluronic nanoparticles as oral delivery of anticancer gemcitabine: preparation and in vitro study." International journal of nanomedicine**7**: 1851.

Hsiao, K. Y., Y.-J. Wu, Z. N. Liu, C. W. Chuang, H. H. Huang and S. M. Kuo (2016). "Anticancer effects of sinulariolide-conjugated hyaluronan nanoparticles on lung adenocarcinoma cells." Molecules**21**(3): 297.

Joe, B. and B. Lokesh (1994). "Role of capsaicin, curcumin and dietary n—3 fatty acids in lowering the generation of reactive oxygen species in rat peritoneal macrophages." BBA-Molecular Cell Research**1224**(2): 255-263.

Kaithwas, G. and D. K. Majumdar (2012). "In vitro antioxidant and in vivo antidiabetic, antihyperlipidemic activity of linseed oil against streptozotocin-induced toxicity in albino rats." European Journal of Lipid Science and Technology**114**(11): 1237-1245.

Khan, N., D. J. Bharali, V. M. Adhami, I. A. Siddiqui, H. Cui, S. M. Shabana, S. A. Mousa and H. Mukhtar (2013). "Oral administration of naturally occurring chitosan-based nanoformulated green tea polyphenol EGCG effectively inhibits prostate cancer cell growth in a xenograft model." Carcinogenesis**35**(2): 415-423.

Kim, S. M., E. Y. Oh, J. H. Lee, D. Nam, S. G. Lee, J. Lee, S. H. Kim, B. S. Shim and K. S. Ahn (2015). "Brassinin Combined with Capsaicin Enhances Apoptotic and Anti-metastatic Effects in PC-3 Human Prostate Cancer Cells." Phytother Res.**29**(11): 1828-1836.

Lee, E.-R., Y.-J. Kang, H.-Y. Choi, G.-H. Kang, J.-H. Kim, B.-W. Kim, Y. S. Han, S.-Y. Nah, H.-D. Paik and Y.-S. Park (2007). "Induction of apoptotic cell death by synthetic naringenin derivatives in human lung epithelial carcinoma A549 cells." Biological and Pharmaceutical Bulletin**30**(12): 2394-2398.

Li, J., M. Huo, J. Wang, J. Zhou, J. M. Mohammad, Y. Zhang, Q. Zhu, A. Y. Waddad and Q. Zhang (2012). "Redox-sensitive micelles self-assembled from amphiphilic hyaluronic acid-deoxycholic acid conjugates for targeted intracellular delivery of paclitaxel." Biomaterials**33**(7): 2310-2320.

Mahato, R. I. and A. S. Narang (2011). Pharmaceutical dosage forms and drug delivery, CRC Press.

Muralidharan, R., J. Panneerselvam, A. Chen, Y. D. Zhao, A. Munshi and R. Ramesh (2015). "HuR-targeted nanotherapy in combination with AMD3100 suppresses CXCR4 expression, cell growth, migration and invasion in lung cancer." Cancer gene therapy**22**(12): 581.

Najlah, M., Z. Ahmed, M. Iqbal, Z. Wang, P. Tawari, W. Wang and C. McConville (2017). "Development and characterisation of disulfiram-loaded PLGA nanoparticles for the treatment of non-small cell lung cancer." European Journal of Pharmaceutics and Biopharmaceutics**112**: 224-233.

Ng, V. W. L., X. Ke, A. L. Lee, J. L. Hedrick and Y. Y. Yang (2013). "Synergistic Co-Delivery of Membrane-Disrupting Polymers with Commercial Antibiotics against Highly Opportunistic Bacteria." Advanced Materials**25**(46): 6730-6736.

O'brien, J., I. Wilson, T. Orton and F. Pognan (2000). "Investigation of the Alamar Blue (resazurin) fluorescent dye for the assessment of mammalian cell cytotoxicity." The FEBS Journal**267**(17): 5421-5426.

Pandey, M., S. Sultana and K. P. Gupta (2014). "Involvement of epigenetics and microRNA-29b in the urethane induced inception and establishment of mouse lung tumors." Experimental and molecular pathology**96**(1): 61-70.

Parashar, P., M. Rathor, M. Dwivedi and S. A. Saraf (2018). "Hyaluronic Acid Decorated Naringenin Nanoparticles: Appraisal of Chemopreventive and Curative Potential for Lung Cancer." Pharmaceutics**10**(1): 33.

Parveen, S. and S. K. Sahoo (2011). "Long circulating chitosan/PEG blended PLGA nanoparticle for tumor drug delivery." European journal of pharmacology**670**(2-3): 372-383.

Perry, S. W., J. P. Norman, J. Barbieri, E. B. Brown and H. A. Gelbard (2011). "Mitochondrial membrane potential probes and the proton gradient: a practical usage guide." Biotechniques**50**(2): 98.

Reyes-Escogido, M. d. L., E. G. Gonzalez-Mondragon and E. Vazquez-Tzompantzi (2011). "Chemical and pharmacological aspects of capsaicin." Molecules**16**(2): 1253-1270.

Sahay, S., P. Tiwari and K. P. Gupta (2015). "Onset of the lymphocytic infiltration and hyperplasia preceding the proliferation in F1 mouse lungs from the N-ethyl-N-nitrosourea exposed mothers: Prevention during the lactation period by inositol hexaphosphate." Toxicology reports**2**: 590-599.

Semete, B., L. Booysen, L. Kalombo, J. D. Venter, L. Katata, B. Ramalapa, J. A. Verschoor and H. Swai (2010). "In vivo uptake and acute immune response to orally administered chitosan and PEG coated PLGA nanoparticles." Toxicology and applied pharmacology**249**(2): 158-165.

Singh, N., P. Parashar, C. B. Tripathi, J. Kanoujia, G. Kaithwas and S. A. Saraf (2017). "Oral delivery of allopurinol niosomes in treatment of gout in animal model." Journal of liposome research**27**(2): 130-138.

Tiwari, G., R. Tiwari, B. Sriwastawa, L. Bhati, S. Pandey, P. Pandey and S. K. Bannerjee (2012). "Drug delivery systems: An updated review." International journal of pharmaceutical investigation**2**(1): 2.

Vangara, K. K., J. L. Liu and S. Palakurthi (2013). "Hyaluronic acid-decorated PLGA-PEG nanoparticles for targeted delivery of SN-38 to ovarian cancer." Anticancer research**33**(6): 2425-2434.

Wang, T., J. Hou, C. Su, L. Zhao and Y. Shi (2017). "Hyaluronic acid-coated chitosan nanoparticles induce ROS-mediated tumor cell apoptosis and enhance antitumor efficiency by targeted drug delivery via CD44." Journal of nanobiotechnology**15**(1): 7.

Wickens, J. M., H. O. Alsaab, P. Kesharwani, K. Bhise, M. C. I. M. Amin, R. K. Tekade, U. Gupta and A. K. Iyer (2017). "Recent advances in hyaluronic acid-decorated nanocarriers for targeted cancer therapy." Drug discovery today**22**(4): 665-680.

Yang, J., T. Li, G. Xu, B. Luo, Y. Chen and T. Zhang (2013). "Low-concentration capsaicin promotes colorectal cancer metastasis by triggering ROS production and modulating Akt/mTOR and STAT-3 pathways." Neoplasma**60**(4): 364-372.

Zhang, J.-Y., Z.-G. Shen, J. Zhong, T.-T. Hu, J.-F. Chen, Z.-Q. Ma and J. Yun (2006). "Preparation of amorphous cefuroxime axetil nanoparticles by controlled nanoprecipitation method without surfactants." International journal of pharmaceutics**323**(1-2): 153-160.

Zhang, S.-s., Y.-h. Ni, C.-r. Zhao, Z. Qiao, H.-x. Yu, L.-y. Wang, J.-y. Sun, C. Du, J.-h. Zhang and L.-y. Dong (2017). "Capsaicin enhances the antitumor activity of sorafenib in hepatocellular carcinoma cells and mouse xenograft tumors through increased ERK signaling." Acta Pharmacologica Sinica.

Chapter IV

Folic Acid Conjugated Nanoparticles

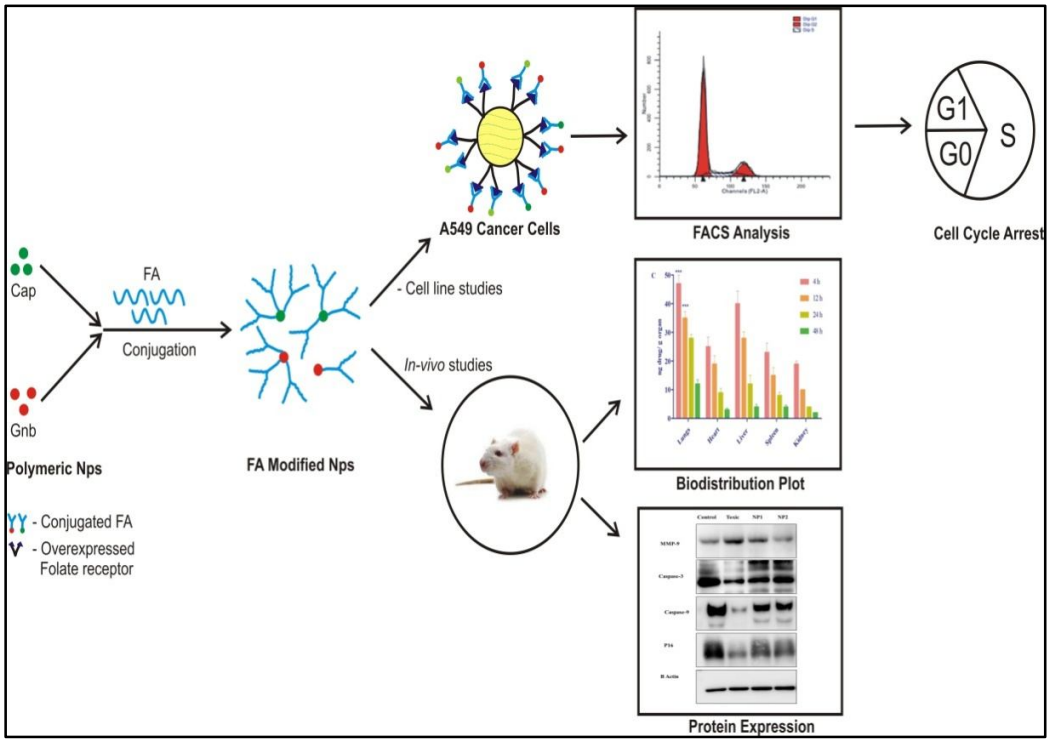

4. Development and Characterizationof Folic acid Conjugated PLGA Nanoparticles of Capsaicin and Gefitinib

4.1 Introduction

Polymeric PLGA nanoparticles possess various desirable properties such as biocompatibility, tailored biodegradation rate, facile surface modification for desirable delivery and interaction with biological membranes and are approved for clinical use in humans (Houston et al. 2014).Preceding investigations have stated such surface modified NPs to have remarkable capability of improved cellular uptake and specificity in reaching tumor cells/tissues (Soppimath et al. 2001). Thus, surface engineered NPs could be an alternative technique for targeted delivery to tumor cells which may increasetherapeutic efficacy and reduce toxicity during cancer therapy.Also, being nanosized, they may bypass the reticuloendothelial system (RES) uptake,leading to repeated circulation in the blood stream(Vangara et al. 2013). Folic acid (FA) is widely used in the delivery of anticancer drugs due to its small size, low price, high tumor tissue specificity and non-immunogenic nature. The other important reason for folic acid (FA) surface modificationis its interaction with overexpressed folate receptors present over the surface of cancer cells as they require a surplus amount of such nutrients and vitamins for their growth and proliferation (Brigger et al. 2002, Guo et al. 2015, Kouchakzadeh et al. 2017). This causes rapid uptake of FA modified NPs leading to selective deliveryto the targeted site and prevention of undesirable toxic effects of the drug on non-targeted cells/tissues(Muralidharan et al. 2016).

The chief spicy component of chili peppers,capsaicin (Cap) (trans-8methyl-N-vanillyl-6-nonenamide),belongs to the genus *Capsicum annum.* Ithas been reported to be bestowedwith several medicinal properties(Surh et al. 1996). It is a derivative of homovanillic acid and is being recounted to inherit anticancer and anti-proliferativepotential. It also possessesanalgesic, antioxidant, anti-inflammatory and anti-obesityproperties.Caphas been broadly studied for a variety of cancers including lung carcinoma (Kim et al. 2015).

Gefitinib (Gnb), is a tyrosine kinase inhibitor which holds a high affinity towards epithelial growth factor receptor (EGFR) which is over expressed in lung cancer (LC) (Chen et al. 2017). Gnb is capable of inhibiting angiogenesis, metastasis and induce apoptosis in LC

tumor cells(Ni et al. 2017). It mainly acts by competitive binding of Mg-ATP situated on the catalytic domain of EGFR-TK (Epidermal growth factor receptor tyrosine kinase) resulting in activation of mitogen activated protein kinase, leading to blocking of the signal transmission(Wang et al. 2015). Extensive circulation of Gnb in the body leads to an almost equal concentration of drug in healthy as well as cancer cells. This results in severe drug-related toxicity in normal cells whereas resistance may develop in cancer cells due to limited sub therapeutic exposure to the drug. If the dose is increased to a concentration which does not allow resistance to develop in the cancer cells, the toxicity in healthy cells would increase even further. Thus, it leads to vicious cycle.

This chapter envisioned on the development and characterization ofCap/Gnbloaded Folic acid (FA) modified PLGA(poly(lactic-co-glycolic acid)) nanoparticles. The present study is aimed at themethodical development and in-depth evaluation of folic acid conjugated PLGA nanoparticles for the selective delivery of Gefitinib (Gnb) and Capsaicin (Cap) to lung cancer cells, utilizing synergetic approach.The feasibility of co-administration of Gnb and Cap loaded in separate NPs as a therapeutic system against LC is being explored. The Cap/Gnb loaded FA conjugated NPs were developed utilizing oil in water emulsion technique and optimized through central composite design (CCD) to achieve enhanced and specific delivery specially to cancer cells. The FA conjugated NPswere systematically characterized for various parameters viz.particle size, zeta potential, *in vitro* release. The cytotoxicity and cell cycle analysis was performed on A549 cells. The formulations were also evaluated for their therapeutic potential *in vivo* in urethane-induced lung carcinoma in rat model.

4.2 Materials

Gefitinib (Gnb) was obtained as a generous gift from M/s United Biotech, Solan, India. Capsaicin was purchased from M/s Vandeep Suppliers Pvt. Ltd, Kolkata, India. PLGA polymers, i.e. PLGA 50:50 (d, l-lactide :glycolide), molecular weight 40,000-75,000 Da, was obtained as a gift sample from Evonik India Pvt. Ltd, Mumbai, India. Polyvinyl alcohol (PVA) and folic acid were procured from Sigma Chemicals (St Louis, MO, USA). N-hydroxysuccinimide (NHS), N,N'-Dicyclohexylcarbodiimide (DCC), Poly(ethylene glycol) bis (amine) (PEG-bisamine, MW 3.4kDa), 2-mercaptoethanol, Propidium Iodide, RNase A, DMEM (Dulbecco's Modified Eagle's medium), Fetal Bovine Serum (FBS) (previously

heat-inactivated), tris-buffered saline (TBS) and tween 20 (TBST), MTT (3-(4,5-Dimethylthiazol-2-yl)-2,5-diphenyl tetrazolium bromide), Nonidet P-40 (NP-40s) were purchased from M/s SigmaAldrich, USA. Di-methyl Sulfoxide (DMSO) and dichloromethane were obtained from Fisher Scientific (Pittsburgh, PA, USA). All antibodies were purchased from M/s Santa Cruz, CA, USA. All other chemicals used in the study were of analytical grade. In-house double distilled water was used throughout the experiment.

4.2.1. Animals

The *in vivo* study was performed according to the Declaration of Helsinki as amended in Seoul 2008 for humans and the European Community guidelines as accepted principles for the use of experimental animals and approved by the Institutional Animal Ethics Committee as per approval number SDCOPVS/AH/CPCSEA/01/0028. Albino wistar rats (male/female, seven-week-old) were fed with synthetic pellet diet (M/S Provimi Animal Nutrition India Pvt. Ltd. Bangalore) and water ad libitum. Animals were kept in polypropylene cages in a well-ventilated animal house at temperature 22°C±2°C. Animals were divided into 06 groups having 9 animals each, under a 12 h light/ dark cycle, and acclimatized for 2 weeks. All animals were handled as per institutional animal ethics norms, and care was taken that all guidelines were followed with a human approach.

4.2.2.Cell Lines

Human non-small-cell lung carcinoma (NSCLC) cell lines (A549) were obtained from American Type Culture Collection (ATCC, Rockville, MD, USA). Cells were maintained in appropriate culture medium in Dulbecco's Modified Eagle's Medium (DMEM) supplemented with 10%w/v fetal bovine serum and 1%w/v antibiotic (penicillin) solution. A549 cells were maintained at 37°C with 5% CO_2 in an incubator(Parashar et al. 2018).

4.3. Methods

The conjugation of folic acid to the polymer PLGA was done in three steps as per scheme 1-3 (Figure 4.1)

4.3.1. Preparation of Folate NHS ester

The active ester of FA was formulated according to previously reported method(Yoo et al. 2004, Boddu et al. 2012)**.** Folic acid (308.7 mg, 0.70mmol) and triethylamine (0.15 mL, 1.0 mmol) were dissolved in 10 mL dry dimethyl sulfoxide (DMSO), to which DCC (144.4 mg, 0.70mmol) was added. The mixture was stirred for 1 h at room temperature under dark condition, and NHS (115 mg, 1.0 mmol) was added. The reaction was stirred overnight at room temperature in the dark. The dicyclohexylureaprecipitate (a side product of the reaction) was filtered via glass wool and folate-NHS ester was precipitated using diethylether. The yellow precipitate (active ester of folic acid) was filtered, washed several times with dry tetrahydrofuran, dried under vacuum, and stored as a yellow powder (**Scheme 1)**.

4.3.2.Activation of PLGA

PLGA (100 mg, 0.002mmol) was dissolved in DMSO and DCC (0.5 mg, 0.002mmol) (PLGA: DCC, 1:1 molar ratio) was added to it with subsequent stirring in dark for 12 h to complete the reaction. Thereafter, PEG-bis-amine (18 mg, 0.006mmol) (PLGA:DCC:PEG-bis-amine, 1:1:3 molar ratio) was added to the above mixture and the reaction was completed under continuous stirring for 3 h to obtain PEG-amino PLGA*i.e.*, PLGA-PEG-NH_2 (**Scheme 2**). The dicyclohexylurea precipitate, by product of reaction, was filtered via glass wool and the filtrate was precipitated using diethylether and dried under vacuum to collect PLGA-PEG-NH_2.

4.3.3. Folate conjugated PLGA Nanoparticles

Folate-NHS ester (25 mg/mL) suspended in phosphate buffer saline (PBS pH 7.4) was poured in equimolar ratio into activated PLGAfor folic acid conjugation as per **Scheme 3**. This mixture was stirred gently overnight at room temperature. To complete the reaction, 2-mercaptoethanol (10 mmol) was added into the above mixture. Subsequently, folate

conjugated PLGA wasdialyzed (12–14 kDa MWCO) to remove unreacted 2-mercaptoethanol and folate-NHS ester

4.3.3.1. FTIR characterization

Synthesis of folate NHS, PLGA-PEG-NH_2 was confirmed by FTIR spectra. The samples were preparedby compressingsamples (freeze dried)withKBr in 1: 100 ratios to get a thin transparent pellet using a hydraulic press. The characteristics peak confirming conjugation of folate to PLGA (PLGA-PEG-FA) was recordedthroughFTIR (Perkin Elmer FT-IR Spectrometer) (He et al. 2015).

4.3.3.2. ^{1}H-NMR characterization

The conjugation of folate to PLGA through PEG was characterized through ^{1}H-NMR spectroscopy (BrukerAvance 400, FT-NMR) using DMSO-D6 as solvent. Chemical shifts (δ) were expressed as parts per million (ppm) relative to the NMR solvent signal (d6-DMSO) using tetramethylsilane (internal standard).

Scheme- 1

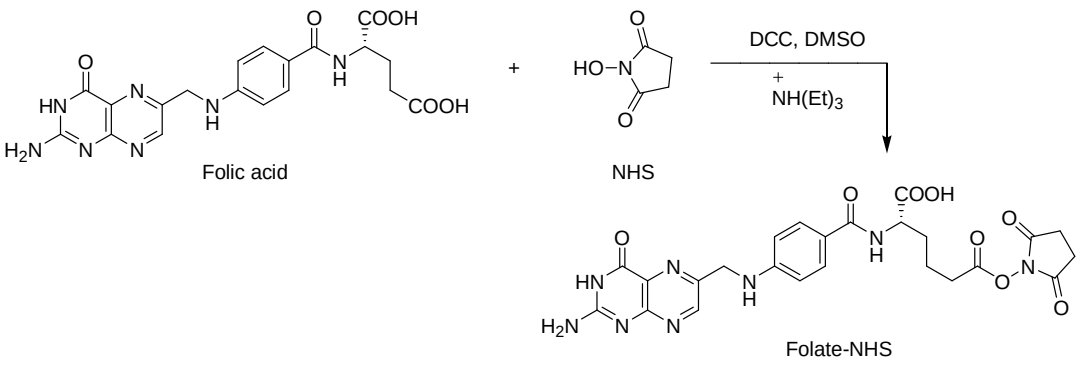

Scheme- 2

Scheme- 3

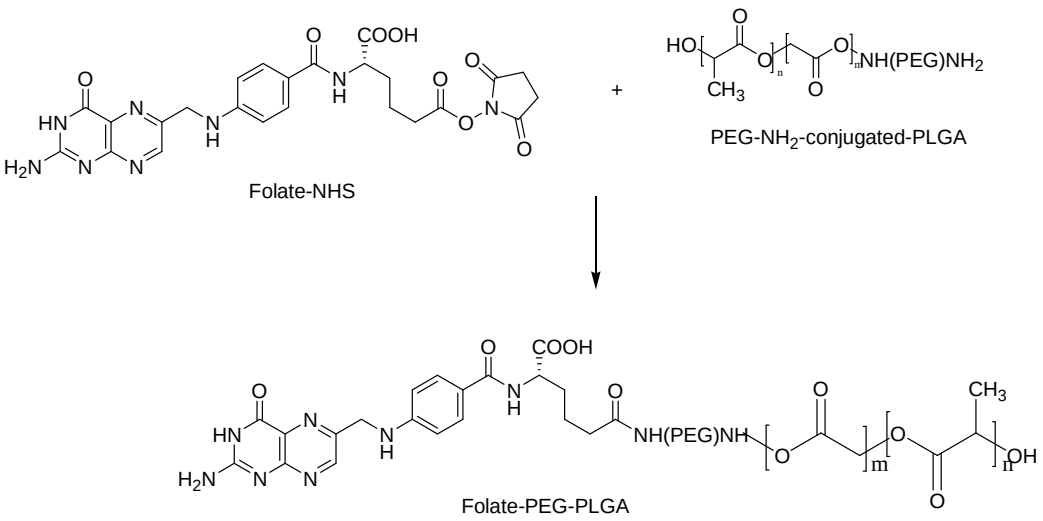

Figure 4.1 Schematic representation of folic acid conjugation synthesis **Scheme 1:** Synthesis of activated folic acid (Folate NHS); **Scheme 2:** Synthesis of PEG-NH_2 conjugated PLGA(PLGA-PEG-NH_2); **Scheme 3:** Synthesis of folate attached PLGA(PLGA-PEG-NH_2).

4.4. Preparation of Gnb-PLGA and Cap-PLGA

Gnb/Cap loaded NPs were prepared using oil in water emulsion technique. Gnb/Cap each was dissolved (separately) in 1 ml chloroform in a 2:1 molar ratio of PLGA. To form o/w emulsion the polymer-drug solution was added to 5 ml of 2.5%v/v aqueous PVA solution under sonication for 5 min at 80% energy, using probe-type sonicator (Labsonic-M, Sartorius Stedium) on an ice bath. The emulsion was stirred overnight, and chloroform was removed by keeping solution under vacuum for 2 h. The mixture was centrifuged at 30,000 rpm for 30 min at 4°C to obtain the NPs in form of a pellet. The pellet was re-suspended in proteomic grade water to remove any excess of PVA and the procedure was repeated thrice(Boddu et al. 2012).

4.4.1. Optimization of Gnb- PLGA and Cap- PLGA NPs

The optimization of NPs was done through central composite design (CCD) to optimize the modified NPs. Polymer:drug ratio (X1) and copolymer PVA (X2) levels were selected on the basis of pre-optimization studies. Overall, a set of 09 experimental runs each were conducted for optimization and data recorded in **Table 4.1** shown in result section. ANOVA (analysis of variance) was applied to find out the significance of the polynomial models and modal terms on the responses and their quantitative effects. Regression equations were established for dependent variables, i.e., Y1, Y2, Y3, and Y4. Response surface analyses were plotted to describe the effects and interaction of two independent variables on the dependent variables.

For nine batches, the various combinations resulted in nanoparticles having particle size ranging from 147-305nm, percentage release 78-88%, drug loading variation from 1.2 to 3.8% and entrapment varying from 35 to 49%.

4.4.2. Preparation of folate conjugated Gnb-PLGA-PEG-FA and Cap-PLGA-PEG-FA NPs

Folate conjugated PLGA NPs were prepared utilizing a similar technique as opted for Gnb-PLGA and Cap-PLGA NPs as described above. The combination of PEG-conjugated PLGA and non-activated PLGA (PLGA-PEG-NH_2 and PLGA in 90:10) was taken for preparation of FA conjugated NPs.

4.4.2.1. Folate content estimation on PLGA-PEG-FA

The FA present on the surface of modified NPs was determined by UV spectrophotometry. The NPs were dissolved in CH_2Cl_2:DMSO in 1:4 ratio and absorbance was recorded at 358 nm. The experiment was performed in triplicate.

4.5. Characterization of Prepared HA-PCL-CAP NPs

4.5.1. Particle size analysis and Zeta potential

The particle size of various modified NPs was determined using laser light scattering-based particle size analyzer (NanoPlus-3, Japan). Study was performed in triplicate, and average values with standard deviation were reported. The samples were reconstituted in phosphate buffer pH 7.4 prior to analysis.

4.5.2. Transmission Electron Microscopy

TEM (H-750, Hitachi, Japan) was employed for analyzing the surface morphology of surface modified Gnb-PLGA-PEG-FA and Cap-PLGA-PEG-FA NPs. The samples were prepared, observed and photographed as described in chapter IIIsections3.4.2.

4.5.3. Entrapment Efficiency (%EE)and Drug loading

Entrapment efficiency was determined by centrifugation method. Formulation (1.5 ml each) was centrifuged (REMI CPR -24) for 15 min at 10,000 rpm at 4°C to separate free drug. The pellet and supernatant were separated. The supernatant was collected to determine free drug present in it. The amount of Gnb in modified NPs was calculated using a standard curve obtained by measuring the UV absorbance (Labtronics LT-2900) of Gnb at a wavelength of 338 nm. Similarly amount of Cap was measured at a wavelength of 279 nm. The Gnb/Cap, loading in NPs was determined by dissolving accurately weighed amounts of NPs (10mg/10ml) into DMSO and concentration was determined by measuring the UV spectrophotometer at wavelength stated above. All the experiments were performed in triplicate. The entrapment efficiency was calculated using formula in equation (i) and drug loading by using formula in equation (ii)

$$\%EE = \frac{W\ initial\ drug - W\ free\ drug}{W\ initial\ drug} X100 \text{.....} \textbf{\textit{(i)}}$$

$$\%DL = \frac{Drug}{(polymer + drug)} X100 \text{.....} \textbf{\textit{(ii)}}$$

4.5.4. In Vitro Dissolution Studies

In-vitro drug release of Gnb/Cap loaded unmodified and modified NPs viz. Gnb-PLGA,Cap-PLGA, Gnb-PLGA-PEG-FA and Cap-PLGA-PEG-FA, was performed through dialysis method using dialysis membrane (Visking tubing, Spectra/Por®, cutoff 12–14 kD). Dialysis membrane was activated with phosphate buffer pH 6.8 for 12 h, prior to experiment. USP dissolution apparatus type-II (Veego, India) was used for performing *in-vitro* release study. The cylinders were filled with 250 mL phosphate buffer maintained at pH 6.8 (containing 0.1% v/v Tween-80) and maintained at 37±0.5°C temperature and 50 rpm. Formulation(s) equivalent to 10 mg of Gnb and 10 mg of Cap (separately) were suspended in 10 mL phosphate buffer (pH 6.8) and filled in the dialysis membrane sac.The sac was tangled to the paddle shaft in such a way that membrane the just touches the dissolution medium surface. The release study was carried out over a period of 80 h and an aliquot of 3ml of the sample was withdrawn from the cylinder at pre-determined time intervals and replacedwith fresh medium. The aliquots were filtered through 0.45 µm membrane filters. Drug concentration was determined spectrophotometrically at 338 nm/279 nm for Gnb and Cap respectively, using UV spectrophotometer (Labtronics LT-2910).The cumulative percent release of modified and unmodified NPs was determined by plotting cumulative percent release as a function of time. All the experiments were conducted in triplicate.

4.5.5. Release Kinetics Modeling

The optimized formulation Gnb-PLGA-PEG-FA and Cap-PLGA-PEG-FA were subjected to graphical treatment to predicting the mechanism of drug release using goodness of data fit

methodology. The obtained *in vitro* release data was analyzed for various kinetic models viz. zero order, first order, Higuchi model, Korsmeyer-Peppas etc.

4.6. *In Vitro* Cell Culture Study

4.6.1. Cell Cytotoxicity Study by MTT Assay

Cytotoxicity of CAP/Gnb was assessed on cancer cells by MTT assay to evaluate the cell viability overA549 cells as described in chapter III section 3.5.1.The cells were treated with various concentrations of CAP, Gnb, Gnb-PLGA, CAP-PLGA, Gnb-PLGA-PEG-FA and Cap-PLGA-PEG-FA ranging from 0 to 50 µM equivalents CAP/Gnb (n=3). For control samples plain PBS was taken and cell were considered as untreated cells. To confirm the synergism, we treated cells with a combination of the two agents in a constant ratio to one another and used CompuSyn software to calculate the combination index (CI) following Chou and Talalay's method.

4.6.2. In vitro Cellular Uptake Study

FACS (Fluorescence activated cell sorter instrument, BD Biosciences, FACS Aria, Germany) was employed for assessing quantitative uptake of drug in A549 (lung cancer) cells so as to explore the effect of FA conjugation on the uptake of NPs. The evaluation of the delivery potential of NPs was done in terms of enhanced cellular uptake of drug in the cancer cells. Gnb-PLGA, Cap-PLGA NPs, FA conjugated NPs were tested to compare the uptake percentage among the various modified and unmodified NPs. FITC loaded NPs were taken as control. A549 cells were cultured in 96 well plates containing fresh DMEM media in a similar manner as described in MTT assay and incubated in a CO_2 incubator over a period of 24 h maintained at 37°C. Thereafter, the cells were treated with FITC labeled Gnb-PLGA-PEG-FA, Cap-PLGA-PEG-FA, Gnb-PLGA and Cap@Gnb-PLGA-PEG-FA for 4 h. At the end of incubation period, the cells were washed with PBS thrice and analyzed by flow cytometric analysis at an excitation wavelength of 480 nm and an emission wavelength of 550 nm.

4.6.3. Cell proliferation studies

The cell proliferation assay of various formulation was performed utilizing Alamar blue® reduction method as perdetails described in chapterIIIsection 3.5.3. The cells were treated with various formulations at sub IC_{50}concentration equivalent of CAP/Gnb for 24 h.

4.6.4. Mitochondrial membrane potential assay (MMP) and Reactive Oxygen Species (ROS) generation analysis

Mitochondrial membrane potential assay was conducted employing dye Rhodamine 123 (Rh-123) on specified A549 cells. ROS generation was analyzed employing DCFDA dye. The experiments were conducted as per method described in chapter III section 3.5.4

4.6.5.Cell Cycle Arrest through Fluorescence-Activated Cell Sorting

Cell cycle arrest by various formulations of Gnb, Cap and Gnb combined with Cap was evaluated to estimate synergistic effect in NSCLC using propidium iodide method through flow cytometry (BD FACS Array).The specified A549 cell lines were plated in a 96-well plate having density of $1X10^6$ cells/well. The cells were exposed to Gnb, Gnb-PLGA, Gnb-PLGA-PEG-FA and Cap@Gnb-PLGA-PEG-FA, over a period of 48h. For conducting the study, cells were grown in PBS (phosphate buffer saline) followed by fixation using 70% cold ethanol for 30 min at 4°C. Thereafter the cells were washed twice with PBS. The obtained cells were centrifuged at 850g for 15 min using cold centrifuge (REMI CPR -24). Lysis of cells was done using ribonuclease (50 µl of a 100 µg/ml stock of RNase). After addition of 200 µl propidium iodide histograms for side scatter and forward scatter were obtained and analyzed. The samples were analyzed at a low flow rate of 500 events/second.

4.7. *In vivo* Study

4.7.1. *In Vivo* Therapeutic Efficacy of FA conjugated NPs

The protocol for animal experiment was approved through institutional ethical committee, approval no. SDCOPVS/AH/CPCSEA/01/0028.The *in vivo* studies were performed as per the protocol detailed in chapter III section 3.6.1. The animals were randomly divided into six groups as described below.

Group I negative control

Group II toxic control, Urethane 1g/kg, i.p

Group III Urethane 1g/kg, i.p + Gnb,20mg/kg

Group IV Urethane 1g/kg, i.p+ Gnb-PLGA-PEG-FA dose: 20mg/kg, i.v.

Group V Urethane 1g/kg, i.p+ Cap-PLGA-PEG-FA dose: 10mg/kg, i.v.

Group VI Urethane 1g/kg, i.p along with Cap@GnbPLGA-PEG-FA (comprising 20 mg/kg of Gnb and 10mg/kg of Cap i.v.simultaneously).

4.7.2. Histopathology

Lung tissues from all the six groups were isolated and stored in 10% buffered formalin for histopathological investigation. The tissues were embedded with paraffin wax, and sections of 3-5 µm made using rotary microtome (YSI-060 Yorco, Ghaziabad, deparaffinized, and stained with hematoxylin and eosin. The sections were observed under 40X magnification India). The fine sections were unruffled over the glass slide, and images were captured using digital biological microscope (N120, BR-Biochem Life Sciences, New Delhi, India).

4.7.3. Oxidative stress markers

The tumor-bearing lungs challenged by urethane were isolated from all the six groups, and investigated for oxidative stress as per methods given in chapter III section 3.6.3 (Kaithwas et al. 2012). Experiments were performed in triplicate and statistically analyzed using software Graph Pad Prism (5.01), San Diego, California.

4.7.4. Western Blotting

Lung tissues were excised and processed for western blotting as described in chapter III section 3.6.4.

Antibodies and dilutions for immunoblotting were as follows: Anti caspase-9 (rabbit polyclonal 1:500), Anti caspase-3 (rabbit polyclonal 1:500) Anti MMP-9 (goat polyclonal 1:500), Anti-actin (rabbit polyclonal 1: 500), Anti P-16 (rabbit polyclonal 1:500), and HRP-conjugated secondary antibodies (anti-rabbit, 1:500). β-actin (MA5-15739-HRP) was used as a standard reference.Quantitative analyses of protein expression in immunoblots were performed using scanning densitometry (ImageJ, NIH).

4.7.5. Biodistribution studies

Biodistribution of modified, unmodified and plain Gnb was evaluated to determine the targeting potential of the FA conjugation. Biodistribution of formulation was examined by injecting Gnb-PLGA-PEG-FA, Cap@Gnb-PLGA-PEG-FA, Gnb-PLGA and Gnb equivalent dose, to 20 mg/kg of Gnb, through tail vein of urethane induced LCs rats. The animals were sacrificed at specific time intervals and various body organs, *viz.*, lungs, liver, heart, kidney, spleen were excised at predetermined time points i.e. 4, 12, 24 and 48 h and stored at -80°C until further analysis. The organs were weighed and homogenized and concentration of Gnb was measured through the validated HPLC method (Waters 2489, Milford, Massachusetts, USA). The system was equipped with Spherowsorb C18, 3.5 µm, 4.6×250 mm column at flow rate 1.0 mL/min. The mobile phase comprised of methanol and 0.1 M potassium dihydrogen phosphate in a ratio of 40:60 (v/v) and a flow rate of 1.0 mL/min with runtime 20 min and detection was doneat 254nm (Pandey et al. 2014).The Cap concentration was measured through the validated HPLC method (Waters 2489, Milford, Massachusetts, USA). The system was equipped with Spherisorb C18, 3.5 µm, 4.6×250 mm column at flow rate 1.5 mL/min. The mobile phase comprised of water-acetonitrile in 50:50 ratio and a flow rate of 1.5 mL/min with runtime 15 min and detection was done at 222nm(Othman et al. 2011).

4.8. Stability Studies

Stability of Gnb-PLGA-PEG-FA and Cap-PLGA-PEG-FA was performed at 5±2°, 25 ±2° (60±5% RH) and 40±2° (75±5% RH) as per ICH guidelines over a period of 90 days. Samples were assessed for particle size, zeta potential and percent drug loading at 0, 15, 30, 45, and 90 days.All experiments were performed in triplicate and mean values reported.

4.9.Statistical analysis

All results were presented as mean ± standard deviation (n=3). One-way analysis of variance (ANOVA) followed by the Turkey-Kramer multiple comparison test was performed to compare differences between formulations using Graph Pad Instat software (Graph Pad Software Inc. CA, USA). Levels of significance were set as $p<0.05$ explaining significant

difference in the therapeutic efficiencies of all formulations in comparison to Cap@Gnb-PLGA-PEG-FA.

4.10. Results

Present investigation aimed at designing of FA modified PLGA NPs, for intravenous delivery to ameliorate urethane-induced LC in rats. The procedure opted from previous literature for conjugation was simple and was found to be successful in entrapping hydrophobic drug Gnb and Cap in folate conjugated PLGA nanoparticles.

4.10.1 Synthesis of PLGA-PEG-FA

The FTIR spectra of PLGA, PLGA-PEG-FA and PLGA-PEG revealed appearance of new peaks when compared to standard PLGA and FA. The spectra of folate displayed peak at 897.2 cm^{-1} (aromatic C–H bending and benzene 1,4-disubstitution), 1,478.9 cm^{-1} (CH–NH–CO amides bending), 1,702.5 cm^{-1} (aromatic C-C bending and stretching), 2996.4 cm^{-1} (alkyl C–H and O-H stretch), and 3,439.3 cm^{-1} (N–H stretch of primary amine and amide, C-H stretch) (**Figure. 4.2a**) which indicating the presence of NH_2. For PLGA characteristic peaks were identified at 2995.91 cm^{-1} (carboxylic acid O–H stretching) 1761.34 cm^{-1} (C=O stretch of COOH group), 2912.95 cm^{-1} (alkyl C-H stretching) (**Figure. 4.2b**). For the Folate-PEG-PLGA, the peaks were observed at 3,431.16 cm^{-1} (amide N–H stretching), 2997.25 and 2914.19 cm^{-1} (O–H stretching COOH and C-H stretching), 1,436.74 cm^{-1} (CH–NH–CO amides bending), 1,660.47 cm^{-1} (aromatic C-C bending and stretching), 698.2, 897.8, 932.2 cm^{-1} (aromatic C-H bending and stretching) and 1312.18 cm^{-1} (PEG C-O-C stretching) confirmed the attachment of the folic acid to PLGA through PEG (**Figure 4.2 c**). For the Folate-NHS ester, the peaks were observed at 1,551.37 cm^{-1} (CH–NH–CO amides bending), 3,491.8 cm^{-1} (amide N–H and C=O stretching), 2913.7 and 2996.1 cm^{-1} (carboxylic acid COOH and O–H unconjugated stretching), 1,663.8 cm^{-1} (ketone C=O stretch), 697.4, 896.9, 931.29 cm^{-1} (aromatic C-H bending and stretching) confirmed the formation of folic acid NHS ester. The formation of PLGA-PEG-FA was confirmed by the presence of bands for amide linkage which were absent in FA and PLGA.

^{1}H-NMR spectrum of PLGA-PEG-FA

Folic acid was conjugated with the polymeric NPs with the aid of the NHS. ^{1}H-NMR of folate attached PLGA was performed and characteristic peaks were identified and appropriately marked to confirm the conjugation of folate to PLGA. Important peaks for folate decorated PLGA (PLGA-PEG-FA conjugate) are **1** (1.24-1.34, 1H, d, aliphatic CH); **2** (3.55, 2H, d, broad peak of protonated NH_2 protons); **3** (3.73-3.98, 2H, dd two adjacent peaks for PEG); **4** (5.58, 3H, m, CONH); **5** (6.60, 2H, m, NH); **6** (6.87, 2H, d, aromatic CH); **7** (7.55, 2H, d, aromatic CH); **8** (8.56, 1H, s, dihydropteridine CH) as shown in Figure. 4.3.

The Folate- NHS ester, synthesized formerly, was endorsed to react with free PEG amine groups available at Gnb-PLGA-PEG surface. The conjugation of folate to PLGA-PEG was found to be 5.67 µM of folate/g of polymer (expressed in molar ratio).

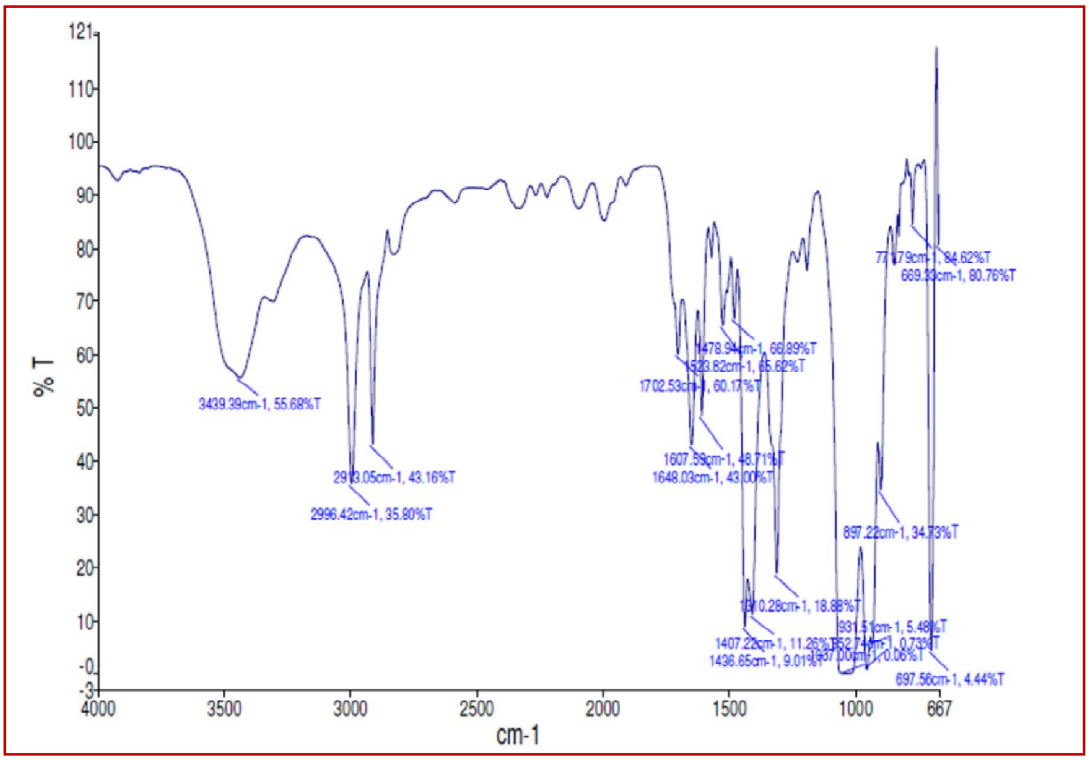

Figure 4.2a.FTIR spectra of Folate NHS (Activated folate)

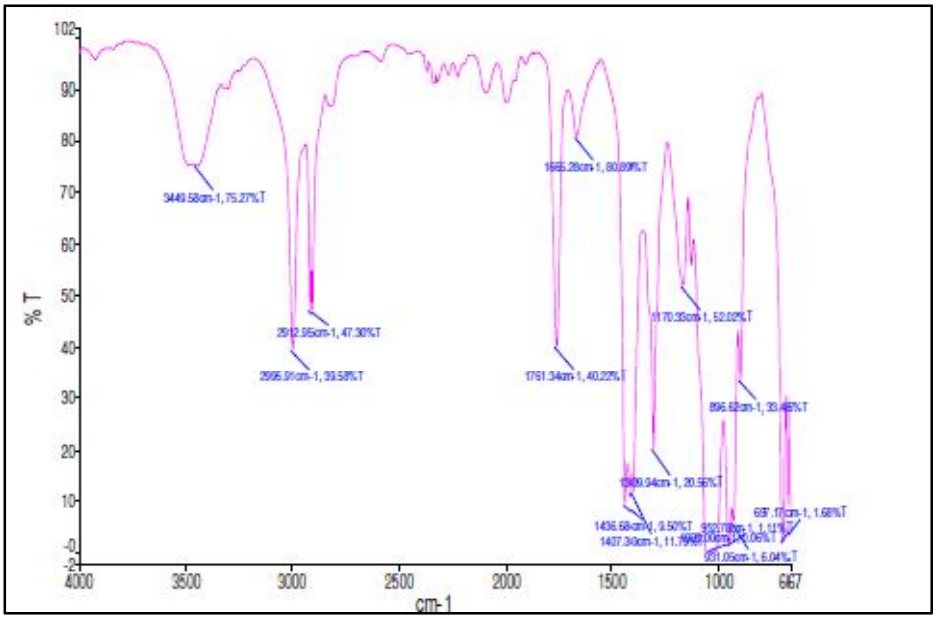

Figure 4.2b.FTIR spectra of PLGA

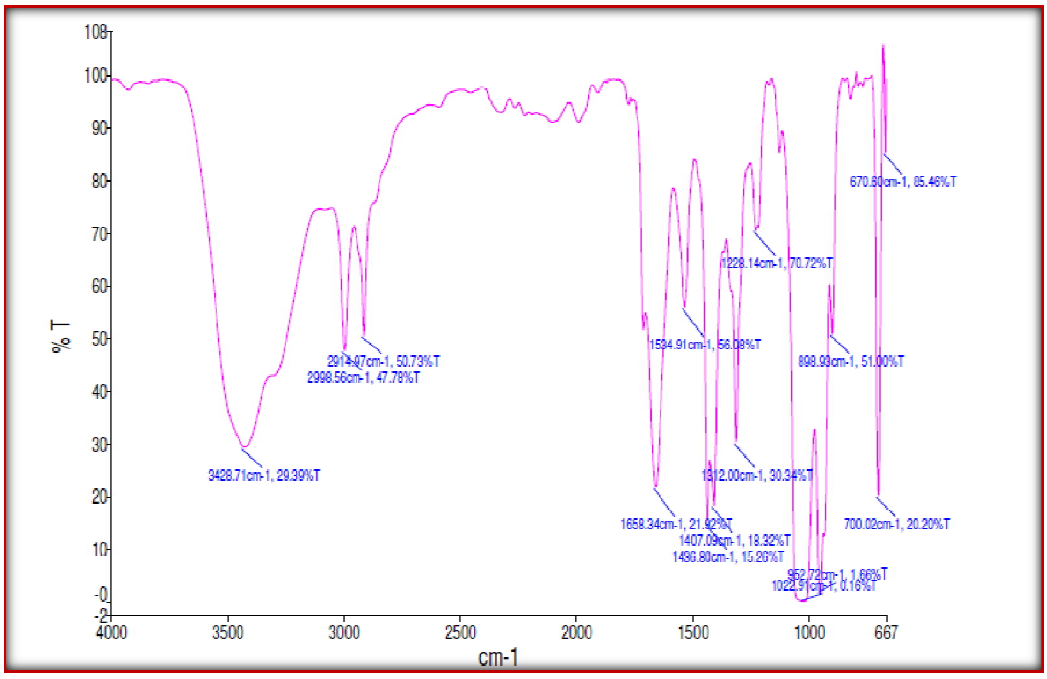

Figure 4.2c.FTIR spectra of folate conjugated PLGA (PLGA-PEG-FA)

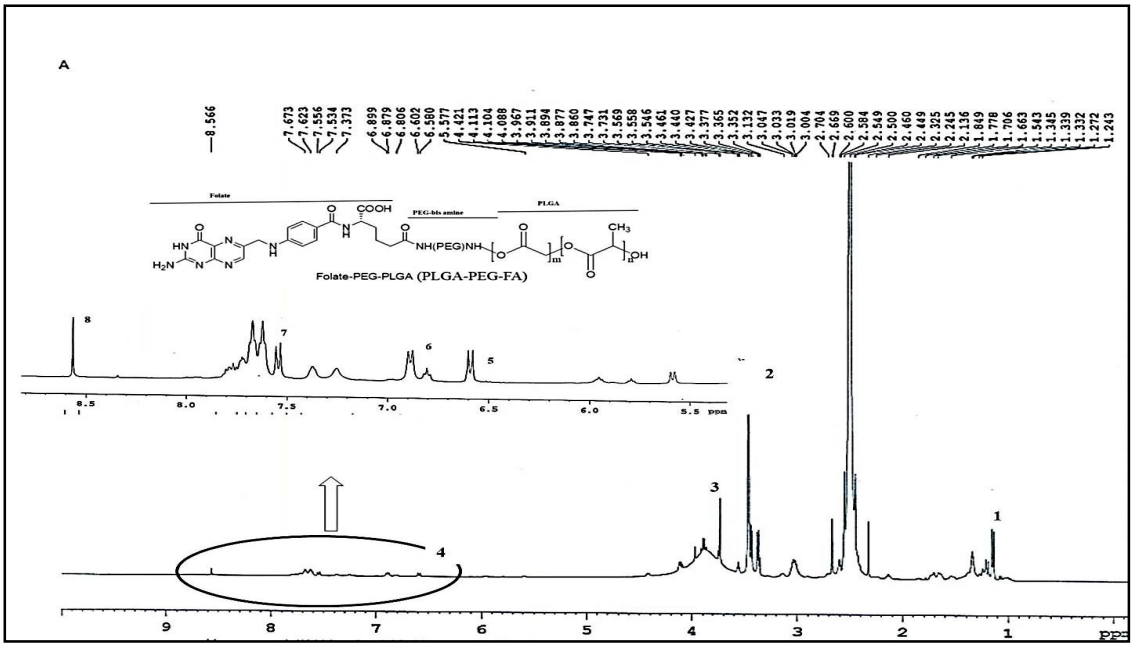

Figure.4.3 ^{1}H-NMR spectrum of PLGA-PEG-FA

4.10.2. Formulation and Optimization of Gnb@PLGA-PEG-FA and Cap@PLGA-PEG-FA

Synthesized polymer PLGA-PEG-NH_2 was utilized to entrap Gnb and Cap which were further conjugated with activated FA to form Gnb-PLGA-PEG-FA and Cap-PLGA-PEG-FA employing oil in water emulsion technique. The data obtained after the analysis reveals that the independent factor i.e., polymer:drug ratio, has a significant effect on drug loading, percentage entrapment, percentage release and particle size. The quantitative estimation of the significant model terms indicated that a nonlinear quadratic relationship was observed among X1 and X2 with all the dependent variables. It was observed that as the polymer ratio increases the particle size increases. However, PVA plays an insignificant role in the process as depicted from figure. 4.4 a-d. The relationship can be explained through the equation given below-

Particle size =+64.88889 +60.83333 * PLGA:Drug+10.00000 * PVA……(iii)

Log_{10}(Entrapment efficiency) = +1.66+0.061* A+0.020 * B-0.052* A^2-0.039* B^2……..(iv)

Drug loading = +3.64+1.05 * A+0.18 * B+0.050 * A * B-0.78 * A^2-0.58* B^2…….(v)

%Release=+81.88889 ……(vi)

4.10.2.1. Optimization and Validation

After analyzing the regression equations, to illustrate correlation between the dependent and independent variables, advance optimization and validation process was performed, employing design expert software (Design Expert 8.0 software; Trial version, M/s Stat-Ease, Minneapolis, USA). The design space (area of desirable characteristics) and the optimal formula for modified NPs depended on the prescriptive criteria of minimization of particle size (<250), drug loading (>10%) and %EE (>40%). The composition of the optimum formulation identified was 2:1 ratio (X1 PLGA) and 2.5%v/v (X2, PVA), which fulfilled the requirements of optimization. At these levels, the predicted values [Figure4.4 e] of particle size, percent drug release, percent entrapment and percent drug loading was 211.56 nm, 81.88%, 40.23% and 18.19% respectively. As per results of the advance validation of predicted values by this model, a new batch of modified NPs (OPT-NPs) were prepared and characterized. This optimized batch exhibited a particle size of 210±9.75 nm, percentage entrapment of 49.11±1.1%, percent drug release of 87.22±4.32% and percentage drug loading of 25.88% respectively, which was in righteous alignment with the predicted values. The parameters for Gnb and Cap have been reported in**Table 4.1 a & b.**The optimization through FbD approach gives the design surface area for formulating desired formulation using suitable excipients in the variable concentration within minimum number of experiments.

Table 4.1 a. Various dependent parameters for PLGA NPs of Gnb prepared as per CCD [Data is presented as mean±SD (n=3)]

Run	Factor1 PLGA: drug	Factor 2 PVA%	Particle size(nm)	%Entrapment	%Drug loading	%Drug Release (Gnb)
1	1	1.0	147± 10.51	30± 1.2	12.2± 0.12	80.32± 1.7
2	3	1.0	257± 10.15	43±2.2	21.1± 0.24	88.31± 4.1
3	1	4.0	154± 10.67	35± 1.4	14.5± 0.16	83.27± 2.2
4	3	4.0	305± 11.21	45±1.3	19.6± 0.11	80.11± 1.2
5	1	2.5	172± 12.31	35± 1.3	12.6± 0.27	81.76± 3.4
6	3	2.5	276± 11.42	44± 3.1	23.9± 0.31	79.09± 3.9
7	2	1.0	174± 12.45	39±1.2	17.8± 0.23	81.34± 3.4
8	2	4.0	209± 8.29	42± 2.1	18.1± 0.30	78.43± 3.2
9	2	2.5	210± 9.75	49±1.1	23.88± 0.24	87.22± 2.8

Table 4.1 b. Various dependent parameters for PLGA NPs of Capprepared as per CCD [Data is presented as mean±SD (n=3)

Run	Factor 1 PLGA: drug	Factor 2 PVA%	Particle size(nm)	%Entrapment	%Drug loading	%Drug Release (Cap)
1	1	1.0	143± 3.21	31± 2.1	13.7± 0.10	79.05± 3.2
2	3	1.0	252± 6.34	42±1.5	20.1± 0.25	85.21± 3.5
3	1	4.0	149± 4.32	36± 1.9	15.1± 0.32	81.90± 4.2
4	3	4.0	308± 5.21	45±2.3	18.5± 0.11	79.31± 1.5
5	1	2.5	169± 2.09	36± 2.3	11.9± 0.73	80.46± 4.5
6	3	2.5	278± 3.31	45± 1.1	25.1± 0.22	79.25± 2.9
7	2	1.0	175± 1.22	37±1.2	15.9± 0.86	80.94± 3.9
8	2	4.0	207± 3.99	40± 2.1	16.1± 0.15	76.23± 4.3
9	2	2.5	215± 4.90	45±3.1	21.3± 0.4	84.10± 2.5

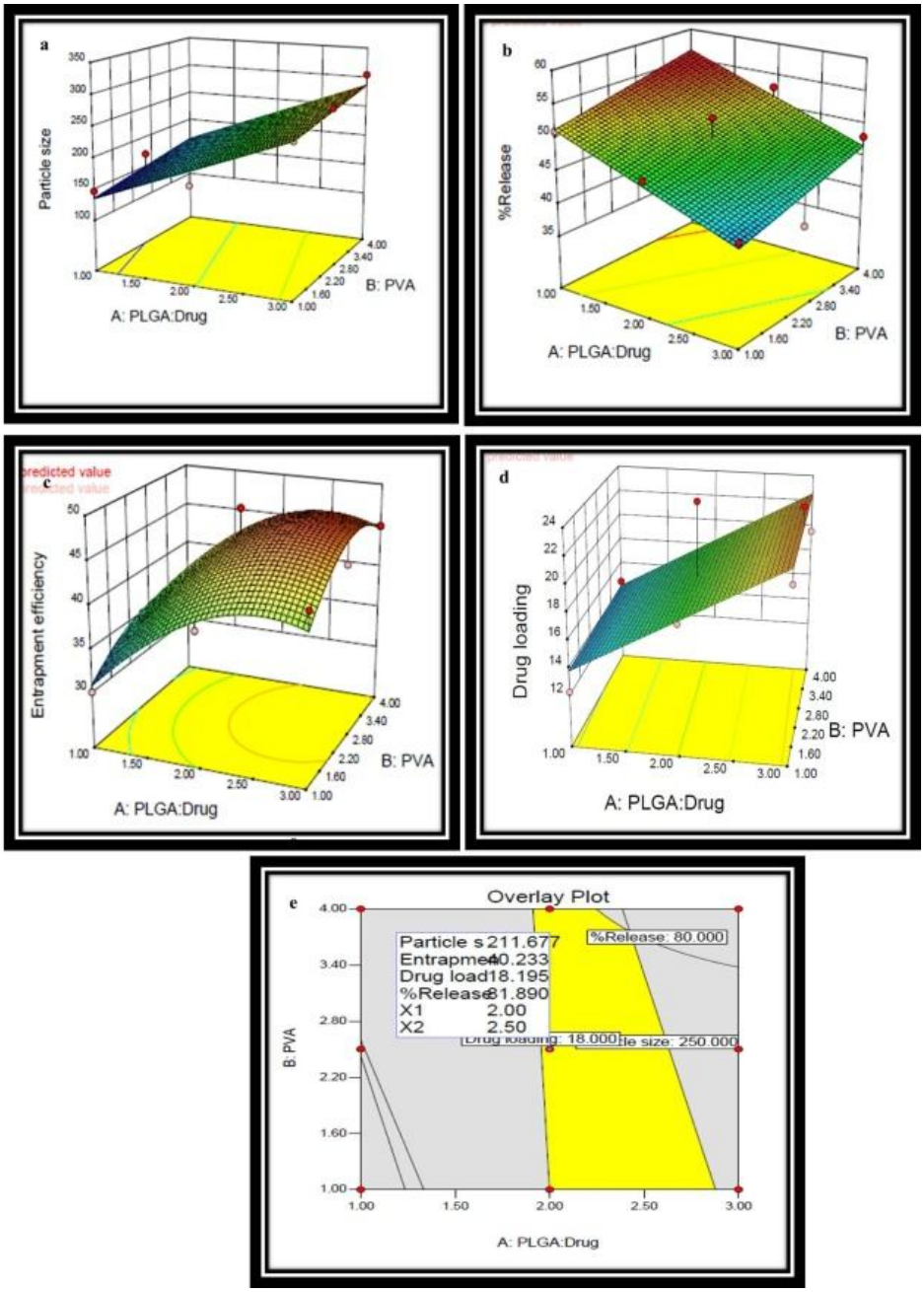

Figure 4.4. Response surface plots depicting the effect of independent variables on dependent variable, effect of independent variable on (a) particle size (b) % release (c) entrapment (d) drug loading (e) overlay plot defining predictable values

4.10.3. Particle size, Zeta potential, Drug loading and %EE

The physical characteristics of Gnb/Cap loaded PLGA–PEG–FA NPs (optimized formulation) viz. particle size, %EE, drug loading and zeta potential are shown in **Table 4.2**. It was observed that there was a slight increase in particle size as well as zeta potential after FA conjugation. The drug loading ranges from 20.88±1.7% to 24.72±0.2% in case of PLGANPsandPLGA-PEG-FA conjugated NPs. The polydispersity index of all the formulations was found to be below 0.3.The highest %EE of 53± 2.4% was observed in case of Gnb-PLGA, while least % EE of 43±1.5% was observed in case of Gnb-PLGA-PEG-FA. The zeta potential was found to be in the ranges of−13.19±2.01mV to 23.71±3.1mV in various formulations.

Table 4.2 Characterization of Gnb-PLGA-PEG-NH_2 and Cap-PLGA-PEG-NH_2 NPs.

Nanoparticles	Particle size (nm)	Zeta Potential (mV)	% Drug loading	%EE
Gnb-PLGA	207.0±4.1	-21.34±2.1	23.92±1.5	53±2.4
Gnb-PLGA-PEG-FA	217.0±3.2	-13.19±2.01	20.88±1.7	49±1.5
Cap-PLGA	201.0±6.1	-23.71±3.1	24.72±1.2	50±2.1
Cap-PLGA-PEG-FA	213.0±5.2	-14.45±0.88	21.77±1.3	46±2.3

4.10.4. Transmission Electron Microscopy (TEM)

The TEM image is represented in Figure4.5. TEM images aids in determination of the surface morphology of a formulation. The particles displayed a smooth surface, spherical morphology and a mean particle size ranging from 50-200 nm.

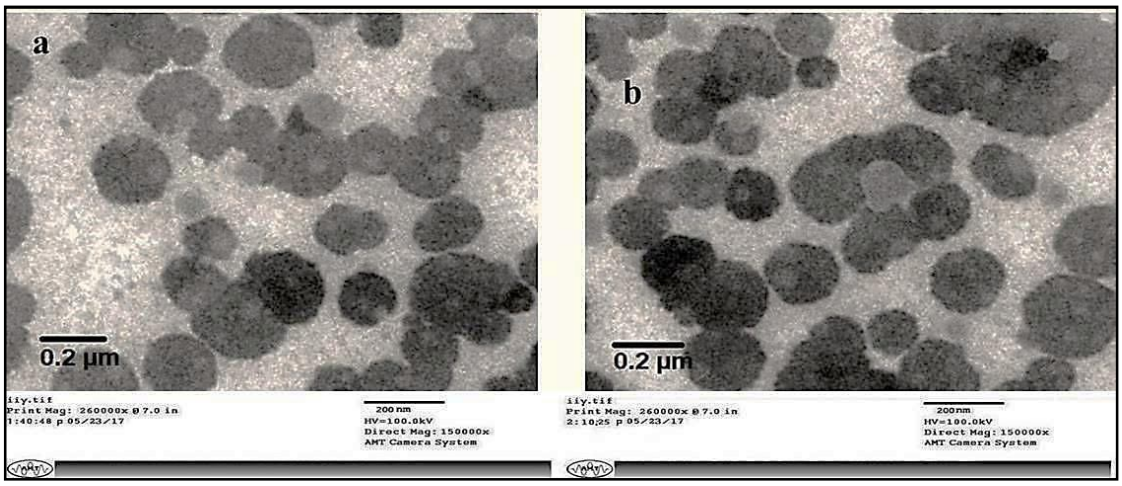

Figure 4.5.TEM images of a) Gnb-PLGA-PEG-FA and b) Cap-PLGA-PEG-FA

4.10.5. *In-vitro* Release Studies

The *in-vitro* release of modified NPs, Gnb-PLGA-PEG-FA and Cap-PLGA-PEG-FA showed biphasic release pattern with an initial faster release within 4 h followed by a sustained release profile. The unmodified NPs Gnb-PLGA and Cap-PLGA respectively exhibited a release of about 91.08±1.34% and 86.78±3.11% each over a period of 80 h. About 85.65±3.21% of Gnb and 81.43±4.32% of Cap were respectively released from modified NPs over a period of 80 h. Approximately 61.29±3.90% of Gnb and 59.93±4.24% of Cap was released from modified NPs over a period of 24 h. Almost 80% of the drug was released over a period of 80 h in case of both modified as well as unmodified NPs of Gnb and Cap respectively as shown in **Figure 4.6.**

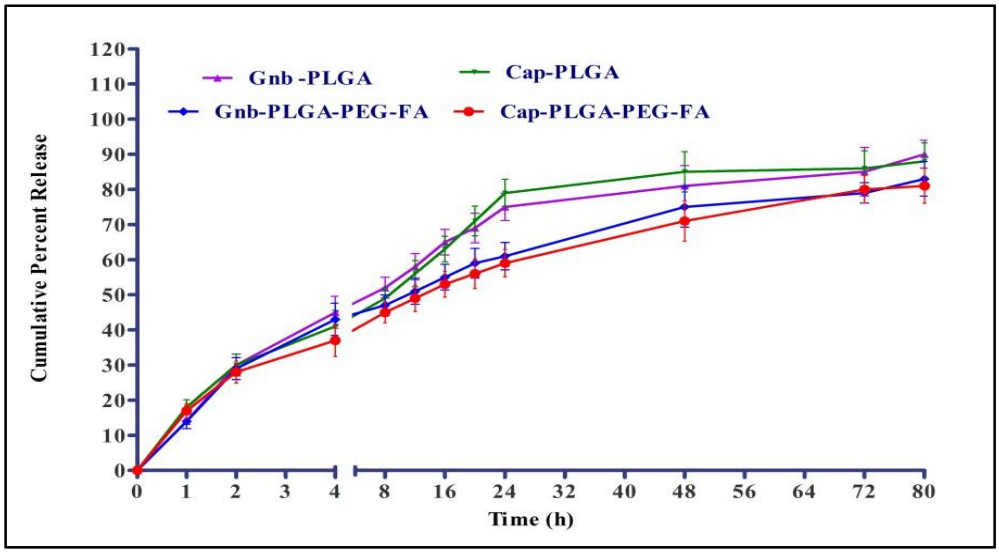

Figure 4.6. Drug release comparisons of modified and unmodified NPs in PBS pH 6.8 buffer[Data is presented as mean±SD (n=3)]

4.10.5.1. Release Kinetics Modeling

Different kinetic models were applied on the data obtained from release study for finding the kinetics of drug release. From the mathematical model data it was concluded that the Higuchi model was found to be most suitable for Cap-PLGA-PEG-FA and Korsmeyer Peppas model for Gnb-PLGA-PEG-FA as it reached highest value of the squared correlation coefficient (R^2), describing the release of the Cap and Gnb from PLGA nanoparticles as recorded in **Table 4.3**. It indicates that the release of drugs (Cap/Gnb) from PLGA nanoparticles is controlled by diffusion. The predicted release mechanism of the drug could be that the penetration of dissolution media penetrates into polymeric matrix which slowly dissolves the drug, and finally drug is released by diffusion into the medium. However, Korsmeyer Peppas model in case of Gnb suggests that there is absence of lag time, describing non-Fickianrelease mechanism.

Table 4.3 Release kinetics for dissolution data of Gnb-PLGA-PEG-FA and Cap-PLGA-PEG-FA

Correlation co-efficient R^2 value	**Gnb-PLGA-PEG-FA**	**Cap-PLGA-PEG-FA**
Zero order	0.6885	0.7318
First order	0.8379	0.8853
Higuchi model	0.892	0.9232
Korsmeyer Peppas model	0.9327	0.9076

4.10.7. Cytotoxicity Study

Cap@GnbPLGA-PEG-FA, Gnb-PLGA-PEG-FA, Cap-PLGA-PEG-FA, Gnb-PLGA, Cap-PLGA, Cap and Gnb were incubated with A549 cell lines in a concentration of 10 nM–100 µM for 48 h to establish the cell viability after treating with NPs. Proliferation and metabolic status of the cells was investigated through the MTT assay. The changes in percent cell viability against the drug treatment of various formulations are presented in **Figure 4.7 a.** The obtained results depicted IC50 value of Cap@GnbPLGA-PEG-FA (23.5±0.76µM), Gnb-PLGA-PEG-FA (31.76±1.54 µM), Cap-PLGA-PEG-FA (45.32±0.86 µM), Gnb (59.43±1.00 µM) and Cap (61.45±1.43 µM). The unmodified formulations also demonstrated a lower IC50 value when compared to free drug i.e., Gnb-PLGA (47.34 ±0.31 µM) and Cap-PLGA (51.27±0.16 µM) respectively. The isobolomic curve analysis revealed that an enhanced percent inhibition of cell proliferation was completed through combination therapy demonstrating their synergistic effect (**Figure 4.7 c)** when compared to Gnb and Cap individual treatment. The combination index (CI) calculated through CompuSyn software was found to be 0.2940The CI below 1 confirms the synergism, aptitude of the system.

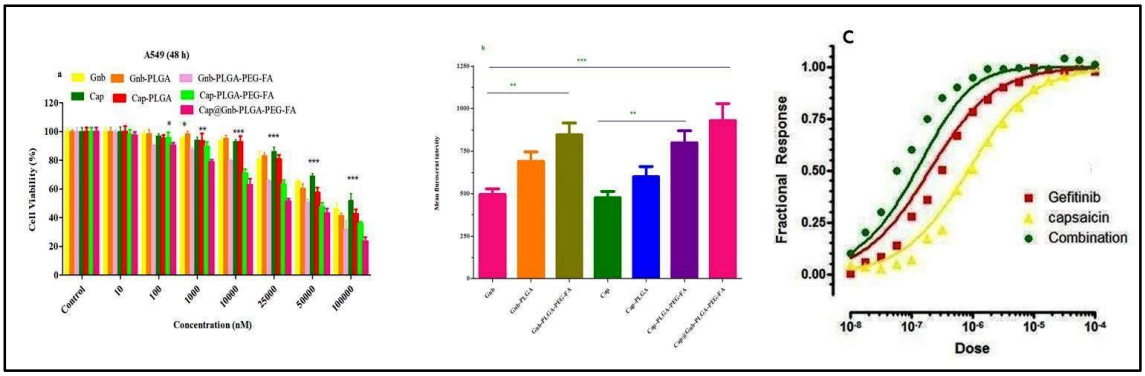

Figure4.7.(a) Cytotoxic effect on A549 cells treated with Gnb, unmodified NPs and modified NPs for 48 h (b) bar graph representation of Cell uptake study (c) Fractional dose-effect curve (isobologram curve) for two drugs (capsaicin and gefitinib) in A549 cells at IC_{50} levels.

4.10.7.1. *In vitro* Cellular Uptake Study

Modified NPs Gnb-PLGA-PEG-FA and Cap-PLGA-PEG-FA showed a significant ($p<0.01$) improvement in quantitative cellular uptake of Gnb and Cap when compared to unmodified NPs in A549 cell lines as represented in **Figure 4.7 b**. However no significant difference in uptake was observed in case of Cap@Gnb-PLGA-PEG-FA when compared to Gnb-PLGA-PEG-FA and Cap-PLGA-PEG-FA. Approximately 1.95 fold increase was observed in case of modified NPs when compared to free Gnb whereas 1.99 fold increase was observed when Cap@Gnb-PLGA-PEG-FA compared to free Gnb. Approximately 1.3 fold increase was observed in case of Gnb-PLGA-PEG-FA and Cap-PLGA-PEG-FA NPs when compared to unmodified Gnb-PLGA and Cap-PLGA. *In vitro* cellular uptake study illustrated that the cell internalization of drug(s) in A549 cells is profoundly enhanced when formulated as FA conjugated NPs. Enhanced cellular uptake can be interconnected with depressed IC_{50} of modified NPs. This uptake study served as relevant proof for functionalization of FA modified nanoparticles.

4.10.8. Cell Cycle Arrest

Cell cycle arrest by Gnb, Gnb-PLGA, Gnb-PLGA-PEG-FA, Cap-PLGA-PEG-FA and Cap@Gnb-PLGA-PEG-FA was investigated in A549 cell lines. Gnb is known to cause cancer cell apoptosis by inhibiting MMP-2 and MMP-9 and also reduces the AKT activity in A549 cell lines. The results demonstrated noticeable arrest in cancer cell growth in G2/M phase consequent to apoptosis when treated with surface modified NPs. **Figure 4.8 (A-F)** represents data for cell cycle arrest in A549 cells lines with free Gnb, Gnb-PLGA, Gnb-PLGA-PEG-FA, Cap-PLGA-PEG-FA and Cap@Gnb-PLGA-PEG-FA. A549 treated with free Gnb, Gnb-PLGA-PEG-FA triggered cell cycle arrest in G2/M phase. Cap@Gnb-PLGA-PEG-FA NPs arrested the cell in G2/M phase as well as in G0/G1 phase significantly at a higher magnitude when compared to modified NPs individually. The magnitude of cell growth inhibition was much higher in combined therapy when compared with either Cap or Gnb individually. A gradual elevation in G2/M population to 19.55±6.47% after 24 h indicates limited cell growth restriction and cell division. In control cells, distribution of cell population in G0/G1, S and G2/M phases of cell cycle were 81.14±6.78%, 11.79±5.26%, and 7.32±3.43%, respectively (**Figure4.8A**). When these cells were treated with Gnb, it resulted in reduction of cell numbers in G0/G1 phase (74.60± 5.31%). The A549 cells treated with Cap@Gnb-PLGA-PEG-FA resulted in significant ($P < 0.05$), G0/G1 phase arrest and increased apoptotic rate in comparison to control (60.36±4.47%) while no significant rise in cell death at S phase was observed. The treatment of A549 cells with various formulation enforced cells to move to the programmed cell death process.

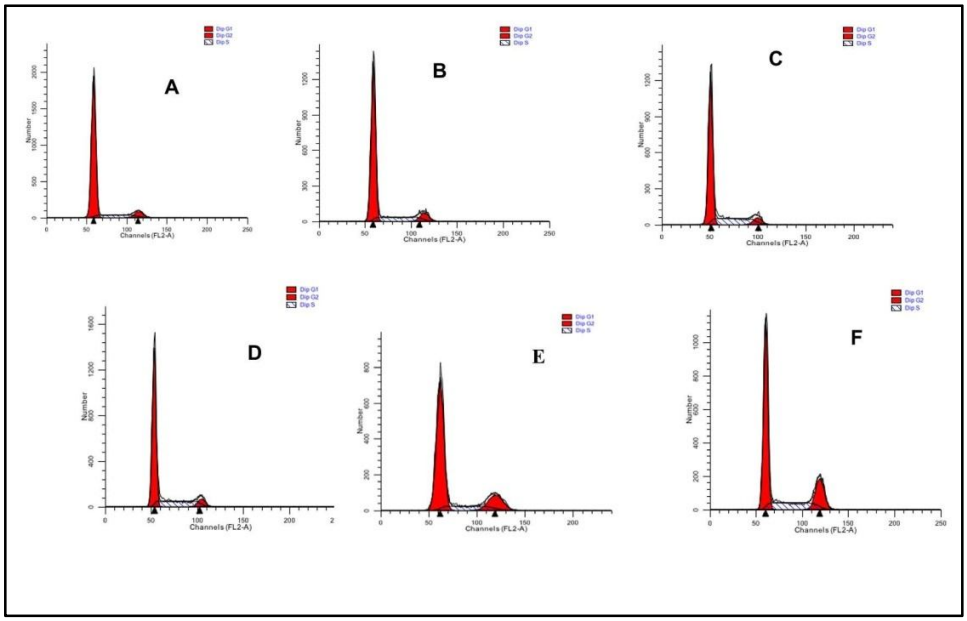

Figure 4.8. Representation of cell cycle distribution in A549 cells after treatment with (A) Control (B) Gnb (C) Gnb-PLGA (D) Gnb-PLGA-PEG-FA (E) Cap@Gnb-PLGA-PEG-FA (F) Cap-PLGA-PEG-FA, at sub IC50 drug concentration and analysis was performed using flow cytometry. Each Figure individually represents the population present in G1-S and G2-M phases, (n=3)

4.10.9. Cell Proliferation Assay

Cell proliferation studies revealed maximum inhibition of A549 cells when treated withmodified NPs. The inhibition potential followed an order of Cap@Gnb-PLGA-PEG-FA>Gnb-PLGA-PEG-FA>Cap-PLGA-PEG-FA>Gnb-PLGA>Cap-PLGA>Gnb>Cap. As shown in **Figure 4.9 a,** Gnb, modified, unmodified and Cap@Gnb-PLGA-PEG-FA NPs(co-therapy) inhibited A549 cell proliferation. Further, percentage viability was measured after treating cells with various formulations for 48 h. It was perceived that percentage viability was significantly reduced ($p<0.001$) as compared to control in treated group in a similar manner as of cell proliferation i.e. Cap@Gnb-PLGA-FA displayed least cell viability. The formulation Gnb-PLGA-PEG-FA and Cap-PLGA-PEG-FA displayed a percentage inhibition of about 71.13±3.29% and 70.43±4.09% which was significantly higher when compared to control ($p<0.001$). The fluorescence intensity of Alamar Blue® is directly related to cell proliferation. The viable cells possess instinctive metabolic activity.

Following metabolization chemical reduction of dye Alamar Blue® occurs which changes its non-fluorescent oxidized (blue) form to the reduced fluorescent (red) form. This intrinsic metabolic activity is not observed with the dead cells, thus an oxidized environment is maintained, constraining dye reduction and hence lack florescence(O'brien et al. 2000).

4.10.10. Mitochondrial Membrane Potential Assay

Maximum disruption of mitochondrial membrane potential (MMP) in A549 cells was instigated by Cap@Gnb-PLGA-PEG-FA which was found significantly higher when compared with control samples ($p<0.01$). It was observed that Cap-PLGA-PEG-FA and Gnb-PLGA-PEG-FA had significant effect on MMP disruption; however a declined effect was observed withCap-PLGA as compared to control. A significant difference in MMP disruption was observed when a comparison was made between modified and unmodified NPs ($p<0.01$). **Figure4.9 b** represents the fluorescence intensity (indicating cell viability) of cells which increases differentially when treated with various NPs. Higher fluorescence intensity in control revealed least lethal capability while least fluorescence intensity in the case of Cap@Gnb-PLGA-PEG-FA indicated highest mortality of A549 cell lines. The effect of the formulations on the MMP can be explained by lower uptake and retention of the Rhodamine-123 in the mitochondria of cells undergoing apoptosis. Rhodamine-123 uptake is MMP-dependent, thus favors its accumulation in the mitochondria of the living cells. This affects the quenching of fluorescence and consequences in red spectral shifts indicating that the cells are undergoing apoptosis.This enhanced mortality proves the synergistic potential of Cap and Gnb.

4.10.11. ROS Generation Analysis

Minimum ROS generation was observed in Cap@Gnb-PLGA-PEG-FA treated cells, which was found to be significantly higher ($p< 0.001$), when compared to Gnb or Cap individually. ROS generation was also found to be significantly higher in free Gnb treated group when compared to free modified NPs($p< 0.001$) indicating superiority of modified NPs over plain drug as shown in **Figure 4.9 c.** Moreover supremacy of modified NPs over unmodified NPs was also perceived, with a significance level of $p< 0.01$. The treatment with the unmodified and the plain Gnb formulation exhibited higher fluorescence of DCF in the A549 cells

demonstrating elevated cellular growth and production of higher ROS that oxidizes the reduced form of DCF to fluorogenic oxidized form. DCFDA, a fluorogenic dye is widely used for direct measurement of the oxidation-reduction state of the cell.

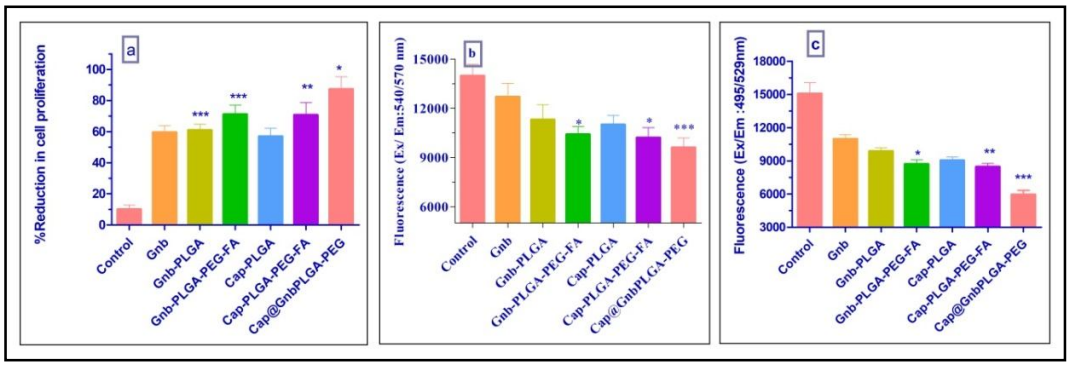

Figure 4.9 a) Inhibition of A549 cell proliferations by Gnb NPs. b) Loss in mitochondrial membrane potential: graph represents the change in mitochondrial potential in A549 cells c) Intracellular ROS level in A549 cells after modified and unmodified Gnb NPs measured by fluorimetry. *: $p<0.05$, **: $p<0.01$, ***: $p<0.001$.

4.11.*In vivo* study

4.11.1.Tumor Regression Studies

Treatment through different formulations i.e. Gnb, Gnb-PLGA, Gnb-PLGA-PEG-FA, Cap-PLGA-PEG-FA and Cap@Gnb-PLGA-PEG-FA were compared for their anticancer potential *in-vivo,* in urethane induced tumor model. After completion of treatment (16 weeks) the rats were sacrificed and the lungs were isolated. The lung weight was recorded and tumors were identified in various groups (**Figure 4.10a & e)**. Cap@Gnb-PLGA-FA and Gnb-PLGA-PEG-FA displayed a marked reduction in lung weight when compared to Gnb-PLGA.Free Gnb and Cap-PLGA-PEG-FA exhibited minor regression in tumor at the end point of experiment when compared with modified NPs and combination therapy through Cap and Gnb. Kaplan Meier survival plot (**Figure 4.10 c**) revealed reduced animal mortality (upto 16 weeks) and demonstrated improved antitumor activity *in vivo*, in both Cap@Gnb-PLGA-FA and Gnb-PLGA-PEG-FA treated group when compared with Gnb and Cap treated and toxic groups respectively. Weight variation plots for different groups displayed a remarkable continuous weight loss among toxic groups when compared to groups receiving

Cap@Gnb-PLGA-PEG-FA and Gnb-PLGA-PEG-FA over a period of 16 weeks as shown in **Figure 4.10 b**. A significant reduction in tumor volume was observed in group receiving Cap@Gnb-PLGA-PEG-FA as compared to group receiving plain Gnb ($p < 0.001$) as well as individual therapy, explaining superiority of combination therapy over single drug. A significant reduction in tumor volume (**Figure 4.10 d**) was observed when Cap@Gnb-PLGA-PEG-FA was compared to the toxic group ($p<0.001$). Groups receiving plain Gnb (Group III), Gnb-PLGA-PEG-FA (Group IV) and Cap-PLGA-PEG-FA (Group V) also displayed reduction in tumor volume but to a lesser extent when compared with group co administered with Cap and Gnb and FA conjugated modified NPs individually. Moreover a significant reduction in tumor volume was observed in Gnb-PLGA-PEG-FA treated group when compared with Gnb-PLGA treated group ($p < 0.05$). However Cap-PLGA-PEG-FA also displayed insignificant reduction in tumor volume when compared with co- therapy by Gnb and Cap.

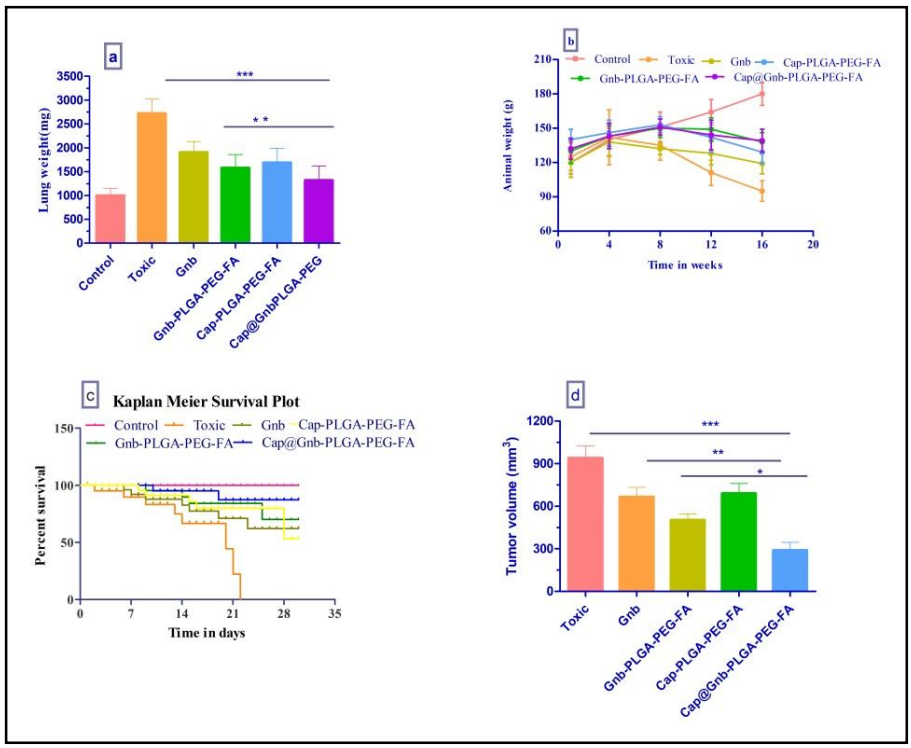

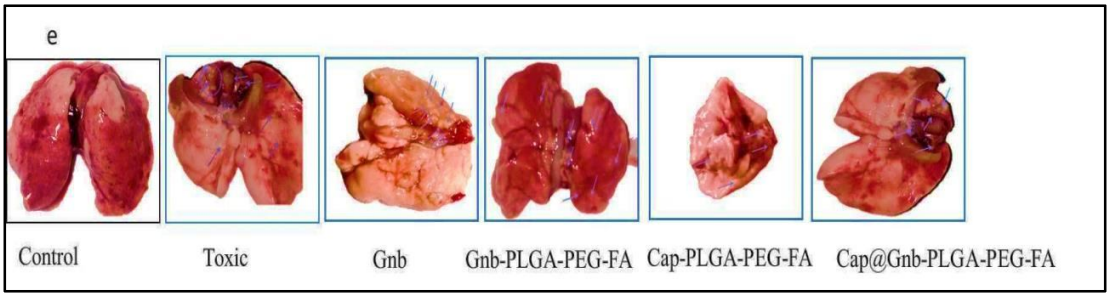

Figure 4.10 a) Bar graph representing lung weight b) change in animal body weight c) Kaplan meier survival plot d) tumor volume data (e) tumor localization of various groups (*: $p<0.05$, **: $p<0.01$, ***: $p<0.001$ Compared to toxic)

4.11.2. Histopathology

The histopathological changes are specified in **Figure 4.11**among the lung tissue of various groups. The normal control group exhibited adipocytes, alveoli and bronchiole structure (marked by arrows) whereas the toxic tissues displayed the presence of developed rosette shaped structured tumor cells and peribronchial cells, which infiltrate the bronchial submucosa. The toxic group exhibited moderately segregated, growing adenocarcinoma, having abundant cytoplasm and some nucleoli, suggesting a non-small cell lung carcinoma. The Gnb treated groups displayed the bronchiole having smooth muscle in the inner airway wall with alveolar attachment while group IV and V showed declining tumor cells and a distinguished alveoli structure and outer airway wall, which somewhat regained their structure during treatment although insignificant in nature.

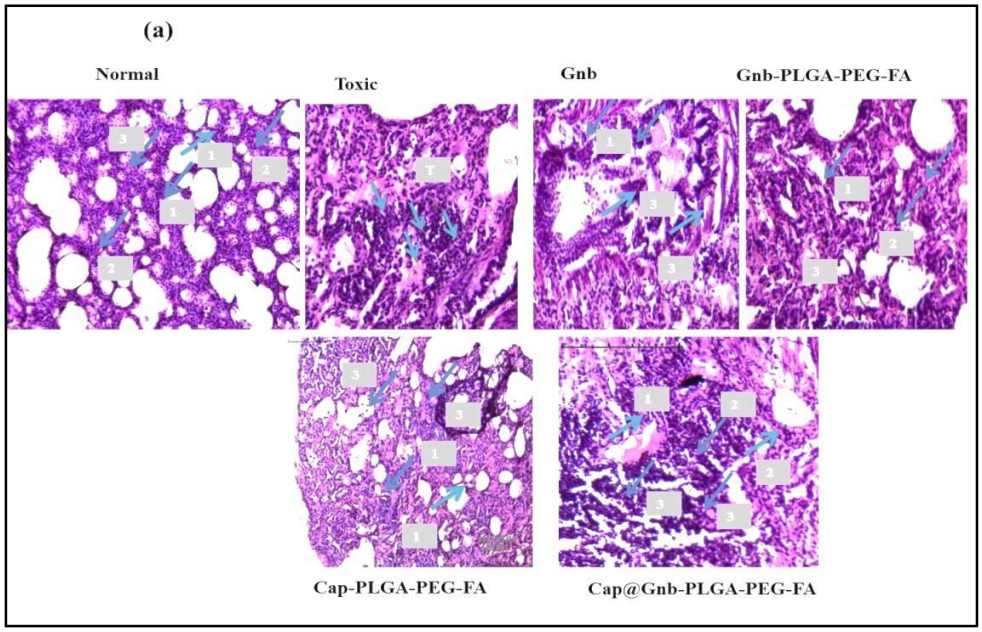

Figure 4.11.H&E staining micrographs of various group. Arrows represents tumor stroma cells in toxic group, bronchiole structure and inner airway in Gnb treated group and distinguished alveoli structure in modified NPs treated group

1: Adipocytes, 2: Alveoli, 3: Bronchiole and T: tumor cells

4.11.3.Biochemical Estimation

The effect of plain Gnb, Gnb-PLGA-PEG-FA, Cap-PLGA-PEG-FA and Cap@Gnb-PLGA-PEG-FAin lung homogenate on various oxidative stress markersenumerated aboveis summarized in table 4.4. The tumor bearing lungs were isolated from albino wistar rats confronted by intraperitonial injection of urethane, which was investigated for oxidative stress study. The TBARS and SOD levels were considerablyincreasedafter urethane administration which was significantly decreased by Cap@Gnb-PLGA-PEG-FA NPs. As revealed by the results Cap@Gnb-PLGA-PEG-FA also restored the tissue catalase and GSH level that had formerly reduced after urethane administration in various groups. The toxic group showed an increased level of protein carbonyl above normal. This increased protein carbonyl level was significantly reduced ($p<0.05$) by Cap@Gnb-PLGA-PEG-FA to an almost normal level. FA modified NPs individually also displayed a reduction in TBARS and SOD levels and restoration of catalase levels but to a lesser extent as compared to Cap@Gnb-PLGA-PEG-FA. Therefore, Cap@Gnb-PLGA-PEG-FA conveyed an overall,

overlaid antioxidant effect to restore the oxidative stress markers balance in Cap@Gnb-PLGA-PEG-FA received group in comparisons to therapy through Gnb-PLGA-PEG-FA and free Gnb group.

Table 4.4. Effect of free Gnb, unmodified NPs and modified NPs on oxidative stress markers, from lung homogenate in Urethane induced lung cancer.

Groups	TBARS (nm of MDA/µg of protein	SOD (units of SOD/mg of protein)	GSH (Mg %)	CATALASE (nm of H_2O_2/ min/mg of protein)	PROTEIN CARBONYL nmol/mg of protein
Control	203.51±12.2	0.0359±0.005	1.26±0.05	0.445±0.012	16.52±0.06
Toxicant	509.81±16.14	0.0432±0.0036	0.93±0.07	0.116±0.11	41.26±6.75
Gnb	298.7±15.3	0.0369±0.0051**	1.09±0.09**	0.127±0.21	34.05±9.8
Gnb-PLGA-PEG-FA	269.11±11.04	0.036±0.002***	1.14±0.11**	0.320±0.015***	29.14±0.73**
Cap-PLGA-PEG-FA	305.7±19.5	0.039±0.0011***	1.11±0.06**	0.301±0.12	31.05±7.5
Cap@Gnb-PLGA-PEG-FA	210.45±7.25	0.0357±0.0042**	1.21±0.08***	0.393±0.032***	20.5±11.7***

Values are (Mean ± SD), each group contains 09 animals. Comparisons were made on the basis of the one-way ANOVA followed by Bonferroni test. All groups were compared to the toxic control group (*p<0.05, **p<0.01, ***p<0.001).

4.11.3.*Western Blotting*

Further, to elucidate the possible mechanisms underlying the superior antitumor effect of modified NPs, western blot analysis was performed. The results of our study indicate varied influences on the expression of different pro-apoptotic (caspase-3 caspase-9 and P-16) and anti-apoptotic (MMP-9) proteins (**Figure 4.12**). It was observed that there was a significant down regulation of MMP-9 proteins when treated with modified NPs. Concurrently, an up regulation was observed in caspase-3 caspase-9 and P-16, suggesting that Gnb-PLGA-PEG-

FA and Cap-PLGA-PEG-FA are intimately involved in the process of cell apoptosis. Moreover, co-therapy of Cap and Gnb produced the greatest inhibition of cancer proliferation, as a remarkable restoration of pro-apoptotic and anti-apoptotic genes occurred, subsequent to treatment. It was revealed from immunoblots that a significantly higher ($p<0.05$) up-regulation of pro-apoptotic proteins and down-regulation of anti-apoptotic proteins was observed with Cap@Gnb-PLGA-PEG-FA when compared with Cap-PLGA-PEG-FA and Gnb-PLGA-PEG-FA individually. This evidences a synergistic effect and capability to reinstate the markers as compared to the toxic group constructively demonstrating apoptosis. Thus, enhanced anticancer potential of Cap and Gnb co-therapy was observed. The result suggested that co-therapy through FA conjugated NPs competently restricted the LC cell proliferation and invasion in the cancer induced animals. This also revealed that Cap potentiated the activity of Gnb leading to enhanced therapeutic efficacy.

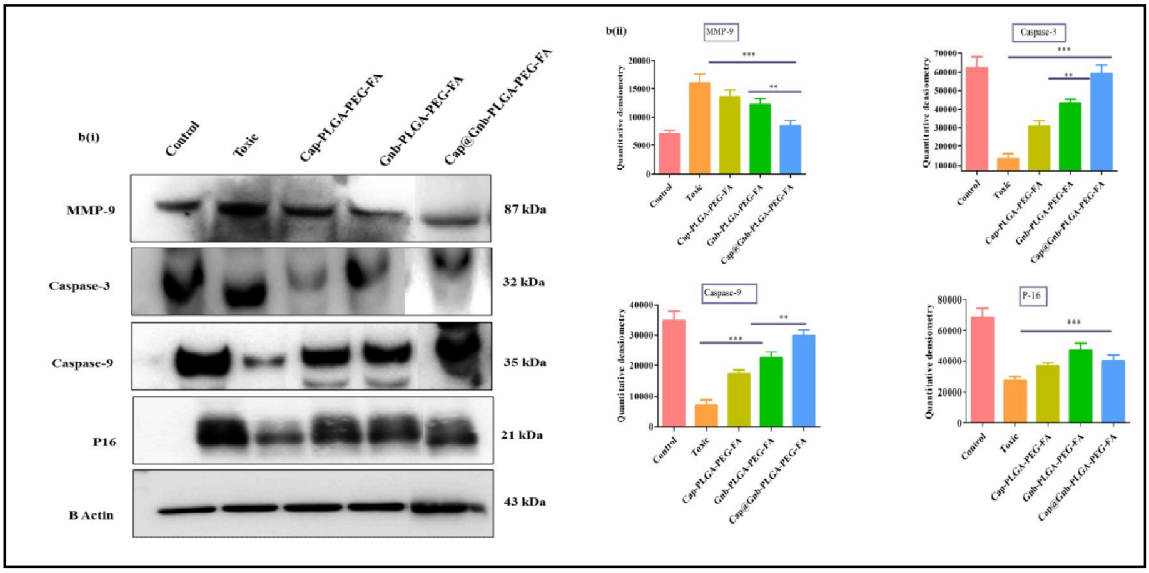

Figure 4.12. Effects of Gnb modified NPs on Pro-apoptotic and anti-apoptotic proteins. Three individual samples from each group were analyzed and subjected to statistical analysis (n = 3) *p < 0.05, **p < 0.01, ***p < 0.001**.**

4.11.4.Biodistribution Studies

The biodistribution study was performed to further investigate the targeting ability of FA modified NPs. Superior targeting potential of a delivery system is a principal prerequisite for effective anticancer therapy. It was observed that there was an enhanced concentration of

modified NPs in tumor tissue when compared with unmodified NPs and plain Gnb. As shown in **Figure 4.13a-d**, significantly higher concentration of Gnb accumulated in tumor tissues from Gnb-PLGA-PEG-FA and Cap@Gnb-PLGA-PEG-FA therapy i.e 45.17±3.23 µg/g and 47.31±2.19µg/g over a period of 4 h respectively. The Gnb levels were significantly higher at 4 h after administration and were scarcelyquantifiable after 48 h in case of unmodified NPs, while modified NPs retained themselves over a long span of time. Significant levels of Gnb were maintained in the tumor organ (39.87±1.33 µg/g) for12 h and 21.45±1.09 µg/g over a period of 48 h in case of Gnb-PLGA-PEG-FA treated group. While the co-therapy administered group maintained Gnb level at 23.98 ±1.32 µg/g and 40.03±2.11 µg/g over a period of 24 and 48 h in tumor organ respectively. Approximately, a 5 fold greater accumulation of drug was observed in tumor tissues when compared with free drug administration at all the time points. This specifies the interaction and accumulation of the folate conjugated NPs into over-expressed folate receptors present in lung tumor cells. This further proves the ability of FA functionalized NPs to localize preferentially in the tumor tissue when compared to free Gnb, specifying its reduced entry into other vital organs. However, no significant difference in biodistribution was observed in case of Cap@Gnb-PLGA-PEG-FA and Gnb-PLGA-PEG-FA as both the formulation were FA conjugated. Comparative biodistribution of Cap and Cap-PLGA-PEG-FA (individually) is presented in **Figure 4.14 a &b**.The biodistribution of Cap was found to be much higher when formulated as folate conjugated NPs. Approximately 5.5 times enhanced accumulation of Cap formulated as Cap-PLGA-PEG-FA was observed in lungs when compared with plain Cap. The concentration of Cap was found to be 39.21 ±1.22 µg/g and 7.50±1.87 µg/g at 4 h time point in lungs for Cap-PLGA-PEG-FA and plain Cap respectively.

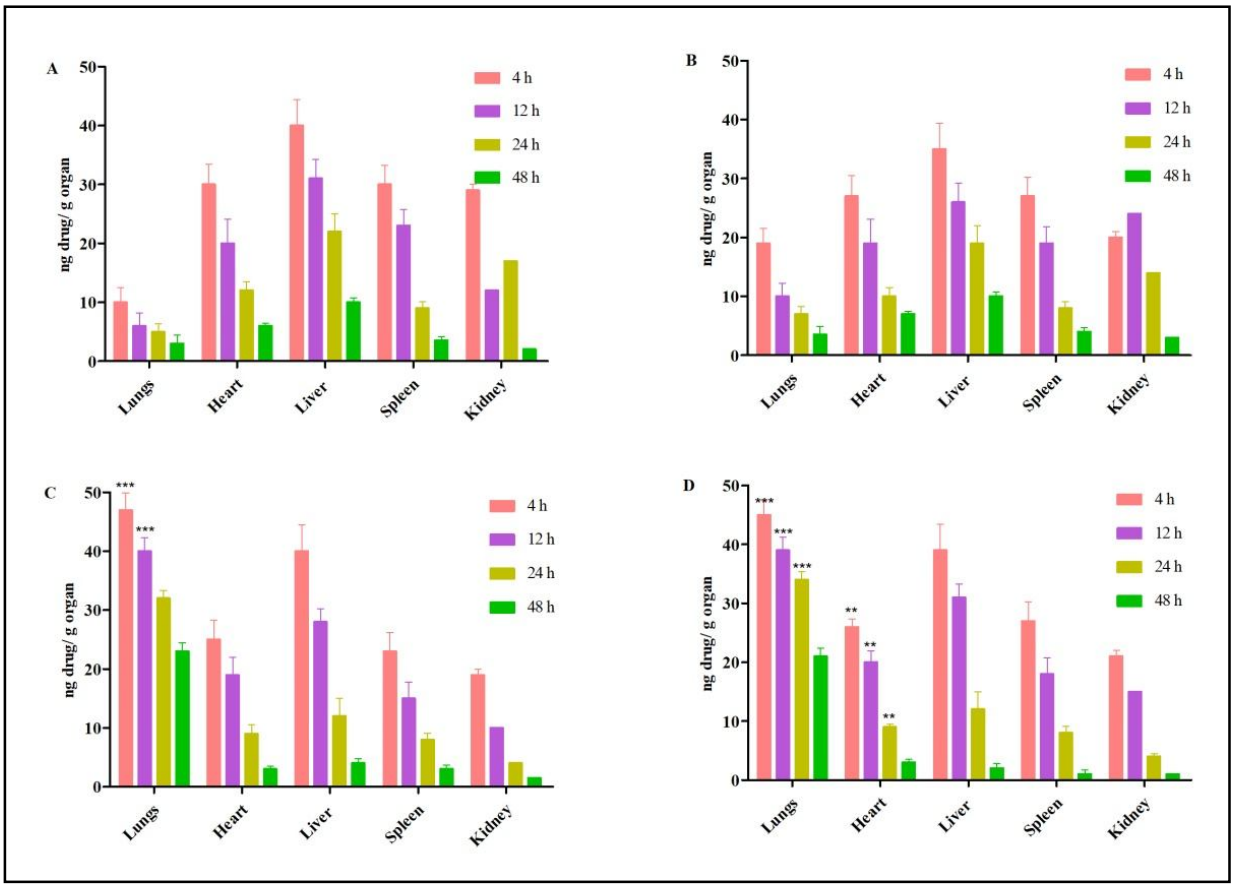

Figure 4.13. Amount of Gnb in different organs (lung, heart, liver, spleen, and kidney) after i.v. administration through tail vein (20 mg/kg Gnb equivalent dose) of (a) Plain Gnb (b) Gnb-PLGA (c) ap@Gnb-PLGA-PEG-FA (d) Gnb-PLGA-PEG-FA (n=6). [Values are presented as Mean ± SD (n=6); *** $p<0.001$ as compared to standard and marketed; ** $p<0.05$ as compared to other groups]

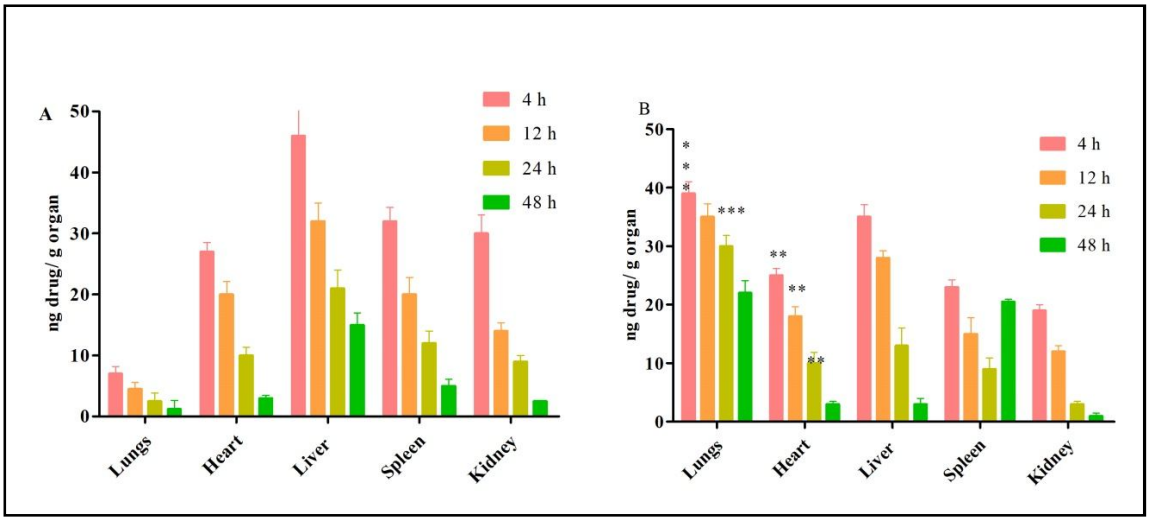

Figure 4.14. Amount of Cap in different organs (lung, heart, liver, spleen, and kidney) after i.v. administration through tail vein (10 mg/kg Cap equivalent dose) of (a) Plain Cap (b) Cap-PLGA-PEG-FA (n=6). [Values are presented as Mean ± SD (n=6); *** $p<0.001$ as compared to standard and marketed; ** $p<0.05$ as compared to other groups] Biodistribution of Cap in various organs (a) Plain Cap (b) Cap-PLGA-PEG-FA

4.12. Stability

This study was designed to investigate the storage stability of the developed Gnb-PLGA-PEG-FA and Cap-PLGA-PEG-FA over a prolonged period of time. The results revealed that the particle size, zeta potential and drug loading did not significantly change after storage period of 90 days under various conditions viz. stored under refrigeration (5±1°C), ambient temperatures (25±5°C, 60±5% RH) and elevated temperature (40±5°C, 75±5% RH). The results obtained validate the selected method for formulations as précise and accurate. The data is presented in **Table 4.5a&b** respectively.

Table 4.5. a) Stability of Gnb-PLGA-PEG-FA at various temperatures as per ICH guidelines

Sampling Interval (days)			Particle size (nm)			Zeta Potential (mV)		%Drug loading		
Gnb-PLGA-PEG-FA		**25°C ±2°C**	**5°C ±1°C**	**40°C ±2°C**	**25°C±2° C**	**5°C ±1°C**	**40°C ±2°C**	**25°C ±2^{0}C**	**5°C ±1°C**	**40°C ±2°C**
1	0	237.0 ± 3.2	237.0± 3.2	237.0± 3.2	−13.19± 2.01	−13.19 ± 2.01	−13.19 ± 2.01	20.88 ± 0.5	20.88±0. 51	20.88± 0.53
2	15	238.2 ±2.6	236.2±1 .9	240.2± 1.6	−14.09 ± 3.01	−12.14 ± 2.31	−15.19 ± 1.01	19.87 ± 0.4	19.86 ± 0.2	18.82 ± 0.3
3	30	238.3 ±2.3	238.2±2 .9	241.6± 3.6	−13.32 ± 2.09	−13.13 ± 2.31	−14.09 ± 2.11	19.85 ± 0.3	19.86 ± 0.3	18.79 ± 0.4
4	45	239.2 ±3.1	239.2±1 .2	243.2± 1.1	−14.09 ± 3.01	−12.20 ± 2.31	−15.09 ± 2.01	18.85 ± 0.4	17.83 ± 0.4	16.79 ± 0.1
5	90	240.2 ±3.6	239.7±3 .1	242.9± 1.9	−14.12 ± 3.01	−12.14 ± 2.31	−15.39 ± 1.31	18.82 ± 0.6	17.01 ± 0.1	15.99 ± 0.4

Table 4.5 b) Stability of Cap@Gnb-PLGA-PEG-FA at temperatures as per ICH guidelines

Sampling Interval (days)			Particle size (nm)		Zeta Potential (mV)				% Drug loading		
Cap-PLGA-PEG-FA			**25° C±2 °C**	**5°C ±1° C**	**40°C ±2°C**	**25°C±2 °C**	**5°C ±1°C**	**40°C ±2°C**	**25°C±2 ^{0}C**	**5°C ±1° C**	**40°C ±2°C**
1	0	243.0 ±5.2	243.0±5.2		243.0 ±5.2	−14. 45±0 .88	−14.45±0.88		−14.45± 0.88	21.92 ±0.2	21.92 ±0.2	21.92± 0.2
2	15	243.0 ±5.2	244.2±1.3		244.0 ±1.7	−14. 45±0 .88	−14.45±1.07		−14.45± 0.90	21.92 ±0.1	21.92 ±0.2	19.89± 0.1
3	30	243.0 ±5.2	244.5±1.1		245.0 ±1.8	−14. 45±0 .88	−13.92±0.36		−12.99± 1.30	18.87 ±0.4	20.40 ±0.3	18.86± 0.2
4	45	244.0 ±3.2	244.5±2.4		247.0 ±3.2	−13. 98±0 .25	−14.45±0.19		−12.45± 0.10	18.84 ±0.3	19.91 ±0.4	18.85± 0.4
5	9	245.0 ±2.9	246.0±3.6		249.0 ±4.2	−13. 6±.6	−13.90±0.76		−12.05± 0.99	17.82 ±0.1	19.89 ±0.2	16.80± 0.3

4.13. Discussion

PLGA possess various desirable properties such as biocompatibility, tailored biodegradation rate, facile surface modification for better delivery and interaction with biological membranes and is approved for clinical use in humans(Gentile et al. 2014). FA is widely used in the delivery of anticancer agents due to its small size, low cost, high tumor tissue specificity and non-immunogenic nature. The peaks of FA could be attributed to the stretching vibrations of C=C in the aromatic ring of folic acid(Choy et al. 2004). The bands at 1478.9 and 1761.34 cm−1 could be due to the formation of amide linkage in PLGA-PEG-FA between carbonyl (C=O) and amine (N−H) groups respectively(Chen et al. 2017). The most significant FTIR absorption peak at 3431.16 cm^{-1} in PLGA-PEG-FA is due to the presence of -CONH- linkage (Esmaeili et al. 2008).The folate conjugation was successfully achieved and was further asserted by, ^{1}H-NMR spectrum and folate content assay were found to be similar as reported in proceeding studies(Liu et al. 2017).The process adopted in formulating modified and unmodified NPs yields particles within the nano range having low polydispersity index indicating the system to be homogenous. A high negative charge on the surface as revealed by zeta potential confirms a well dispersed and less aggregated nanoparticulate system. PVA was used as an emulsifier which contributed to formation of uniform nanosized particles. PVA is known to have a unique property of interaction with PLGA co-polymer due to the presence of vinyl acetate and vinyl alcohol groups in the polymer chain. The increase in particle size upon FA conjugation is attributed to the fact that FA attaches itself on the surface of PLGA-PEG through crosslinking via linker DCC (Sharma et al. 2013). The modified NPs showed a slight decrease in %EE which could be due to the loss of free drug from the surface of unmodified NPs during conjugation with activated FA. The modified and unmodified formulations showed a slow release in the later stage because of slow erosion of the polymer in pH 6.8, and the drug was available for dissolution only after the erosion of polymeric layers(Singh et al. 2017). This was further proven by Higuchi fit model, which indicates that the release is diffusion controlled.

Four parameters of enhanced cellular uptake, reduced cell viability; lower IC50 and better biodistribution in case of modified NPs are attributed to FA conjugation. FA receptors are highly expressed in tumor cells, and modified NPs hold high affinity towards them, thus

readily taken up by the tumor cells. FA has high binding affinity (Kd ~10-10 m) towards folate receptors, which facilitates modified NPs to enter the cells through FA receptor-mediated endocytosis as displayed by modified NPs (Yameen et al. 2014, Butt et al. 2015). The improved anticancer activity of FA modified NPs could be due to ligand receptor interaction between folate group of NPs and folate receptorson the cancer cells, which alters the percent of NPsto internalize more into the tumors(Han et al. 2017). The least viability of cancerous cells indicates synergistic effect of Cap and Gnb modified NPs, which could again be due to enhanced penetration of the drugs into the cells due to their nanosize and higher affinity towards folate receptors and higher accumulation of drug.

The aim of this work was to investigate whether combination therapy with Cap and Gnb may hold any promise for improved LC treatment. Furthermore, in view of high toxicity and resistance development associated with the Gnb chemotherapy, the use of rational chemotherapeutic combinations, in which a natural agent with a different mechanism of action was used for a synergistic approach. Combination therapy through various anticarcinogenic agent NPs has the capability of enhancing the apoptotic effect as reported in previous literature (Zhang et al. 2012, Nie et al. 2015, Chen et al. 2017). The synergistic effect was further proved by isobologram analysis. As is evident in the isobologram, the maximum effect was shown by the combination of gefitinib and capsaicin, rather than either capsaicin or gefitinib. Thus, when the combined effect is greater than that of individual drug candidates, the combination is said to be synergistic(Tallirada 2011). Such combinations demonstrating synergism have been proven beneficial in cancer therapies, as they may lower doses of the combination neoplastic agents, a probability of reduced adverse reactions (Gravitz 2011). Further, the CI value of 0.29409 was found in a range of 0.1–0.3 confirming strong synergism, validating the potential of our delivery system (Chou 2006).

Various reports suggest the apoptosis producing mechanisms for Cap. Cap causes apoptosis by inhibiting NF-κ activation by hindering its nuclear migration. Subsequent tumor necrosis factor-α–stimulates the degradation of IκBα, a factor associated with the inhibition of proteasome activity (Zhang et al. 2017). Cap is known to alter the production of reactive oxygen species by inhibition of the NADH dependent plasma membrane electron transport system with a consequent disruption of mitochondria transmembrane potential (Kim et al. 2015).These altered ROS and peroxynitrite levels result in inhibition of NADH oxidase

activity in cancer cells.The most important mechanism underlying enhanced apoptosis as co-therapy with Cap, is the property of Cap to cause production of heat-sensation over cancer cells, mediated by the transient receptor potential vanilloid 1 (TRPV1) receptor (Reyes-Escogido et al. 2011). This activation sensitizes the cancer cells to respond towards other therapeutic agents (Gnb) as evident from cell line studies. It has also been reported that Cap hinders chemotherapy induced autophagy through activation of the phosphoinositide 3-kinase (PI3K)/protein kinase B (AKT)/ (mTOR) pathway in cancer cells, which make the cells more susceptible to responddesirably to chemotherapeutic agents (Joe et al. 1994, Hong et al. 2015).

Keeping in mind the above mechanisms, we can explain the rationale behind taking Cap and Gnb in combination, which was confirmed by the additive inhibitory effects *in vitro* (A549 cell lines) as well as via *in vivo* animal studies. Synergistic effects were observed on ROS generation, MMP disruption, cell cycle arrest and apoptosis. The co-therapy through Cap@Gnb-PLGA-PEG-FA has proven to be more effective against lung cancer cell growth as compared to individual therapy either by Cap or Gnb. This can be further supported by the significant reduction in IC_{50} values (47.34±0.31 µM to 23.5±0.76µM) by Cap@Gnb-PLGA-PEG-FA when compared to Gnb or Cap NPs, individually. The cell arrest was found to be maximum in case of modified Cap@Gnb-PLGA-PEG-FA which could be associated with dual action of both drugs at different phasesi.e G2/M phase arrest caused by Gnb and Cap causes cell growth arrest in the G0/G1 phase of the cell cycle and a decrease of cells in the S phase as shown in Figure 4.8 F&E. Enhanced apoptosis due to synergistic effect of Gnb and Cap can be clearly observed from the Figure 4.8 E. Second possible reason for enhanced apoptosis could be binding of NPs to overexpressed FA receptors as stated above and augmented delivery of drug into the cells as proven by cellular uptake studies.

The highest disruption of MMP was observed in case of Cap@Gnb-PLGA-PEG-FA, because of the presence of Cap with Gnb, since Cap is known to modulate the ROS levels which disrupt the MMP and result in apoptosis as stated above (Sánchez et al. 2007). On the other side Gnb induces apoptosis by blocking the signal transmission by competitive binding Mg-ATP situated on the catalytic domain of EGFR-TK which inhibits the activation of mitogen activated protein kinase in the cancer cell (Morabito et al. 2013).

The differential effect on lung weight, animal weight and tumor regression among various groups can be correlated to the synergetic effect of Cap and Gnb. Superior therapeutic efficacy by Cap@Gnb-PLGA-PEG-FA could be due to additional properties like anti-proliferative and anticarcinogenic activity of Cap in combination with Gnb which would be further enhanced by surface modification.

Cap has been reported to enhance caspase-3, caspase-6 and caspase-9 activation and inhibit interleukin-6-induced STAT3 activation. The results of western analysis of our study are in good agreement with the ability of Cap for inducing DNA damage through upregulation of pro-apoptotic proteins Caspase- 3/9 suggesting that this is one reason for enhanced apoptosis. Another mechanism suggests binding of Cap to the TRPV1 receptor which prompts p38 MAP kinase stimulation. This results in enhancement of mitochondrial permeability and causes downstream activation of caspase-9 (Reilly et al. 2003, Sánchez et al. 2007, Ziglioli et al. 2009).

To further address the underlying mechanism of this enhanced cell apoptosis, the activity of MMP-9 expression was examined in tumor tissue via western analysis. These findings indicate that the co therapy restricts cancer cell invasion by suppressing MMP-9 activities. The results indicate down regulation of MMP-9, and up regulation of P-16,which could be a primary reason for reduced tumor volume and improved survival of animals in the groups receiving combination therapy (Goren et al. 2000, Sharma et al. 2017). Also, it can be concluded that these factors are important markers in LC prognosis (Krug et al. 2003, Takenaka et al. 2017).

Biochemical estimation of various parameters viz, SOD, TBARS, GSH, catalase etc. are strongly evidenced by diminished oxidative stress. Histopathological and biochemical results also evidenced supremacy of Cap@Gnb-PLGA-PEG-FA over individual therapy by Gnb/Cap, which could be attributed to enhanced targeting potential of FA as well as the property of Cap to cut oxidative stress (Reyes-Escogido et al. 2011). As described in preceding studies, intracellular ROS accumulation, consecutive Akt pathway inactivation, and the successive alteration of apoptotic-regulated proteins can trigger the apoptotic cascade resulting in better therapeutic outcome (Najlah et al. 2017). The biodistribution studies further strengthen the evidences for potential targeting of FA functionalized NPs into tumor. This may be explained on the basis of the presence of folate receptors on tumor

tissues that favored discriminatory entry of Gnb-PLGA-PEG-FA and Cap@Gnb-PLGA-PEG-FA in tumors. The presence of folate receptors on the tumor surface offers an interesting platform and accelerates targeting. This scheme will help to augment the therapeutic efficacy by reducing the dose of therapeutic moiety. The modified NPs were stable for a period of 90 days indicating that the opted method for formulation and optimization of NPs was accurate and precise. The advantages of co-therapy comprise use of two drugs at lower concentrations which reduced toxicity and side effects during treatment while promoting enhanced cell apoptosis. The newer more promising natural agents could also be investigated in combination with Gnb in future studies. Further, formulating them as modified NPs couldenable better interaction with biological membranes, enhanced targeting potential and higher accumulation of drug in the tumor cells.

4.14. Conclusions

The lung-targeted drug delivery of FA anchored NPs (Gnb-PLGA-PEG-FA and Cap-PLGA-PEG-FA) were successfully prepared and characterized. The presents study indicates the targeting potential, spatial delivery, augmented therapeutic prospective and higher retention potential of the modified NPs into tumor tissues. Further, the presence of folic acid receptors in tumor tissues offers a platform and diverse imitation of ligand to facilitate the tumor targeting. Various *in vitro* and *in vivo* studies proved remarkably higher drug accumulation in tumor tissues with FA-anchored NPs when compared to plain Gnb/Cap. Moreover, *in vitro* cell uptake results displayed that surface modification with FA to Gnb/Cap might significantly intensify the affinity of NPs, towards A549 cell lines. Finally, the present investigation exhibits the prospects of co-administration of FA anchored Cap and Gnb NPs as synergistic therapy to offer enhanced therapeutic efficacy and antitumor effect. In conclusion, developed Cap@Gnb-PLGA-PEG-FA nano-particulate system demonstrated minimal toxicity, facilitated targeted delivery to tumor sites, with diminished access to normal cells as a result of surface modification. In light of the above studies it can be concluded that a safe natural anticancer agent like Cap can be an alternative to synergize synthetic anticarcinogenic agents to be prepared as nanoformulations. Further, studies can be performed to recognize the effect of combination therapy on carcinomas and subsequent scale-up from bench to bedside.

REFERENCES

Boddu, S. H., R. Vaishya, J. Jwala, A. Vadlapudi, D. Pal and A. Mitra (2012). "Preparation and characterization of folate conjugated nanoparticles of doxorubicin using PLGA-PEG-FOL polymer." Med. Chem**2**(4): 68-75.

Brigger, I., C. Dubernet and P. Couvreur (2002). "Nanoparticles in cancer therapy and diagnosis." Adv. Drug Deliv. Rev.**54**(5): 631-651.

Butt, A. M., M. C. I. M. Amin and H. Katas (2015). "Synergistic effect of pH-responsive folate-functionalized poloxamer 407-TPGS-mixed micelles on targeted delivery of anticancer drugs." Int. J. Nanomedicine**10**: 1321.

Chen, D., F. Xie, D. Sun, C. Yin, J. Gao and Y. Zhong (2017). "Nanomedicine-Mediated Combination Drug Therapy in Tumor." Open Pharm. Sci. Journal**4**(1).

Choy, J.-H., J.-S. Jung, J.-M. Oh, M. Park, J. Jeong, Y.-K. Kang and O.-J. Han (2004). "Layered double hydroxide as an efficient drug reservoir for folate derivatives." Biomaterials**25**(15): 3059-3064.

Esmaeili, F., M. H. Ghahremani, S. N. Ostad, F. Atyabi, M. Seyedabadi, M. R. Malekshahi, M. Amini and R. Dinarvand (2008). "Folate-receptor-targeted delivery of docetaxel nanoparticles prepared by PLGA–PEG–folate conjugate." J. Drug Target.**16**(5): 415-423.

Gentile, P., V. Chiono, I. Carmagnola and P. V. Hatton (2014). "An overview of poly (lactic-co-glycolic) acid (PLGA)-based biomaterials for bone tissue engineering." International journal of molecular sciences**15**(3): 3640-3659.

Goren, D., A. T. Horowitz, D. Tzemach, M. Tarshish, S. Zalipsky and A. Gabizon (2000). "Nuclear delivery of doxorubicin via folate-targeted liposomes with bypass of multidrug-resistance efflux pump." Clin. Cancer Res.**6**(5): 1949-1957.

Guo, C.-L., H.-Y. Chen, B.-L. Cui, Y.-H. Chen, Y.-F. Zhou, X.-S. Peng and Q. Wang (2015). "Development of a HPLC method for the quantitative determination of capsaicin in collagen sponge." International Journal of Analytical Chemistry**2015**.

Han, N., L. Pang, J. Xu, H. Hyun, J. Park and Y. Yeo (2017). "Development of surface-variable polymeric nanoparticles for drug delivery to tumors." Molecular pharmaceutics**14**(5): 1538-1547.

He, Z., J. Huang, Y. Xu, X. Zhang, Y. Teng, C. Huang, Y. Wu, X. Zhang, H. Zhang and W. Sun (2015). "Co-delivery of cisplatin and paclitaxel by folic acid conjugated amphiphilic PEG-PLGA copolymer nanoparticles for the treatment of non-small lung cancer." Oncotarget**6**(39): 42150.

Hong, Z.-F., W.-X. Zhao, Z.-Y. Yin, C.-R. Xie, Y.-P. Xu, X.-Q. Chi, S. Zhang and X.-M. Wang (2015). "Capsaicin enhances the drug sensitivity of cholangiocarcinoma through the inhibition of chemotherapeutic-induced autophagy." PloS one**10**(5): e0121538.

Houston, K. A., S. J. Henley, J. Li, M. C. White and T. B. Richards (2014). "Patterns in lung cancer incidence rates and trends by histologic type in the United States, 2004–2009." Lung Cancer**86**(1): 22-28.

Joe, B. and B. Lokesh (1994). "Role of capsaicin, curcumin and dietary n—3 fatty acids in lowering the generation of reactive oxygen species in rat peritoneal macrophages." BBA-Molecular Cell Research**1224**(2): 255-263.

Kaithwas, G. and D. K. Majumdar (2012). "In vitro antioxidant and in vivo antidiabetic, antihyperlipidemic activity of linseed oil against streptozotocin□induced toxicity in albino rats." European Journal of Lipid Science and Technology**114**(11): 1237-1245.

Kim, S. M., E. Y. Oh, J. H. Lee, D. Nam, S. G. Lee, J. Lee, S. H. Kim, B. S. Shim and K. S. Ahn (2015). "Brassinin Combined with Capsaicin Enhances Apoptotic and Anti□metastatic Effects in PC□3 Human Prostate Cancer Cells." Phytother Res.**29**(11): 1828-1836.

Kouchakzadeh, H., T. Soudi, A. N. Heshmati and S. Shojaosadati (2017). "Ligand-modified biopolymeric nanoparticles as efficient tools for targeted cancer therapy." Curr. Pharm. Des.
Krug, L. M., V. A. Miller, D. A. Filippa, E. Venkatraman, K. K. Ng and M. G. Kris (2003). "Bcl-2 and bax expression in advanced non-small cell lung cancer: lack of correlation with chemotherapy response or survival in patients treated with docetaxel plus vinorelbine." Lung Cancer**39**(2): 139-143.
Liu, Y., X.-M. Yu, R.-J. Sun and X.-L. Pan (2017). "Folate-Functionalized Lipid Nanoemulsion to Deliver Chemo-Radiotherapeutics Together for the Effective Treatment of Nasopharyngeal Carcinoma." AAPS PharmSciTech**18**(4): 1374-1381.
Morabito, A., R. Costanzo, A. M. Rachiglio, R. Pasquale, C. Sandomenico, R. Franco, A. Montanino, E. De Lutio, G. Rocco and N. Normanno (2013). "Activity of Gefitinib in a Non–Small-Cell Lung Cancer Patient with Both Activating and Resistance EGFR Mutations." J. Thorac. Oncol.**8**(7): e59-e60.
Muralidharan, R., A. Babu, N. Amreddy, K. Basalingappa, M. Mehta, A. Chen, Y. D. Zhao, U. B. Kompella, A. Munshi and R. Ramesh (2016). "Folate receptor-targeted nanoparticle delivery of HuR-RNAi suppresses lung cancer cell proliferation and migration." J. Nanobiotechnology**14**(1): 47.
Najlah, M., Z. Ahmed, M. Iqbal, Z. Wang, P. Tawari, W. Wang and C. McConville (2017). "Development and characterisation of disulfiram-loaded PLGA nanoparticles for the treatment of non-small cell lung cancer." Eur. J. Pharm. Biopharm.**112**: 224-233.
Ni, X. L., L. X. Chen, H. Zhang, B. Yang, S. Xu, M. Wu, J. Liu, L. L. Yang, Y. Chen and S. Z. Fu (2017). "In vitro and in vivo antitumor effect of gefitinib nanoparticles on human lung cancer." Drug Deliv.**24**(1): 1501-1512.
Nie, P., W. Hu, T. Zhang, Y. Yang, B. Hou and Z. Zou (2015). "Synergistic induction of erlotinib-mediated apoptosis by resveratrol in human non-small-cell lung cancer cells by down-regulating survivin and up-regulating PUMA." Cell Physiol Biochem**35**(6): 2255-2271.
O'brien, J., I. Wilson, T. Orton and F. Pognan (2000). "Investigation of the Alamar Blue (resazurin) fluorescent dye for the assessment of mammalian cell cytotoxicity." The FEBS Journal**267**(17): 5421-5426.
Othman, Z. A. A., Y. B. H. Ahmed, M. A. Habila and A. A. Ghafar (2011). "Determination of capsaicin and dihydrocapsaicin in Capsicum fruit samples using high performance liquid chromatography." Molecules**16**(10): 8919-8929.
Pandey, M., S. Sultana and K. P. Gupta (2014). "Involvement of epigenetics and microRNA-29b in the urethane induced inception and establishment of mouse lung tumors." Experimental and molecular pathology**96**(1): 61-70.
Parashar, P., M. Rathor, M. Dwivedi and S. A. Saraf (2018). "Hyaluronic Acid Decorated Naringenin Nanoparticles: Appraisal of Chemopreventive and Curative Potential for Lung Cancer." Pharmaceutics**10**(1): 33.
Reilly, C. A., W. J. Ehlhardt, D. A. Jackson, P. Kulanthaivel, A. E. Mutlib, R. J. Espina, D. E. Moody, D. J. Crouch and G. S. Yost (2003). "Metabolism of capsaicin by cytochrome P450 produces novel dehydrogenated metabolites and decreases cytotoxicity to lung and liver cells." Chem. Res. Toxicol.**16**(3): 336-349.
Reyes-Escogido, M. d. L., E. G. Gonzalez-Mondragon and E. Vazquez-Tzompantzi (2011). "Chemical and pharmacological aspects of capsaicin." Molecules**16**(2): 1253-1270.
Sánchez, A. M., S. Malagarie-Cazenave, N. Olea, D. Vara, A. Chiloeches and I. Díaz-Laviada (2007). "Apoptosis induced by capsaicin in prostate PC-3 cells involves ceramide accumulation, neutral sphingomyelinase, and JNK activation." Apoptosis**12**(11): 2013-2024.
Sharma, G., A. Kumar, S. Sharma, M. Naushad, R. P. Dwivedi, Z. A. ALOthman and G. T. Mola (2017). "Novel development of nanoparticles to bimetallic nanoparticles and their composites: a review." J. King Saud Univ. Sci.

Sharma, M., R. Malik, A. Verma, P. Dwivedi, G. S. Banoth, N. Pandey, J. Sarkar, P. R. Mishra and A. K. Dwivedi (2013). "Folic acid conjugated guar gum nanoparticles for targeting methotrexate to colon cancer." J. Biomed. Nanotechnol.**9**(1): 96-106.

Singh, N., P. Parashar, C. B. Tripathi, J. Kanoujia, G. Kaithwas and S. A. Saraf (2017). "Oral delivery of allopurinol niosomes in treatment of gout in animal model." Journal of liposome research**27**(2): 130-138.

Soppimath, K. S., T. M. Aminabhavi, A. R. Kulkarni and W. E. Rudzinski (2001). "Biodegradable polymeric nanoparticles as drug delivery devices." J. Control. Release**70**(1): 1-20.

Surh, Y.-J. and S. Lee (1996). "Capsaicin in hot chili pepper: carcinogen, co-carcinogen or anticarcinogen?" Food Chem. Toxicol.**34**(3): 313-316.

Takenaka, T., M. Katayama, A. Sugiyama, M. Hagiwara, I. Fujii, T. Takatani-Nakase, S. S. Kobayashi and I. Nakase (2017). "Gefitinib Enhances Mitochondrial Biological Functions in NSCLCs with EGFR Mutations at a High Cell Density." Anticancer research**37**(9): 4779-4788.

Vangara, K. K., J. L. Liu and S. Palakurthi (2013). "Hyaluronic acid-decorated PLGA-PEG nanoparticles for targeted delivery of SN-38 to ovarian cancer." Anticancer Res.**33**(6): 2425-2434.

Wang, S.-J., Z.-J. Huo, K. Liu, N. Yu, Y. Ma, Y.-H. Qin, X.-C. Li, J.-M. Yu and Z.-Q. Wang (2015). "Ligand-conjugated pH-sensitive polymeric micelles for the targeted delivery of gefitinib in lung cancers." RSC Advances**5**(89): 73184-73193.

Yameen, B., W. I. Choi, C. Vilos, A. Swami, J. Shi and O. C. Farokhzad (2014). "Insight into nanoparticle cellular uptake and intracellular targeting." Journal of Controlled Release**190**: 485-499.

Yoo, H. S. and T. G. Park (2004). "Folate receptor targeted biodegradable polymeric doxorubicin micelles." J. Control. Release**96**(2): 273-283.

Zhang, S.-s., Y.-h. Ni, C.-r. Zhao, Z. Qiao, H.-x. Yu, L.-y. Wang, J.-y. Sun, C. Du, J.-h. Zhang and L.-y. Dong (2017). "Capsaicin enhances the antitumor activity of sorafenib in hepatocellular carcinoma cells and mouse xenograft tumors through increased ERK signaling." Acta Pharmacologica Sinica.

Zhang, Z., J. C. Lee, L. Lin, V. Olivas, V. Au, T. LaFramboise, M. Abdel-Rahman, X. Wang, A. D. Levine and J. K. Rho (2012). "Activation of the AXL kinase causes resistance to EGFR-targeted therapy in lung cancer." Nature Genet**44**(8): 852-860.

Ziglioli, F., A. Frattini, U. Maestroni and F. Dinale (2009). "Vanilloid-mediated apoptosis in prostate cancer cells through aTRPV-1 dependent and a TRPV-1-independent mechanism." Acta Biomed.**80**(1): 13-20.

Chapter V

Biotinylated Nanoparticles

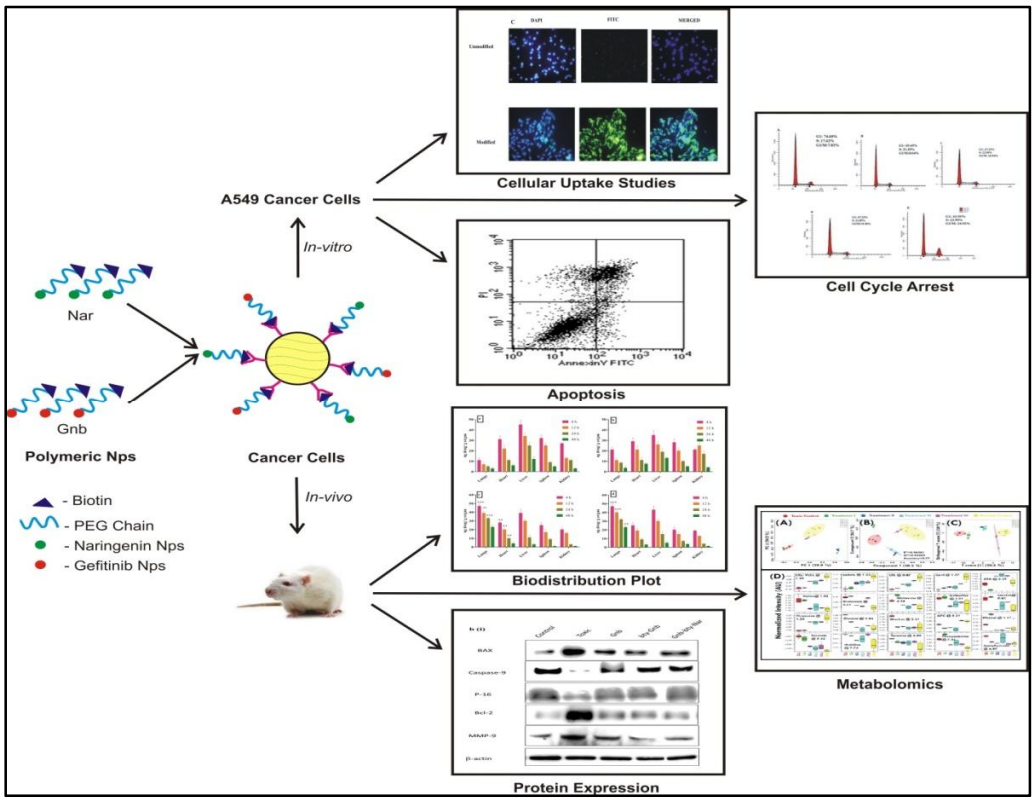

5. Formulation and Evaluation of Biotin Decorated PCL Nanoparticles of Naringenin and Gefitinib

5.1 Introduction

Numerous biodegradable polymers, of synthetic origin have been utilized in formulating NPs(Mogoşanu et al. 2016). PCL-PEG was selected in particular, as it is known to form a stable hydrophobic core while PEG forms the external coating which shields the carrier from immediate systemic clearance(Sinha et al. 2004). Furthermore, many functional groups on PCL such as hydroxyl and ketone groups make it a suitable candidate for surface modification with cancer-overexpressed molecules(Blanco et al. 2011). Currently receptor targeted drug delivery is the most frequently used methodology for delivering drug to the specific tumor cells. Receptor targeting helps in the easy uptake of NPs via endocytosis. The specific ligands such as monoclonal antibody, folic acid, biotin, aptamers, oligopeptides and hyaluronic acid were frequently conjugated to the surface of NPs and employed as tumor-specific "guiding modules"(Chen et al. 2010).Biotin (bty) commonly known as vitamin H or B-7 is a growth promoter at the cellular level, and its concentration in tumors is significantly higher than that in normal tissues(Brannon-Peppas et al. 2012). Biotin receptors are overexpressed in a number of cancer cells such as leukemia (L1210FR), breast (MMT06056), colon (Colo-26), lung (NCI-H69, A549), renal (RENCA, RD0995) and many more(Tseng et al. 2007, Tseng et al. 2009). Accordingly, we designated biotin as tumor targeting molecule for delivering polymeric NPs.

In order to target multiple growth promoting pathways, combination therapies using different anticarcinogenic agents have been reported earlier. Over the past few decades the use of natural components specifically vitamins and flavonoids have seen recognized as chemopreventive and therapeutic agents against cancer. Naringenin (Nar) is a flavonoid primarily found in citrus fruits and has a bioactive effect on human health. Several reportssay that Nar possess antioxidant, anti-mutagenic and anti-carcinogenic activities(Jin et al. 2009, Chang et al. 2017).

Gefitinib (Gnb) is a tyrosine kinase inhibitor which holds a high affinity towards epithelial growth factor receptor (EGFR) which is over expressed in lung cancer (LC)(Morabito et al.

2013). Gnb is capable of inducing angiogenesis, metastasis and apoptosis in LC tumor cells(Ni et al. 2017). It mainly acts by competitive binding of Mg-ATP situated on the catalytic domain of EGFR-TK (Epidermal growth factor receptor tyrosine kinase) resulting in activation of mitogen activated protein kinase leading to blocking the signal transmission(Cataldo et al. 2011). Biotin at the cellular levelplays has an imperative role in epigenetic gene regulation;cell signaling and chromatin structure (Zempleni et al. 2009).Biotin is not synthesized in mammalian cells as they lack biotin synthetic pathway. Therefore, it has to be taken externally through other sources likeplants and bacteria. The mammalian cells achievebiotin uptake throughbiotin transporter which hold high-affinity for biotin. Also, fractional biotin uptake is done through sodium-dependent multivitamin transporter(Azhar et al. 2015). The aforementionedleadingtransporter for biotin uptake, are overexpressed in several aggressive tumors such as lung, colon, leukemia, breast, ovarian and renal tumor (Ren et al. 2015).

This chapter deals withthe development and characterization ofNar/Gnb loadedbiotindecorated PCL nanoparticles. The present study is aimed at themethodical development and in-depth evaluation of biotin decorated PCL nanoparticles for the selective delivery of Gefitinib (Gnb) and Naringenin (Nar) to lung cancer cells, utilizing synergistic approach.The Nar/Gnb loaded biotin decorated NPs were developed utilizing o/w emulsion and solvent extraction evaporation technique and optimization through central composite design (CCD) to achieve enhanced and specific delivery as well as target specificity.The drug delivery and anticancer potentials of the NPs was ascertained by means of particle size analysis, zeta potential and drug release kinetics study. The MTT assay[3-(4,5-dimethylthiazol-2-yl)-2,5-diphenyltetrazolium] bromide was employed to examine *in vitro* cytotoxicity of the free drug as well as of the biotin decorated NPs. Finally, the effect of free drug, unmodified NPs and surface modified NPs was evaluated in urethane-induced LC in experimental animals. Dysregulation of various pro-apoptotic (BAX, MMP-9, Caspase-3 and Caspase-9) and anti- apoptotic proteins (Bcl-2 and P-16) wass analyzed via western blot.

5.2 Materials

Gefitinib (Gnb) was obtained as a generous gift from M/s United Biotech, Solan, India. Naringenin was purchased from M/s Vandeep Suppliers Pvt. Ltd, Kolkata, India. PCL (Mw:80,000 Da), was purchased from Sigma-Aldrich, USA. Polyvinyl alcohol (PVA) and biotin were procured from Sigma Chemicals (St Louis, MO, USA). N-hydroxysuccinimide (NHS), N,N'-Dicyclohexylcarbodiimide (DCC), Poly(ethylene glycol) bis(amine) (PEG-bisamine, MW 3.4kDa), Propidium Iodide, RNase A, DMEM (Dulbecco's Modified Eagle's medium), Fetal Bovine Serum (FBS), tris-buffered saline (TBS) and tween 20 (TBST), MTT (3-(4,5-Dimethylthiazol-2-yl)-2,5-diphenyl tetrazolium bromide), DAPI 2-(4-amidinophenyl)-1H -indole-6-carboxamidine,Nonidet P-40 (NP-40s) were purchased from M/s Sigma Aldrich, USA. Di-methyl Sulfoxide (DMSO) and dichloromethane were obtained from Fisher Scientific (Pittsburgh, PA, USA). All antibodies were purchased from M/s Santa Cruz, CA, USA. All other chemicals used in the study were of analytical grade. In house double distilled water was used throughout the experiment.

5.2.1. Animals

The *in vivo* study was performed according to the CPCSEAguidelines as accepted principles for the use of experimental animals and approved by the Institutional Animal Ethics Committee as per approval number SDCOPVS/AH/CPCSEA/01/0028. Albino wistar rats (male/female, seven-week-old) were fed with synthetic pellet diet (M/S Provimi Animal Nutrition India Pvt. Ltd. Bangalore) and water ad libitum. Animals were kept in polypropylene cages in a well-ventilated animal house at temperature 22°C±2°C. Animals were divided into 06 groups having 9 animals each, under a 12 h light/ dark cycle, and acclimatized for 2 weeks. All animals were handled as per institutional animal ethics norms, and care was taken that all guidelines were followed with a human approach.

5.2.2.Cell Lines

Human non-small-cell lung carcinoma (NSCLC) cell lines (A549) were obtained from American Type Culture Collection (ATCC, Rockville, MD, USA). Cells were maintained in

appropriate culture medium in Dulbecco's Modified Eagle's Medium DMEM supplemented with 10% fetal bovine serum and 1% antibiotic (penicillin) solution. A549 cells were maintained at 37°C with 5% CO_2 in incubator(Chang et al. 2011).

5.3. Methods

5.3.1. Preparation of Biotin Decorated PCL Nanoparticles

The PCL polymer was surface decorated with biotin as per scheme 1-3 (Figure 5.1)discussed below-

The active NHS ester of biotin was prepared as per previous reported method (Lee et al. 1994, Wu et al. 2016). Biotin (17.10 mg), DCC (14.44 mg) and NHS (8.05 mg) (1:1:1 molar ratio) in DMSO at 50°C, was stirred for 2 h and allowed to react overnight at room temperature. Biotin-NHS was obtained by precipitation with acetone (**Figure 5.1, Scheme 1)**. PCLderivative was synthesized by dissolving PCL (1g) in DMSO and DCC (2.57 mg) in equimolar ratio and kept under stirring in dark for 12 h (**Figure 5.1, Scheme 2)**. Thereafter, PEG-bis-amine (37.5 mg) was added to the above solution and was stirred for 3 h to obtain primary amine terminal of PCL (PCL-PEG-NH_2). The dicyclohexylurea precipitate was filtered through glass wool and the filtrate was dried under vacuum. Further, Biotin–NHS (4.49 mg) was added to PCL-PEG-NH_2 (137.5mg) dissolved in DMF and allowed to react overnight under stirring (**Figure 5.1, Scheme 3)**. After stirring overnight at room temperature, the product was placed in a dialysis bag (8-12 kDa MWCO) and dialyzed against distilled water for 2 h. The dialyzed product was freeze dried and stored at 4 °C for further use.

Scheme- 1

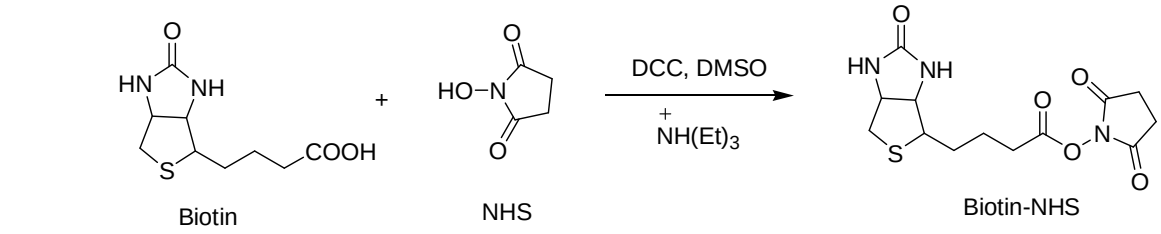

Scheme- 2

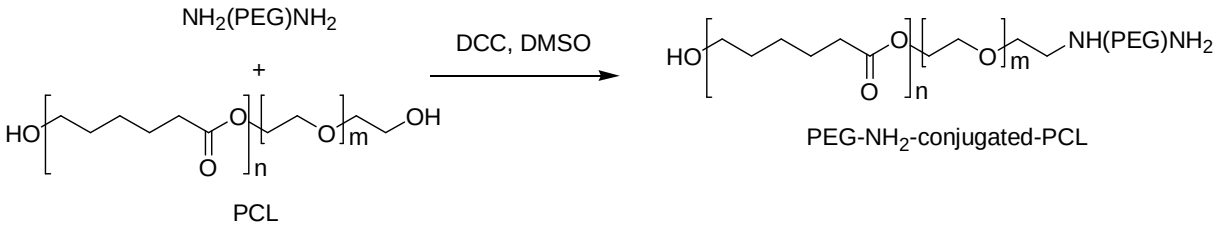

Scheme- 3

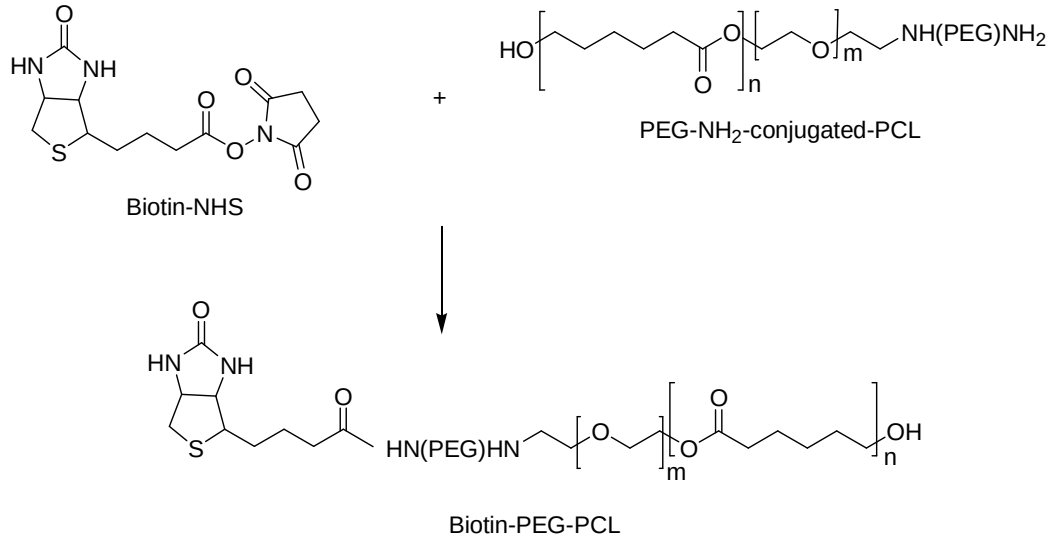

Figure 5.1 Schematic representation of biotin conjugation synthesis **Scheme 1:** Synthesis of activated biotin (biotin NHS); **Scheme 2:** Synthesis of PEG-NH_2 conjugated PCL (PCL-PEG-NH_2); **Scheme 3:** Synthesis of biotin attached PCL (bty- PEG-PCL).

5.3.1.1. Characterization of Biotin decorated PCL

5.3.1.1.1. FTIR characterization

Synthesis of biotin NHS, PCL-PEG-NH_2 and bty- PEG-PCL was confirmed by FTIR analysis. Further, ^{1}H-NMR of bty- PEG-PCL was conducted to ascertain biotin surface attachment.

5.3.1.1.2. ^{1}H-NMR characterization

The conjugation of biotin to PCL through PEG was established through protonNMR spectroscopy (Bruker Avance 400, FT-NMR) and chemical shifts (δ) were presented as parts per million (ppm) relative to the NMR solvent signal (d6-DMSO) using tetramethylsilane (internal standard).

5.4. Preparation of Gnb loaded poly (e-caprolactone) nanoparticles (PCL-Gnb/Nar)

Gnb loaded PCL NPs were formulated employing o/w emulsion and solvent extraction evaporation technique as reported elsewhere(Mattu et al. 2013). Briefly PCL and Gnb/Nar were dissolved in 5 ml of methylene chloride and added dropwise into 1% w/v PVA solution, followed by sonication at 200W under ice bath for 2 seconds (Labsonic-M, Sartorius Stedium). The cycle was repeated 10 times in breaks of 2 seconds each to get primary o/w emulsion. The obtained primary emulsion was added dropwise to 50 ml of 0.5% w/v aqueous PVA solution and was homogenized at 10000 rpm for 15 min. The dispersion was kept overnight under continuous stirring to remove organic solvent. The dispersion was then centrifuged at 15,000 rpm for 20 min. followed by three washes with distilled water to obtain NPs. Finally the NPs were freeze dried (Christ Alpha 1-4 lyophilizator, Osterodo, Germany) over a period of 24 h.

5.4.1. Optimization of bty-Gnb/Nar

The NPs were designed and optimized using central composite design (CCD). Polymer:drug ratio (X1),copolymer PVA (X2) levels were selected on the basis of pre-optimization studies. Totally, a set of 09 of experimental runs each were conducted for optimization and data recorded in table 1. ANOVA (analysis of variance) was applied to find out the significance of the polynomial modals and model terms on the responses and

their quantitative effects. Regression equations were established for dependent variables, i.e. Y1 and Y2. Response surface analyses were plotted to describe the effects and interaction of independent variables on the dependent variables. Particle size, entrapment efficiency and drug loading were taken as dependent variables.

5.4.1.1.Preparation of optimized bty-Gnb and bty-Nar (Biotinylated NPs)

For biotin-decorated NPs(bty-Gnb/bty-Nar), biotin-conjugated PCL (20% of total PCLweight) was employed and NPswere prepared using oil in water emulsion technique as described above for formulating Pcl-Gnb/Nar.

5.4.2.Biotin content assay

The biotin content in bty-Gnb/Nar was determined by HABA/avidin Assay(Tseng et al. 2008). 0.1 mM of HABA (4'-Hydroxyazobenzene-2-carboxylic acid) was dissolved in 10 ml of aqueous sodium hydroxide solution (0.01 M). Separately 5 mg of Avidin was dissolved in 9.7 ml of PBS pH 7.2. To this HABA solution was added to obtain HABA-avidin solution. HABA-avidin solution (300 µl) was added to bty-Gnb/Nar to get 1 mg ml $^{-1}$ concentration. The solution was kept for 2 h under stirring to assure complete mixing. The amount of biotin was estimated using UV/Vis microplate spectrophotometer (Multiskan GO, Thermo Fisher) at 500nm. The change in absorbance was recorded before and after addition of bty-Gnb. Similar procedure was performed to determine biotin content in bty-Nar.

5.5. **Characterization of Prepared bty-Gnb and bty-Nar**

5.5.1. Particle size analysis and Zeta potential

The particle size of various modified NPs was determined using laser light scattering-based particle size analyzer (NanoPlus-3, Japan). Study was performed in triplicate, and average values with standard deviation were reported. The samples were reconstituted in phosphate buffer pH 7.4, prior to analysis.

5.5.2. Transmission Electron Microscopy

TEM (H-750, Hitachi, Japan) was employed for analyzing the surface morphology of surface modified bty-Gnb and bty-Nar NPs. The samples were prepared, observed and photographed as described in previous chapter III section 3.4.2.

5.5.3. Entrapment Efficiency (%EE)and Drug loading

Entrapment efficiency was determined by dialysis method. Breifly, entrapment efficiency was estimated by keeping 1 mL of drug loaded NPs in dialysis membrane (12-14 kDa MWCO) for 2 h, and the dialyzed drug (free drug) was estimated using UV-Vis spectrophotometer. The amount of drug in the aqueous phase was calculated. The amount of Gnb in modified NPs was calculated using a standard curve obtained by measuring the UV absorbance (Labtronics LT-2900) of Gnb at a wavelength of 338 nm. Similarly amount of Nar was measured at a wavelength of 285 nm. The Gnb/Nar, loading in NPs was determined by dissolving accurately weighed amounts of NPs (10mg/10ml) into DMSO and concentration was determined by measuring the UV absorbance stated above. All the experiments were done in triplicate. The entrapment efficiency was calculated using formula in equation (i) and drug loading by using formula in equation (ii)

$$\%EE = \frac{W\ initial\ drug - W\ free\ drug}{W\ initial\ drug} X100 \text{.....} \textit{(i)}$$

$$\%DL = \frac{Drug}{(polymer+drug)} X100 \text{.....} \textit{(ii)}$$

5.5.4. *In Vitro* Dissolution Studies

In-vitro drug release of Gnb/Nar loaded unmodified and modified NPs viz. Pcl-Gnb,Pcl-Nar, bty-Gnb and bty-Nar, was performed using dialysis membrane having molecular cut off range between 12,000-14,000 dalton. Dialysis membrane (Visking tubing, Spectra/Por®, cutoff 12–14 kD) was activated with phosphate buffer pH 6.8 for 12 h, prior to experiment.

USP dissolution apparatus type-II (Veego, India) was used for *in-vitro* release study. The cylinders were filled with 250 mL phosphate buffer maintained at pH 6.8 (containing 0.1% v/v Tween-80) and 37.0±0.5°C temperature. Formulation(s) equivalent to 10 mg of Gnb and 30 mg of Nar was suspended in 10 mL phosphate buffer (pH 6.8) and packed in the sac made of dialysis membrane. The sac was then tied to the paddle shaft in such a way that membrane just touches the dissolution medium surface. The dissolution medium was stirred at 50 rpm. The release study was carried out for 80 h and an aliquot of 3ml each was withdrawn from the cylinder at pre-determined time intervals and replenished with fresh medium. The aliquots were filtered through 0.45 μm membrane filters. Drug concentration was determined spectrophotometrically at 338 nm/285 nm for Gnb and Nar respectively, using UV spectrophotometer (Labtronics LT-2910).The cumulative percent release of modified and unmodified NPs was determined by plotting cumulative percent release as a function of time. The experiments were performed in triplicate.

5.5.5. Release kinetics modeling

The data was analyzed for various kinetic models viz. zero order, first order, Higuchi model, Korsmeyer-Peppas, etc. The optimized formulation bty-Gnb and bty-Nar were subjected to graphical treatment to predict the kinetics of drug release using goodness of data fit approach. The release kinetic modeling gives a prediction of release pattern of drug from the formulation.

5.6. *In Vitro* Cell Culture Study

5.6.1. Cell Cytotoxicity Study by MTT Assay

Cytotoxicity of CAP/Gnb was assessed on cancer cells by MTT assay to evaluate the anticancer efficacy *over* A549 cells as described in chapter III section 3.5.1.The optimized formulations bty-Gnb, bty-Nar, Pcl-Gnb and Pcl-Nar were taken concomitantly to study the effect of over A549 cell lines. Similarly a combined effect of bty-Gnb and bty-Nar (Gnb-bty-Nar) over A549 cells (2:1 ratio) was evaluated and subsequently compared with effect of concomitant treatment of Gnb or Nar individually(n=3). Plain PBS was taken as control i.e. untreated cells.

*5.6.2.*Qualitative and quantitative cell uptake

A549cells were seeded on a cover-slip placed in a 6-well plate at density of $2x10^5$in DMEM supplemented with 10% fetal bovine serum (FBS) and 100 U/ml antibiotic (penicillin) solution. Next day, cells were treated with free FITC solution and FITC loaded modified and unmodified formulation. The cells were then incubated at 37˚C in humidified incubator maintained at 5% CO_2. Following treatment, the cells were washed with PBS and fixed using 4% formaldehyde. The cover-slip were then mounted on glass slide with DAPI (nuclear stain) and observed under florescence microscope. Quantitative estimation of cell uptake was performed using FACS. The cells were seeded as mentioned above without cover-slip and following treatment, they were trypsinized and collected for flow cytometry (FACS Calibur, Cell Quest; BD Bioscience) at an excitation wavelength of 485 nm and an emission wavelength of 538 nm.

5.6.3. Cell proliferation studies

The cell proliferation assay of various formulation was performed utilizing Alamar blue® reduction method as per method described in chapter III section 3.5.3. The cells were treated with various formulations at sub IC_{50}concentration equivalent of Nar/Gnb for 24 h.

5.6.4.Cell Cycle Arrest through Fluorescence-Activated Cell Sorting

Cell cycle arrest through Fluorescence-activated cell sorting

Cell cycle arrest by various formulations of Gnb, Nar and Gnb combined with Nar was evaluated to estimate synergistic effect in NSCLC using propidium iodide method through flow cytometry (BD FACS Array).The specified A549 cell lines were plated in a 96-well plate having density of 1×10^6 cells/well. The cells were exposed to Gnb, Pcl-Gnb, Pcl-Nar, bty-Gnb and bty-Nar, as well as combined bty-Gnb and bty-Nar over a period of 48h. For conducting the study, cells were grown in PBS (phosphate buffer saline) followed by fixation using 70% cold ethanol for 30 min at 4°C. Afterwards, cells were washed two times with PBS. The obtained cells were centrifuged at 850g for 15 min using cold centrifuge

(REMI CPR -24). Lysis of cells was done using ribonuclease (50 µl of a 100 µg/ml stock of RNase). After addition of 200 µl propidium iodide,histograms obtained for side scatter and forward scatter were analyzed. The samples were analyzed at a low flow rate of 500 events/second.

5.6.5. Mitochondrial membrane potential assay (MMP) and Reactive Oxygen Species (ROS) generation analysis

Mitochondrial membrane potential assay was conducted employing dye Rhodamine 123 (Rh-123) on specified A549 cells as per method described in chapter III section 3.5.4.

5.7. *In vivo* Study

5.7.1.*In Vivo* Therapeutic Efficacy of biotin decorated NPs

The protocol for animal testing was approved through institutional ethical committee, approval no. SDCOPVS/AH/CPCSEA/01/0028. The in vivo studies were performed as per the protocol detailed in chapter IIIsection 3.6.1(Pandey et al. 2014).

Group I Negative control

Group II Toxic control, Urethane 1g/kg, i.p

Group III Urethane 1g/kg, i.p + Gnb,20mg/kg

Group IV Urethane 1g/kg, i.p+bty-Gnb dose: 20mg/kg, iv

Group V Urethane 1g/kg, i.p +bty-Nar dose: 30 mg/kg, ip.

Group VI Urethane 1g/kg, i.p along with bty-Gnb dose: 20mg/kg, iv and bty-Nar dose: 30 mg/kg, ipsimultaneously).

5.7.2. Histopathology

Lung tissues from all the six groups were isolated and stored in 10% buffered formalin for histopathological investigation. The samples were prepared as described in section 3.6.2 of chapter IIIand were observed under 40X magnification. The images were captured using digital biological microscope (N120, BR-Biochem Life Sciences, New Delhi, India.

5.7.3. Oxidative stress markers

The tumor-bearing lungs challenged by urethane were isolated from all the six groups, and investigated for oxidative stress as per methods given in chapter III section 3.6.3. Experiments were performed in triplicate and statistically analyzed using software Graph Pad Prism (5.01), San Diego, California(Rani et al. 2016).

5.7.4. Western Blotting

Lung tissues were excised and processed for western blotting as described in chapter III section 3.6.4.

Antibodies and dilutions for immunoblotting were as follows: Anti caspase-9 (rabbit polyclonal 1:500), Anti caspase-3 (rabbit polyclonal 1:500) Anti MMP-9 (goat polyclonal 1:500), Anti-actin (rabbit polyclonal 1: 500), Anti P-16 (rabbit polyclonal 1:500), Bcl-2 (mouse monoclonal 1:500), BAX (mouse monoclonal 1:500), and HRP-conjugated secondary antibodies (anti-rabbit, 1:500). β-actin (MA5-15739-HRP) was used as a standard reference.Quantitative analyses of protein expression in immunoblots were performed using scanning densitometry (ImageJ, NIH).

5.7.5. Biodistribution studies

Biodistribution of modified, unmodified and plain Gnb was evaluated to determine the targeting potential of the biotin conjugation. Biodistribution of formulation was examined by injecting bty-Gnb, Gnb-bty-Nar, Pcl-Gnb and Gnb equivalent dose, to 20 mg/kg of Gnbthrough tail vein,in urethane induced LCs rats. The animals were sacrificed at specific time intervals and various body organs, *viz.*, lungs, liver, heart, kidney, spleen were excised at predetermined time points i.e. 4, 12, 24 and 48 h and stored at -80°C until further analysis. The organs were weighed and homogenized and concentration of Gnb was measured through the validated HPLC method (Waters 2489, Milford, Massachusetts, USA). The system was equipped with Spherowsorb C18, 3.5 μm, 4.6×250 mm column at flow rate 1.0 mL/min. The mobile phase comprised of methanol and 0.1 M potassium dihydrogen

phosphate in a ratio of 40:60 (v/v) and a flow rate of 1.0 mL/min with runtime 20 min and detection was done at 254nm (Faivre et al. 2011).

5.8. Metabolomics study

5.8.1. ^{1}H NMR spectroscopic analysis of serum samples

5.8.1.1 Serum sample preparation

Serum samples from -20°C temperature were thawed and centrifuged at relative centrifugal force (rcf) of 16278 for 5 min to remove precipitates just before acquiring the NMR data. A total of 440 µl of sample was used in 5 mm NMR tube (Wilmad Glass, USA) for data acquisition. Serum (220 µl) was takenand final volume adjusted by adding 220 µl of saline sodium phosphate buffer of strength 20 mM and pH 7.4 with 0.9 % saline prepared in D_2O(Guleria et al. 2016).In 5 mm NMR tubes, a sealed co-axial was inserted containing the known concentration of 0.1 mM TSP (Sodium salt of 3-trimethylsilyl-(2, 2, 3, 3-d4)-propionic acid) to provide lock for NMR experiments, and as an external standard reference to aid chemical shift referencing for metabolite quantification and assignment (Beckonert et al. 2007).

5.8.1.2. NMR measurements

All the NMR spectra were acquired at 300 K on Bruker NMR spectrometer (Avance-III) operating at a proton frequency of 800.21 MHz and equipped with Cryoprobe. The raw NMR data was processed in Bruker software Topspin-v2.1 (Bruker BioSpin GmbH, Silberstreifen 476287 Rheinstetten, Germany). On each serum sample, the 1D 1H transverse relaxation-edited CPMG (Carr–Purcell–Meiboom–Gill) NMR spectra were recorded using the standard Bruker's pulse program library sequence (cpmgpr1d) with pre-saturation of the water peak through irradiating it continuously during the recycle delay (RD) of 5 sec. Each spectrum consisted of the accumulation of 128 scans and lasted for approximately 15 min. To remove broad signals from triglycerides, proteins, cholesterol, and phospholipids, a total spin-spin relaxation time of 60 ms (n=300 and 2τ=200µs) were applied. Each FID (free induction decay) was zero filled and Fourier-transformed to 64 K data points following

manual phase and baseline-correction. A line broadening factor of 0.3 Hz and a sine–bell apodisation function was applied to FIDs before Fourier Transformation (FT).

5.8.1.3. Spectral assignment

The 1D 1H CPMG NMR spectra metabolite resonances were assigned using the Chenomx NMR suite (Chenomx Inc., Edmonton, AB, Canada). The remaining peaks in the CPMG 1H NMR spectra were assigned as far as possible, by comparing them with the chemical shifts available using previously reported NMR assignments of metabolites, data obtained from BMRB database (Biological Magnetic Resonance Data Bank) and HMDB (The Human Metabolome Database) (Nicholson et al. 1995, Ulrich et al. 2008, Guleria et al. 2014). The serum spectra contained peaks mainly from lipoproteins, glycoproteins, glucose, amino acids, lactate, and choline-containing metabolites. No additional NMR signals were observed in the sera of treated rats compared to the normal control rats suggesting that the sera of treated rats either did not contain any drug molecules or their concentrations in the sera were below the NMR detection range (i.e. <5 uM) (Wishart et al. 2007).

5.8.1.4. Multivariate Statistical analysis

Before multivariate data analysis, all the NMR spectra were manually phased, baseline corrected and referenced internally to Lactate peak (at δ =1.3102 ppm). The CPMG δ(0.7−8.6 ppm) spectra were binned and automatically integrated using AMIX package (Version 3.9.15, Bruker).The region δ(4.66-5.1 ppm) distorted due to water suppression were excluded from the CPMG data set to avoid the effects of imperfect water suppression. Finally, the selected regions were reduced to spectral bins of δ0.02 ppm and each spectral bin further normalized using the total spectral intensity. The binned data from CPMG experiments were submitted to a multivariate data analysis performed using the open access web-based metabolomics data processing tool, named MetaboAnalyst. Principal Component Analysis (PCA) was used for the initial overview of the grouping trend within the data set and outlier detection. Next, the data were modeled with the supervised method of Partial Least Squares Discriminant Analysis (PLS-DA) to reveal class separations between the groups and to further identify the metabolites responsible for class separation. For both PCA

and PLS-DA, the data were scaled using Pareto scaling. As PLS-DA inclines to over fit the data and, therefore, the model needs to be strictly validated to see whether the separation is statistically significant or is due to random noise. To avoid the over-fitting of the PLS-DA model, 10-fold cross-validation algorithm –which helps to evaluate 100% classification accuracy using the top 5 latent variables, was used. The quality of the models was described by the cross-validation parameters R2 and Q2, representing the explained variance and predictive capability of the model, respectively. The PLS-DA model was further used to identify the metabolites responsible for the discrimination based on their higher values of variable importance on projection scores (i.e. VIPs). The VIP score represents a weighted sum of squares of the PLS loadings and takes into account the amount of explained Y-variation in each dimension to measure the impact of each metabolite in the model. A 0.05 level of probability i.e. p-value ≤0.05 (calculated using Mann Whitney test for pairwise comparisons) was used as the standard for statistical significance(Xia et al. 2009, Worley et al. 2013, Xia et al. 2015).

5.9. Stability Studies

Stability of bty-Gnb and bty-Nar was performed at 5±2°, 25±2° (60±5% RH) and 40±2° (75±5% RH) as per ICH guidelines over a period of 90 days. Samples were assessed for particle size, zeta potential and percent drug loading at 0, 15, 30, 45, and 90 days.

5.10.Statistical analysis

All results were presented as mean ± standard deviation (n=3). One-way analysis of variance (ANOVA) followed by the Turkey-Kramer multiple comparison test was performed to compare differences between formulations using Graph Pad Instat software (Graph Pad Software Inc. CA, USA). Levels of significance were set as $p<0.05$ explaining significant difference in the therapeutic efficiency of all formulations in comparison to Cap@Gnb-PLGA-PEG-FA.

5.11. Results

Present investigation aimed at designing of biotin decorated PCL NPs, for intravenous delivery to ameliorate urethane-induced LC in rats. The procedure opted from previous literature for conjugation was simple and was found to be successful in entrapping hydrophobic drug Gnb and Nar in biotin decorated PCL nanoparticles. Also, targeted therapy gives advantage of chemotherapy combined with nanotechnology in a pre-modulated delivery system.

5.11.1.Synthesis of PCL-PEG-bty

FTIR spectroscopy was employed to access NHS ester of biotin. The peaks of NHS ester of biotin displayed important peaks at 3,440 cm^{-1} imidazole band that overlap with the (N–H) absorptions, $–CH_2$ groups stretching at 2995 cm^{-1} and deformations at 2,921.7 cm^{-1}, C=O stretch at 1644.5 cm^{-1}, N-H bending 1550 cm^{-1},$–CH_2$ group bending at 1435 cm^{-1} and (C–O) stretching of ester at 1026.9 cm^{-1}as shown in **Figure 5.2 A&B**. The spectra of biotinylated-PEG-PCL were characterized by bands at 3,440 cm^{-1} imidazole band overlapped with (N–H) stretch of secondary amide group, (C=O) stretch at 1712.84 cm-1, (C–O) stretching of PEG chain at 1210 cm^{-1} and1,042.95 cm^{-1}, –CH2 group stretching at 2911.3 cm^{-1} and $–CH_2$ group bending at 1435.76 cm^{-1} as shown in **Figure. 5.2C**.

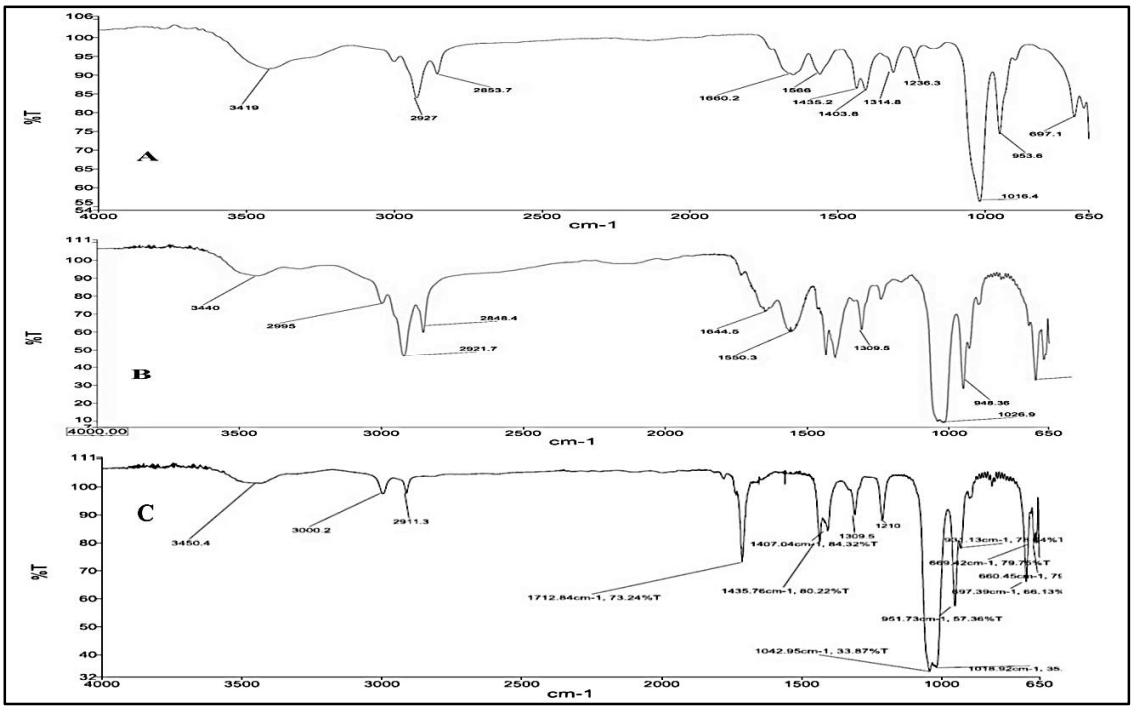

Figure 5.2 FTIR spectra of (A) biotin, (B) NHS-Biotin, and (C) biotin-PEG-PCL

5.11.2. ^{1}H-NMR spectrum of PCL-PEG-bty

^{1}H-NMR analysis of biotin decorated PCL NPs was done to confirm the formation of **PCL-PEG-bty**. The characteristic peaks were correctly marked as shown in **Figure 5.3.**Theimportant peaks can be designated as **1**, (6.50, 1H); **2**(6.38, 1H); **3**(4.49, 1H);**4**(two adjacent peaks for PEG);**5**(2.7, 2H);**6**(3.07, 1H)foroxohexahydrothienoimidazol ring of biotin;**7,** (2.98 6H, CH_2); **8**(1.49, 2H) for pentanoic chain of biotin;**9**(1.39, 2H, CH_2, C_2);**10**(~1.34, 28H, CH_2, $C_{3\text{-}16}$);**11**(1.31, 2H, CH_2, C_{17});**12**(1.21, 3H, CH_3, C_{18}) for PCL.

The conjugated biotin in bty-Gnb and bty-Nar determined by HABA/ avidin assay was found to be 39.43 µg mg-1 and 38.57 µg mg-1 respectively.

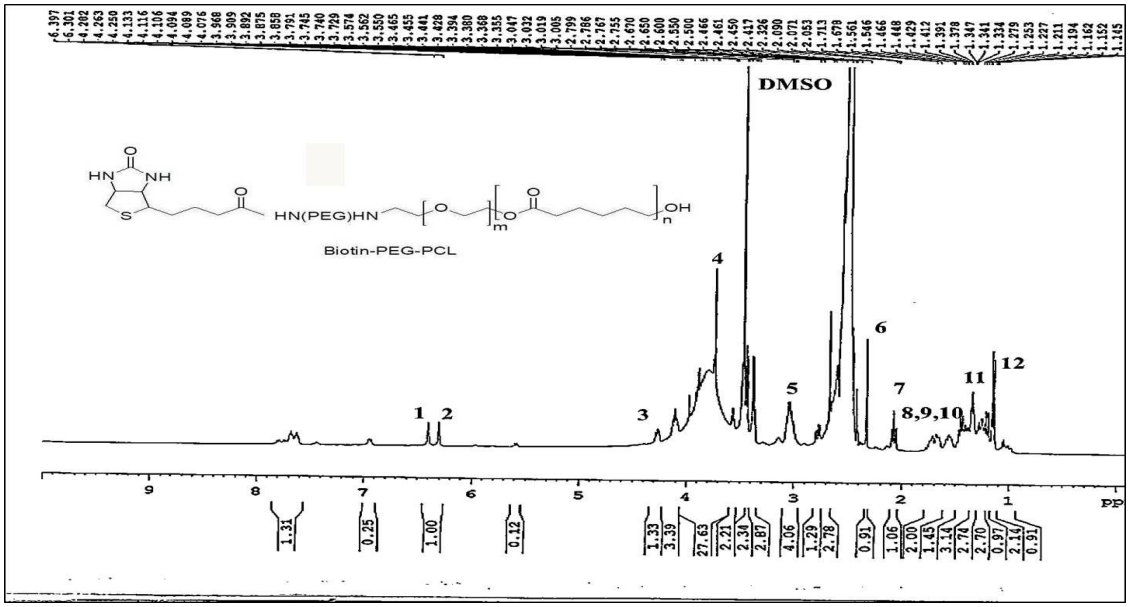

Figure.5.3[1]HNMR spectra of Biotin-PEG-PCL

5.11.3.Formulation and optimization of bty-Gnb and bty-Nar

Synthesized polymer PCL-PEG-NH_2 was utilized to entrap Gnb and Nar which were further conjugated with activated biotin to form bty-Gnb and bty-Nar employing oil in water emulsion technique. The data obtained after the analysis revealed that the independent factor i.e., polymer:drug ratio, has a significant effect on particle size, percentage entrapment and drug loading. The quantitative assessment of the significant modal terms showed that a nonlinear quadratic relationship was observed among X1 and X2 with all the dependent variables. It was observed that the particle size and drug loading increases as polymer ratio was enhanced. However, PVA plays an insignificant role in the process as shown in **Figure 5.4 a-c.** The effects of various factors on dependent variables are summarized in **Table 5.1 a&b.**The linear quadratic equations obtained are as-

Particle size =+51.55556+38.33333 * PCL:drug+13.55556 * PVA ……(i)

Entrapment efficiency =+24.55556+3.55556 * PCL:drug+2.22222* PVA ……..(ii)

Drug loading = =+7.44444+2.77778* PCL:drug+0.22222 * PVA …….(iii)

5.11.4. Optimization and validation

After analyzing the regression equations, to illustrate correlation between the dependent and independent variables, advance optimization and validation process was performed, employing design expert software (Design Expert 8.0 software; Trial version, M/s Stat-Ease, Minneapolis, USA). The design space (area of desirable characteristics) and the optimal formula for modified NPs depended on the prescriptive criteria of minimization of particle size (<200), drug loading (>15%) and %EE (>35%). The composition of the optimum formulation identified was 3.5:1 ratio (X1 PCL) and 1.25%v/v (X2, PVA), which fulfilled the requirements of optimization.At these levels, the predicted values (**Figure 5.4 d**) of particle size, percent entrapment and percent drug loading was 202.62 nm, 39.77% and 17.44% respectively. As per results of the advance validation of predicted values by this model, a new batch modified NPs (OPT-NPs) were prepared and characterized. This optimized batch exhibited particle size of 199±3.70 nm, percentage entrapment of 45.31±2.1% and percentage drug loading 21.65%, which were in righteous alignment with the predicted values.

Table 5.1 Various dependent parameters for PCL NPs of Gnb prepared as per CCD

Run	Factor1 PCL:drug	Factor 2 PVA%	Particle size(nm)	%Entrapment	%Drug loading
1	2.0	1.25	162± 3.51	35±1.2	12.2± 0.13
2	2.0	2.0	154± 3.21	35±2.3	14.1± 0.34
3	3.5	1.25	199± 2.46	45± 1.3	21.5± 0.26
4	2.0	0.5	147± 1.21	30±1.4	12.6± 0.12
5	5.0	1.25	246± 2.14	44±1.3	23.6± 0.14
6	3.5	2.0	180± 2.12	42±1.3	18.9± 0.22
7	5.0	2.0	305± 2.45	45±1.1	19.8± 0.31
8	5.0	0.5	257± 4.90	43± 2.3	21.1± 0.30
9	3.5	0.5	174± 4.94	39±1.9	17.88± 0.11

Table 5.1 b Various dependent parameters for PCL NPs of Nar prepared as per CCD

Run	Factor1 PCL:drug	Factor 2 PVA%	Particle size(nm)	%Entrapment	%Drug loading
1	2.0	1.25	159± 1.22	37±1.3	13.3± 0.12
2	2.0	2.0	152± 2.31	36±1.5	14.4± 0.29
3	3.5	1.25	200± 2.90	46± 1.7	21.9± 0.45
4	2.0	0.5	145± 1.82	31±2.1	13.8± 0.13
5	5.0	1.25	244± 1.24	42±0.9	25.3± 0.19
6	3.5	2.0	178± 3.12	40±1.4	17.5± 0.11
7	5.0	2.0	309± 5.30	46±1.1	20.1± 0.15
8	5.0	0.5	259± 3.23	44± 2.7	20.9± 0.32
9	3.5	0.5	170± 4.11	38±2.9	18.9± 0.13

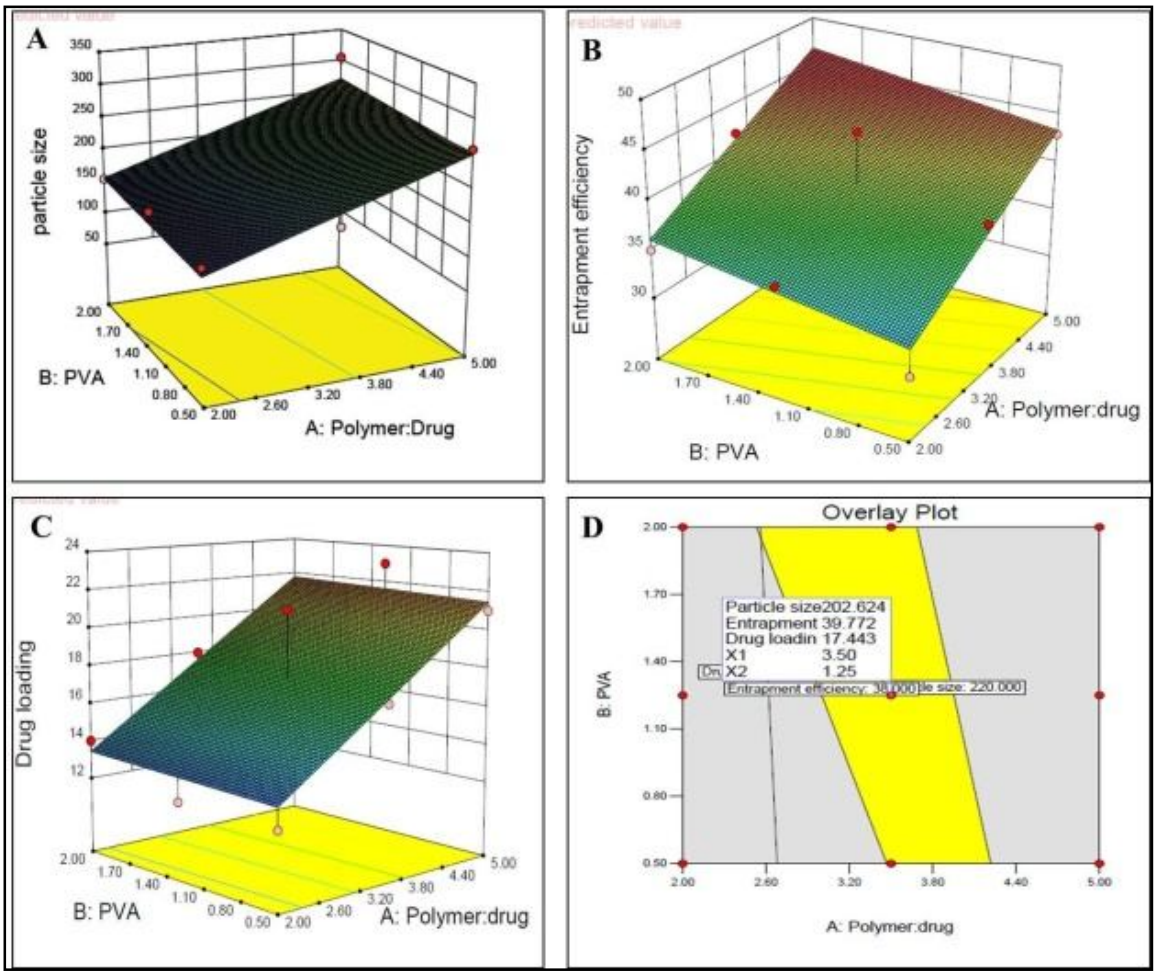

Figure 5.4. Response surface plots depicting the effect of independent variables on dependent variable, effect of independent variable on (a) particle size (b) % entrapment (c) drug loading (d) overlay plot defining predictable values

5.11.5. Particle size, Zeta potential, Drug loading and %EE

The physical characteristics of Gnb/Nar loaded PCl-PEG-NH_2 NPs viz. particle size, %EE, drug loading and zeta potential are shown in Table 5.2. It was observed that there is an increase in particle size as well as zeta potential after biotin conjugation. The particle size was found to be 211±1.4% and 203±2.7% for bty-Gnb and bty-Nar respectively. The observed drug loading ranges from 21.23±1.3% to 29.72±2.1% in case of modified and

unmodified NPs. The polydispersity index of all the formulations was found to be below 0.2.The %EE ranges from to 47±3.5% to 56± 3.1%. The highest %EE of was observed in case of Pcl-Gnb, while least % EE was observed in case of bty-Gnb. The zeta potential ranges from -21.04±1.4 mV to -23.21±2.1 mV in various formulations.

Table 5.2 Characterization of bty-Gnb and bty-Nar NPs.

Nanoparticles	Particle size (nm)	Zeta Potential (mV)	% Drug loading	%EE
Pcl-Gnb	197±1.4	-23.21±2.1	29.72±2.1	46± 3.1
bty-Gnb	201±3.2	-21.04±1.4	23.23±1.7	44±2.9
Pcl-Nar	199±1.8	-22.77±2.3	25.23±2.1	45±1.4
bty-Nar	203±2.7	-21.19±2.3	21.23±1.3	43±2.3

5.11.6. Transmission Electron Microscopy (TEM)

TEM images revealed biotin conjugated nanoparticles to be spherical in shape having smooth surface as shown in **Figure** 5.5. The image confirms the formation of NPs in a mean particle size ranging from 50-200 nm and uniform distribution.

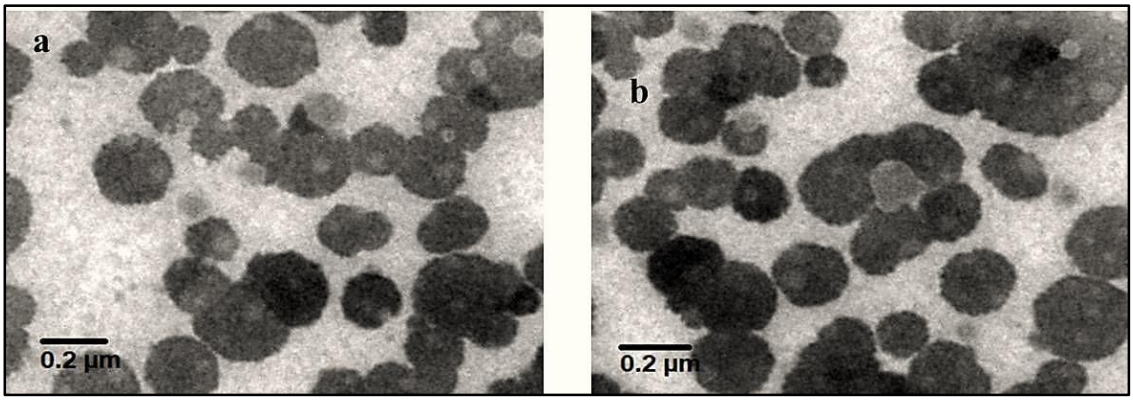

Figure 5.5.TEM images of a) bty-Gnb and b) bty-Nar

5.11.7.In-vitro Release Studies

The *in-vitro* release of modified NPs, bty-Gnb and bty-Nar showed biphasic release pattern with an initial faster release within 4 h,followed by a sustained release profile. About 86.54±4.2% and 83.43±3.29% of Gnb and Nar respectively was released from Pcl-Gnb and Pcl-Nar respectively over a period of 80 h. About 81.99±4.23 % of Gnb and 80.54±2.71 % of Nar were respectively released from modified NPs over a period of 80 h. Approximately 63.17±3.70% of Gnb and 65.80±3.4% of Nar was released from modified NPs over a period of 24 h. Almost 80% of the drug was released over a period of 80 h in case of both modified as well as unmodified NPs of Gnb and Nar respectively as shown in **Figure 5.6.**

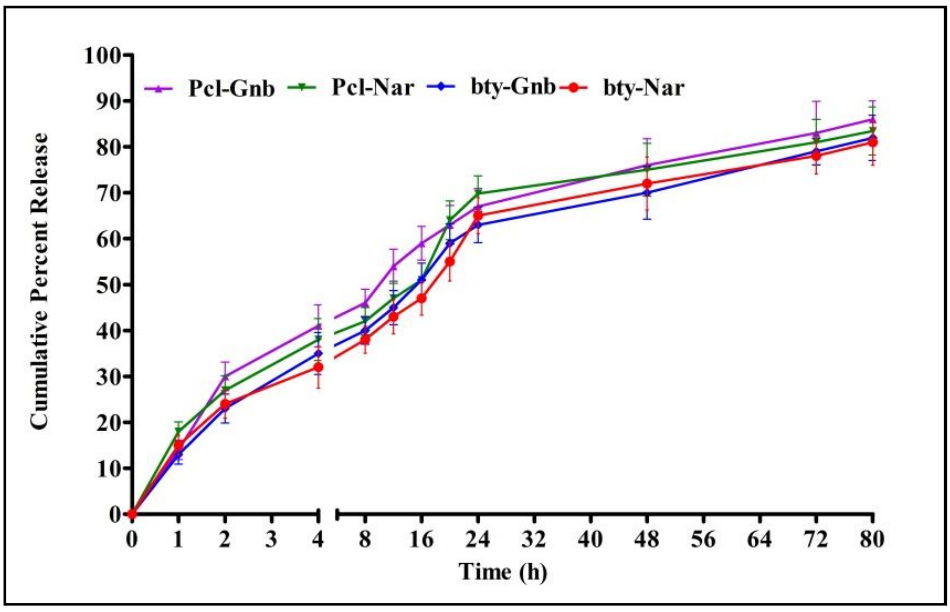

Figure5.6. Drug release comparisons of modified and unmodified NPs in PBS pH 6.8 buffer [Data is presented as mean±SD (n=3)]

5.11.7.1.Release Kinetics Modeling

Different kinetic models were applied on the data obtained from release study for categorizing the kinetics of drug release. From the mathematical model data it was concluded that the Higuchi model was best fitted for modified formulations as it reached

highest value of the squared correlation coefficient (R^2), describing the release of the Gnb and Nar from PCL nanoparticles as diffusion controlled. The data is recorded in Table 5.3. The predicated release mechanism of the drug could be that the penetration of dissolution media into polymeric matrix which slowly dissolves the drug, and finally drug is released by diffusion in the medium.

Table 5.3. Release kinetics for dissolution data of bty-Gnb and bty-Nar

Correlation co-efficient R^2 value	**bty-Gnb**	**bty-Nar**
Zero order	0.6328	0.6974
First order	0.8126	0.8368
Higuchi model	0.9124	0.9252
Korsmeyer Peppas model	0.8314	0.9011

*5.11.8.*Cell cytotoxicity study

Pcl-Gnb, Pcl-Nar, bty-Gnb, bty-Nar, Gnb-bty-Nar and Gnb were incubated with A549 cell lines to investigate the enhanced anti-cancer activity of modified NPs. Proliferation and metabolic status of the cells was investigated through the MTT assay. The changes in percent cell viability against the drug treatment of various formulations are presented in **Figure 5.7 a**. The obtained results depicted IC_{50} value of Gnb-bty-Nar (25.4±0.32µM), bty-Gnb (32.71±2.71 µM), bty-Nar (7.46 ±0.86 µM) and Gnb (59.43±1.00 µM). The unmodified formulations also demonstrated a lower IC_{50} value i.e., Pcl-Gnb (48.21 ±0.34 µM) and Pcl-Nar (14.5 ±0.16 µM) respectively. The isobolomic curve analysis revealed that an enhanced percent inhibition of cell proliferation was completed through combination therapy demonstrating their synergistic effect (**Figure 5.7 c)** when compared to Gnb and Cap individual treatment. The combination index (CI) calculated through CompuSyn software was found to be 0.2940. The CI below 1 confirms the synergism, aptitude of the system.

5.11.8.1. *In vitro* Cellular Uptake Study

In vitro cellular uptake study demonstrated that the cell internalization of drug(s) in A549 cells was profoundly enhanced in biotin decorated NPs. Enhanced cellular uptake can be interconnected with depressed IC_{50} of modified NPs. Modified NPs bty-Gnb and bty-Nar displayed a significant ($p<0.01$) enhancement of Gnb and Nar uptake when compared to Pcl-Gnb and Pcl-Nar in A549 cell lines as represented in **Figure5.7 b**. However, no significant difference in uptake was perceived in case of Gnb-bty-Nar when compared with bty-Gnb and bty-Nar taken individually. About 2 fold increase was observed in case of modified NPs when compared to free Gnb whereas 1.97 folds increase was observed when Gnb-bty-Nar compared to free Gnb. Approximately 1.5 folds increase was observed in case of bty-Gnb and bty-Nar NPs when compared to unmodified Pcl-Gnb and Pcl-Nar. The combination index value as revealed through isobologram was found to be 0.2940. the value below 1 indicates synergistic potentialof cotherapy.

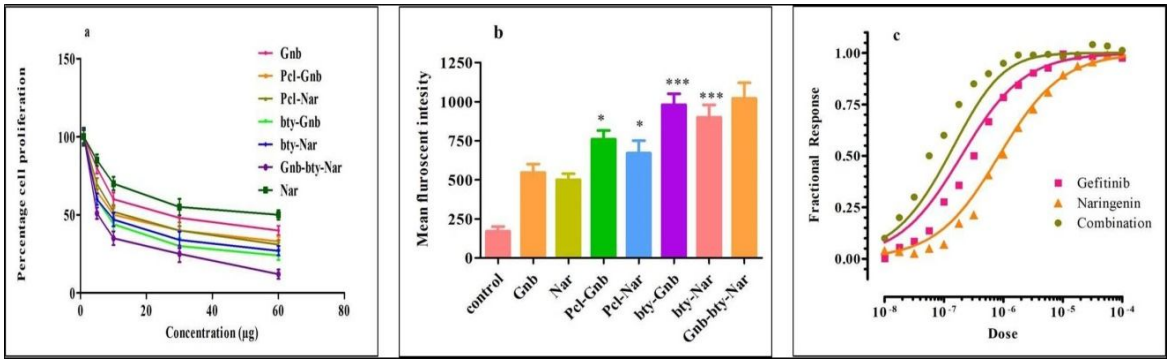

Figure5.7(a) Cytotoxic effect on A549 cells treated with Gnb, unmodified NPs and modified NPs for 48 h (b) bar graph representation for Cellular uptake (c) Fractional dose-effect curve (isobologram curve) for two drugs (naringenin and gefitinib) in A549 cells at IC_{50} levels.

5.11.8.2. Qualitative Cell internalization

Florescence images reflected that uptake of biotin modified NPs was enhanced to a greater extent in A549 cells than unmodified (**Figure 5.8**). These studies served as supplementary evidence for biotin functionalization in NPs.

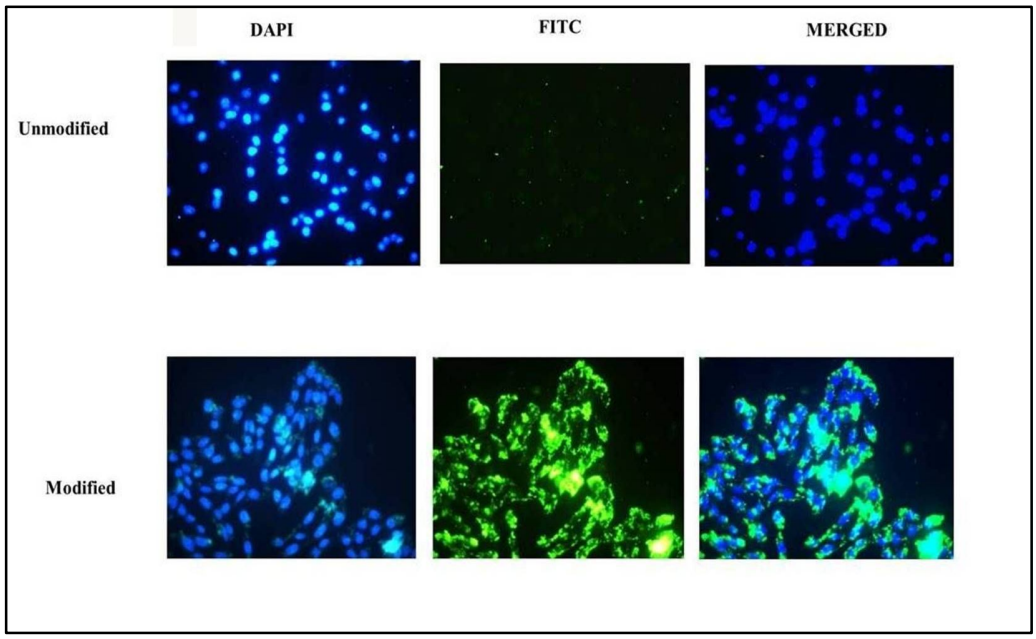

Figure 5.8. Fluorescence images of A549 cells incubated with FITC-labeled unmodified NPs and biotin modified NPs: cell nuclei stained with DAPI**.** (***p<0.001, *p<0.05 n=3)

5.11.9. Cell Cycle Arrest

Cell cycle analysis demonstrated cell cycle arrests in A549 cells after incubation with Gnb, bty-Gnb, bty-Nar and Gnb-bty-Nar (**Figure 5.9**). In our findings, a noticeable arrest was observed in G2-M phase succeeding apoptosis in A549 cells. Treatment with bty-Nar, initiated cell cycle arrest in G2-M phase whereas Gnb-bty-Nar arrested the G2-M phase to a higher extent than individual therapy through bty-Nar and bty-Gnb respectively. A steady rise in G2-M population to 18.99% after 24 h demonstrates a significantly low ($p<0.05$) cell growth and cell division. In control samples, distribution of cell population in G0/G1, S and G2/M phases of cell cycle were 74.60± 3.16%, 17.62±1.39%, and 7.82±0.14%, respectively (**Figure 5.9 A**). The cell population reduced to 63.95±1.76% in G0/G1 phase after Gnb-bty-Nar incubation. The treatment of A549 cells with various formulation enforced cells to move in programmed cell death process.

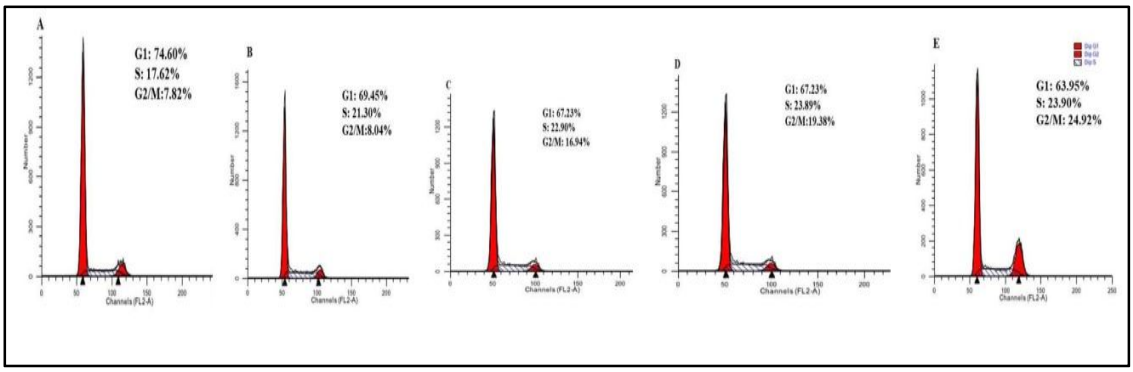

Figure 5.9. Representation of cell cycle distribution in A549 cells after treatment with (A) Control (B) Gnb (C) bty-Gnb (D) bty-Nar (E) Gnb-bty-Nar, at sub IC50 drug concentration and analysis was performed using flow cytometry. Each Fig. individually represents the population present in G1-S and G2-M phases, (n=3)

5.11.10.Cell Proliferation Assay

Biotin modified NPs displayed superlative inhibition of cell proliferation in A549 cells lines. The inhibition potential followed an order of Gnb-bty-Nar>bty-Gnb>bty-Nar>Pcl-Gnb>Pcl-Nar>Gnb>Nar. **Figure5.10a,** revealed that percentage viability was significantly reduced ($p<0.001$) as compared to control in surface modified treated group and Gnb-bty-Nar exhibited least cell viability of about 15%. The formulation bty-Gnb and bty-Nar displayed a percentage inhibition of about 72.31±2.90% and 63.14±2.17% which was significantly higher when compared with control ($p<0.001$). Gnb-bty-Nar provokes highest inhibition of 85.67±4.16% in A549 cells. The fluorescence intensity of Alamar Blue® is directly related to cell proliferation. The viable cells possess instinctive metabolic activity which causes chemical reduction of Alamar Blue® from the non-fluorescent oxidized (blue) form to the reduced fluorescent (red) form. The dead cells lack the intrinsic metabolic activity and maintain an oxidized environment, constraining reducing the dye and thus lack florescence(O'brien et al. 2000).

5.11.11. Mitochondrial Membrane Potential Assay

Gnb-bty-Nar instigated maximum disruption of mitochondrial membrane potential (MMP) in A549 cells which was found significantly higher than control samples ($p<0.01$). It was

observed that bty-Gnb and bty-Nar had significant effect on MMP disruption; however a declined effect was observed with plain Nar and Gnb treated groups. A significant difference in MMP disruption was observed when a comparison was made between modified and unmodified NPs ($p<0.01$), as unmodified NPs displayed lower MMP disruption as compared to modified NPs. **Figure 5.10b** represents the fluorescence intensity (indicating cell viability) of cells which alters differentially when treated with various NPs. Higher fluorescence intensity in control revealed minor deadly population while least fluorescence intensity in the case of Gnb-bty-Nar designated highest mortality of A549 cell lines. This enhanced mortality proves the synergistic potential of Nar and Gnb. The effect of the formulations on the MMP can be described as the cells undergoing apoptosis which hold lower uptake and retention of the Rh-123 in their mitochondria. Rh-123 uptake is MMP-dependent and favors accumulation in the mitochondria of the live cells. This effects the quenching of fluorescence and consequences in red spectral shifts indicating that the cells are undergoing apoptosis(Tang et al. 2007).

5.11.12.ROS Generation Analysis

Gnb-bty-Nar inhibits maximum ROS generation, which was found to be significantly higher ($p< 0.001$) when compared to Gnb or Nar individually. ROS generation was also found to be significantly higher in modified NPs as compared to free Gnb ($p< 0.001$) indicating superiority of modified NPs over plain drug as shown in **Figure 5.10c.** Moreover supremacy of modified NPs over unmodified NPs was also apparent, with a significance level of $p< 0.01$. DCFDA, a fluorogenic dye is widely used for direct measurement of the oxidation-reduction state of the cell.The treatment with the unmodified and the plain Gnb/Nar formulation revealed higher fluorescence of DCF in the A549 cells demonstrating raised cell population and production of higher ROS that oxidized the reduced form of DCF to fluorogenic oxidized form. On the contrary the least fluorescence was observed with the Gnb-bty-Nar treated group representing greater cell death(Eruslanov et al. 2010).

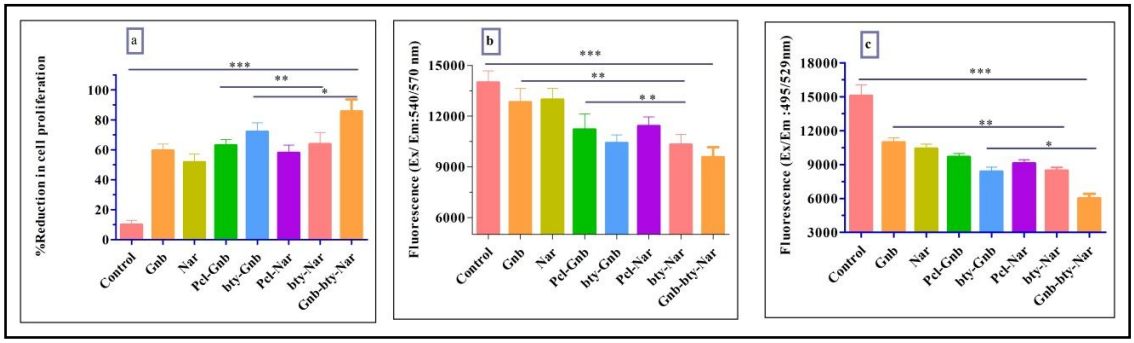

Figure 5.10a) Inhibition of A549 cell proliferations by Gnb NPs. b) Loss in mitochondrial membrane potential: graph represents the change in mitochondrial potential in A549 cells c) Intracellular ROS level in A549 cells after modified and unmodified Gnb NPs measured by fluorimetry. *: $p<0.05$, **: $p<0.01$, ***: $p<0.001$.

5.12.*In vivo* study

5.12.1.Tumor Regression Studies

Various formulations i.e Gnb, Pcl-Gnb, bty-Gnb, bty-Nar and Gnb-bty-Nar were compared for their anticancer potential *in-vivo* in urethane induced tumor model. Co-therapy with Nar and Gnb (Gnb-bty-Nar) and bty-Gnb revealed a marked reduction in lung weight when compared to Pcl-Gnb as shown in **Figure 5.11 a**. Free Gnb and bty-Nar exhibited minor regression in tumor at the end point of experiment when compared with modified NPs and combination therapy through Nar and Gnb. Weight variation plots for different groups displayed a remarkable constant weight loss among toxic and Gnb treated group when compared to groups receiving Gnb-bty-Nar and bty-Gnb over a period of 16 weeks as shown in **Figure 5.11 b**. Kaplan Meier survival plot (**Figure 5.11 c**) revealed declined animal death (over 16 weeks), establishing superior antitumor activity *in vivo*, in both Gnb-bty-Nar and bty-Gnb treated group when compared with plain Gnb treated and toxic groups respectively. A significant reduction in tumor volume was observed in group receiving Gnb-bty-Nar as compared to group receiving plain Gnb ($p< 0.001$) as well as individual therapy, elucidating superiority of combination therapy over single drug. **Figure 5.11 d** revealed a significant reduction in tumor volume when Gnb-bty-Nar was compared with toxic group ($p<0.001$). Plain Gnb (Group III), bty-Gnb (Group IV) and bty-Nar (Group V) receiving groups also

displayed reduction in tumor volume but to a lesser extent when compared with group co administrated with Nar and Gnb. Biotin decorated NPs individually displayed higher therapeutic efficacy in comparison to plain Gnb. Moreover a significant reduction in tumor volume was observed in bty-Gnb treated group when compared with Pcl-Gnb treated group ($p < 0.05$). Conversely bty-Nar displayed insignificant drop in tumor volume when compared with co- therapy by Gnb and Nar.

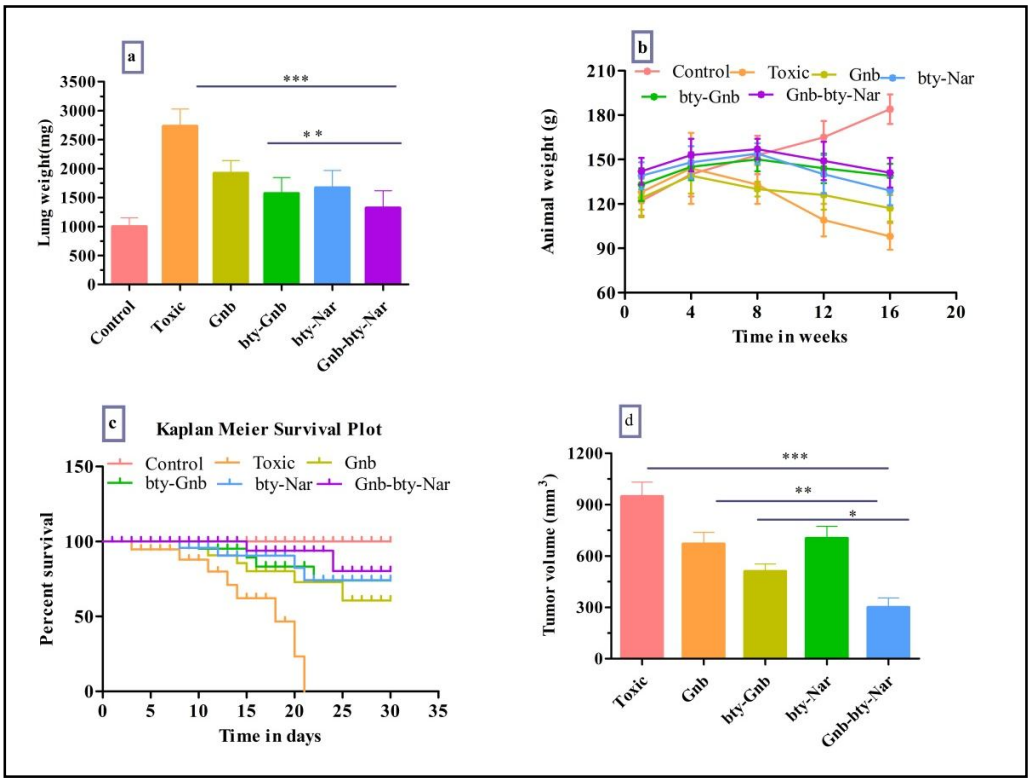

Figure 5.11a) Bar graph representing lung weight b) change in animal body weight c) Kaplan meier survival plot d) tumor volume data *: $p<0.05$, **: $p<0.01$, ***: $p<0.001$

5.12.2. Histopathology

The histopathological changes among the lung tissue of various group is detailed in **Figure 5.12.** The adipocytes, alveoli and bronchiole structure (marked by arrows) are seen in normal control whereas the toxic tissues displayed well developed tumor cells and moderately segregated, growing adenocarcinoma, having abundant cytoplasm and some

nucleoli, suggesting a developedNon-SmallCell Lung Cancer. The Gnb treated groups displayed the bronchiole having smooth muscle in the inner airway wall with alveolar attachment while group IV and V and VI revealed reduced tumor cells and a distinguished alveoli structure and outer airway wall, which somewhat regained their structure during treatment although statistically insignificant in nature.

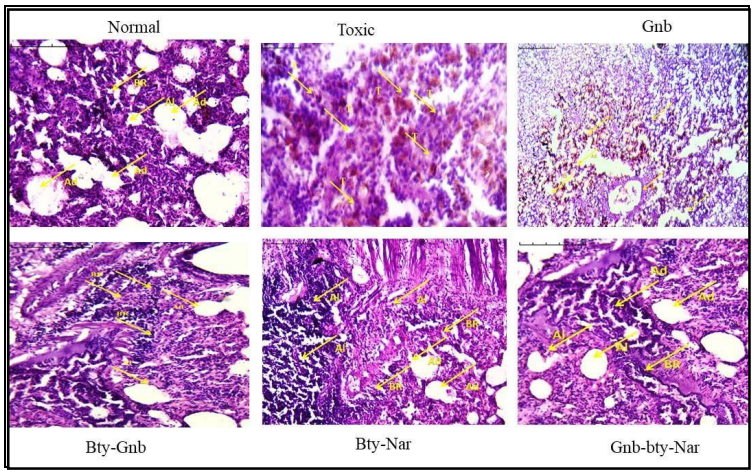

Figure 5.12.H&E stained micrographs of various groups. Arrows represents tumor cells in toxic group, bronchiole structure and inner airway in Gnb treated group and distinguished alveoli structure in modified NPs treated group

1: Adipocytes, 2: Alveoli, 3: Bronchiole and T: tumor cells

5.12.3.Biochemical Estimation

The therapeutic outcome of free Gnb, bty-Gnb, bty-Nar and Gnb-bty-Nar on oxidative stress markers i.e, TBARS, SOD, Catalase and Protein Carbonyl in lung homogenate are recorded in **Table 5.4**. The elevated TBARS and SOD levels with urethane administration were significantly dropped by Gnb-bty-Nar NPs ($p<0.001$). As revealed by the results Gnb-bty-Nar also restored the tissue catalase and GSH level that had formerly reduced after urethane administration in various groups. The increased level of protein carbonyl above normal among various groups was also significantly ($p<0.001$) reduced by Gnb-bty-Nar to an almost normal level. Individually bty-Nar and bty-Gnb also displayed a marked reduction

in TBARS and SOD levels and restoration of catalase levels but to a lesser extent as compared to Gnb-bty-Nar. Therefore, Gnb-bty-Nar conveyed an overall, superimposed antioxidant effect to restore the redox balance when compared with therapy through free Gnb, bty-Gnb and bty-Nar group.

Table 5.4. Effect of free Gnb, unmodified NPs and modified NPs on oxidative stress markers, from lung homogenate in Urethane induced lung cancer.

Groups	TBARS (nm of MDA/µg of protein	SOD (units of SOD/mg of protein)	GSH (Mg %)	CATALASE (nm of H_2O_2/ min/mg of protein)	PROTEIN CARBONYL nmol/mg of protein
Control	204.51±10.3	0.0367±0.005	1.31±0.05	0.459±0.22	18.51±0.09
Toxicant	512.31±13.10	0.0452±0.0021	0.98±0.02	0.121±0.11	43.13±5.11
Gnb	310.3±11.5	0.0381±0.0050**	1.10±0.05**	0.129±0.21	36.01±7.2
bty-Gnb	271.31±10.03	0.0374±0.002***	1.15±0.11**	0.327±0.051***	29.13±1.43**
bty-Nar	301.2±10.3	0.039±0.001***	1.13±0.04**	0.314±0.21	31.03±3.5
Gnb-bty-Nar	209.4±10.5***	0.0352±0.002***	1.24±0.03***	0.399±0.06***	21.3±9.5***

Values are (Mean ± SD), each group contains 09 animals. Comparisons were made on the basis of the one-way ANOVA followed by Bonferroni test. All groups were compared to the toxic control group (*p<0.05, **p<0.01, ***p<0.001) (n=6).

5.12.4. Western Blotting

The result of western analysis indicates varied influences on the expression of different pro-apoptotic (BAX, caspase-3, caspase-9 and P-16) and anti-apoptotic (Bcl-2 and MMP-9) proteins (**Figure 5.13 a)**. The densitometric data suggested that the treated groups restored various markers when compared with toxic group **(Figure 5.13 b)**. Moreover, co-therapy of

Nar and Gnb produced the highest restoration of the anti-apoptotic and pro-apoptotic markers in comparison to the plain Gnb ($p<0.05$). This evidences a synergistic effect and competence to reinstate the markers as compared to the toxic group constructively demonstrating apoptosis, thus enhanced anticancer potential of Nar and Gnb co-therapy. The result suggested that co-therapy through biotin decorated NPs competently restricted the LC cell proliferation and invasion in the cancer induced animals. Further, it has been demonstrated that the above mentioned proteinsare critical factors for LC proliferation and invasion.

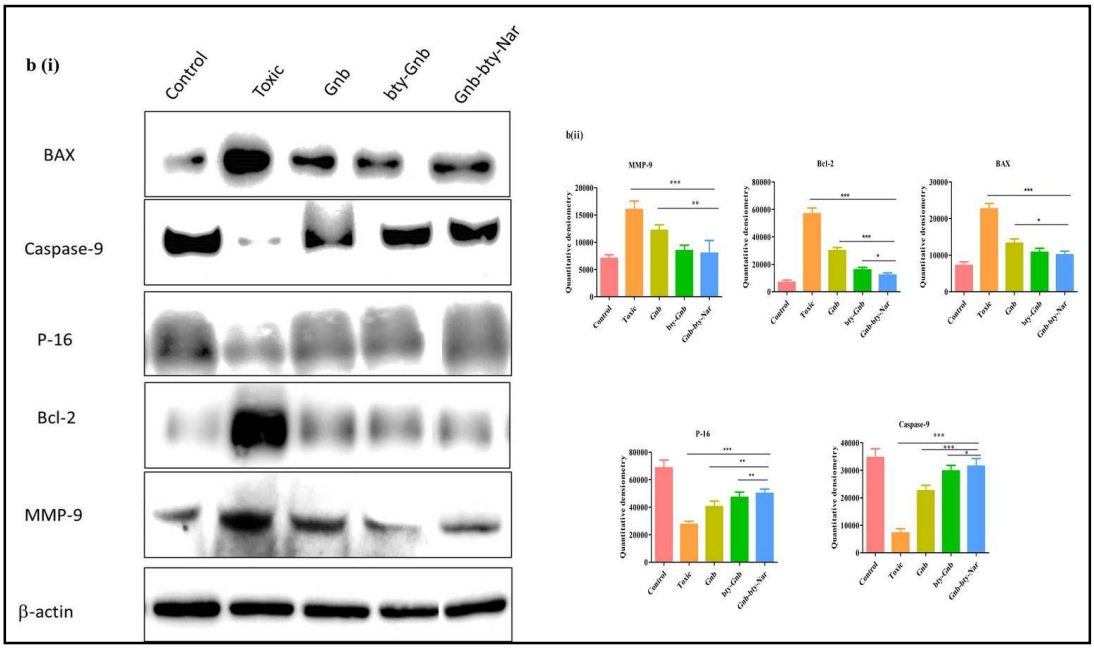

Figure 5.13. Effects of Gnb modified NPs on Pro-apoptotic and anti-apoptotic proteins. Three individual samples from each group were analyzed and subjected to statistical analysis (n = 3). *p < 0.05,**p < 0.01, ***p < 0.001.

5.12.5.Biodistribution Studies

The biodistribution study was performed to further investigate the targeting ability of biotin decorated NPs. Superior targeting potential of a delivery system is foremost criterion for an effective anticancer therapy. A comparative interpretation of the Gnb distribution in the various organs is presented in **Figure 5.14a-d**. It was revealed from the study that there was

greater concentration of modified NPs in tumor tissue when compared when unmodified NPs and plain Gnb. The results demonstrated a significantly higher ($p<0.001$) concentration of Gnb accumulation in tumor tissues after bty-Gnb and Gnb-bty-Nar therapy i.e 47.13±2.91 ng/g and 47.30±3.15 ng/g at 4 h respectively. Conversely, considerably low levels of Gnb were retained in tumor organ at 4 h (21.34±3.27 ng/g) and over a period of 12 h (11.90±1.45 ng/g) in case of Pcl-Gnb treated group. While the co-therapy administered group maintained Gnb level at 32.98 ±1.90 ng/g and 23.15±2.31 ng/g over a period of 24 and 48 h in tumor organ respectively. Approximately, a 5 fold higher accumulation of drug was observed in tumor tissues when compared with free drug administration at all the time points suggesting retention of Gnb in tumor vicinity over long span of time. This specifies the interaction and accumulation of the biotin decorated NPs with over-expressed biotin receptors present in lung tumor cells. This further proves the ability of biotin functionalized NPs to localize preferentially in the tumor tissue when compared to free Gnb, specifying its reduced entry into other vital organs. However, no significant difference in biodistribution was observed in case of Gnb-bty-Nar and bty-Gnb as both the formulation were surface modified with biotin.

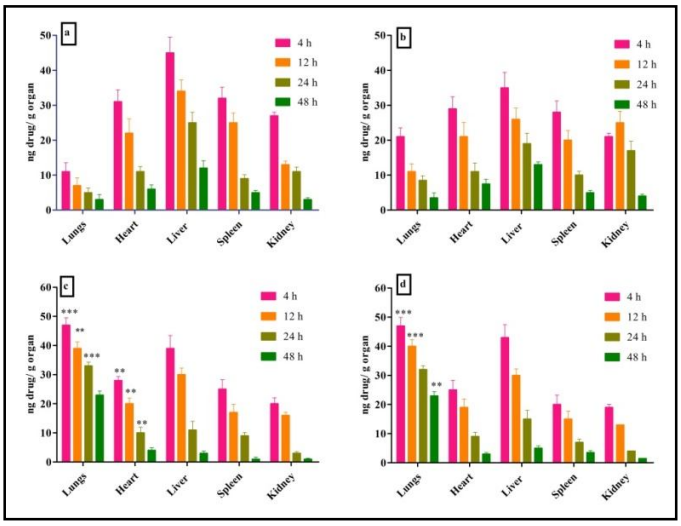

Figure 5.14. Amount of Gnb in different organs (lung, heart, liver, spleen, andkidney) after i.v. administration through tail vein (20 mg/kg Gnb equivalent dose) of (a) Plain Gnb (b) Pcl-Gnb (c) bty-Gnb (d) Gnb-bty-Nar (n=6). [Values are presented as Mean ± SD(n=6); *** $p<0.001$ as compared to standard and marketed; ** $p<0.05$ as compared toother groups]

5.13. Metabolomics

2.1 Serum Metabolic profiling using 1D ^{1}H NMR

In this *in vivo* study the therapeutic efficacy of biotin decorated co-therapy of Gnb and Nar was evaluated. The serum samples of animal were scoped using NMR based metabolomics and serum metabolic perturbations were compared with respect to toxicgroup. The representative 1D ^{1}H CPMG NMR spectra of rat serum samples obtained from different groups with the assigned resonances of relevant metabolites are shown in **Figure 5.15.** The NMR spectra showed signals mainly from lipids/lipoproteins (e.g. low-density lipoprotein (LDL), very low density lipoprotein (VLDL), polyunsaturated fatty acids (PUFAs) etc., and amino acids (e.g. alanine, valine, lysine, leucine, isoleucine, phenylalanine, histidine, tyrosine, glutamine, glutamate etc.). Other identified metabolites were glucose, choline, creatine, creatinine, pyruvate, acetate, citrate, ethanol, methanol and lactate. In this result, multivariate data analysis was performed to find out the toxicant-induced metabolic alterations and further the effect of nanoformulation of the drug treatment on toxicant-induced metabolic alterations was studied **(Figure 5.16).** Unsupervised PCA score plots were constructed for an initial overview of the data set identifying the outlier samples **(Figure 5.16A)**. The outliers were excluded from both the data sets and the resultant data sets were then subjected to supervised PLS-DA to minimize the possible contribution of intergroup variability and to further improve the separation between the 6 groups **(Figure 5.16B).** The combined PCA score plot **(Figure 5.16A)** showed a clear trend of clustering in different groups and no further outlier sample was detected. The combined PLS-DA score plot for all the six groups **(Figure 5.16B)** showed that treated rat groups are well separated from normal control (NC) group with a significantly higher quality of fit and predictability (i.e. R2, Q2 > 0.5, **Figure 2B**). The careful inspection of combined PLS-DA score plot also revealed that nanoformulations mitigate the effect of toxicant-induced toxicity, as inferred by the progressive shift of these groups back towards the control group. The ameliorative effect of the nanoformulation became further evident from the 2D score plot obtained from

combined OPLS-DA analysis (orthogonal projection to the latent structure with discriminant analysis) for all the five groups **(Figure 5.16C).**

The visual inspection of pairwise score plots showed a clear differentiation between Gnb-bty-Narnanoformulation and toxicant which indicates that the separation decreases progressively after treatment **(Figure5.16A&C).** Next, to evaluate the biochemical effects of nanoformulation on urethane-induced toxicity, we identified the metabolic markers using variable importance on projection (VIP) score >1 for discrimination significance and further tested for statistical significance at the level of $p<0.05$ derived from Wilcoxon Mann–Whitney test (**Figure 5.16**). Overall, we identified 20 metabolic markers significantly perturbed in the sera of toxicant treated rats compared to normal control rats. These marker metabolic entities along with their chemical shifts and relative serum levels (in the form of box plots) are shown in **Figure 5.16D.** Compared with control group, toxicant group had significant elevation of lipids, VLVL/LDL lipoprotein, lactate, polyunsaturated fatty acids and pyruvate in their sera, whereas, they were having decreased levels of glucose and several amino acids including glycine, alanine, leucine, isoleucine, valine, glutamate and glutamine were observed**(Figure5.16D).** Further, we found that the metabolic alterations which were observed in the toxicant treated group get ameliorated after Gnb-bty-Nar cotherapy. For example, the metabolites which were increased in the toxicant treated group such as lipids, LDL/VLDL, PUFAs, pyruvate decreased in the drug-treated groups depicted through representative box plots **(Figure 5.16D).** Similarly, the levels of amino acids were partly reset back towards normal after the treatment of Gnb-bty-Nar.

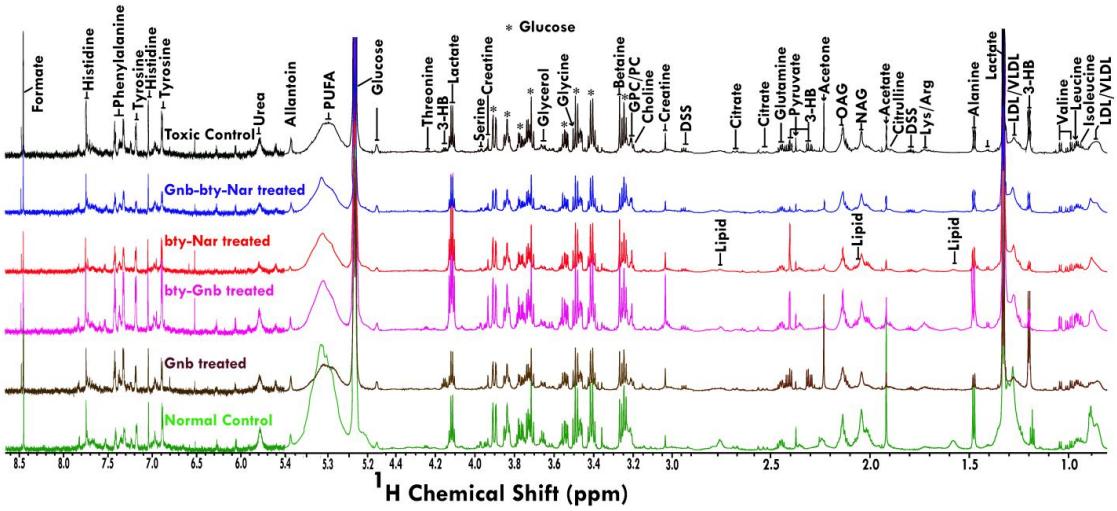

Figure 5.15. Stack plot of representative 1D ^{1}H CPMG (δ 0.7–4.6 and δ 5.2–8.6) . The peaks annotated in the figure show the assignments of serum metabolites. The inset shows the CPMG NMR spectra (δ 0.7–4.66 & 5.2-8.6) of serum The abbreviations used are: LDL/VLDL: Low/very-low-density lipoproteins; PUFA: polyunsaturated fatty acids; Ile: isoleucine; Leu: leucine; Val: Valine, Pyr: pyruvate; Ch: choline; GPC: glycerophosphocholine; Glucose resonances have been indicated using symbol asterisk "*"; NC: Normal Control; TC; Toxic Control; T1: Gnb; T2: bty-Gnb; T3: bty-Nar; T4: Gnb-bty-Nar.

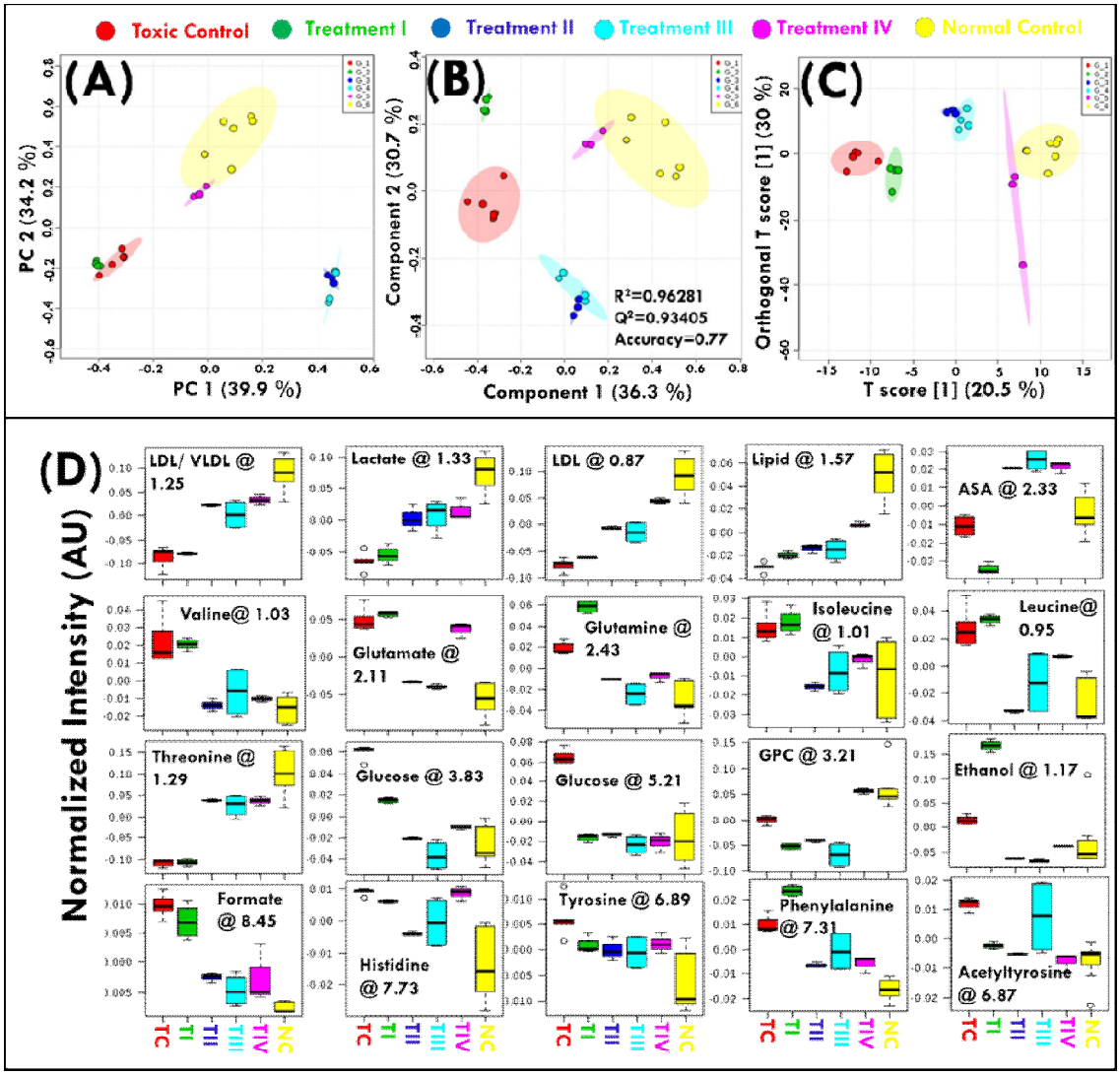

Figure 5.16. Multivariate analysis revealed Biochemical effects of treatment**.**

The multivariate analysis of the serum sample that combined in the 2D PCA, PLS-DA, and OPLS-DA in the Fig1 (A), (B), and (C) respectively, the score plots derived from cumulative analysis of 1D ^{1}H CPMG NMR spectra comprising of all the groups: NC: Normal Control; TC; Toxic Control; T1: Gnb; T2: bty-Gnb; T3: bty-Nar; T4: Gnb-bty-Nar representative box-cum-whisker plots showing quantitative variations of relative signal integrals for serum metabolites relevant in the context of the pathophysiology of lung cancer. For presented metabolite entities, the VIP score >1 and statistical significance is at the level of p□≤□0.05 (the metabolites highlighted in red are having p>0.05).

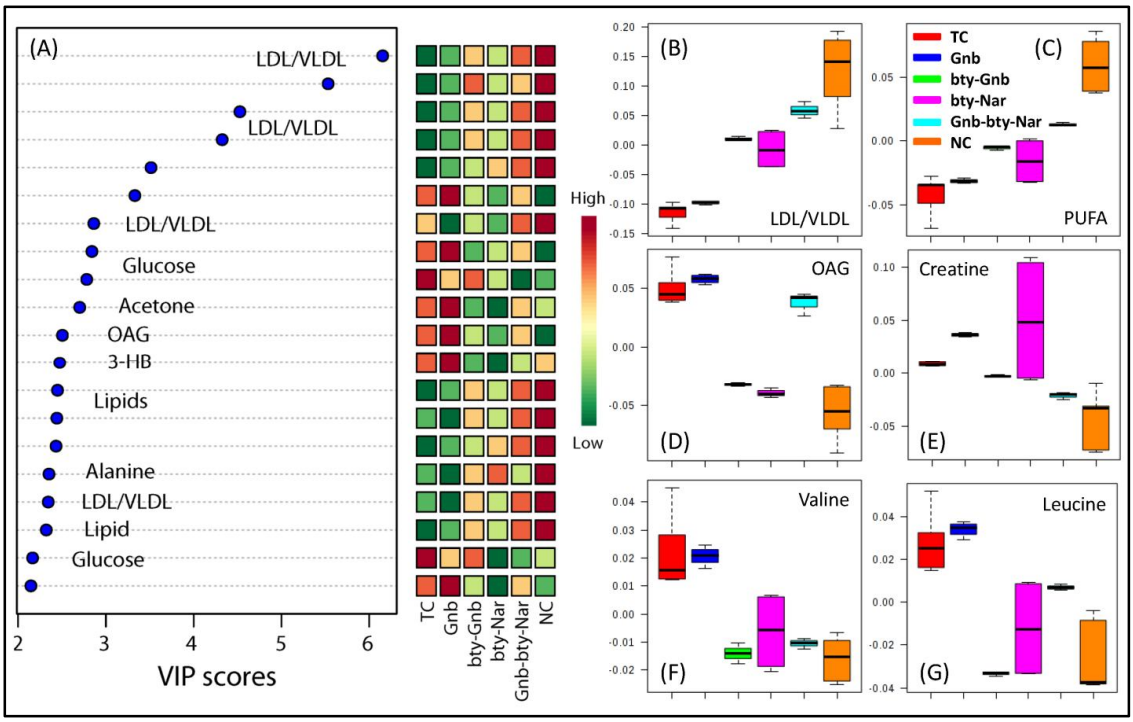

Figure 5.17 Multivariate PLS-DA based discriminatory analysis

The potential biomarker metabolite entities were identified from PLS-DA analysis and are listed in decreasing order of VIP score to highlight their discriminatory potential as show in**figure 5.17**. The complete NMR data matrix was used for PLS-DA modeling and resultant VIP scores for top 35 metabolite entities are shown in **figure 5.17 (A & D).** Most of these metabolite entities correspond to membrane and lipid metabolites. The PLS-DA modeling identified with the excluded lipid regions (0.7 to 0.9, 1.2 to 1.42, 1.5 to 1.6, 2.17 to 2.3, 2.69 to 3.0, 4.67 to 5.4) that revealed the discriminatory importance of other serum metabolites mainly amino acids and metabolites of the tricarboxylic acid cycle show in VIP score shown in **figure 5.17(B&E).**The **figure 5.17 (C & F),** the down-field spectral region from 5.4 to 8.6 ppm was separately used for PLS-DA modeling and revealed the discriminatory importance of aromatic amino acids like Histidine, Tyrosine, and phenylalanine seen in the **figure (F).** In each case, the model parameters for the explained variation, R2, and the predictive capability, Q2, were significantly high (R2, Q2 > 0.9, displayed in the respective PLS-DA score-plots), indicating that the PLS-DA models constructed from complete and truncated CPMG data matrix possessed satisfactory fit with good discriminatory power.

5.14. Stability

This study was designed to investigate the storage stability of the developed bty-Gnb and bty-Nar over a prolonged period of time. The results revealed that the particle size, zeta potential and drug loading did not significantly change after storage period of 90 days under various conditions viz. stored under refrigeration (5±1°C), ambient temperatures (25±5°C, 60±5% RH) and elevated temperature (40±5°C, 75±5% RH). The results obtained validates the selected method for formulations as precise sand accurate. The data is presented in **Table 5.5 a&b** respectively.

Table 5.5. a) Stability of bty-Gnb at various temperatures as per ICH guidelines

Sampling interval (days)	Particle size (nm)			Zeta potential (mV)			% Drug content		
bty-Gnb	5°C± 2°C	25°C± 1°C	40°C ±2°C	5°C±2°C	25°C±1°C	40°C ±2°C	5°C±2°C	25°C± 1°C	40°C ±2°C
0	201±2.4	201±2.4	201± 2.4	-21.04±0.4	-21.04±0.4	-21.04±0.4	44±2.1	44±2.1	44±2.1
15	201±3.1	202±1.1	204± 2.9	-21.04±0.3	-21.99±0.8	-21.99±0.5	44±1.9	44±3.1	44±1.1
30	201±1.9	203±1.3	206± 3.6	-20.31±0.3	-22.93±0.6	-22.14±0.3	43±3.1	42±3.9	42±1.5
45	203±2.1	204±2.5	206± 3.9	-20.22±0.1	-23.21±0.2	-25.32±0.9	43±1.1	41±3.2	40±1.3
90	205±3.2	206±3.4	210± 3.6	-22.17±0.5	-23.39±0.5	-25.19±0.3	42±3.2	41±2.9	40±1.3

Table 5.5b) Stability of bty-Nar at various temperatures as per ICH guidelines

Sampling interval (days)	Particle size (nm)			Zeta potential (mV)			% Drug content		
bty-Nar	5°C±2°C	25°C±1°C	40°C±2°C	5°C±2°C	25°C±1°C	40°C±2°C	5°C±2^{0}C	25°C±1°C	40°C±2°C
0	203±1.2	203±1.2	203±1.2	-21.19±0.4	-21.19±0.4	-21.19±0.4	43±1.3	43±1.3	43±1.3
15	203±3.1	203±1.3	204±1.1	-21.20±0.3	-21.19±0.2	-21.31±0.4	43±1.3	43±1.3	43±1.3
30	203±1.8	203±2.1	206±2.9	-21.81±0.3	-23.09±0.8	-22.49±0.1	43±2.9	41±3.6	41±2.1
45	203±3.0	205±3.7	208±2.2	-20.71±0.5	-23.11±0.2	-24.99±0.7	42±3.2	41±1.1	40±1.9
90	205±4.1	206±1.2	210±3.7	-20.21±0.1	-24.19±0.3	-24.09±0.1	42±1.8	41±3.2	40±0.9

5.15. Discussion

Biocompatibility, biodegradability and easy surface modificationfor targeted delivery are some of the properties owned by PCL (Varan et al. 2017). Biotin is widely used in the delivery of anticancer agents due to its high tumor tissue specificity with overexpressed biotin-specific receptors (Chen et al. 2010, Morral-Ruíz et al. 2015). The peaks in biotin-NHS could be attributed to the C=O stretch at 1644.5 cm^{-1}, N-H bending at 1550 cm^{-1},CH_2 group bending at 1435 cm^{-1} and (C-O) stretching of ester at 1026.9 cm^{-1}. The ^{1}H-NMR further confirms the formation of biotin decorated PCL.A high negative surface charge, confirmed by zeta potential evidences a well dispersed and less aggregated nanoparticulate system. The increase in particle size upon biotin conjugation is attributed to the fact that

biotin attaches itself on the surface PCL-PEG through crosslinking. The modified NPs displayed a minor decrease in %EE which could be due to the loss of free drug from the surface of unmodified NPs during conjugation with activated biotin. The formulations exhibited a slow release in the later stage as the polymer erodes slowly in pH 6.8, and the drug is available for dissolution only after the erosion of polymeric layers(Singh et al. 2017). Functionalization of NPs with biotin enables improved interactions with the overexpressed factors in tumor cells and leads to enhanced cellular uptake, better internalization, reduced cell viability, lower IC_{50} and improved biodistribution. The raised anticancer activity and low viability of A549 cells could be due to rapid cellular uptake of biotinylated NPs as they have high affinity towards biotin receptors and their nanosize, which facilitates effortless NPs internalization. The uptake study supported as an important evidence for functionalization of biotin-modified nanoparticles (Russell-Jones et al. 2004).

The aim of this work was to investigate whether co-therapy with Nar and Gnb hold any promise for improved LC treatment. Previous literatures has reports of various mechanism of Nar, to inhibit cell proliferation by interfering with the PI3K (phosphoinositide 3-kinase) and MAPK pathways resulting in up-regulation of autophagic protein followed by autophagy-mediated cell death. It also causes ERK1/2 inhibition, up-regulation of CYP1A1, PCNA and NF-κB, a caspase cascade signaling pathway and inhibition of matrix metalloproteinases-2 and 9 (Du et al. 2009, Jin et al. 2009, Raha et al. 2015, Eanes et al. 2016).

Keeping in mind the above mechanisms, we can explain the rationale behind taking Nar and Gnb in combination which was confirmed by the additive inhibitory effects *in vitro* (A549 cell lines) as well as via *in vivo* animal studies. The co-therapy through Gnb-bty-Nar has proven to be more effective against LC cell growth. This was supported by the significant reduction in IC_{50} values. The synergistic effect was further proved by isobologram analysis. As is evident in the isobologram, the maximum effect was shown by the combination of gefitinib and naringenin, rather than only naringenin or gefitinib. Thus, when the combined effect is greater than that of individual drug candidates, the combination is said to be

synergistic (Tallirada 2011). Such combinations demonstrating synergism have been proven beneficial in cancer therapies, as they may lower doses of the combination anticancer drugs, a probability of reduced adverse reactions (Gravitz 2011). Further, the CI value of 0.2892 was found in a range of 0.1–0.3 confirms strong synergism, validating the potential of our delivery system (Chou 2006).The enhanced ROS and MMP alteration, cell cycle arrest and apoptosis by Gnb-bty-Nar when compared to Gnb or Nar NPs, individually also supports the superiority of co-therapy. This could be due tothe Nar property to modulate the ROS levels which disrupt the MMP and result in apoptosis as stated above as well as the binding of NPs to overexpressed biotin receptors. On the other side Gnb induces apoptosis by blocking the signal transmission through competitive binding of Mg-ATP situated on the catalytic domain of EGFR-TK, which inhibits the activation of mitogen activated protein kinase in the cancer cell (Lynch et al. 2004, Cataldo et al. 2011).

Superior therapeutic efficacy evidenced by restored levels of biochemical parameters through Gnb-bty-Nar could be due to additional properties like anti-proliferative and anticarcinogenic activity of Nar in combination with Gnb, which was further enhanced by surface modification. The results of western analysis of our study are in good agreement with the ability of Nar for inducing DNA damage through caspase- 9 upregulation and MMP-9 down-regulation, suggesting enhanced therapeutic potential of Gnb-bty-Nar .

Elevated levels of amino acids in toxic group indicated an enhanced catabolism, while decreased glucose level indicates glucose metabolism through glycolysis to generate ATP instead of oxidative phosphorylation requirement of quick proliferation(Wishart et al. 2007, Worley et al. 2013). The restoration towards normal levels in treated groups reveals inhibition of cell growth indicating reduced metabolism and catabolism thus cell death is induced by co-therapy(Bodduluru et al. 2016).

The stability data indicates that the opted method for formulation and optimization of NPs was accurate and precise. The advantages of co-therapy involve utilizing two drugs at lower concentration which reduce toxicity and side effects during treatment, also promoting enhanced cell apoptosis. The newer more promising natural agents could also be investigated in combination with Gnb in future studies. Further formulating them as

modified NPs facilitates better interaction with biological membranes, improved targeting potential and greater accumulation of drug in the tumor cells.

5. 16. Conclusion

The existence of biotin receptors in tumor tissues offers a platform and diverse imitation of ligands to facilitate the tumor targeting. The present investigation exhibits the prospects of co-administration of biotin anchored Nar and Gnb NPs as synergistic therapy to offer enhanced therapeutic efficacy, antitumor effect, targeting potential and greater retention of the biotin modified NPs into tumor tissues.The lung-targeted drug delivery of biotin decorated NPs (bty-Gnb and bty-Nar) were successfully prepared and characterized. In conclusion, developed Gnb-bty-Nar nano-particulate system demonstrated minimal toxicity, facilitated targeted delivery to tumor sites, with reduced access to normal cells as a result of surface modification. Various *in vitro* and *in vivo* studies evidenced remarkably higher drug accumulation in tumor tissues with biotin decorated NPs when compared to plain Gnb/Nar. To sum up, the present investigation exhibits the prospects of co-administration of biotin decorated Nar and Gnb NPs as synergistic therapy to offer improved therapeutic efficacy and antitumor effect. As witnessed by studies it can be concluded that a safe natural anticancer agents like Nar can be an alternative to synergize synthetic anticarcinogenic agents to be formulated as nanoformulations. Further studies can be performed to recognize the effect of combination therapy on carcinomas and subsequent scale-up from bench to bedside.

REFERENCES

Azhar, A., G. Booker and S. Polyak (2015). "Mechanisms of biotin transport."

Beckonert, O., H. C. Keun, T. M. Ebbels, J. Bundy, E. Holmes, J. C. Lindon and J. K. Nicholson (2007). "Metabolic profiling, metabolomic and metabonomic procedures for NMR spectroscopy of urine, plasma, serum and tissue extracts." Nature protocols**2**(11): 2692.

Blanco, E., A. Hsiao, A. P. Mann, M. G. Landry, F. Meric-Bernstam and M. Ferrari (2011). "Nanomedicine in cancer therapy: innovative trends and prospects." Cancer science**102**(7): 1247-1252.

Bodduluru, L. N., E. R. Kasala, R. M. Madhana, C. C. Barua, M. I. Hussain, P. Haloi and P. Borah (2016). "Naringenin ameliorates inflammation and cell proliferation in benzo (a) pyrene induced pulmonary carcinogenesis by modulating CYP1A1, NFκB and PCNA expression." International immunopharmacology**30**: 102-110.

Brannon-Peppas, L. and J. O. Blanchette (2012). "Nanoparticle and targeted systems for cancer therapy." Advanced drug delivery reviews**64**: 206-212.

Cataldo, V. D., D. L. Gibbons, R. Pérez-Soler and A. Quintás-Cardama (2011). "Treatment of non–small-cell lung cancer with erlotinib or gefitinib." New England Journal of Medicine**364**(10): 947-955.

Chang, H. L., Y. M. Chang, S. C. Lai, K. M. Chen, K. C. Wang, T. T. Chiu, F. H. Chang and L. S. Hsu (2017). "Naringenin inhibits migration of lung cancer cells via the inhibition of matrix metalloproteinases-2 and-9." Experimental and therapeutic medicine**13**(2): 739-744.

Chang, Y., S.-T. Yang, J.-H. Liu, E. Dong, Y. Wang, A. Cao, Y. Liu and H. Wang (2011). "In vitro toxicity evaluation of graphene oxide on A549 cells." Toxicology letters**200**(3): 201-210.

Chen, S., X. Zhao, J. Chen, J. Chen, L. Kuznetsova, S. S. Wong and I. Ojima (2010). "Mechanism-based tumor-targeting drug delivery system. Validation of efficient vitamin receptor-mediated endocytosis and drug release." Bioconjugate chemistry**21**(5): 979-987.

Du, G., L. Jin, X. Han, Z. Song, H. Zhang and W. Liang (2009). "Naringenin: a potential immunomodulator for inhibiting lung fibrosis and metastasis." Cancer research**69**(7): 3205-3212.

Eanes, L. and Y. M. Patel (2016). "Inhibition of the MAPK pathway alone is insufficient to account for all of the cytotoxic effects of naringenin in MCF-7 breast cancer cells." Biochimie Open**3**: 64-71.

Eruslanov, E. and S. Kusmartsev (2010). Identification of ROS using oxidized DCFDA and flow-cytometry. Advanced protocols in oxidative stress II, Springer**:** 57-72.

Faivre, L., C. Gomo, O. Mir, F. Taieb, A. Schoemann-Thomas, S. Ropert, M. Vidal, D. Dusser, A. Dauphin and F. Goldwasser (2011). "A simple HPLC-UV method for the simultaneous quantification of gefitinib and erlotinib in human plasma." Journal of Chromatography B**879**(23): 2345-2350.

Guleria, A., N. K. Bajpai, A. Rawat, C. Khetrapal, N. Prasad and D. Kumar (2014). "Metabolite characterisation in peritoneal dialysis effluent using high-resolution 1H and 1H–13C NMR spectroscopy." Magnetic Resonance in Chemistry**52**(9): 475-479.

Guleria, A., A. Pratap, D. Dubey, A. Rawat, S. Chaurasia, E. Sukesh, S. Phatak, S. Ajmani, U. Kumar and C. L. Khetrapal (2016). "NMR based serum metabolomics reveals a distinctive signature in patients with Lupus Nephritis." Scientific reports**6**: 35309.

Jin, C.-Y., C. Park, J.-H. Lee, K. T. Chung, T. K. Kwon, G.-Y. Kim, B. T. Choi and Y. H. Choi (2009). "Naringenin-induced apoptosis is attenuated by Bcl-2 but restored by the small molecule Bcl-2 inhibitor, HA 14-1, in human leukemia U937 cells." Toxicology in Vitro**23**(2): 259-265.

Lee, R. J. and P. S. Low (1994). "Delivery of liposomes into cultured KB cells via folate receptor-mediated endocytosis." J Biol Chem**269**(5): 3198-31204.

Lynch, T. J., D. W. Bell, R. Sordella, S. Gurubhagavatula, R. A. Okimoto, B. W. Brannigan, P. L. Harris, S. M. Haserlat, J. G. Supko and F. G. Haluska (2004). "Activating mutations in the epidermal growth factor receptor underlying responsiveness of non–small-cell lung cancer to gefitinib." New England Journal of Medicine**350**(21): 2129-2139.

Mattu, C., R. Pabari, M. Boffito, S. Sartori, G. Ciardelli and Z. Ramtoola (2013). "Comparative evaluation of novel biodegradable nanoparticles for the drug targeting to breast cancer cells." European Journal of Pharmaceutics and Biopharmaceutics**85**(3): 463-472.

Mogoşanu, G. D., A. M. Grumezescu, C. Bejenaru and L. E. Bejenaru (2016). "Polymeric protective agents for nanoparticles in drug delivery and targeting." Int. J. Pharm.**510**(2): 419-429.

Morabito, A., R. Costanzo, A. M. Rachiglio, R. Pasquale, C. Sandomenico, R. Franco, A. Montanino, E. De Lutio, G. Rocco and N. Normanno (2013). "Activity of Gefitinib in a Non–Small-Cell Lung Cancer Patient with Both Activating and Resistance EGFR Mutations." J. Thorac. Oncol.**8**(7): e59-e60.

Morral-Ruíz, G., P. Melgar-Lesmes, A. López-Vicente, C. Solans and M. J. García-Celma (2015). "Biotinylated polyurethane-urea nanoparticles for targeted theranostics in human hepatocellular carcinoma." Nano Research**8**(5): 1729-1745.

Ni, X. L., L. X. Chen, H. Zhang, B. Yang, S. Xu, M. Wu, J. Liu, L. L. Yang, Y. Chen and S. Z. Fu (2017). "In vitro and in vivo antitumor effect of gefitinib nanoparticles on human lung cancer." Drug Deliv.**24**(1): 1501-1512.

Nicholson, J. K., P. J. Foxall, M. Spraul, R. D. Farrant and J. C. Lindon (1995). "750 MHz 1H and 1H-13C NMR spectroscopy of human blood plasma." Analytical chemistry**67**(5): 793-811.

O'brien, J., I. Wilson, T. Orton and F. Pognan (2000). "Investigation of the Alamar Blue (resazurin) fluorescent dye for the assessment of mammalian cell cytotoxicity." The FEBS Journal**267**(17): 5421-5426.

Pandey, M., S. Sultana and K. P. Gupta (2014). "Involvement of epigenetics and microRNA-29b in the urethane induced inception and establishment of mouse lung tumors." Experimental and molecular pathology**96**(1): 61-70.

Raha, S., S. Yumnam, G. E. Hong, H. J. Lee, V. V. G. Saralamma, H.-S. Park, J. D. Heo, S. J. Lee, E. H. Kim and J.-A. Kim (2015). "Naringin induces autophagy-mediated growth inhibition by downregulating the PI3K/Akt/mTOR cascade via activation of MAPK pathways in AGS cancer cells." International journal of oncology**47**(3): 1061-1069.

Rani, A., S. Roy, M. Singh, U. Devi, R. K. Yadav, S. Gautam, J. K. Rawat, M. N. Ansari, A. S. Saeedan and A. Prakash (2016). "α-Chymotrypsin regulates free fatty acids and UCHL-1 to ameliorate N-methyl nitrosourea induced mammary gland carcinoma in albino wistar rats." Inflammopharmacology**24**(5): 277-286.

Ren, W. X., J. Han, S. Uhm, Y. J. Jang, C. Kang, J.-H. Kim and J. S. Kim (2015). "Recent development of biotin conjugation in biological imaging, sensing, and target delivery." Chemical Communications**51**(52): 10403-10418.

Russell-Jones, G., K. McTavish, J. McEwan, J. Rice and D. Nowotnik (2004). "Vitamin-mediated targeting as a potential mechanism to increase drug uptake by tumours." Journal of inorganic biochemistry**98**(10): 1625-1633.

Singh, N., P. Parashar, C. B. Tripathi, J. Kanoujia, G. Kaithwas and S. A. Saraf (2017). "Oral delivery of allopurinol niosomes in treatment of gout in animal model." Journal of liposome research**27**(2): 130-138.

Sinha, V., K. Bansal, R. Kaushik, R. Kumria and A. Trehan (2004). "Poly-ϵ-caprolactone microspheres and nanospheres: an overview." International journal of pharmaceutics**278**(1): 1-23.

Tang, B., Y. Xing, P. Li, N. Zhang, F. Yu and G. Yang (2007). "A rhodamine-based fluorescent probe containing a Se– N bond for detecting thiols and its application in living cells." Journal of the American Chemical Society**129**(38): 11666-11667.

Tseng, C.-L., W.-Y. Su, K.-C. Yen, K.-C. Yang and F.-H. Lin (2009). "The use of biotinylated-EGF-modified gelatin nanoparticle carrier to enhance cisplatin accumulation in cancerous lungs via inhalation." Biomaterials**30**(20): 3476-3485.

Tseng, C.-L., T.-W. Wang, G.-C. Dong, S. Y.-H. Wu, T.-H. Young, M.-J. Shieh, P.-J. Lou and F.-H. Lin (2007). "Development of gelatin nanoparticles with biotinylated EGF conjugation for lung cancer targeting." Biomaterials**28**(27): 3996-4005.

Tseng, C.-L., S. Y.-H. Wu, W.-H. Wang, C.-L. Peng, F.-H. Lin, C.-C. Lin, T.-H. Young and M.-J. Shieh (2008). "Targeting efficiency and biodistribution of biotinylated-EGF-conjugated gelatin nanoparticles administered via aerosol delivery in nude mice with lung cancer." Biomaterials**29**(20): 3014-3022.

Ulrich, E., H. Akutsu, J. Doreleijers, Y. Harano, Y. Ioannidis, J. Lin, M. Livny, S. Mading, D. Maziuk and Z. Miller (2008). "BioMagResBank Nucleic Acids Res. 36." D402–D408.

Varan, C. and E. Bilensoy (2017). "Cationic PEGylated polycaprolactone nanoparticles carrying post-operation docetaxel for glioma treatment." Beilstein journal of nanotechnology**8**: 1446-1456.

Wishart, D. S., D. Tzur, C. Knox, R. Eisner, A. C. Guo, N. Young, D. Cheng, K. Jewell, D. Arndt and S. Sawhney (2007). "HMDB: the human metabolome database." Nucleic acids research**35**(suppl_1): D521-D526.

Worley, B. and R. Powers (2013). "Multivariate analysis in metabolomics." Current Metabolomics**1**(1): 92-107.

Wu, J.-L., X.-Y. He, P.-Y. Jiang, M.-Q. Gong, R.-X. Zhuo and S.-X. Cheng (2016). "Biotinylated carboxymethyl chitosan/CaCO 3 hybrid nanoparticles for targeted drug delivery to overcome tumor drug resistance." RSC Adv**6**(73): 69083-69093.

Xia, J., N. Psychogios, N. Young and D. S. Wishart (2009). "MetaboAnalyst: a web server for metabolomic data analysis and interpretation." Nucleic acids research**37**(suppl_2): W652-W660.

Xia, J., I. V. Sinelnikov, B. Han and D. S. Wishart (2015). "MetaboAnalyst 3.0—making metabolomics more meaningful." Nucleic acids research**43**(W1): W251-W257.

Zempleni, J., S. S. Wijeratne and Y. I. Hassan (2009). "Biotin." Biofactors**35**(1): 36-46.

Chapter VI

Summary &Conclusion

Summary and Conclusion

The present study is focused on development and assessment of polymeric nanoparticulate system designed to target lung carcinoma. The targeted delivery system is believed to deliver drug specifically to the cancer cells, resulting in high payload thus enhanced therapeutic efficacy. Such systems are capable to easily discriminate between the cancer and normal cells, thereby reducing dose related toxicity.Some xenobiotics (Capsaicin and Naringenin in current study)bestowed with antioxidant, anti-inflammatory, antiproliferative and anticancer properties. These xenobiotics were taken along with synthetic drug widely employed in lung cancer (gefitinib) in combination and co-therapy was executed, to get a synergistic effect. Also, the antioxidant property of xenobioticsreduces the oxidative stress and aided in overcoming multidrug resistance. Taking advantage ofthis approach the therapeutic outcome of anticancer agents can be enhanced when compared with therapy through single drugs.

The anticancer drug selected for current study was gefitinib (Gnb) as it is one of the most widely adopted drugs for treating lung cancer. Further, to improve its therapeutic potential xenobiotics capsaicin (Cap) and naringenin (Nar) were taken for co-therapy. The selected drug candidates for the present study were characterized for identification and purity by FTIRand UV spectroscopy.

Based upon the compatibility, desired biocompatible, biodegradable and ease in surface tailoring properties PCL and PLGA polymers were selected. The selected polymers were anticipated to possess capability of giving stable formulation(s), having high %EE and ability to deliver drug to the targeted site. For polymeric nanoparticles (NPs), polymer and drug ratio was selected on the basis of stability, particle size, %EE, drug loading and *in vitro* release.

For the optimization of NPs formulation(s) different factors selected includeddrug:polymer ratio (1:2), copolymer PVA concentration, cremophore EL concentration and stirring speed. A 3-factor 3-level central composite design (CCD) was selected for optimization of polymeric NPs which suggested 09 experimental trials with different combination of factors. All the trials for PCL and PLGA NPs were individually formulated and evaluated for response variables like, particle size, %EE, drug release and drug loading.

The experiential data for both the NPs systems were analysed mathematically, using quadratic equations andbest fit model that generated best fitted equations was obtained. Response Surface Model (RSM) was implementedwhich best validated the relationships among selected factors and responses accompanied by interactions among factors, if any. The RSM advised significant effect of drug:polymer ratio on various responses i.e., particle size, %EE, drug release and drug loading of NPs.

Further, the design space was generatedusing overlay plot and optimized formulation was recognised by putting definite criteria for different response factors. The criteria applied for the NPs optimizations were fixed at the values *viz.*particle size below 250 nm, entrapment efficiency above50%, drug release not less than 80% and drug loading above10%.

The formulation composition optimized for PLGA NPs were drug:polymer ratio(2:1), PVA concentration (2.5%v/v), whereas for PCL NPs the composition taken wasdrug:polymer ratio (2:1), and PVA concentration (2.5%v/v)with a stirring speed (500 rpm) which was found suitable to yield NPs of desired characteristics. A good agreement was witnessed between predicted values and observed values of response variables for all the systems.

The targeting module folate was successfully conjugated on the surface of PLGA NPs with the help of NHS and DCC as evidencedby means ofFTIR and NMR spectrum. The characteristic peaks for various groups and structural configurationswere observed and confirmed through aforementioned spectra. Estimation of folate content further witnessed the folate conjugation to the PLGA NPs surface.The amount of folate attached was found to be 5.67 µM of folate/g of polymer. The physicochemical characterization of folate conjugated NPs (Gnb-PLGA-PEG-FA and Cap-PLGA-PEG-FA) revealed the particle size of 217.0±3.2nm and 213.0±5.2 nm, zeta potential -13.19±2.01mV and -14.45±0.88 mV, entrapment efficiency of 49±1.5% and 46±2.3% percent drug loading of 20.88±1.7% and 21.77±1.3%,respectively.

The biotin was successfully anchored on the surface of PCL NPs with help of NHS and DCC as denoted by characteristic peaks of FTIR and NMR spectrum. The estimation of biotin content through HABA/avidin assay,further confirmed the biotin anchoring to the surface of PCL NPs. The biotin content was found to be 39.43 µg mg^{-1} and 38.57 µg mg^{-1} for bty-Gnb and bty-Nar respectively. The physicochemical characterization of biotin

anchored NPs (bty-Gnb and bty-Nar)displayed the particle size of 201±3.2nm and 203±2.7 nm, zeta potential -21.04±1.4mV and -21.19±2.3 mV, entrapment efficiency of 44±2.9% and 43±2.3% and drug loading of 23.23±1.97% and 21.23±1.3% respectively.

The hyaluronic acid (HA) was successfully anchored on the surface of capsaicin loaded PCL NPs employing layer by layer technique (LBL).A polycationic layer of a polymer was utilized as a linker between two polyanionic layers. Chitosan (CH) was sandwiched between PCL and HA so as to form a polycationic layer for fabrication of the LBL assembly. The physicochemical characterization of HA decorated NPs (HA-PCL-CAP) displayed the particle size of 194±2.90nm, zeta potential -27.87±3.21 mV mV, entrapment efficiency of 52.89±2.19% and drug loading of 13±0.37%respectively.

The release pattern in case of PCL/PLGA NPs was found to be sustained.Approximately 85.65±3.21% and 81.43±4.32% for Gnb and Cap were released from Gnb-PLGA-PEG-FA and Cap-PLGA-PEG-FA over a period of 80 h. About 81.94±3.12% of Gnb and 80.99±4.99% of Nar were released from biotin modifiedPCL NPs over a period of 80 h.HA-PCL-CAP NPs exhibited sustained release behaviour with 82.43±1.93% drug release in 48 h. An insignificant change in the release profiles was observed before and after surface modification of NPs in all the three formulations, since these experiments were done *in vitro*. Further, the isobologram evidenced the synergistic effect of combination therapy. The combination index value obtained was below 0.3, which indicates a very good synergistic effect of Gnb when combined with Cap/Nar.

The folate modified, biotin modified and HA modified NPs were found to be stable during the studies performed as per ICH guidelines over a period of three months.

In vitro cell lines studies executedoverA549 cell lines,displayed superiority of folate, biotin and HA decorated NPs over unmodified formulations. The supremacyof surface engineered formulationwas ascertainedthrough cell cytotoxicity assay, cell cycle analysis, cellular proliferation studies, apoptosis assay, cellular internalization, MMP and ROS studies. Further superlative response of cotherapy over individual therapy either by Gnb/Nar/Cap was evidenced by aforementioned studies in case of folate and biotin conjugated formulations.

MTT assay displayed a supressed IC_{50} value of formulation when given in combination as modified NPs. The IC_{50}values were found to be 23.5±0.76µM in cells treated with

Gnb and Cap combination (Cap@GnbPLGA-PEG-FA) and 25.4±0.32µM in case of combination treatment through Nar and Gnb (Gnb-bty-Nar) which was relatively lowwhen compared with the IC_{50} values obtained in Gnb/Nar/Cap treated cells individually. Also, the HA decorated Cap displayed a depressed IC_{50} value of 39.74±2.11 µM when compared withunmodified Cap.

Cell cycle studies through FACS demonstrated that Cap@GnbPLGA-PEG-FA (co-therapy) arrested the A549 cells in G0/G1, S and G2/M phases respectively. While, A549 cells were preferentially arrested in G1 phase, G1phase and G0/G1 phase respectively in case of Gnb-bty-Nar co-therapy.

Cell proliferation studies revealed that the inhibition of cellular proliferation for Cap and Gnb cotherapywas much higher than individual therapy.The inhibition potential followed an order of **1**Cap@Gnb-PLGA-PEG-FA>**2**Gnb-PLGA-PEG-FA>**3**Cap-PLGA-PEG-FA>**4**Gnb-PLGA>**5**Cap-PLGA>**6**Gnb>**7**Cap. While, the order for inhibition of cellular proliferation various formulationof PCL NPs, was found in order of Gnb-bty-Nar>bty-Gnb>bty-Nar>PCl-Gnb>PCl-Nar>Gnb>Nar. The data suggested that modified formulations when given in combination displayedmaximum cellular mortality when compared to individual drug formulations treated cells.Correspondingly, ROS and MMP data suggested the superiority of the HA decorated NPs,biotinylated NPs and folate anchored NPsover unmodified formulations. Also, it was demonstrated that when natural agents were given in combination, the effect obtained was superior in comparison to response obtained through individual drug. Cellular internalization studies through florescence microscopy demonstrated enhanced internalization of modified formulation in comparison to unmodified formulation.

The supremacy of modified formulations over unmodified formulation as concludedfrom *in vitro* cell lines data specified that surface modifications facilitated these formulations in improved cellular internalization through overexpressed receptors. Also, formulation being nanosized,possess passive targeting resulting in enhanced permeation and retention. Further xenobiotics, including phytopharmaceutical agents are expelled out from the cells due to efflux pumps present in prokaryotes and eukaryotes, leading to sub-therapeutic concentrations at desired site. Howeverformulating them as surface modified, receptor specific, nanoformulations can lead to higher internalization into the targeted cells.Also, phytochemicals are known to act through several pathways thus a

combination of natural and synthetic drug can lead to enhanced apoptosiseffected through different pathways.

In vivo studies were performed on albino wistar ratsweighing 120-150 g, of either sex. The protocol for animal testing was approved through institutional ethical committee and experiments werecompletedin accordance to the CPCSEA guidelines for laboratory animals and ethics, Department of Animal Welfare, Government of India. Animals were randomized and divided into six groups of 12 animals each for folate conjugated and biotin conjugated NPs, while animals were divided into five groups in case of HA modified NPs. Lung cancer was induced by three consecutive i.p. injections of urethane, within a gap of 48 h over a period of one week. The development of lung tumors was initiated over a period of 8-12 weeks.During treatment period, various formulations were administered (20 mg/kg e.q. Gnb, 10 mg/kg e.q. Cap and 30 mg/kg e.q. Nar) to respective groups via intravenous tail injection at an interval of three days. The treatment was continued for a period of four weeks, followed by observation of the animals for indication of toxicity, weight loss and mortality, of animals during the study. A gap of 12 weeks was taken to develop the cancer in animals. Toxic group exhibitedhighest incidence of mortality,highest tumor volume and reduction in animal weight, followed by pure drug receiving group, Gnb-PLGA-PEG-FA/Cap-PLGA-PEG-FA and Cap@GnbPLGA-PEG-FA. Highest recovery was observed in the group receiving co-therapy through Cap and Gnb. In case of biotin decorated formulation reduction in animal weight declined to 46% for toxic group, 31.23% reduction for bty-Nar, 11.32% for cotherapy (Gnb-bty-Nar)group. Similarly for HA modified formulation, toxic group showed mean reduction in animal weight of 49%, PCL-CAP treated group showed 35.32% reduction, HA-PCL-CAP group displayed10.25% reduction.

Themortality incidents of animal were found to be lowest in groups receiving cotherapy, followed by biotin decorated/folate conjugated groups. Similarly the highest survival was observed in case of group receiving HA modified CAP. Toxic groupspresented lowest animal survival rate, in all the three formulations (folate/ biotin/ Hyaluronic acid conjugated formulation). Likewise, trends were observed for tumor volumes and tumor incidence forall the three formulations.

The urethane-inducedlung carcinoma brings abouta significant imbalance in biochemical mechanisms of cells. It was clearly indicated by noticeablealteration in the levels of

oxidative stress markers like TBARS, protein carbonyl, GSH, SOD and catalase. Treatment with different formulation restoredthe levels of these imbalanced markers towards normal and order of activity observed was cotherapy>folate conjugated NPs>unmodified NPs>pure drug. Likewise, biotin modified co-therapy and HA modified NPs revealed highest efficiency in restorationof altered levels of oxidative stress markers towards normal.

Western blotting analysisadvocated that administration of urethane to the animals triggered the up-regulation of antiapoptotic proteins such as bcl-2, and MMP-9 and down-regulation of pro-apoptotic markers such as bax, caspase-3, P-16 and caspase-9. The treatment of animal with Gnb and folate decorated formulationsreinstated the level of these proteins towards normal but the effect was more intense in case of cotherapy through Cap@Gnb-PLGA-PEG-FA. Parallel trends were observed in case of cotherapy throughNar and Gnb, and therapy through HA modified formulations.Treatment of urethaneadministered group with various formulations resulted in down-regulation of anti-apoptotic proteins bcl-2 and MMP-9 while upregulation ofpro-apoptotic proteins like BAX, caspase-9 and p16 expression was observedrepresenting tumor inhibitory potential of all the three modified formulation. Further, highestrestoration was observed with cotherapy through Gnb and Nar as well as Gnb and Cap.Concomitantly, the proteins p-16, MMP-9 and members of the bcl-2 family protein, comprising bcl-2, BAX *etc*.plays an important role in migration, invasion and metastasis of lung cancer. The outcomesof our study demonstrated that the biotin decorated NPs, folate decorated NPs and HA decorated NPs can efficiently reduce the lung tumor development in the cancer induced rats. Further, the cotherapy has proved its enhanced therapeutic potential for treating urethane-induced lung carcinoma when compared with individual therapy through either of drugs (Gnb/Cap/Nar).

Angiogenesis and cellproliferation isimportant characteristicfeature of cancer growth. The development of carcinoma was represented through rosette shaped structured tumor cells and peribronchial cells which infiltrate the bronchial submucosa after urethane administration.The co-therapy through Cap@Gnb-PLGA-PEG-FA and Gnb-bty-Nar formulations revealed restoration of cellular architecture towards normal. Parallel results were demonstrated in HA-PCL-CAP treated animals.

The Gnbconcentration accumulated in the lung carcinoma was highest in the case of the Gnb-PLGA-PEG-FA (45.17±3.23 µg/g in 4 h) followed by the Gnb-PLGA (37.43±2.91 µg/g organ in 4 h) indicating the site-specific accumulation of the folate conjugatedNPs in folate over-expressed tumor cells in lung carcinoma. Further, Gnb-PLGA-PEG-FA substantiallymaintained greaterGnb levels in the tumor organover a period of 48 h (21.45±1.09 µg/g tumor organ) ($p<0.001$) and37.87±1.33 µg/gorganupto 12 h.The concentration of Gnb was found significantly lower($p<0.01$)in groups *vis-à-vis* pure Gnb (10.53±3.46 µg/g in 12 h, 3.05±0.53 µg/g in 48 h) and the Gnb-PLGA (13.32±2.34 µg/g in 12 h, 1.49±0.393 µg/g in 48 h) treated groups. In case of unmodified NPs highest Gnb concentration was detected in the liver among various organs, followed by the spleen, the heart and the kidney. Overall,Gnbaccumulation was found significantly lower in aforementioned organs in folate decorated NPstreated groups than that of groups treatedwith unmodified formulations. Similar, results were perceivedwith biotinylated NPs. The highest concentration was maintained by bty-Gnb in cancer cells followed by Pcl-Gnb and Gnb.The biodistribution data further confirmed the discriminatoryentry of the biotinylated NPs towards the biotin receptor that are over-expressed in diseases like lung carcinoma. Parallel results were revealed by HA decorated NPs. The maximum concentration of Cap was achieved in cancer tissue after HA-PCL-CAP administration(49.35±3.22 µg/g) followed by PCL-CAP (29.34± 1.45 µg/g) and CAP (09.21±1.02 µg/g). However, an insignificant difference in drug concentration was found when a comparison was made between co-therapy and individual therapy through modified NPs.

Further, the metabolomics study revealed restoration of elevated levels of amino acids and decreased glucose level towards normal levels in biotinylated NPs (cotherapy) treated groups. The resultsrevealed inhibition of cell growth indicating reduced metabolism and catabolism thus it can be said that the cell death induced by co-therapy when formulated as modified NPs.

On the basis of results summarized above, ligand directed drug delivery system was found therapeutically effective and safe for regulating the cancer proliferation, in lung carcinoma. The mammalian cells standincompetentin synthesizing some of the essential biomolecules obligatory for their growth and proliferation. Thus,these have to be taken up through some transport systems such as sodium-dependent multivitamin transporter (SMVT), high-affinity biotin transporter for biotin uptake and high affinity folate

receptor for folate uptake. Also, CD44 over expressed in cancer cells that binds to its primary ligand HA and is stated to be responsible for cellular signaling, leading to regulation of biological process within cells. Thus a swift uptake of NPs carrying such molecules is witnessed via these overexpressed receptors, delivering the drug payload.The overexpression of these receptors over cancer cell and selective uptake of such targeting modules in the cancer cells could be a probablejustification for selective uptake of molecularly designed targeted NPs for lung cancer. Conjugation of targeting moietyutilizing a moderately long PEG chain linker yieldedan effective ligand-receptor molecule and supports its internalization into cancer cells. Further, it has been demonstrated that co-therapy with Cap/Nar has cancer suppression and inhibitory effect. Additionallyphytoconstituents have antioxidant propertyand are known to act through several pathways because of whichmulti drug resistance can also be addressed. Further,prolonged drug release maintains higher concentration of antineoplastic agents/xenobiotic leading to greater cell cytotoxicity. The combination therapy,that too as a targeted delivery, would successfully address lung carcinoma. Finally, the present investigation exhibits the prospects of co-administration of targeted module conjugated NPs as synergistic therapy to offer enhanced therapeutic efficacy and antitumor effect. In conclusion, developed nano-particulate system(s) demonstrated minimal toxicity, facilitated targeted delivery to tumor sites, with diminished access to normal cells as a result of surface modification. In light of the above studies it can be concluded that safe, natural, anticancer agents like Cap/Nar can be an alternative to synergize synthetic anticarcinogenic agents to be formulated as nanoformulations and conventional formulations for management of lung carcinoma. Further studies can be performed to recognize the effect of combination therapy on carcinomas and subsequent scale-up from bench to bedside after suitable clinical evaluations.

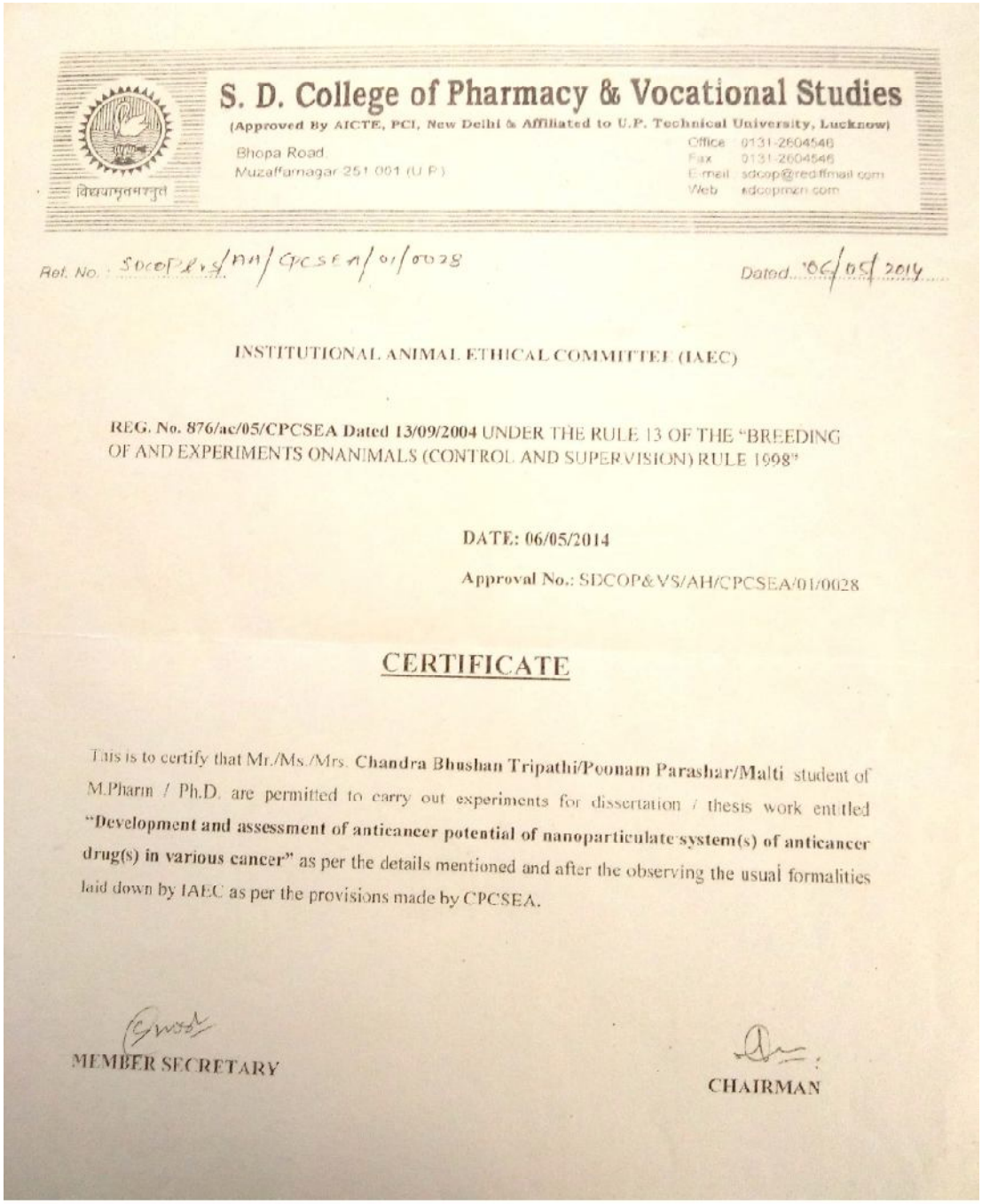

S. D. College of Pharmacy & Vocational Studies

(Approved By AICTE, PCI, New Delhi & Affiliated to U.P. Technical University, Lucknow)

Bhopa Road
Muzaffarnagar 251 001 (U.P.)

Office 0131-2604546
Fax 0131-2604546
E-mail sdcop@rediffmail.com
Web sdcopmzn.com

Ref. No.: SDCOP&VS/MM/CPCSEA/01/0028 Dated: 06/05/2014

INSTITUTIONAL ANIMAL ETHICAL COMMITTEE (IAEC)

REG. No. 876/ac/05/CPCSEA Dated 13/09/2004 UNDER THE RULE 13 OF THE "BREEDING OF AND EXPERIMENTS ONANIMALS (CONTROL AND SUPERVISION) RULE 1998"

DATE: 06/05/2014

Approval No.: SDCOP&VS/AH/CPCSEA/01/0028

CERTIFICATE

This is to certify that Mr./Ms./Mrs. **Chandra Bhushan Tripathi/Poonam Parashar/Malti** student of M.Pharm / Ph.D. are permitted to carry out experiments for dissertation / thesis work entitled **"Development and assessment of anticancer potential of nanoparticulate system(s) of anticancer drug(s) in various cancer"** as per the details mentioned and after the observing the usual formalities laid down by IAEC as per the provisions made by CPCSEA.

MEMBER SECRETARY

CHAIRMAN

Plagiarism Report

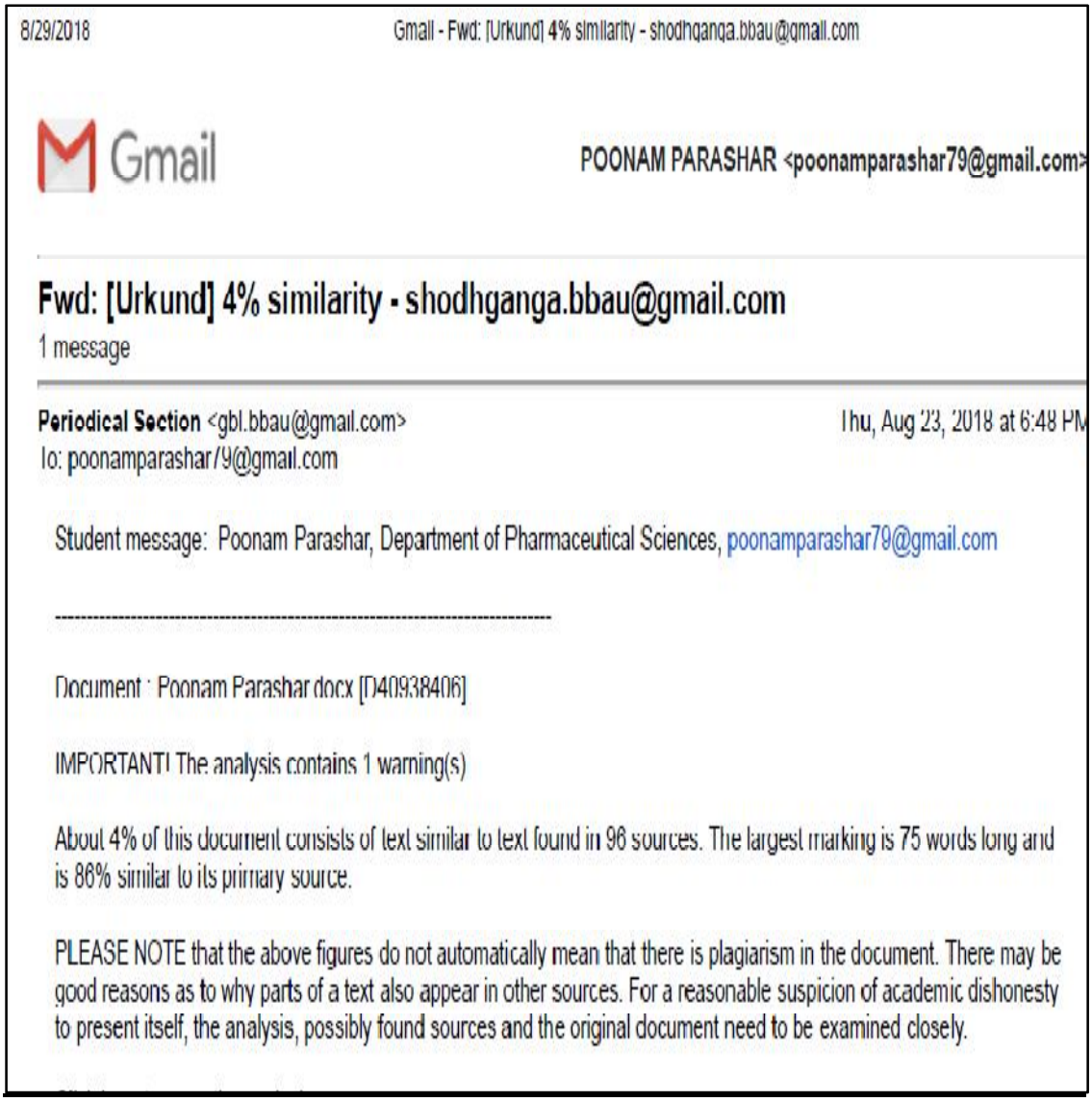

8/29/2018 Gmail - Fwd: [Urkund] 4% similarity - shodhganga.bbau@gmail.com

Gmail

POONAM PARASHAR <poonamparashar79@gmail.com>

Fwd: [Urkund] 4% similarity - shodhganga.bbau@gmail.com

1 message

Periodical Section <gbl.bbau@gmail.com> Thu, Aug 23, 2018 at 6:48 PM
To: poonamparashar79@gmail.com

Student message: Poonam Parashar, Department of Pharmaceutical Sciences, poonamparashar79@gmail.com

---

Document : Poonam Parashar.docx [D40938406]

IMPORTANT! The analysis contains 1 warning(s)

About 4% of this document consists of text similar to text found in 96 sources. The largest marking is 75 words long and is 86% similar to its primary source.

PLEASE NOTE that the above figures do not automatically mean that there is plagiarism in the document. There may be good reasons as to why parts of a text also appear in other sources. For a reasonable suspicion of academic dishonesty to present itself, the analysis, possibly found sources and the original document need to be examined closely.

Publications

Publications from the Present Research Work

1. **Poonam Parashar,** Meena Rathor, Monika Dwivedi, Shubhini A Saraf. Hyaluronic Acid Decorated Naringenin Nanoparticles: Appraisal of Chemopreventive and Curative Potential for Lung Cancer, Pharmaceutics 2018;10: 1-33. **(Impact factor-3.74)**

2. **Poonam Parashar**, Chandra Bhushan Tripathi, Malti Arya, Jovita Kanoujia, Mahendra Singh, Abhishek Yadav, Amit Kumar, Anupam Guleria, Shubhini A Saraf. Biotinylated Naringenin Intensified Anticancer Effect of Gefitinib in Urethane-Induced Lung Cancer in Rats: Favorable Modulation of Apoptotic Regulators and Serum Metabolomics, Artificial cell, nanomedicine and biotechnology. 2018 **(Accepted manuscript) (Impact factor-3.02)**

3. **Poonam Parashar**, Chandra Bhushan Tripathi, Malti Arya, Jovita Kanoujia, Mahendra Singh, Abhishek Yadav, Shubhini A Saraf. A Facile Approach for Fabricating CD44 Targeted Delivery of Hyaluronic Acid Functionalized PCL Nanoparticles in Urethane-Induced Lung Cancer: Bcl-2, MMP-9, Caspase-9 and BAX as Potential Markers. DDTR.(**Accepted manuscript**) **(Impact factor-3.39)**

4. **Poonam Parashar**, Preeti Rana, Monika Dwivedi, Shubhini A Saraf. "Dextrose Modified Bilosomes for Peroral Delivery: Improved therapeutic potential and stability of Silymarin in Diethylnitrosamine-induced hepatic carcinoma in rats" Journal of Liposomal Research. 2018 **(Accepted manuscript) (Impact factor-2.5)**

Publications Related to otherResearch Work

5. Chandra Bhushan Tripathi, **Poonam Parashar**, Malti Arya, Jovita Kanoujia, Mahendra Singh, Shubhini A Saraf, QbD based Development of α-Linolenic Acid Potentiated Nanoemulsion for Targeted Delivery of Doxorubicin in DMBA Induced Mammary Gland Carcinoma: In Vitro and In Vivo Evaluation, Drug Deliv Transl Res. 2018. (**Impact factor- 3.3)**

6. Neelu Singh, **Poonam Parashar**, Chandra Bhushan Tripathi, Jovita Kanoujia, Gaurav Kaithwas & Shubhini A. Saraf. Oral delivery of allopurinol niosomes in treatment of gout in animal model , Journal of liposomal Research 2017 ;27(2):130-138. (**Impact factor- 2.5**)

7. Jyoti Verma, Jovita Kanoujia, **Poonam Parashar**, Chandra Bhushan Tripathi & Shubhini A. Saraf.Wound healing applications of sericin/ chitosan-capped silver nanoparticles incorporated hydrogel, Drug delivery and translational research 2017 ;7(1):77-88. (**Impact factor- 3.3**)

8. Sanju Singh, **PoonamParashar**, Jovita Kanoujia, Indu Singh, Shubhini A. Saraf. Transdermal potential and anti-gout efficacy of febuxostat from niosomal gel. Journal of drug delivery science and technology 2017, 39: 348-361 **(Impactfactor- 2.2)**

9. **Poonam Parashar**, Yogesh Kumar, Jovita Kanoujia, Indu Singh, Shubhini A. Saraf. "Coformer Selection and Engineering of Co Crystals of Felodipine for Enhanced Solubility". Thai Journal of Pharmaceutical Sciences. 2018 (**Accepted Manuscript**).

10. Deepika Rawat, Chandra Bhushan Tripathi, **Poonam Parashar**, Mahendra Singh, Gaurav Kaithwas, Shubhini A. Saraf, "Development and Characterization of Nanostructured Lipid Carriers of Vetiveria zizanoides oil for Therapeutic Potential in Prickly Heat Treatment" Journal of Pharmacy and Pharmaceutical Sciences, 2015; 2: 162–171.

11. Nidhi Ganggwar, Mahendra Singh, **Poonam Parashar**, Chandra Bhushan Tripathi, Malti Arya, Shubhini A Saraf and Sudipta Saha. Topical Delivery of Fluconazole via Microemulsion Incorporated Hydrogel for the Management of Fungal Dermatophytosis. Current Drug Therapy, 2016; 11(2):129 – 141.

12. Mahendra Singh, Jovita Kanoujia, **Poonam Parashar**, Malti Arya, Chandra B. Tripathi, Vivek Sinha, Shailendra K. Saraf, Shubhini A. Saraf. Augmented bioavailability of felodipine through an α-linolenic acid-based microemulsion. Drug delivery and translational research. 2017:1-22. **(Impact factor- 3.094)**

13. Mahendra Singh, Jovita kanoujia, Pooja Singh, **Poonam Parashar**, Malti Arya**,** Chandra Bhusan Tripathi, Vivek Sinha, Shubhini A. saraf, Development of an a-linolenic acid containing soft nanocarrier for oral delivery part II: buccoadhesive gel, RSC Advances. 2016;6:101602-101612 **(Impact factor- 3.108)**

14. Mahendra Singh, Jovita Kanoujia, Pooja Singh, Chandra B. Tripathi, Malti Arya, **Poonam Parashar,** Vivek R. Sinha, Shubhini A. Saraf, Development of ana-linolenic acid containing soft nanocarrier for oral delivery: in vitro and in vivo evaluation, RSC Advances, 2016;6:77590–77602. **(Impact factor- 3.108)**

15. Mahendra Singh, Jovita Kanoujia, **Poonam Parashar**, Malti Arya, Chandra B. Tripathi, Vivek R. Sinha, Shailendra K. Saraf, Shubhini A. Saraf . Assessment of improved buccal permeation and bioavailability of felodipine microemulsion-based cross-linked polycarbophil gel. (DrugDeliv Transl Res. 2018 Jun;8(3):591-601. **(Impact factor- 3.3)**

16. Malti Arya, Prakash Tiwari, Chandra B. Tripathi, **Poonam Parashar**, Mahendra Singh, Priyam Sinha, Narayan P. Yadav, Gaurav Kaithwas, Krishna P. Gupta, Shubhini A. Saraf. Novel niosomal lotion of Inositol hexaphosphate against inflammation/ hyperplasia in epidermal layer of Swiss albino mice. Molecular Pharmaceutics. 2017;14(3):928–939. **(Impact factor- 4.440)**

17. Jovita Kanoujia, Mahendra Singh, Pooja Singh, **Poonam Parashar,** Chandra Bhusan Tripathi, Malti Arya**,** Shubhini A. Saraf**,** Genipin crosslinked soy-whey based bioactive material for atorvastatin loaded nanoparticles: Preparation, characterization and in vivo antihyperlipidemic study. RSC Advances. 2016;6:93275-93287. **(Impact factor- 3.108)**

18. Chandra B. Tripathi, Neha Gupta, Pranesh Kumar, Ashok Kumar Singh, Vinit Raj, **Poonam Parashar**, Mahendra Singh, Jovita Kanoujia, Malti Arya**,** Shubhini A. Saraf**,** Sudipta Saha. ω-3 Fatty Acid Synergized Novel Nanoemulsifying System for Rosuvastatin Delivery: In Vitro and In Vivo Evaluation. AAPS Pharm SciTech. 2017:1-14. **(Impact factor- 2.451)**

19. Md. Meraj Anjum, Jovita Kanoujia, **Poonam Parashar**, Malti Arya, Alok Kumar Yadav, Shubhini A. Saraf, Evaluation of a Polymer-Lipid-Polymer type of System Utilising Hybrid Nanoparticles for Dapsone as a Novel Antiacne Agent. Current Drug Therapy. 2016; 11(2):86-100.

Presentations/Conference Attended

1. Presented poster entitled "Targeted drug delivery of nanoparticles in lung carcinoma" in International Conference on Updates in Cancer Prevention and Research (ICUCPR-2017) & Satellite Conference on Translational Research: Trends and Implications (IPCBBAU-2017). February 14th-16th & 20th, 2017.
2. Attended a sixteen days' workshop of DBT course in Biotechnology on the topic "Techniques in Molecular Biology", held at S.G.P.G.I.M.S., Lucknow, U.P., India. September 15th to September 30th, 2015.
3. Attended seven days' Workshop on NMR/MRI: From molecules to human behaviour. Sponsored by Department of Science and Technology (DST), India. Held at BBAU, Lucknow, U.P., India. June 21st to 27th, 2015.
4. Attended and presented poster in 2nd National Seminar on "Profession of Pharmacy: Challenges & Opportunities", Lucknow. 18th October, 2015.

5. Attended and participated in oral presentation "Oral delivery of allopurinol niosomes in treatment of gout" in 3rd Lucknow Science Congress LUSCON-2015 on "Hope for Society through Drug Research", Lucknow, 31stOctober-2ndNovember, 2015.
6. Attended and presented poster in 2nd National Seminar on "Profession of Pharmacy: Challenges & Opportunities", Lucknow, 18th October, 2015.
7. Attended 15th Indo-US Flow Cytometry Workshop on Application of Flow Cytometry in Biomedical Research, Lucknow, October 29-31, 2014.
8. Attended International Symposium on advances in Material Characterization, Lucknow. July 14, 2014.
9. Attended and presented poster entitled "Optimization and evaluation of microemulsion loaded topical gel for fungal treatment" in 2nd Lucknow Science Congress, Lucknow. March 27-28, 2014.
10. Presented scientific poster entitled "A multiple drug therapy approach for muscular pain relief: challenges & opportunities", held at I.P.S.R., Lucknow, U.P., India. 18th October, 2015.
11. Presented scientific poster entitled "Assessment of multikinase nanoparticles in lung cancer therapy" at International Pharmaceutical Conference-2015 on "Nanoformulations and Translational Research: Small Getting Bigger", held at B.B.A. University, Lucknow, U.P., India. February 2nd – 3rd, 2015
12. Presented scientific poster entitled "Development and Characterization of Targeted Delivery System(s) for Cancer Therapy" at 2nd Lucknow Science Congress on "Leveraging Science and Innovation for Development", held at B.B.A. University, Lucknow, U.P., India. March 27th – 28th, 2014.
13. Presented scientific poster entitled "Development and characterization of nanostructured lipid carriers of vetiveria zizanoides oil for therapeutic potential in prickly heat treatment" at IHPA GOLDCON- 2104 on "Restructuring Pharmacy Curricula: Need of Health Sector", held at B.B.A. University, Lucknow, U.P., India. March 1st – 2nd, 2014.

Brief CurriculumVitae

Name: Poonam Parashar

Date of birth: 03-08-1979

Education: B.Pharm(2005) from Rajiv Academy for Pharmacy (affiliated to UPTU, Lucknow), Mathura, U.P. and M.Pharm(Pharmaceutics, 2007) from Rajiv Academy for Pharmacy (affiliated to UPTU, Lucknow), Mathura, U.P.

M.Pharm project: Formulation and development of proniosomal gel for transdermal drug delivery of clonazepam, under the guidance of Prof KamlaPathak.

PhD project: Assessment of Drug Delivery and Anticancer Potential of Multikinase Inhibitor Nanoparticles in Lung cancer under the guidance of Prof. Shubhini A saraf (Head and Dean) at Dept. of Pharmaceutical Sciences, Babasaheb Bhimrao Ambedkar University, Lucknow.

Research Publications:

1. Twenty two (22) international/national research/review articles
2. Thirteen (13) oral/poster presentation in national/international seminars/conferences

Research expertise: Polymeric nanoparticulate system, Colloidal vesicular systems such asliposomes, niosomes, Targeted drug delivery, carcinogenesis.

Permanent Address

N-1/99, Aashiana
Lucknow U.P. 226012

Parashar

(Poonam Parashar)